Cerebral Blood Flow Measurement Using Intra-arterial Bolus Injection of ^2H_2O Monitored with Magnetic Resonance Spectroscopy

by

Chun-Bun Kwok

A thesis
presented to the University of Manitoba
in partial fulfillment of the requirements for the degree of
PhD
in
Physics

Winnipeg, Manitoba

(c) Chun-Bun Kwok, 1997

National Library of Canada
Acquisitions and Bibliographic Services
395 Wellington Street
Ottawa ON K1A 0N4
Canada

Bibliothèque nationale du Canada
Acquisitions et services bibliographiques
395, rue Wellington
Ottawa ON K1A 0N4
Canada

Your file Votre référence

Our file Notre référence

The author has granted a non-exclusive licence allowing the National Library of Canada to reproduce, loan, distribute or sell copies of this thesis in microform, paper or electronic formats.

The author retains ownership of the copyright in this thesis. Neither the thesis nor substantial extracts from it may be printed or otherwise reproduced without the author's permission.

L'auteur a accordé une licence non exclusive permettant à la Bibliothèque nationale du Canada de reproduire, prêter, distribuer ou vendre des copies de cette thèse sous la forme de microfiche/film, de reproduction sur papier ou sur format électronique.

L'auteur conserve la propriété du droit d'auteur qui protège cette thèse. Ni la thèse ni des extraits substantiels de celle-ci ne doivent être imprimés ou autrement reproduits sans son autorisation.

0-612-23622-6

Canada

THE UNIVERSITY OF MANITOBA

FACULTY OF GRADUATE STUDIES

*****

COPYRIGHT PERMISSION PAGE

CEREBRAL BLOOD FLOW MEASUREMENT USING INTRA-ARTERIAL BOLUS INJECTION OF $^{2}H_2O$ MONITORED WITH MAGNETIC RESONANCE SPECTROSCOPY

BY

CHUN-BUN KWOK

A Thesis/Practicum submitted to the Faculty of Graduate Studies of The University of Manitoba in partial fulfillment of the requirements of the degree

of

DOCTOR OF PHILOSOPHY

Chun-Bun Kwok 1997 (c)

Permission has been granted to the Library of The University of Manitoba to lend or sell copies of this thesis/practicum, to the National Library of Canada to microfilm this thesis and to lend or sell copies of the film, and to Dissertations Abstracts International to publish an abstract of this thesis/practicum.

The author reserves other publication rights, and neither this thesis/practicum nor extensive extracts from it may be printed or otherwise reproduced without the author's written permission.

I hereby declare that I am the sole author of this thesis.

I authorize the University of Manitoba to lend this thesis to other institutions or individuals for the purpose of scholarly research.

Chun-Bun Kwok

I further authorize the University of Manitoba to reproduce this thesis by photocopying or by other means, in total or in part, at the request of other institutions or individuals for the purpose of scholarly research.

Chun-Bun Kwok

The University of Manitoba requires the signatures of all persons using or photocopying this thesis. Please sign below, and give address and date.

ACKNOWLEDGEMENTS

I would like to acknowledge the many individuals who contributed in various capacities to this thesis.

I thank my supervisors Drs. J.A. Bews and D. Abrams. I thank Dr J.A. Bews who directed and guided my research. His suggestions and sound explanations have many times helped me to focus on the important aspects of my project. Most importantly, he took interest in my professional development. I thank Dr. D. Abrams for his guidance and helpful advice, and taking time out from his extremely busy schedule to proofread the thesis.

I would also like to thank Drs. R. Buist, J. Peeling, Mr. F. W. Yan and Drs. T. Lee, R. Palser and N. Davison. I thank Dr. R. Buist, system manager of the NMR laboratory of the department of radiology, Health Sciences Center, for many helpful discussions we shared. Most of the animal experiments were performed in evenings and Dr. R. Buist was always on standby to help with the Bruker Biospec 7/21 MR scanner. I thank Dr. J. Peeling for the use of the MR scanner, Mr. F.W. Yan for his lessons in microsurgery and for developing the indicator injection technique, and Drs. T. Lee, R. Palser, N. Davison for being members of my Ph.D. program committee.

I would like to express my love and gratitude to my wife and my parents, whose love and support played a critical role in the completion of this thesis.

Abstract

The brain is a relatively poor nutrient storage organ and as such is greatly dependent on an adequate and constant blood flow to remain viable. It is therefore proposed that a technique for measuring cerebral blood flow (CBF) will constitute an extremely useful tool in assessing the health state of the brain. This thesis reports the development of a MR based, non invasive CBF measurement method. The technique is a 3 step process:

1. Introduce a certain amount of tracer into the brain
2. Monitor the kinetics of the tracer in the brain, namely the accumulation and dissipation
3. Fit a theoretical model to the monitored result to measure CBF

Measurements were performed on Sprague-Dawley rats pre-treated with Atropine™, anaesthetized with Na-Pentobarbital. Animal preparation was a 3 step process. The first involved setting up mechanisms to monitor rat physiology during experiments. The rats were placed on a heated water bag so as to maintain a constant tympanic temperature of 38 ± 0.5 °C. Temperature was monitored constantly throughout the experiments using a thermocouple inserted into the animal's ear. The rat was then mechanically ventilated using a mixture of nitrogen and oxygen gases, with the ventilation rate and volume adjusted so as to achieve the desired level of $PaCO_2$ and PaO_2. Next, a tail artery was catheterized to enable blood sampling for determination of the blood gas levels before and after each experiment as well as to allow blood pressure monitoring. The 2nd stage of animal preparation was the placement of the injection catheter. A neck incision was made to expose the junction of the common carotid, internal carotid and external carotid arteries. A gauge 24 Teflon catheter was then inserted retrograde into the external carotid artery until its tip was positioned just before the junction with the common and internal carotids. The 3rd stage of animal preparation

involved the placement of the MR surface coil. The skin and muscle were retracted from the top of the rat's head and an approximately 1.5 cm diameter surface coil positioned tightly against the skull. Once prepared the animal was inserted into a Bruker Biospec 7/21 MR scanner for ^2H spectral acquisition. After tuning and shimming, a series of 360 free induction decays (FID) were taken. The ^2H labeled water indicator, usually 200 micro-liters, was injected as an instantaneous bolus at the beginning of the 15^{th} FID. The serial data acquisition procedure was repeated five times to yield 5 sets of data per rat. The FID in the series was used to generate 360 ^2H spectra. The peak heights of the spectra represent the relative amount of indicator in the brain at a particular time and a plot versus time of this data constituted the indicator washin and washout curve for the tracer.

The theoretical model fit to the washin and washout data was modified from the Stimulus-Response theorem. The model enabled measurement of the fast CBF (fCBF) and average CBF (aCBF) using the same indicator washin and washout curve: with the fCBF utilizing the initial portion of the washout curve and the aCBF utilizing the area under the entire curve.

The validity of the CBF measurement method developed was tested, by examining its ability to track changes in CBF with changes in $PaCO_2$. Experiments were conducted in which $PaCO_2$ levels were purposefully altered to hypocarbia and hypercarbia by adjusting ventilation rate and volume. CBF values obtained in these experiments demonstrated the technique was able to track the anticipated changes in CBF with changes in $PaCO_2$.

The reproducibility of the CBF measurement method developed was evaluated by repetitive CBF measurements on the same animal at the same $PaCO_2$ level. It was found that the method was qualitatively reproducible.

The CBF results obtained with the method developed were compared with values published in the literature using other techniques. The developed quantitative CBF

method in this thesis, if not corrected for, yielded an average CBF for normal Sprague Dawley rats of 73 ml/100g/min. This value is 37% lower than the average of all values appearing in the literature (115 ml/100g/min). It is proposed that CBF underestimation is due to indicator (used in the CBF method) not being freely diffusible and due to indicator recirculation. A consequence of the indicator not being freely diffusible was that the rate of indicator washout from the brain was slower than predicted by our model; hence CBF was underestimated. A consequence of the indicator recirculation was that the rate of indicator washout from the brain 'appeared' to be slower due to replenishment of indicator that washed-out earlier but recirculated back to the brain.

Two methods were employed to eliminate the CBF underestimation due to the indicator not being freely diffusible. The first was the extraction coefficient (E) method that employed the concept of the capillary permeability surface area product of the indicator (PS). In this method E was obtained by separating the brain into the intravascular and extravascular space. E was the ratio of indicator extracted by the extravascular to the total amount injected. The obtained E was then related to PS to assess the degree of CBF underestimation. The second method employed deuterated alcohols (ethanol, isopropanol, and t-butanol) as the indicators for the reason that they are more freely diffusible than water. A dual indicator technique was employed where deuterated water and deuterated alcohol were simultaneously introduced into the brain. Due to the difference in the chemical shifts (CS) of the two, their respective washins and washouts were simultaneously monitored; hence their respective CBFs were measured. The more freely diffusible alcohol indicator resulted in a CBF that was larger. This enabled assessing the degree of CBF underestimation due to the diffusion limitation of deuterated water.

A convolution analysis was employed to account for CBF underestimation due to indicator recirculation. This technique utilized an input function obtained from the derivative of the washout curve and a point spread function from injecting an

instantaneous bolus downstream of the brain while monitoring at the brain. This technique was successful in delineating and removing indicator recirculation from the CBF measurements. It was found that the diffusibility and recirculation corrected CBF values agree with a gold standard from the literature.

CONTENTS

Chapter 1: Introduction

The *in vivo* measurement of fluid (blood, plasma) flow or mass flux is based on the principles of tracer kinetics. Briefly, an indicator or tracer is introduced into the subject's vascular system and its accumulation and/or dissipation as a function of time in the tissue/organ of interest is monitored. The change in system indicator concentration with time is the result of fluid flowing into and out of the system. As such, an appropriate theoretical kinetic model can be fit to this data set to yield a best fit estimate of flow or flux. The form of the theoretical model used in the fitting procedure will depend on a number of factors, including:

1. the kinetic properties of the indicator
2. the manner in which the indicator is introduced into the subject's vascular system
3. whether or not recirculation of indicator is significant
4. the protocol used to monitor the indicator

Three main classes of indicators exist:

1. vascular (non-diffusible) indicators, which remain in the vascular bed
2. extracellular (hydrophilic) indicators, which can pass through the capillary wall *via* water-filled pores but are nevertheless confined to the extracellular space due to their inability to cross cell membranes

3. freely diffusible (lipophilic) indicators, which distribute throughout the entire tissue/organ, quickly establishing equilibrium

The indicator is usually introduced into the subject in one of two ways, constant infusion or bolus injection, the period over which the latter is carried out being either instantaneous or extended.[1] The principles (e.g., the Stewart principle,[2] the Fick principle[3]) underlying constant indicator infusion flow measurements are simple and have been in use since the last century. Similarly, the Henriques-Hamilton[4,5] principle, the Bergner[6] principle, and the stimulus – response theorem for bolus injection have also been known for quite some time. All of these principles and theorems, which constitute the foundation of flow measurement in biological systems, have been reviewed extensively in a monograph by N.A. Lassen and W. Perl.[7] Using the constant infusion method, either the washin (ie. build-up or accumulation) of the indicator in tissue or the washout (ie. clearance or dissipation) following cessation of infusion is monitored. The rate at which a new equilibrium is established will depend on flow. In the case of bolus injection, indicator concentration in tissue will rise from an initial value of zero to some maximum and then back down to a new baseline value. Flow is related to the ratio of the amount of indicator injected to the area under this build-up curve. Since the tracer kinetic principles are well established, the major task in any new flow measurement will be to optimize their application to different clinical or experimental environments.

A. A Field Driven by New Tools

Chapter 2 reviews in detail how cerebral blood flow (CBF) measurements have developed over time. It will become apparent that the major advances in flow measurements were driven by the development of new physical imagers and spectrometers (i.e monitoring methods), such as single photon emission computed tomography (SPECT), x-ray computed tomography (CT), positron emission tomography (PET) and magnetic resonance (MR) imaging (MRI) and spectroscopy (MRS). With the arrival of each new modality its strengths and limitations for CBF measurement were tested. The testing usually concentrated on the applicability of a particular flow principle, rather than on the capability of the instrument, which tends to be well known. In the end, however, it is the capability of the instrument that determines the unique modifications needed for the application of the existing flow principles. For example, consider one very important constraint of SPECT, its long image acquisition time. This constrains one to employ indicators that behave as so-called 'chemical microspheres', which can diffuse freely into the tissue of interest and remain in the tissue for a relatively long period of time, (e.g., 2 hours). On the other hand, if the monitoring device is an x-ray film, then the ideal flow measurement technique is autoradiography using radioactive microspheres. Therefore it is fair to say that recent advances in flow measurement have been driven by new monitoring tools, in an attempt to find ways to utilize them in conjunction with existing tracer kinetic principles.

B. CBF is Critical to the Well Being of the Brain

The importance of CBF information can not be over emphasized. The brain is a poor storage organ and it can neither store nutrients for metabolism nor tolerate waste products. As such, a certain CBF level has to be maintained at all times to keep the brain viable. The very critical dependence of the brain on CBF can also be illustrated by the fact that this organ receives an unusually large portion of cardiac output per tissue weight.

From the vantage point of cancer management, CBF information can be useful in the diagnosis, treatment and post treatment follow-up of brain tumours. For diagnosis, CBF may help to delineate lesions better through spatial blood flow (BF) anomalies.[8] Prior to radiotherapy, CBF can be used to determine the state of oxygenation of tumour cells, so that the most appropriate treatment regimes (fractionation) can be chosen.[9] The importance of CBF applies equally well to brain tumour chemotherapy, for the up-take of antineoplastic drugs into the tumour is a function of CBF and other factors.[10] For post-treatment follow-up, CBF can be used to assess the cerebral vascular damage[11,12,13] due to radiotherapy.

In so far as perfusion is concerned, the brain is a fairly simple organ to model. To a first order approximation, it can be thought to consist of four major arteries (two internal carotids and two vertebralis) and two major veins (the internal jugulars), all in bilateral pairs. In addition, the imaging modalities in use today, such as CT, PET, SPECT and MR, are ideally suited for sampling the

indicator washin and/or washout data (required in CBF measurements) on the brain. For example, in comparison to the abdomen, motion artifacts in head scans can be minimized.

C. The Goal: To Develop a Clinical CBF Technique

We have set our goal to develop a non-invasive MR based CBF measurement technique that can be used routinely as a procedure in brain tumour management. We can achieve our proposed goal by accomplishing three tasks:

1. Develop a 'non-invasive', indicator based CBF technique in rats that will allow us to investigate the fundamental principles on which it is based. 'Non-invasive' will refer to the method used to sample the washin/washout data. Injection of the indicator will be invasive, at least initially, so as to allow us to study fundamental principles.
2. Formulate procedures to evaluate the accuracy and precision of the technique.
3. Make the technique truly non-invasive for human usage, in particular, the injection of indicator.

D. Organization: Outline of the Thesis

The outline of the thesis, besides this introduction, is as follows:

a) Chapter 2 reviews the history of CBF measurements, past to present.

b) Chapter 3 formulates the theoretical basis of CBF measurement using MR.

c) Chapter 4 consists of two parts; the first part summarizes a variety of experiments undertaken in the development of our CBF measurement protocol and the second part provides a practical manual for the final protocol developed.

d) Chapter 5 presents CBF results obtained using the final protocol and examines the experimental reproducibility of the protocol.

e) Chapters 6 and 7 study the accuracy of the CBF technique

f) Chapter 8 study the suitability of deuterated alcohols for accuracy assessment of the CBF technique.

g) Finally, Chapter 9 summarizes the study and suggests the direction for future research.

References

[1] Zierler K, 'Theoretical Basis for Indicator-Dilution Methods for measuring Flow and Volume', *Circulation Research* 10:393, 1962.

[2] Stewart GN in *J. Physiol.* 22:159, 1897.

[3] Fick A in *Sitzungsb. der Phys.-Med. Ges. zu Wurzburg* p.36, 1870.

[4] Henriques V in *Biochem. Zeitschr.* 56:230, 1913.

[5] Hamilton WR, *et al.*, in *Am. J. Physiol.* 84:338, 1928.

[6] Bergner PEE in *J.Theor.Biol.* 6:137, 1964.

[7] Lassen NA and Perl W in *Tracer Kinetic Methods in Medical Physiology*, Raven Press, New York, 1979.

[8] Aizawa S, Sako K and Yonemasu Y, 'Measurement of cerebral blood flow, cerebral blood volume and cerebral capillary permeability in glioma bearing rats', *Neurol.Med.Chin.* 30(2):113-8, 1990.

[9] Dgawa T, Uemura K, Shishindo F, *et al.*, 'Changes of cerebral blood flow, and oxygen and glucose metabolism following radiochemotherapy of gliomas: a PET study', *J.Comput.Assist.Tomogr.* 12(2):290-7, 1988.

[10] Suzuki N, Sako K, Yonemasu Y, 'Effects of induced hypertension on blood flow and capillary permeability in rats with experimental brain tumors', *J.Neurooncol.* 10(3):213-8 1991.

[11] Lo EH, Frankel KA, Steinberg GK, DeLaPaz RL, Fabrikant JI, 'High-dose single-fraction brain irradiation: MRI, cerebral blood flow, electrophysiological, and histological studies', *Int.J.Radiat.Oncol.Biol.Phys.* 22(1): 47-55 1992.

[12] Sakai N, Nakatani K, Shirakami S, *et al.*, 'Delayed effects of radiation of patients with germ-cell tumor, with special attention to cerebral blood flow', *No.To.Shinkei.* 42(2):161-6, 1990.

[13] Mineura K, Suda Y, Sasajima T, *et al.*, 'Prognostic significance of regional blood flow, blood volume, oxygen extraction fraction, and metabolic rates of oxygen and glucose as measured by positron

emission tomography in patients with gliomas',
Nippon.Gan.Chiryo.Gakkai.Shi. 24(11): 2556-62, 1989.

Chapter 2: Review of CBF Research

A. Introduction

Indicator based techniques have been employed to measure the blood flow of numerous organs and tissues, with CBF being just one of the many applications. A common characteristic of all indicator techniques is that the flow measurement procedure can be described as a 'three step' procedure:

1. introduction of an indicator into the system of interest, (e.g., an organ or tissue)
2. monitoring the time course accumulation and/or dissipation of the indicator in the system and
3. applying a suitable mathematical model to the monitored data to predict flow

Out of this simple 'three step' procedure, many blood flow measurement methods have been developed, each differing in the way the three steps are carried out. For example, step one can consist of bolus injection, or constant infusion,[1] intravenous injection, intra-arterial injection, interstitial[2] injection or inhalation.[1]

Furthermore, the indicators themselves can differ substantially, falling into one of three distinct categories:

1. vascular indicators (remain in the vascular bed)

2. extracellular indicators (pass through the capillary walls by way of water filled pores but are unable to cross the cell membranes and hence are confined to the extracellular spaces)

3. freely diffusible indicators (cross cell membranes and distribute throughout the entire tissue)

Examples of indicators used to measure CBF are given in Table 2.1. The table also illustrates some of the variations in CBF measurement techniques which have arisen from applying different methods for monitoring indicator build-up.

Further variations in techniques developed to measure CBF have also resulted from the third step. This is simply due to the fact that different mathematical algorithms will be required for different types of indicators, different kinds of monitoring techniques and different methods of introducing the indicators into the organ of interest. Chapter 3 details this discussion.

B. CBF Measurement Methods

1. The Coming of Age of CBF Studies

Research into CBF determination assumed prominence when Kety and Schmidt demonstrated that CBF can be measured quite conveniently using inert gases, such as nitrous oxide, xenon, argon, *etc.*[3,4] This monumental piece of work provided a simple technique for global CBF measurement, as recognized by all research groups. In my opinion the most important contribution of the work is in the example it gives, on how an existing, well-known flow principle (the Fick principle) can be modified for application to CBF measurement.[5]

Table 2.1 Indicators and Monitoring Methods Used to Measure CBF.

Type of Monitoring Method	Indicator
Geiger-Muller Tube, Gamma Camera, Planar x-ray Film.	Argon[3] N_2O[4] ^{85}Kr[6] ^{133}Xe[7]
Hydrogen Clearance *via* Platinum Eletroodes	H_2[8]
Autoradiography	^{131}I Trifluoroiodomethane[9] ^{14}C Iodoantipyrine[10]
CT	Stable Xenon[11]
PET	$H_2{}^{15}O$[1] $C^{15}O$[12] ^{11}C-radiopharmaceuticals[6] ^{13}N- radiopharmaceuticals[6] ^{18}F- radiopharmaceuticals[6] ^{82}Rb[6]
SPECT	^{123}I-IMP[13] ^{123}I-HIPDM[14] ^{99m}Tc-HMPAO[15] ^{99m}Tc-ECD[16]
MR	$^{2}H_2O$[17] ^{19}F-tracers CFC-22[18] FC-23[19] ^{19}F-Blood Replacement[20] Gadolinium DTPA[21]

2. Classification of CBF Measurement Methods

From a practical point of view, all CBF measurement methods can be classified into either invasive or non-invasive groupings (with respect to the brain). Among all methods, the most used invasive CBF method is autoradiography. This CBF measurement method was developed by Landau and co-workers in 1955.[9] It is applicable only to animal studies, as in using this technique, the brain has to be cut into thin slices after infusion of a radioactive indicator. These slices are then placed on a photographic film, the level of optical density (or darkening) being a measure of the concentration of indicator and hence perfusion. This invasive procedure has been used to provide information on the local blood perfusion rate in the brain. The autoradiography method has contributed greatly to the understanding of brain diseases, especially in the pathophysiology of cerebral ischaemia,[22,23,24] cerebral metabolism and drug response[25] and neurological function, *etc.*[26]

When used in humans, the minimum requirement of any CBF measurement technique is non-invasiveness. Modern imaging modalities are therefore ideal candidates for CBF studies. To date, all existing imaging modalities have been investigated, or are being investigated, for their potential use in CBF measurement. By far the most common clinical implementation of CBF measurement utilizes single photon emission computed tomography (SPECT) with ^{99m}Tc derivatives such as HMPAO and ECD[27,28,29,30,31,32,33,34] and prior to the ^{99m}Tc era with iodinated amines such as ^{123}I IMP[35,36,37,38,39,40] Next on the list is positron emission

tomography (PET) with ^{15}O-labeled tracers,[41,42,43,44,45,46] followed by stable xenon contrast computed tomography (CT) and iodinated contrast CT.[47,48,49,50,51] CBF using magnetic resonance (MR) is currently a developing technique[17,18,52,53,54,55,56] that has not seen wide spread clinical application. (See a later section on CBF using MR for more details.) The following sections review in detail both the invasive and the non-invasive CBF measurement methods.

a) Invasive CBF Measurement Methods

The two invasive CBF measurement methods most frequently used in animals are autoradiography and hydrogen clearance. The autoradiographic technique was developed by Landau *et al.* in 1955 using ^{131}I-trifluoroiodomethane (^{131}I-CF_3I).[9] Since then, the indicator of choice for this technique has been ^{14}C-iodoantipyrine (^{14}C-IAP). This preference followed a study by Sakurade *et al.*,[10] in which they discovered that ^{14}C-IAP is less diffusion limited than ^{131}I-CF_3I. Other indicators used in the past[57,58] were shown to be inferior to ^{14}C-IAP in diffusion properties. The autoradiography technique assumes that:

1. the indicator used can be detected once introduced into the flow system
2. the extraction of the indicator is tissue independent (including diseased tissues)
3. the extraction coefficient (E) is the same for all flow rates

Because of these assumptions an ideal autoradiographic indicator is one that is initially freely diffusible, and upon reaching the tissue of interest is retained in proportion to the perfusion rate of the tissue. To measure CBF after indicator injection, the brain is cut into thin slices and placed on a photographic film. After exposure and development the optical densities of the film are related to flow. To summarize, the 'three step' procedure of the autoradiography technique are:

1. Introducing an amount of an indicator, by means of constant infusion or bolus injection, into the brain. The indicator must be radioisotopically labeled, extracted by the brain and retained in the brain for a long period of time
2. Sampling the spatial distribution of the indicator retained by cutting the brain into thin slices, and placing the slices on photographic film
3. Developing the exposed films and relating the optical density on the films to relative regional CBF (rCBF)

Another invasive CBF method worth mentioning is the hydrogen clearance method.[59,60] Aukland[8] was the first to explore this technique. In this method, one relies on the fact that the quantity of hydrogen gas in tissue can be detected by microelectrodes imbedded in a discrete fashion over a well-defined region of interest.[8,26] The 'three step' procedure of the hydrogen clearance technique are:

1. Ventilating the subject with a mixture of hydrogen and other gases

2. Detecting the hydrogen concentration in various locations of the brain using implanted microelectrodes

3. Relating the local CBF (lCBF) to the hydrogen concentrations *via* mathematical modeling

The difference between rCBF and lCBF is that the former refers to a spatial location in the brain while the latter refers to a specific brain region, such as frontal cortex.

b) Non-Invasive CBF Methods

Invasive techniques for the study of CBF in the brain have limitations. The most obvious one is the fact that the relationship between CBF and human brain diseases are studied indirectly through animal models. Unfortunately, findings from the animal studies cannot always be extrapolated to humans, herein lies the strength of non-invasive techniques.

(1) CBF Measurements Using CT

Since the earlier 80's, the most investigated CBF CT technique used CT in its dynamic mode.[11,47,48,49,50] This was in order to monitor the build-up or clearance of xenon in the brain. In CBF measurements, stable xenon (atomic number of 54) was used as CT image contrast agent. Iodinated contrast agents had been used previously but with only limited success.[51] With minor exceptions, the vast majority of xenon enhanced dynamic CT based CBF techniques consisted of the following 'three step' procedure:

1. Aerating the subject with a mixture of stable xenon and air (oxygen)

2. Acquiring three or more CT images during and/or after 4 to 6 minutes of xenon and air inhalation. Simultaneously sampling the time course of end-tidal xenon concentration of the expired xenon/air mixture

3. Using the time dependent concentration of xenon in the brain and the end-tidal xenon concentration in the Kety[61] or the Kety and Schmidt[4] equation to predict rCBF or CBF and λ_i or λ for xenon (*via* deconvolution or curve fitting). This technique assumes that the arterial time course concentration of xenon, required in the Kety or Kety and Schmidt equation, was proportional to the end-tidal time course concentration.

The Kety equation provided a simultaneous estimation of regional CBF (rCBF) and regional partition coefficients (λ_i), and the Kety and Schmidt equation provided a global CBF and average partition coefficient (λ). In CBF studies, λ was defined as the ratio of indicator concentration in tissue (the brain) to that in carrier fluid (the blood), under steady-state equilibrium. Both the build-up and clearance of xenon in brain tissue have been used for CBF estimation.

Compared to PET, a strength of the stable xenon CT technique was that the measured CBF was more accurately linked to anatomy. Also, researchers have demonstrated that the xenon CT technique could provide more accurate

measurements of CBF in the low blood flow regions (such as white matter) of the brain.[48]

Although CT is capable of fast dynamic scanning, each scan delivers a radiation dose of approximately 4 mSv,[62] resulting in either an unacceptably high risk to the patient, or insufficient temporal resolution if fewer scans are used. The xenon concentration used in the air mixture was around 35%, with higher xenon concentrations often being associated with sedation and agitation.[63,64,65] This factor limited the available CT contrast, and hence the signal to noise,[66,67] resulting in limited CBF accuracy.[68]

Recently CBF measurements using stable xenon enhanced CT has been gaining clinical acceptance, especially in cases of brain death, acute stroke, occlusive vascular disease, etc.[48] In these cases the xenon CT technique was specially suited, due to its ability to measure low more CBF accurately (compared to PET).

(2) CBF Measurements Using SPECT

(a) Introduction

The most common CBF study using SPECT is the non-invasive autoradiographic technique.[69] An obvious reason is in the longer imaging time required for SPECT (autoradiography requires a minimum of one scan). The tendency towards using the non-invasive autoradiographic technique imposed strict requirements that the indicator used in SPECT behave more or less like a chemical microsphere. Physical microspheres may not be used because of their

potential invasiveness in blocking blood flow to the brain. At present the most studied SPECT perfusion indicator is ^{99m}Tc-Bicisate (or ECD)[16,30,31,34,70]. It has the potential to replace ^{99m}Tc-HMPAO[15,27,28,29,32,33] which had superseded the ^{123}I-labeled amines (IMP)[13,36,37,38,39,40] and (HIPDM).[14,35,71] ^{99m}Tc HMPAO is more desirable than ^{123}I IMP because ^{99m}Tc is physically more desirable than ^{123}I (for example, ^{99m}Tc has a shorter half life and therefore radiation dose to patient will be less). ^{99m}Tc HMPAO, however, has a number of short-comings. It is chemically unstable[72] and its labeled metabolites demonstrate slow blood clearance.[73] ^{99m}Tc ECD is a result of considerable effort in the search for a ^{99m}Tc HM-PAO replacement. ^{99m}Tc ECD has a rapid blood clearance,[74] slow washout from the brain and insignificant intracerebral redistribution. Compared to ^{99m}Tc HM-PAO, ^{99m}Tc ECD appears to be more stable and has higher extraction fractions.[73] Unfortunately, the one time promising non-invasive autoradiography SPECT technique using ^{99m}Tc ECD (or earlier ^{99m}Tc HMPAO) is intrinsically incorrect, due to the fact that the retention of the chemical microsphere is possible only through metabolic conversion of the freely diffusible indicators into forms that are stable and remain in the respective organs/tissues for a considerable amount of time. The very dependence of this mechanism on metabolism results in violation of the requirement that extraction of the microspheres be tissue (both healthy and diseased tissue) independent and that the extraction coefficient be the same for all flow rates. This is especially true when the technique is used to study diseased

brain where tissues may not function normally (that is, diseased tissues may not metabolize the injected tracer normally).

The non-invasive autoradiography based SPECT can be divided further into qualitative SPECT and flow and/or rate constant SPECT.[75]

(b) Qualitative SPECT

Qualitative CBF using SPECT employs perfusion indexes for flow assessment.[75,76] These perfusion indexes include:

1. fractional brain uptake (FBU) of indicator or uptake index (UIs)
2. normalized brain uptake (with respect to, for example, the cerebellum tissue)
3. regional standardized values (SVs, standardized to the injected activity and the acquisition time unit)

The 'three step' procedure in qualitative CBF using SPECT is as follow:

1. intravenous (bolus) injection of tracer
2. SPECT image acquisition and perfusion indexes determination (from regions of interest (ROIs) in the image)
3. qualitative blood flow assessment using the perfusion indexes obtained

An important topic of study for qualitative SPECT is to derive empirical correlation methods for connecting the perfusion indexes to corresponding blood

flow or flow rate constants. There are many examples of qualitative CBF correlation investigations using both ^{99m}Tc HMPAO and ^{99m}Tc ECD.

In one such qualitative CBF correlation investigation using ^{99m}Tc HMPAO, Inugami *et al.*[77] correlated the normalized radioisotope distribution (uptake) of ^{99m}Tc HMPAO in the brain (normalized to the cerebellum tissue) with rCBF images obtained using PET and $C^{15}O_2$ inhalation. They employed a three compartment kinetics model to describe ^{99m}Tc HMPAO in the brain (the so-called linearization correction model).[78] The three compartments were: (a). the lipophilic tracer in the blood pool of the brain, (b). the lipophilic tracer inside the brain and (c). the hydrophilic form retained in the brain. They found that the ^{99m}Tc HMPAO images were very similar to the PET-CBF images obtained the using $C^{15}O_2$ inhalation, steady state method (see section on CBF using PET for more details) for both the linearization corrected and uncorrected cases. The correlation coefficient (r) for the corrected case was 0.93 and for the uncorrected 0.85, except in high blood flow regions. Similarly, Yonekura *et al.*[79] correlated ^{99m}Tc HMPAO SPECT images with rCBF images measured with a PET based, $C^{15}O_2$ inhalation steady state method in patients with stenosis (using the three compartment model for ^{99m}Tc HMPAO brain kinetics). In this clinical application, they had found that although the SPECT technique could not provide absolute CBF values, it could, through the use of a 'linearization algorithm' (linearization correction), provide a better linear correlation between normalized pixel activity (uptake) and CBF. The

correlation coefficient (r) for the uptake and CBF was 0.901. It was also found that the 'linearization algorithm' improved contrast between normal and ischemic regions of the brain. In another study, Langen *et al.*[80] correlated ^{99m}Tc HMPAO SPECT images with CBF images measured with a PET based $C^{15}O_2$ inhalation steady state method in patients with brain tumors. They too employed the three compartment model for ^{99m}Tc HMPAO brain kinetics and found a significant correlation between intracerebral distribution ratios (normalized tumor uptakes) and CBF determined using the $C^{15}O_2$ inhalation steady state method. As a final example, Andersen *et al.*[81] correlated the uptake and retention of ^{99m}Tc HMPAO with CBF image measured using a SPECT based ^{133}Xe inhalation technique. They found that the ^{99m}Tc HMPAO CBF images agreed quite well with that of ^{133}Xe CBF regardless of whether or not the 'linearization algorithm' (the three compartment correction for ^{99m}Tc HMPAO brain kinetics) was used.

In a qualitative CBF correlation investigation using ^{99m}Tc ECD, Huglo *et al.*[76] correlated regional brain ^{99m}Tc ECD standardized values (SVs), uptake indexes (UIs) and asymmetry indexes (AIs) to the corresponding rCBF, flow indexes (FIs) and AIs measured using ^{133}Xe inhalation SPECT. In this preliminary study, they found highly significant correlations between: SV and CBF (r=0.47), UI(normalized to cerebellar lobes) and FI (r=0.57), UI(normalized to occipital cortex) and FI (r=0.69). In another study, Yonekura *et al.*[82] correlated the uptakes of ECT (which have been corrected using a permeability – surface area product

(PS) model, see Chapter 6) with CBF images obtained by PET using $^{15}O_2$ inhalation steady-state. They found that the nonlinear relationship between ^{99m}Tc-ECD uptakes and rCBF could be accounted for by using the PS correction.

(c) Flow and Rate Constant SPECT

The flow and rate constant SPECT CBF techniques measure absolute, quantitative flow and/or rate constants directly, by employing tracer kinetic models of flow. The ^{133}Xe inhalation method is an example. It employs SPECT in the dynamic mode and makes use of an indicator clearance model.[83] Dynamic ^{133}Xe SPECT is less common clinically for the following reasons:

1. It has poor spatial and temporal resolution[77]
2. It requires a dedicated SPECT scanner[76]
3. Compared to ^{99m}Tc it is less suitable for large depth (center of brain) studies due to the softer radiation emitted by this radionuclide[84]

In spite of the above, dynamic ^{133}Xe was sometimes used as a standard for SPECT perfusion studies.[76,81] However, most flow and rate constant SPECT CBF measurements have utilized ^{99m}Tc HMPAO or ^{99m}Tc ECD.

In a ^{99m}Tc HMPAO flow and rate constant CBF SPECT investigation, conducted by Matsuda *et al.*[85] flow and rate constants were obtained using the following 'three step' procedure:

1. intravenous bolus injection of ^{99m}Tc HMPAO (20 to 30 mCi)

2. simultaneous dynamic monitoring and sampling of ^{99m}Tc HMPAO tissue concentration in the brain (using a ring-type SPECT scanner) and in the arterial blood
3. employing a four compartment kinetic model to describe the brain and using the arterial ^{99m}Tc HMPAO concentration information in a convolution operation to predict flow.

The four compartment ^{99m}Tc HMPAO brain kinetic model consisted of: (a). diffusible tracer in the blood, (b). non-diffusible tracer in the blood, (c). lipophilic diffusible tracer in brain tissue, and, (d). hydrophilic nondiffusible tracer in brain tissue. The absolute CBF value they obtained was 40 ± 3 ml/100g/min for gray matter and 23 ± 1 ml/100g/min for white matter.

Pupi *et al.*[75] assessed the accuracy of ^{99m}Tc ECD flow and rate constants by comparing them with results obtained using ^{99m}Tc-microspheres. In addition, they compared the strengths and limitations of flow and rate constant versus qualitative measurements. Their flow and rate constant 'three step' procedure consisted the following:

1. Performing an intravenous (antecubital vein) injection of a slow (~ 15 s) bolus of ^{99m}Tc ECD
2. Acquiring a SPECT image and obtaining arterial blood tracer concentration information. (While the SPECT image was being

acquired, 32 blood samples were taken from the radial artery to establish time-activity curves of artery tracer concentration.)

3. Using the artery time activity information to obtain a DR(t) function (fraction of the tracer that is diffusible across the blood brain barrier, BBB) and using the tracer activity in the brain (obtained from SPECT image) to obtain an influx constant K_i (a constant which related to CBF *via* a two-compartment model for the brain kinetics of ^{99m}Tc-ECD).

The qualitative flow indexes were obtained from the SPECT image in the second step of the above 'three step' procedure. The study demonstrated the possibility of using ^{99m}Tc-ECD for CBF measurement. In addition, it questioned the reliability of using qualitative CBF indexes, as their results indicated that FBU is neither accurate nor precise.

(d) Recent Developments in SPECT Based ^{123}I-labeled IMP CBF Measurements

The ^{123}I-labeled IMP CBF SPECT technique was superceded by ^{99m}Tc HMPAO CBF SPECT for a number of reasons. Despite the fact that the first pass extraction fraction and affinity in the brain for this tracer it, unfortunately:

1. has non negligible clearance from the brain (making it a less than 'ideal' microsphere)[86,87,88,89,90]
2. has inferior imaging and dosimetry characteristics[91]

3. has a potential for inaccurate correlation of uptake of ^{123}I-labeled IMP in the brain and true CBF[92,93]

4. has the potential for redistribution of indicator in the brain over time (again making it a less than 'ideal' microsphere).[86,94,95]

Recently there has been renewed interest in ^{123}I-labeled IMP CBF SPECT research. This renewed interest was in part due to the development of a one-point arterial sampling method,[96] which greatly simplified the technique. Currently this one point arterial sampling is being assessed and applied clinically.[97,98]

(3) CBF Measurements Using PET

(a) Introduction

The distinction between SPECT and PET is that the former employs single photon emitting nuclear isotopes while the latter employs positron emitters (i.e. gamma versus beta nuclide decay followed by electron-positron annihilation). This seemingly singular distinction between the PET and SPECT has far reaching implications. The most important implication is the kind of indicator that one can use. With PET, the most frequently used positron-emitting radionuclides are ^{11}C, ^{13}N, ^{15}O, ^{18}F, and ^{82}Rb. Since C, O and N are natural building components of organic matter, PET is currently the only modality capable of simultaneous measurement of CBF, blood volume (BV), oxygen extraction fraction, and oxygen and glucose metabolism with detail and accuracy.[41] Unfortunately such capabilities carry a high monetary cost.[42] As a result, if the goal is to study CBF alone, after many compromises and arguments the end conclusion will be that

SPECT is much more cost-effective than PET. Besides, PET installations are few in number and only major research establishments have access to this technology.

The majority of the quantitative CBF with PET techniques were developed in the 80's and late 70's. In all the techniques, the most common indicator was ^{15}O[44,45,46,47] in the form of gas[43,45] ($C^{15}O_2$ and $^{15}O_2$)[1,2,12,99,100] and water[46] ($H_2{}^{15}O$).[101,102,103,104,105,106,107,108] This is readily understood, as gas can be introduced conveniently into the subject through inhalation and water is naturally present in the body. Recent developments in the area of PET based quantitative CBF techniques have focused on refining and improving the existing techniques.

(b) CBF Measurements Using PET

With all ^{15}O gas CBF PET techniques, an underlying assumption was that the $^{15}O_2$ transfer from gas (CO_2 or O_2) to H_2O in the pulmonary alveolar capillaries *via* carbonic anhydrase.[109] Therefore, the $C^{15}O_2$ technique may be considered an indirect $H_2{}^{15}O$ technique. The 'three step' procedure for the measurement of CBF with ^{15}O gas PET, in many cases, resembles the 'three step' procedure of ^{133}Xe CBF with SPECT.

(i) ^{15}O[Gas] CBF PET

In ^{15}O gas CBF PET investigations, Frackowiak *et al.*[1] developed a continuous steady-state $C^{15}O_2$ method for measuring CBF in humans. The technique developed was subsequently treated by many research groups as a practical CBF measurement standard – a standard for assessing other quantitative

CBF techniques (such as the CBF with SPECT techniques).[77,80] The 'three step' procedure of the Frackowiak *et al.* method involved:

1. Introducing $C^{15}O_2$ into the subject continuously *via* inhalation
2. At indicator steady-state equilibrium, measuring the $H_2{}^{15}O$ activities in the brain using PET and in the femoral artery using blood sampling
3. Utilizing the two activities in a kinetic model, a model derived from the Fick principle, to predict CBF. (See Chapter 3 for more details on the Fick principle. The Fick principle was used to account for the decay of $^{15}O_2$)

Using this method both gray matter CBF and white matter CBF were obtained, with the measured gray matter CBF equal to 65 ml/100ml/min and the measured white matter CBF equal to 21 ml/100ml/min. The CBF results they obtained compared well with those measured by Kety and Schmidt[4] and Kety[110] and Lassen.[111] The accuracy of this technique in measuring CBF has been assessed and reported in a number of papers. Lammertsma *et al.*[112] and Rhodes *et al.*[113] found the technique to be highly accurate. Assured of the technique's accuracy, Ito *et al.*[100] applied it to the study of CBF in patients with cerebral tumors.

In another ^{15}O gas CBF PET study, Huang *et al.*[2] developed a non invasive autoradiographic bolus $C^{15}O_2$ CBF method in humans. The 'three step' procedure of this technique involved:

1. Having the subject inhale a single breath of $C^{15}O_2$, (again assuming the $^{15}O_2$ transfer from CO_2 to H_2O in the pulmonary alveolar capillaries *via* carbonic anhydrase)
2. Acquiring a sequence of five 2-min PET scans to determine brain tracer activity and a series of 15 to 20 artery blood samples over 10 min; the later was used to obtain a time activity curve of artery blood.
3. Employing the two tracer activities in a kinetic model (again derived from the Fick principle of Chapter 3) to predict both gray matter and white matter CBF

Using this method, Huang *et al.* measured a value of 59 ml/100g/min for the gray matter CBF and a value of 20 ml/100g/min for the white matter CBF.

(ii) ^{15}O[Water] CBF PET

In ^{15}O water CBF PET investigations, Raichle *et al.*[108] developed a non invasive autoradiographic $H_2{}^{15}O$ CBF PET technique in baboons. Furthermore, they evaluated the accuracy of the technique by comparing the results to the CBF obtained using residue detection of an internal carotid artery bolus injection. (See Chapter 3 for more details on bolus injection and residual detection theory as well as Chapter 4 on experimental internal carotid tracer bolus injection and residue detection in rats using MRS.) The 'three step' procedure developed by Raichle *et al.* was as follows:

1. Performing an intravenous bolus injection of 5 ml $H_2{}^{15}O$ saline
2. Acquiring a 40 second PET scan (from 7 brain slices in a low resolution mode) for brain tracer activity and drawing internal carotid artery blood (ICA) samples at 5 second intervals to yield an arterial time activity curve
3. Using the tracer activity of the ICA and the instantaneous local radiotracer concentration of the PET scan in Kety's tracer kinetic equation[61] to predict CBF (numerically by means of interactive parameter estimations)

They found that the CBF obtained using the non invasive autoradiographic PET technique related well to the CBF measured by internal carotid bolus injection and residue detection, with CBF (PET) = 0.90 CBF(Ref) + 4.

In another ^{15}O water study, Jones *et al.*[106] developed a continuous intravenous infusion of $H_2{}^{15}O$ CBF PET technique. The 'three step' procedure involved:

1. Introducing $H_2{}^{15}O$ into the subject continuously *via* intravenous infusion (antecubital vein)
2. 10 min into the intravenous infusion, acquiring PET scans of the brain for 10 to 30 min and obtaining artery samples every 3 to 4 min. The PET scans and the arterial blood samples were used to

determine the mean brain tissue concentration and the mean artery activity

3. Employing a working tracer kinetic equation developed by Subramanyam *et al.*[114] to predict CBF

The CBF obtained, after correcting for underestimation due to the nonlinearity of the kinetic model used and after correcting for the whole-brain recovery coefficient, was 47-77 ml/100g/min.

(c) Recent Developments in PET CBF Techniques

The above mentioned quantitative CBF PET techniques have undergone refinements for over the past 10 years. For example, Nelson *et al.*[101] attempted to make the sampling the of the arterial blood (an awkward and difficult task required in all the above mentioned CBF PET techniques) less invasive. Their noninvasive arterial monitoring was as follows:

1. Establishing a time dependent relationship between photon count (measured using a scintillation probe) from the superior right lung to the arterial tracer concentration in humans using $C^{15}O$ inhalation at steady state (same blood concentration of ^{15}O labeled carbon monoxide for the whole body)
2. During the bolus $H_2{}^{15}O$ CBF PET measurement, replacing the arterial blood sampling by photon count from the superior right lung (measured using the scintillation probe)

3. Relating the photon time activity curve from the lung to the arterial time activity curve using the established relation.

Kanno *et al.*[102] investigated the optimal scan time needed to achieve the maximum signal-to-noise (S/N) for CBF measurements using the bolus $H_2{}^{15}O$ CBF PET technique. In this investigation they performed dynamic (sequential) PET scanning in subjects injected with a bolus of $H_2{}^{15}O$ and combined the dynamic data into images corresponding to different scan spans. They found that the maximum S/N ratio for CBF measurements was for scan durations of 90 and 120 seconds.

Finally, Berridge *et al.*[115] attempted to correct for CBF underestimation inherent with $H_2{}^{15}O$ (a tracer that is not entirely freely diffusible and hence does not fully meet the requirements of the kinetic model used in CBF measurement). In an animal (rhesus monkey) study they compared CBF measured using [^{11}C]butanol to CBF measured using $H_2{}^{15}O$ and had found that the average CBF from [^{11}C]butanol (53.1 ml/100g/min) was significantly higher than the average CBF from $H_2{}^{15}O$ (44.4 ml/100g/min).

(4) CBF Measurements Using MR

(a) Introduction

MR is the most recent modality to be used in the study of CBF. Compared to PET, MR has many advantages. For example, a unique feature of MR is that it does not utilize ionizing radiation, and therefore is associated with low or no

radiation risk to the subject. Another advantage of MR is in the kind of indicators that can be used. MR indicators are divided into two groups, endogenous and exogenous.

The endogenous indicator can be generated by manipulating MR pulse sequences.[116,117,118,119] For example, one can selectively saturate the water in blood at or near the internal carotid artery and as the saturated water flows into the brain it can be detected and used to measure flow. In endogenous measurement of CBF with MR, water has been the only tracer employed; (the protons of water possess the highest MR signal available in all stable nuclei).

An exogenous indicator is injected into the subject in much the same way as for SPECT and PET, except that stable (non radioactive) MR indicators are much easier to handle. Using a stable indicator has many other advantages, one being that the correction for radioactive decay is unnecessary, which simplifies flow calculations. Another advantage is that the indicators need not be manufactured on site using an expensive facility, as in the case of ^{15}O CBF PET techniques. Other attractive features of measuring CBF using an exogenous indicator with MR include: 1. availability of scanners, 2. coupling of anatomy to CBF and 3. superior temporal and spatial resolution.

In many of the exogenous MR CBF studies, labeled water indicators were used, including: (a) ^{2}H MR using $^{2}H_2O$,[17,52,53] (b) ^{1}H MR using $H_2{}^{17}O$,[120] and (c) ^{17}O MR using O_2 or $H_2{}^{17}O$.[121,122,123,124] A number of research groups have

employed ^{19}F labeled compounds, such as: (a) [^{19}F]CFC-22 (or Freon-22), (b) [^{19}F]FC-23 (Freon-23 or Trifluoromethane), (c) [^{19}F]halothane, and (d) others.[18,19,20,54,125] In another variation of the exogenous MR CBF studies, contrast enhancement agents were used. In exogenous contrast enhanced MR, CBF was studied indirectly (*via* image contrast enhancements) from relaxation and/or magnetic susceptibility effects.[21,55,122,121,123,126,127,128,129,130,131]

The following section reviews the above mentioned CBF MR techniques. Additional information on the strengths and limitations of the different indicator techniques can be found in a later section of this chapter: 'The Development of Deuterium MRS for CBF Measurement.'

(b) CBF MR Techniques

(i) Endogenous Studies

In an animal (male Sprague-Dawley rats) study, Detre *et al.*[132] utilized water in the blood (as an endogenous tracer) and ^{1}H MR images of the brain to estimate CBF. Their 'three step' procedure for CBF measurement consisted of:

1. Saturating blood water flowing to the brain in the neck region (using a spin echo pulse sequence and spoiler gradients at the time of the 180° refocusing pulse[133])
2. Acquiring an MR brain image at indicator steady state (constant MR signal following the initial signal reduction due to saturated blood water exchange with non saturated brain water)

3. Calculating CBF using: (a) the signal ratio from the saturated and the non saturated image, (b) the T_1 (spin lattice relaxation rate) of blood water, and (c) the brain-water partition coefficient (λ, defined in Chapter 5)

Using the above 'three step' procedure Detre *et al.* obtained an average CBF of 105 ± 16 ml/100g/min in three rats under normocarbia. In addition, they found that the technique was sensitive to increases in arterial $PaCO_2$.

In another paper by the same research group, Williams, Detre, Leigh and Koretsky[116] performed a similar study in which the spin echo pluse spoiling gradients in the neck region were replaced by a spin inversion at the same location using the principles of adiabatic fast passage (see later in this chapter for more detailed discussion). In the study the average CBF measured was 139 ± 19 ml/100g/min (in five rats). As in the previous approach, this technique was found to be sensitive to $PaCO_2$ changes. Further more, the technique was found able to detect anomalous regional perfusion.

Further research on using inverted arterial water spins as endogenous CBF tracers had focused on accounting for factors which affect the accuracy of the technique. For example, Zhang, Williams, Detre *et al.*,[134] Zhang, Silva *et al.*[135] and Silva, Zhang *et al.*[136] have investigated (and accounted for) the effect of unintentional perturbation of tissue macromolecules in the brain volume.

(ii) Exogenous Studies

The exogenous tracers used in the CBF MR methods can be divided further into MR signal indicators and MR contrast enhancement agents (contrast agents for short). The MR contrast agents can enhance MR image contrast *via* magnetic susceptibility and/or relaxation effects.

(a) CBF Using Exogenous MR Signal Indicators

In most of the MR signal indicator based CBF techniques either ^{2}H labeled water ($^{2}H_2O$ or deuterated water) or ^{19}F labeled compounds have been used. Using deuterated water, Corbett, Laptook and Olivares[137] measured CBF in new born piglets *via* ^{2}H MR spectroscopy (MRS). The 'three step' procedure of this study included:

1. Employing an intracarotid bolus injection of deuterated water
2. Immediately following the injection, obtaining an *in vivo* ^{2}H residue time course MR spectrum
3. Using the ^{2}H rate of clearance of deuterated water to calculate CBF. (The rate was obtained by fitting the residue time course with a two-compartment in-series flow model, with the second compartment representing indicator recirculation)

They found that CBF values determined using this technique were highly reproducible.

In another study, Detre, Subramanian *et al.*[52] measured CBF in cat brain using slow (15 to 20 seconds) bolus ^{2}H MRS and MR imaging (MRI). Their 'three step' procedure consisted of:

1. Performing a 1 ml slow bolus, bilateral intracarotid deuterated saline injection
2. At the completion of the injection, acquiring a time course ^{2}H spectrum for 20 minutes (using a two-turn, 2.5 x 3 cm^2 elliptical surface coil double-tuned to the ^{1}H and ^{2}H resonance frequencies) or a series of 16 images in 4 minutes (using the same surface coil and a gradient-echo pulse sequence with a 0.3 x 0.3 x 1 cm^3 nominal voxel size)
3. In the case of MRS CBF measurements, fitting a biexponential decay curve (representing a fast compartment and a slow compartment to describe the kinetics of the indicator in the brain) model to the time course ^{2}H spectra data (using a least squares fitting method). In the case of CBF with MRI, fitting a monoexponential decay curve (representing a single compartment description of the kinetics of indicator in the brain) model to the time course image intensities at every pixel location

They found that, in the case of CBF with MRS, CBF increased directly with $PaCO_2$ and the values were in good agreement with a number of papers in the

literature. In the case of CBF with MRI, ^{2}H images obtained using a unilateral slow bolus injection differ from bilateral slow bolus injection ^{2}H images in terms of image intensity distribution. Furthermore, the average CBF (for the bilateral slow bolus injection case, averaging over the entire image) at a $PaCO_2$ = 37 mmHg was 70 ml/100g/min and at a $PaCO_2$ = 21 mmHg was 48 ml/100g/min.

In a ^{19}F labeled compound study, Ewing, Branch, Helpern *et al.*[138] measured CBF in cats with ^{19}F MRS, using Freon-22 as an indicator. The 'three step' procedure of this method was as follows:

1. Ventilating the animal with a gas mixture of 50 % O_2, 45 % Freon-22 and 5 % N_2 (for CBF measurement at normocapnia) or a gas mixture of 50 % O_2, 45 % Freon-22 and 5 % CO_2 (for CBF measurement at hypercapnia) for 6 minutes
2. Acquiring a series of ^{19}F MR FIDs (at ~ 12 second interval) during the build-up and clearance of Freon-22 in the brain using a surface coil. At the same time, acquiring a series of ^{19}F FIDs (at the same interval) for the arterial blood (using a 6 turn solenoid coil, with the blood from a femoral artery running through the axis of the solenoid and returning to the animal *via* a femoral vein)
3. Using an arterial input function (arterial time course curve, derived from the arterial blood FIDs) and the brain indicator concentration curve (derived from the brain FIDs) in the Kety equation (with gray

and white matter compartments)[61] to estimate the gray and white matter CBF as well as the Freon-22 gray and white matter partition coefficients. (The estimation employed a maximum likelihood curve fitting technique.)

They found that the fast (gray matter) flow in cats at normocapnia was 50 ± 19 ml/100g/min and at hypercapnia was 83 ± 32 ml/100g/min.

In another ^{19}F labeled compound study using the above technique, Ewing, Branch, Fagan *et al.*[19] measured CBF with ^{19}F MR, using Fluorocarbon-23 (Trifluoromethane, FC-23, or Freon-23), in place of Freon-22 in the previous study. At normocapnia, the measured fast (gray matter) flow was 70 ± 15 ml/100g/min. The FC-23 toxicity was also investigated by the same research group in a separate paper.[54] Two findings of this paper were: (a) FC-23 could be suitable for animal studies and, (b) before FC-23 can be used in humans, its toxicity needs to be studied further.

The technique of using FC-23 as an indicator was later modified to measure CBF with low resolution ^{19}F MRI. In a technical note, Branch, Helpern, Ewing and Welch[139] replaced the brain ^{19}F MR FID acquisitons (of the second step above) with a time series of ^{19}F FLASH (gradient field echo) images. In addition, they replaced the time course ^{19}F MR FIDs of the blood from femoral artery with a doped semiconductor oscillator that detected the FC-23 concentration in expired air. Using an arterial FC-23 time course curve (derived from the end-tidal estimate

of FC-23 in the expired air) and a FC-23 brain clearance curve (obtained from the time course signal intensities of a pixel in the images) in a single compartment Kety equation, they calculated CBF at each pixel location. In this study, the rate of image acquisition was 67.5 seconds per image and the nominal voxel size used was 1 x 1 x 2 cm^3. Typically, 6 to 8 voxels were obtained in a cat brain, giving 6 to 8 regional CBF values ranging from 12 ml/100g/min to 125 ml/100g/min in one rat. In another paper, they applied the same technique[20] to study atraumatic cerebral perfusion in cats.

In a similar manner Pekar, Ligeti *et al.*[125] measured CBF with ^{19}F MRI using CHF_3 as a freely diffusible gas indicator. In this study, ^{19}F brain images were acquired at a rate of 33 seconds each, with a nominal voxel size of 0.7 x 0.7 x 0.8 cm^3. A mass spectrometer (UTI instruments Model 100 C) was used to monitor the time concentration of CHF_3 in the expired air. Two CBF values were obtained for each experiment, one from the build-up of CHF_3 in the brain and the other from the clearance, again using the Kety equation for CBF modeling.

In still another study Van Zijl, Ligeti *et al.*[140] measured CBF using volumetric-selective ^{19}F MRS. A major difference between this method and the above CBF ^{19}F MRS studies was that a STEAM[141] (Stimulated Echo Acquisition Mode) pulse sequence was used for the serial ^{19}F spectral acquisitions of the brain. The STEAM method enabled the selection of a volume in the brain for MRS.

Therefore the method was able to elimination MR signal from the skin and other extra-cranial tissues.

(b) CBF Measurements Using Exogenous MR Contrast Agents

The MR contrast agents used to measure CBF have been mostly non-diffusible (intra-vascular) tracers that do not cross the blood brain barrier (BBB). Quantitative CBF with MR using intra-vascular agents is still in the development stage. Initially, attention was focused on developing a kinetic model that can relate, indirectly, the intravascular transit of the agents to CBF (a tissue perfusion). (Recall that a kinetic model was also needed in most of the CBF SPECT techniques, except that this kinetic model was used to describe the process of tracer metabolic conversion leading to retention, redistribution, etc. of the tracer in the brain.) Because CBF is studied indirectly, the accuracy of quantitative tissue perfusion using the intra-vascular agents is model dependent. (The accuracy depends on the exactness of the model that describes the actual kinetics).[55] In addition, the accuracy is also contrast agent dependent. For example, Gore and Majumdar[142] have shown that superparamagnetic iron oxide particles could be a difficult agent to use as a blood flow marker (because the *in vivo* effectiveness of this indicator is tissues dependent).

More recently, development has focused on using fast MRI sequences to track the intravascular transit of Gd-DTPA dynamically.[55,127,131,143] This allows

one to obtain the intravascular mean transit time (MTT = cerebral blood volume divided by tissue flow and therefore CBF.

(c) CBF Using $^{17}O_2$ or $H_2{}^{17}O$ as Exogenous MR Tracer

^{17}O is a stable isotope of oxygen with intrinsic spin 5/2. ^{17}O in the form of a gas ($^{17}O_2$) or water ($H_2{}^{17}O$) can be used as an MR signal indicator or contrast agent. It can be considered a contrast agent because it can enhance water proton (^1H) T_2 relaxation rates through its scalar-coupled interactions.[120]

Using $H_2{}^{17}O$ as an MR signal indicator, Pekar, Ligeti *et al.*[121] measured CBF for a 0.8 ml voxel in the cat brain using ^{17}O MRI. The 'three step' procedure of this technique was as follows:

1. Performing an arterial bolus injection of $H_2{}^{17}O$ enriched saline (0.15 ml at 35% $H_2{}^{17}O$ *via* the lingual artery)
2. Acquiring an ^{17}O MR image using a surface coil (at a rate of 22 seconds per image)
3. Fitting a monoexponential decay curve to the washout of $H_2{}^{17}O$ to predict CBF. (See Chapter 3 for more details.)

In 5 cats at normocarbia ($PaCO_2$ in the range of 35 to 42 mmHg) the CBF was measured to be 39 ± 12 ml/100g/min.

Using $H_2{}^{17}O$ as a contrast agent, Kwong, Hopkins, Belliveau *et al.*[120] measured CBF in dogs with dynamic ^1H MR imaging. The 'three step' procedure of this study was as follows:

1. Injecting a bolus of 2 to 3 ml of saline or $H_2{}^{17}O$ enriched saline (at 45% $H_2{}^{17}O$) at the external carotid artery, alternately. The ordinary saline injection was used for acquiring sham images
2. Acquiring consecutive ^1H MR images at a rate of one image per every 2 seconds (using an echo planar pulse sequence)
3. To calculate CBF, dividing the cortical region of the images into 1.2 x 1.2 x 1.5 cm^3 voxels, calculating a time curve of relative difference ($\Delta R2(t)$) between tissue T_2 rates with $H_2{}^{17}O$ and tissue T_2 rates with the sham, fitting a monoexponential decay function to the washout phase of the $\Delta R2(t)$ curve to predict voxel CBF (see Chapter 3 for more on CBF using a single compartment model).

They obtained, at normocapnia and hypocapnia, CBF values of 72 ± 1 ml/100g/min and 29 ± 1 ml/100g/min.

It is fair to say that CBF using MR is still in its experimental stage. (For example, many studies were performed in animal.) The successful application of CBF measurement using MR in the clinical environment is pending the establishment of a 'preferred' technique, and quantification of its precision and accuracy.

C. Overview

In summarizing the review, one can see that over the years many indicator based techniques have been developed for quantifying CBF. All of these techniques are based on the 'three step' procedure mentioned previously. In the immediate future, the clinical application of CBF measurements, in all likelihood, will center on the continued utilization of SPECT. This is due to the fact that SPECT is readily accessible and relatively low cost. As for PET, it will always play a significant role due to its unique capabilities of providing simultaneous metabolic and pathophysological information. PET will continue to set the stage for new metabolite and functional applications of emission tomography while SPECT will translate the techniques developed with PET into the clinic.

Contrast in CT images is from attenuation (photoelectric effect and compton scattering) of x-rays by electrons in the subject. Because the underlying principles of image formation are relatively simple a thorough investigation of the usefulness CT in CBF measurement has been possible. MR on the other hand is the most complicated modality that can be used in CBF measurements. Besides the intrinsic variations of signal and contrast on parameters such as T_1, T_2, T_2^*, and pulse sequence used, *etc.*, one also has to consider which MR nucleus to use. Because of this MR can be said to have the greatest potential but still requires a great deal more study.

It is obvious that a lot of effort has been invested into finding out whether or not it is possible to use each of the above mentioned imaging modalities for measuring CBF. In the end, all modalities reviewed have been shown capable of measuring CBF. Nevertheless there still exists a gap between feasibility and clinical applicability for all the modalities. The clinical relevance of CBF measurement can be increased substantially if more attention is given to assessing the accuracy and precision and the strengths and weaknesses of the CBF techniques. It is very difficult to comprehend the usefulness of a CBF method, in relation to patient management, when such aspects remain undetermined. Therefore, one way to enhance the clinical potential of CBF measurement will be to understand the fundamental precision and accuracy achievable with CBF techniques. This thesis will emphasize the development of a CBF measurement technique which can be assessed for precision and accuracy at a very fundamental level.

D. The Development of Deuterium MRS for CBF Measurement

The following is a justification of the major components of the MR based CBF measurement technique developed in this thesis.

1. Selecting the Sampling Method

Recall the two categories of sampling methods: invasive and non-invasive. In this study, a strict requirement was that the sampling technique be non-invasive because our goal is to eventually apply it to humans. Also, it eventually has to

allow for measurement of regional CBF. Recall the non-invasive indicator monitoring methods include: 1. PET, 2. SPECT, 3. CT and 4. MR.

Figure 2.1: ^{2}H MR Image of a Bottle of $^{2}H_{2}O$

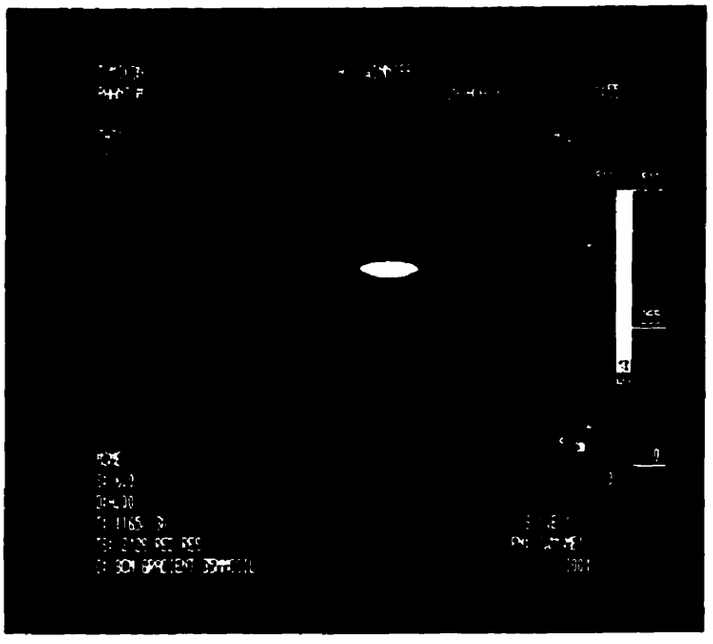

The MR method was selected for the following reasons:

1. MR was the only non-ionizing method among the four
2. PET was not widely available; as such, clinical application of CBF measurement using PET is limited to those major centers having PET facilities
3. The strengths and limitations of the CT technique are well understood. A problem with the CT technique is the amount of

radiation required for acquiring an image. This amount depends on the spatial resolution (image pixel size) and image signal-to-noise ratio (SNR). A higher resolution (smaller pixel size) or a larger SNR image requires a greater amount of radiation. In dynamic CBF techniques the washin and washout of indicator in the brain are monitored continuously and the number of images needed per CBF measurement can be large (for good temporal resolution). Under dynamic CBF measurement condition the application of CT is limited

4. An advantage of SPECT based CBF techniques is the potential connection of CBF measured to physiology. On the other hand the techniques allow less connection of the CBF measured to anatomy. In addition, image acquisition time is longer and indicators used in the CBF measurements are radioactive

MR Spectroscopy was selected over imaging because:

1. It allows better temporal resolution
2. It provides better SNR
3. The data is easier to model and interpret

Eventually spectroscopy based sampling of the indicator will be replaced with imaging, thereby making possible regional CBF measurements. Progress to date in using MRI has consisted of:

1. Acquisition of ^{2}H MR images of a bottle of deuterated water using various pulse sequences. (See Figure 2.1 for an example)
2. With a flow phantom assembly (presented in Figure 2.2), a gradient field echo (GFE) pulse sequence (a FLASH derivative) was used to acquire dynamic ^{1}H MR images of the time course accumulation and dissipation of an indicator. The steps in these experiments were as follows:
    i. Setup a flow of water through the phantom at a rate of 2 to 10 ml/min
    ii. Acquire 12 ^{1}H MR images, 22 seconds apart (image acquisition time was approximately 12 seconds per image)
    iii. After the acquisition of the first image, inject a bolus of $^{2}H_2O$ upstream

Figure 2.3 presents a typical experimental result, where image brightness (a measure of indicator concentration) averaged of all pixels is plotted as a function of time. Evidently the MR signal suppression by $^{2}H_2O$ injection was measurable. Theoretically this washin/washout data can be utilized to predict flow.

Figure 2.2: Phantom Flow Assembly for MR Imaging

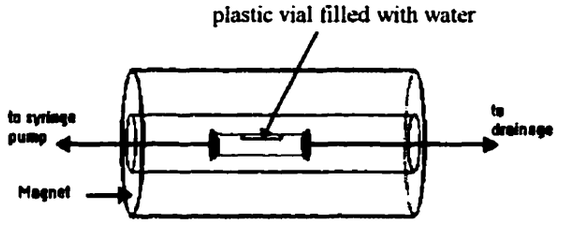

Figure 2.3: Dynamic ^{1}H MR Images (upper) of the Phantom in Figure 2.2 and Image Intensity as a Function of Time (lower).

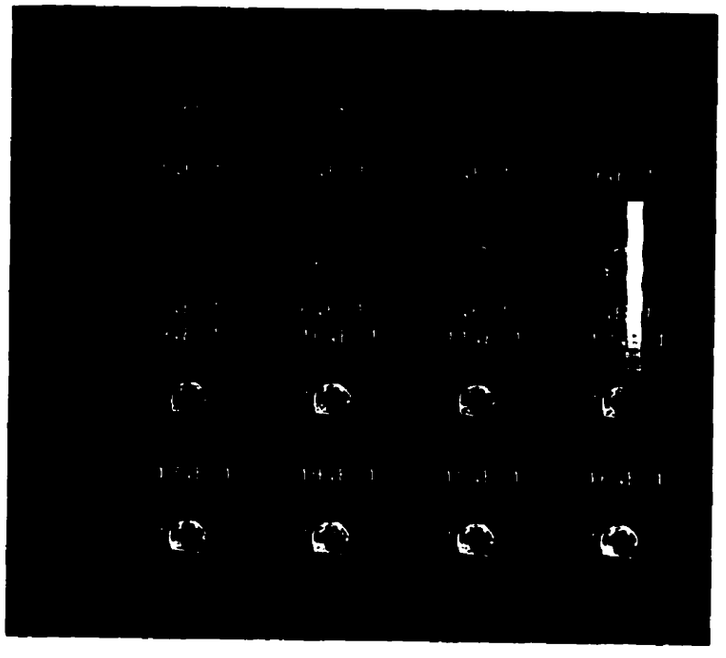

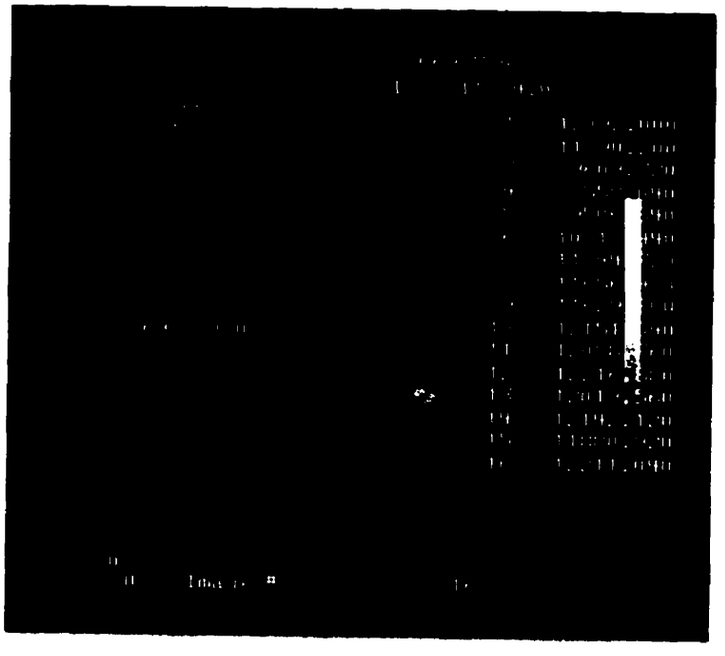

2. Selecting the Indicator

Recall that MR indicators can be classified as endogenous and exogenous. The endogenous indicator involves, for example, labeling the protons of the water in blood. The water protons are labeled magnetically either using adiabatic fast passage[144,145] or other spin saturation methods.[71,116,117,118,132,134,146,147] In the adiabatic fast passage, a constant radio frequency (rf) field is applied to an existing magnetic gradient that is along the direction of flow, usually near the entrance to the brain (ie. internal carotid). When water molecules pass through the rf field, the proton spins are inverted. As the inverted spins enter the brain the MR signal is reduced proportional to the number of inverted spins that enter the tissue. Since the number of inverted spins that enter the tissue is proportional to blood flow, blood flow can be estimated from the MR signal reduction. Others have used a simple method that employs a multi-slice-multi-echo (MSME) sequence with a spoiling rf pulse. In this method only two slices are selected: one at the level of the neck and the other at the brain where perfusion is to be measured. The slice at the neck serves to saturate the spins in water using a 90 degree pulse and a spoiling pulse. As the saturated spins enter the brain, MR signal is reduced (similar to that of the adiabatic fast passage technique).

The use of exogenous indicators involves compounds that possess nuclei with gyromagnetic ratios less than that of the proton's. Some of these indicators include various ^{19}F-labelled[18,19,20,54,123,138,140] and [^{2}H]labelled[52,53] compounds. Also included in the exogenous indicator group are compounds that are

paramagnetic or superparamagnetic[55], such as Gd-DTPA,[125,126] other paramagnetic lanthanide chelates[21,127,129,130,148,149,150,151] and iron oxide particles.[142,152]

a) Indicator Criteria

The indicator selection criteria included:

1. simple mathematical modeling
2. minimal perturbation of the system to be measured
3. good signal to noise

b) Strengths and weaknesses of the endogenous proton indicator

Endogenous indicators are good physiologically but the results are difficult to interpret. The main reason is in the relaxation of the saturated spin as a function of time, which is intricately related to many variables (temperature, flow, molecular electronic environment). On the other hand this type of indicator disturbs the blood flow system the least. In spite of its minimum disturbance to the CBF of the system, the indogenous indicator for CBF measurement can be more complicated to model.

c) Strengths and Weaknesses of the ^{19}F Techniques

The strength of the ^{19}F MR techniques is this large gyromagnetic ratio (γ) of ^{19}F second only to the proton (γ=0.94 of proton).[153] Unfortunately many of the ^{19}F compounds (such as various types of freon) cause physiological disturbances (including changes in blood flow and toxicity effects) in the subject.[54] The ^{19}F MR based CBF method was considered unsuitable for this reason.

d) Strengths and Weaknesses of the Paramagnetic Indicators

Gadolinium-DTPA is routinely employed in clinical imaging as a MR contrast agent. Gadolinium-DTPA is a relaxation agent, which reduces the *in vivo* relaxation time constants T_1 and T_2, with T_1 reduction proportionally greater than T_2. Depending on the kind of pulse sequence employed, the MR signal can either be increased or decreased. The alteration of MR signal provides a means of CBF estimation. In fact, any compound that can enhance T_1 and/or T_2 relaxation constitutes an indicator for the measurement of CBF using MR. For example, Kwong and colleagues have utilized $H_2{}^{17}O$ as MR contrast for CBF measurements[120] because $H_2{}^{17}O$ can selectively reduce T_2. With respect to the goal of the study this type of indicator is unsuitable as modeling the induced T_1 and T_2 relaxation as a function of time is complicated.

e) Strengths and Weaknesses of the ^2H Techniques

The ^2H MR technique has a low signal sensitivity (due to its relatively small gyromagnetic ratio). The relative MR detection sensitivity of ^2H is only 0.00965 or approximately 1%[154] of ^1H. Nevertheless ^2H as water is extremely attractive as a flow indicator, for the obvious reason that deuterated water exists naturally in the body and physically as well as chemically behaves very much like ordinary water. Therefore it will perturb the system to be measured only minimally provided concentrations are kept low enough. By employing a surface coil and MRS (instead of MRI) it is possible to use only a small amount of deuterated

water in the form of a bolus and still achieve the SNR required for estimating CBF. Also, as an indicator, the MR signal properties of the ^2H_2O (or more precisely ^2HOH) indicator does not change over time. (This is not the case with saturated water where the degree of saturation is a decaying function of T_1.) Due to its MR signal stability and chemical simplicity, the use of ^2H_2O as an indicator allows quantitative assessment of the accuracy and precision of the CBF methods at a very fundamental level. For these reasons, ^2H_2O is the indicator of choice for this CBF study.

3. Selecting the Injection Method

The mathematical model used in CBF calculations depends both on the type of indicator employed and on the manner in which it is introduced into the system being measured. The following techniques have been utilized:

1. inhalation[11,23,54,61]
2. intra-tissue injection[155]
3. intra-arterial injection:
    a. intra-carotid[52,105,156]
    b. renal and aortic burification[157]
4. intra-venous injection:
    a. femoral vein[158]
    b. antecubital vein[106]
    c. percutaneous vein[108]

It impressed us that the success or failure of the accuracy and reproducibility assessment of the CBF measurement depended critically on the number of variables introduced into the technique. More variables entail more associated uncertainties that can propagate into the accuracy and reproducibility results obtained, making the assessment less meaningful. In conclusion, ^{2}H MRS using deuterated water as indicator and injecting the indicator instantaneously into the brain of the subject is the most suitable procedure for the proposed investigation. However, this injection site can result in damage to the brain. Instead, an instantaneous internal carotid artery bolus injection technique was developed (see Chapter 4 for details), the site being as close as physically possible to the brain without actually injecting into brain tissues. Constant infusion was not utilized so as to minimize indicator recirculation and prolonged system perturbations.

Note that the injection method is invasive. At this stage an invasive injection method is acceptable, for the goal of the study is to examine some of the fundamentals of indicator based blood flow methods. It is therefore recognize that, if the technique is to be applied to humans, then the injection site will have to be moved to a peripheral blood vessel.

4. Selecting the Mathematical Model

The mathematical models for the CBF measurements were pre-determined by the sampling and indicator injection methods chosen. Chapter 3 discusses in detail

the models used. Briefly, the mathematical models utilized are applications of the so-called stimulus – response theorem. These applications of the theorem, under the assumption of instantaneous intra-arterial bolus injection enable simultaneous measurements of the so-called fast CBF and average CBF. (See Chapter 5 for details.)

Reference

[1] Frackowiak R, Lenzi G, Jones T and Heather J, 'Quantitative Measurement of Regional Cerebral Blood Flow and Oxygen Metabolism in Man Using ^{15}O and Positron Emission Tomography: Theory, Procedure and Normal Values', *J.Comput.Assist.Tomogr.* 4(6):727-736, 1980.

[2] Huang S, Carson R, Hoffman E, Carson J, MacDonala N, Barrio J and Phelps M, 'Quantitative Measurement of Local Cerebral Blood Flow in Humans by Positron Computed Tomography and ^{15}O-Water', *Journal of Cerebral Blood Flow and Metabolism* 3(2):141-153, 1983.

[3] Kety S and Schmidt C, 'The Determination of Cerebral Blood Flow in Man by the Use of Nitrous Oxide in Low Concentrations' *Am.J.Physiol.*, 143:53-56, 1945.

[4] Kety S and Schmidt C, 'The Nitrous Oxide Method for the Quantitative Determination of Cerebral Blood Flow in Man: Theory, Procedure and Normal Values', *J.Clin.Invest.* 27:476-483, 1948.

[5] Sako K, Diksic M, Kato A, *et al.*, 'Evaluation of ^{18}F-4-Fluoroantipyrine as a New Blood Flow Tracer for Multiradionuclide Autoradiography', *Journal of Cerebral Blood Flow and Metabolism* 4:259-263, 1984.

[6] Lassen N and Klee A, 'Cerebral Blood Flow Determined by Saturation and Desaturation with $^{85}Krypton$: An Evaluation of the Validity of the Inert Gas Method of Kety and Schmidt', *Circulation Research* 16:26-32, 1965.

[7] Obrist W, Thompson H, Wang H and Wilkinson W, 'Regional Cerebral Blood Flow Estimated by $^{133}Xenon$ Inhalation', *Stroke* 6:245-256, 1975.

[8] Aukland K, Bower B and Berliner R, 'Meauremenet of Local Blood Flow with Hydrogen Gas', *Circulation Research* 14:164-187, 1964.

[9] Landau W, Freygang W, Rowland L *et al.*, 'The Local Circulation of the Living Brain: Values in the Unanesthetized and Anesthetized Cat', *Trans.Am.Neurol.Assoc.* 80:125-129, 1955.

[10] Sakurada O, Kennedy C, Jehle J, *et al.*, 'Measurement of Local Cerebral Blood Flow with Iodo[^{14}C] Antipyrine', *Am.J.Physiol.* 234:H59-H66, 1978.

[11] Meyer J, Hayman L, Yamamoto M, *et al.*, 'Local Cerebral Blood Flow Measured by CT after Stable Xenon Inhalation', *A.J.R.* 135:239-251, 1980.

[12] Lammertsma A, Frackowiak R, Hoffman J, *et al.*, 'The $C^{15}O_2$ Build-up Technique to Measure Regional Cerebral Blood FLow and Volume of Distribution of Water', *Journal of Cerebral Blood Flow and Metabolism* 9:461-470, 1989.

[13] Winchell H, Baldwin R and Lin T, 'Development of I-123 Label Amines for Brain Studies: Localization of I-123 Iodophenylalkyl Amines in Rat Brain', *J.Nucl.Med.* 21:940-947, 1980.

[14] Kund H, Tramposch K and Blau M, 'A New Brain Perfusion Imaging Agent: [123-I] HIPDM:N,N,N'-trimethyl-N'-[2-hydroxyl-3-methyl-5-benzyl]1,3-propanediamine', *J.Nucl.Med.* 24:66-72, 1983.

[15] Lassen N and Blasberg R (editors), *Journal of Cerebral Blood Flow and Metabolism* 8(S 1):S1-S126, 1988.

[16] Walovitch R, Hill T, Garrity S, *et al.*, 'Characterization of Technetium-99m-L,L-ECD for Brain Perfusion Imaging. Part 1: Pharmacology of Technetium-99m ECD in Nonhuman Primates', *J.Nucl.Med.* 30:1892-1901, 1989.

[17] St Lawrence K, Lee T, Yeung W and Henderson S, 'Diffusion Limitation of Deuterium Oxide in the Measurement of Cerebral Blood Flow', *COMP Conference 1993 proceedings*, Ottawa, 1993.

[18] Barranco D, Sutton L, Florin S, *et al.*, 'Use of ^{19}F NMR Spectroscopy for Measurement of Cerebral Blood Flow: A comparative Study Using Microspheres', *Journal of Cerebrel Blood Flow and Metabolism* 9:886-891, 1989.

[19] Ewing J, Branch C, Fagan S, *et al.*, 'Fluorocarbon-23 Measure of Cat Cerebral Blood Flow by Nuclear Magnetic Resonance', *Stroke* 21(1):100-106, 1990.

[20] Branch C, Ewing J, Helpern J, *et al.*, 'Atraumatic quantitation of cerebral perfusion in cats by ^{19}F magnetic resonance imaging', *Magn.Reson.Med.* 28(1):39-53, 1992.

[21] Rudin M and Sauter A, 'Noninvasive Determination of Regional Cerebral Blood Flow in Rats Using Dynamic Imaging with Gd(DTPA)', *Magnet.Reson.Med.* 22:32-46, 1991.

[22] Todd N, Picozzi P and Crockard H, 'Quantitative Measurement of Cerebral Blood Flow and Cerebral Blood Volume After Cerebral Ischaemia', *Journal of Cerebral Blood Flow and Metabolism* 6:338-341, 1986.

[23] Dirnagl U, 'Cerebral Ischemia: the Microcirculation as Trigger and Target', *Progress in Brain Research* 96:49-65, 1993.

[24] Tamura A, Graham D, McCulloch J and Teasdale G, 'Focal Cerebral Ischaemia in the Rat: 2. Regional Cerebral Blood Flow Determined by ^{14}C Iodoantipyrine Autoradiography Following Middle Cerebral Artery Occlusion', *Journal Cerebral Blood Flow and Metabolism* 4:259-263, 1984.

[25] Mohamed A, McCulloch J, Mendelow A, *et al.*, 'Effect of the Calcium Antagonist Nimodipine on Local Cerebral Blood Flow: Relationship to Arterial Blood Pressure', *Journal of Cerebral Blood Flow and Metabolism* 4:206-211, 1984.

[26] R. von Kummer, F. von Kries and Herold S, 'Hydrogen Clearance Method for Determining Local Cerebral Blood Flow. II. Effect of Heterogeneity in Cerebral Blood Flow', *Journal of Cerebral Blood Flow and Metabolism* 6:492-498, 1986.

[27] Andersen A, '^{99m}Tc-D,L-hexamethylene-propyleneamine oxime (^{99m}Tc-HMPAO): Basic Kinetic Studies of a Tracer of Cerebral Blood Flow' *Cerebrovasc.Brain.Metab.Rev.* 1(4):288-318, 1989.

[28] Nedd K, Sfakianakis G, Ganz W, *et al.*, '^{99m}Tc-HMPAO SPECT of the Brain in Mild to Moderate Traumatic Brain Injury Patients: Compared with CT—a Prospective Study', *Brain.Inj.* 7(6):469-479, 1993.

[29] Neirinckx R, 'Evaluation of Regional Cerebral Blood Flow with ^{99m}Tc-d, 1 HM-PAO and SPECT', *Neurosurg.Rev.* 10(3):181-184, 1987.

[30] Friberg L Andersen A, Lassen N, *et al.*, 'Retention of ^{99m}Tc-Bicisate in the Human Brain after Intracarotid Injection', *Journal of Cerebral Blood Flow and Metabolism* 14(S 1):S19-S27, 1994.

[31] Tsuchida T, Nishizawa S, Yonekura Y, *et al.*, 'SPECT Images of Technetium-99m-ethyl Cysteinate Dimer in Cerebrovascular Diseases: Comparison with other Cerebral Perfusion Tracers and PET', *J.Nucl.Med.* 35(1):27-31, 1994.

[32] Miletich R, Quarantelli M, Di-Chiro G, 'Regional Cerebral Blood Flow Imaging with ^{99m}Tc-Bicisate SPECT in Asymmetric Parkinson's Disease: Studies with and Without Chronic Drug Therapy' *Journal Cerebral Blood Flow and Metabolism* Jan. 14 (S 1):S106-S114, 1994.

[33] Markus HS, Bunker CB, Kouris K, Costa DC and Harrison-MJ, 'rCBF Abnormalities Detected, and Sequentially Followed, by SPECT in Neuro-Behcet's Syndrome with Normal CT and MRI Imaging', *J.Neurol.* 239(7):363-366, 1992.

[34] Mountz JM, Deutsch G and Khan SH, 'Regional Cerebral Blood Flow Changes in Stroke Imaged by Tc-99m HMPAO SPECT with Corresponding Anatomic Image Comparison', *Clin.Nucl.Med.* 18(12):1067-1082, 1993.

[35] O'Leary D, Hill T, Lee R, Clouse M and Holman B, 'The use of ^{123}I-Iodoamphetamine and Single Photon Emission Computed Tomography to Assess Local Cerebral Blood Flow', *AJNR.* 4(3):547-549, 1983.

[36] Jibiki I, Maeda T, Kubota T and Yamaguchi N, '^{123}I-IMP SPECT Brain Imaging in Epileptic Psychosis: a Study of Two Cases of Temporal Lobe Epilepsy with Schizophrenia-Like Syndrome' *Neuropsychobiology*, 28(4):207-211, 1993.

[37] Jibiki I, Kido H, Yamaguchi N, *et al.*, 'Probable Cerebellar Abnormality on N-isopropyl-(iodine-123)-p-iodoamphetamine Single Photon Emission Computed Tomography Scans in an Epileptic Patient Receiving Long-Term High-Dose Phenytoin Therapy', *Neuropsychobiology* 27(4):204-209, 1993.

[38] Suzuki M, Yuasa S, Minabe Y, *et al.*, 'Left Superior Temporal Blood Flow Increases in Schizophrenic and Schizophreniform Patients with Auditory Hallucination: a Longitudinal Case Study Using ^{123}I-IMP SPECT', *Eur.Arch.Psychiatry.Clin.Neurosci.* 242(5):257-261, 1993.

[39] Jibiki I, Matsuda H, Kido H, 'Quantitative Assessment of Regional Cerebral Blood Flow with ^{123}I-IMP in Normal Adult Subjects', *Acta.Neurol.Napoli.* 15(1):7-15, 1993.

[40] Takeshita G, Toyama H, Nakane K, *et al.*, 'Quantitative Measurement of Regional Cerebral Blood Flow with I-123 IMP SPECT: a Correction of the Microsphere Model by Global Extraction between Artery and Internal Jugular Vein', *Ann.Nucl.Med.* 5(4):145-148, 1991.

[41] Broich K, Alavi A, Kushner M, 'Positron Emission Tomography in Cerebrovascular Disorders', *Semin.Nucl.Med.* 22(4):224-232, 1992.

[42] Gardner S, Green J, Bednarczyk E, *et al.*, 'Principles and Clinical Applications of Positron Emission Tomography', *Am.J.Hosp.Pharm.* 49(6):1499-1506, 1992.

[43] Tuohimaa P, Aantaa E, Toukoniitty K and Makela P, 'Studies of Vestibular Cortical Areas with Short-Living $^{15}O_2$ Isotopes', *ORL.J.Otorhinolaryngol.Relat.Spec.* 45(6):315-321, 1983.

[44] Jamieson D, Alavi A, Jolles P, *et al.*, 'Positron Emission Tomography in the Investigation of Central Nervous System Disorders', *Radiol.Clin.North.Am.* 26(5):1075-1088, 1988.

[45] Herscovitch P and Raichle M, 'Effect of Tissue Heterogeneity on the Measurement of Cerebral Blood Flow with the Equilibrium $C^{15}O_2$ Inhalation Technique', *Journal of Cerebral Blood Flow and Metabolism* 3(4):407-415, 1983.

[46] Herscovitch P, Markham J and Raichle M, 'Brain Blood Flow Measured with Intravenous $H_2{}^{15}O$. I. Theory and Error Analysis', *J.Nucl.Med.* 24(9):782-789, 1983.

[47] Takahashi N, Kikuchi H and Karasawa J, 'Dynamic CT in Patients with Superficial Temporal-Middle Cerebral Artery Anastomosis', *AJNR* 4(3):454-457, 1983.

[48] Johnson D, Stringer W, Marks M, *et al.*, 'Stable Xenon CT Cerebral Blood Flow Imaging: Rationale for and Role in Clinical Decision Making', *AJNR* 12(2):201-213, 1991.

[49] Bidabe A, Gense-de-Beaufort D, Gin A and Caille J, 'Measurement of Cerebral Blood Flow by the Stable Xenon Computerized Tomography Method', *J.Neuroradiol.* 17(2):103-124, 1990.

[50] Gur D, Yonas H and Good W, 'Local Cerebral Blood Flow by Xenon-Enhanced CT: Current Status, Potential Improvements, and Future Directions', *Cerebrovasc.Brain.Metab.Rev.* 1(1):68-86, 1989.

[51] Gur D, Wolfson S, Jr., Yonas H, *et al.*, 'Progress in Cerebrovascular Disease: Local Cerebral Blood Flow by Xenon Enhanced CT', *Stroke* 13(6):750-758, 1982.

[52] Detre J, Subramanian V, Mitchell M, *et al.*, 'Communication. Measurement of Regional Cerebral Blood Flow in Cat Brain using Intracarotid ^2H_2O and ^2H NMR Imaging', *Mag.Res.Med.* 14:389-395, 1990.

[53] Kim S. and Ackerman J, 'Quantification of Regional Blood Flow by Monitoring of Exogenous Tracer *Via* Nuclear Magnetic Resonance Spectroscopy', *Magn.Reson.Med.* 14:226-282, 1990.

[54] Branch C, Ewing J, Fagan S, *et al.*, 'Acute Toxicity of a Nuclear Magnetic Resonance Cerebral Blood Flow Indicator in Cat', *Stroke* 21(8):1172-1177, 1990.

[55] Rosen B, Belliveau J, Vevea J and Brady T, 'Perfusion Imaging with NMR Contrast Agents', *Magn.Reson.Med.* 14:249-265, 1990.

[56] Evelhoch J, Larcombe McDouall J, *et al.*, 'Measurement of Relative Regional Tumor Blood Flow in Mice by Deuterium NMR Imaging', *Magn.Reson.Med.* 24:42-52, 1992.

[57] Reivich M, Jehle J, Sokoloff L and Kety S, 'Measurement of Regional Cerebral Blood Flow with 14C-Antipyrine in Awake Cats', *J.Appl.Physiol.* 27:296-300, 1969.

[58] Rapin J, Monique Le Poncin-Lafitte, Duterte D, *et al.*, 'Iodoamphetamine as a New Tracer for Local Cerebral Blood Flow in the Rat: Comparison with Isopropyliodoamphetamine', *Journal of Cerebral Blood Flow and Metabolism* 4:270-274, 1984.

[59] Allen KL, Busza AL, Proctor E, *et al.*, 'Controllable Graded Cerebral Ischaemia in the Gerbil: Studies of Cerebral Blood Flow and Energy Metabolism by Hydrogen Clearance and 31P NMR Spectroscopy', *NMR-Biomed.* 6(3):181-186, 1993.

[60] Fujibayashi T, Sugiura Y, Yanagimoto-M, *et al.*, 'Brain Energy Metabolism and Blood Flow During Sevoflurane and Halothane Anesthesia: Effects of Hypocapnia and Blood Pressure Fluctuations', *Acta.Anaesthesiol.Scand.* 37(8) pp. 806-10, 1993. Corrected and republished: *Acta.Anaesthesiol.Scand.* 38(4):413-418, 1994.

[61] Kety SS, 'The Theory and Applications of The Exchange of Inert Gas at The Lungs and Tissues', *Pharm.Rev.* 3(1):1-41, 1951.

[62] Webster E, *et al.*, 'AAPM Report No. 18: A Primer on Low-Level Ionizing Radiation and Its Biological Effects', *AIP*, New York, 1986.

[63] Meyer JS, Hayman LA, Takahira A, *et al.*, 'Mapping Local Blood Flow of Human Brain by CT Scanning During Stable Xenon Inhalation', *Stroke* 12:426-436, 1981.

[64] Yonas H, Grundy B, Gur D, *et al.*, 'Side Effects of Xenon Inhalation', *J.Comput.Assist.Tomogr.* 5(4):591-592, 1981.

[65] Haughton VM, Donegan JH, Walsh PR, *et al.*, 'A Clinical Evaluation of Xenon Enhancement for Computed Tomography', *Invest.Radiol.* 15:160-163, 1980.

[66] Sakai F, Gotoh F, Ebihara S, *et al.*, 'Xenon Enhanced CT Method for The Measurement of Local Cerebral Blood Flow in Man', *Journal of Cerebral Blood Flow and Metabolism* 1:29-30, 1981.

[67] Ono H, Ono K and Mori K, 'Mapping of CBF Distribution by Dynamic Xe-Enhanced CT Scan Method', *Journal of Cerebral Blood Flow and Metabolism* 1:50-51, 1981.

[68] Good WF and Gur D, 'The Effect of Computed Tomography Noise and Tissue Heterogeneity on Cerebral Blood Flow Determination by Xenon-Enhanced Computed Tomography', *Med.Phys.* 14(4):557-561, 1987.

[69] Wyper D, 'Functional Neuroimaging with Single Photon Emission Computed Tomography (SPECT)', *Cerebrovasc.Brain.Metab.Rev.* 5(3):199-217, 1993.

[70] Greenberg J and Lassen N (editors): *Journal of Cerebral Blood Flow and Metabolism* 14(S 1):S1-S120, 1994.

[71] Drayer B, Jaszczak R, Friedman A, *et al.*, '*In Vivo* Quantitation of Regional Cerebral Blood Flow in Glioma and Cerebral Infarction: Validation of the HIPDM-SPECT Method', *AJNR* 4(3):572-576, 1983.

[72] Neirinckx RD, Canning LR, Piper IM, *et al.*, 'TC-99m d,l-HM-PAO: A New Radiopharmaceutical for SPECT Imaging of Regional Cerebral Blood Perfusion', *J.Nucl.Med.* 28:191-202, 1987.

[73] Greenberg JH and Lassen NA, 'Introduction. Characterization of ^{99m}Tc-Bicisate as an Agent for the Measurement of Cerebral Blood Flow With SPECT', *Journal of Cerebral Blood Flow and Metabolism* 14(S):S1-S3, 1994.

[74] Leveille J, Demonceau G, De Roo M, *et al.*, 'Characterization of Technetium-99m-L, L-ECD for Brain Perfusion Imaging, Part 2: Biodistribution and Brain Imagng in Humans', *J.Nucl.Med.* 30:1902-1910, 1989.

[75] Pupi A, De Cristofaro MTR, Passeri, *et al.*, 'Quantitation of Brain Perfusion with ^{99m}Tc-Bicisate and Single SPECT Scan: Comparison with Microsphere Measurements', *Journal of Cerebral Blood Flow and Metabolism* 14(S 1):S28-S35, 1994.

[76] Huglo D, Rousseaux M, Leys D, *et al.*, 'Regional Cerebral Blood Flow Imaging: A Quantitative Comparison of ^{99m}Tc-Bicisate with ^{133}Xe Using Single Photon Emission Computed Tomography', *Journal of Cerebral Blood Flow and Metabolism* 14(S 1):S76-S83, 1994.

[77] Inugami A, Kanno I, Uemura K, *et al.*, 'Linearization Correction of ^{99m}Tc-Labeled Hexamethyl-Propylene Amine Oxime (HM-PAO) Image in Terms of Regional CBF Distribution: Comparison to $C^{15}O_2$ Inhalation Steady-State Method Measured by Positron Emission Tomography', *Journal of Cerebral Blood Flow and Metabolism* 8(S):S52-S60, 1988.

[78] Lassen NA, Andersen AR, Neirinckx RD, *et al.*, in *rCBF Atlas—The Clinical Application of rCBF Imaging by SPECT*, Ell PJ, Costa DC, Cullum ID, et al. edited, Brier Press, High Wycombe, pp 14-18, 1987.

[79] Yonekura Y, Nishizawa S, Mukai T, *et al.*, 'SPECT with [^{99m}Tc]-d,l-Hexamethyl-Propylene Amine Oxime (HM-PAO) Compared with Regional Cerebral Blood Flow Measured by PET: Effects of Linearization', *Journal of Cerebral Blood Flow and Metabolism* 8(S):S82-S89, 1988.

[80] Langen KJ, Herzog H, Kuwert T, *et al.*, 'Tomographic Studies of rCBF with [^{99m}Tc]-HM-PAO SPECT in Patients with Brain Tumors: Comparison with $C^{15}O_2$ Continuous Inhalation Technique and PET', *Journal of Cerebral Blood Flow and Metabolism* 8(S):S90-S94, 1988.

[81] Andersen AR, Friberg HH, Schmidt JF and Hasselbalch SG, 'Quantitative Measurements of Cerebral Blood Flow Using SPECT and [^{99m}Tc]-d,l-HM-PAO Compared to Xenon-133', *Journal of Cerebral Blood Flow and Metabolism* 8(S):S69-S81, 1988.

[82] Yonekura Y, Tsuchida T, Sadato N, *et al.*, 'Brain Perfusion SPECT with ^{99m}Tc-Bicisate: Comparison with PET Measurement and Linearization Based on Permeability-Surface Area Product Model', *Journal of Cerebral Blood Flow and Metabolism* 14(S 1):S58-S65, 1994.

[83] Kanno I and Lassen NA, 'Two Methods for Calculating Regional Cerebral Blood Flow from Emission Tomography of Inert Gas Concentrations', *J.Comput.Assist.Tomogr.* 3:71-76, 1979.

[84] Lassen NA, Henriksen L and Paulson O, 'Regional Cerebral Blood Flow in Stroke by ^{133}Xe Inhalation and Emission Tomography', *Stroke* 12:284-287, 1981.

[85] Matsuda H, Oba H, Seki H, *et al.*, 'Determination of Flow and Rate Constants in a Kinetic Model of [^{99m}Tc]-Hexamethyl-Propylene Amine Oxime in the Human Brain', *Journal of Cerebral Blood Flow and Metabolism* 8(S):S61-S68, 1988.

[86] Creutzig H, Schober O, Gielow P, *et al.*, 'Cerebral Dynamics of N-Isopropyl-(^{123}I)p-Iodoamphetamine', *J.Nucl.Med.* 27:178-183, 1986.

[87] Nishizawa S, Tanada S, Yonekura Y, *et al.*, 'Regional Dynamics of N-Isopropyl-(^{123}I)p-Iodoamphetamine in Human Brain', *J.Nucl.Med.* 30:150-156, 1989.

[88] Greenberg JH, Kushner M, Rango M, *et al.*, 'Validation Studies of Iodine-123-Iodoamphetamine as a Cerebral Blood Flow Tracer Using Emission Tomography', *J.Nucl.Med.* 31:1364-1369, 1990.

[89] Matsuda H, Higashi S and Tsuji S, 'A New Noninvasive Quantitative Assessment of Cerebral Blood Flow Using N-Isopropy-(Iodine 123)p-Iodoamphetime', *Am.J.Physiol.Imaging* 2:49-55,1987.

[90] Takeshita G, Maeda H, Nakane K, *et al.*, 'Quantitative Measurement of Regional Cerebral Blood Flow Using N-Isopropyl-(Iodine-123)p-Iodoamphetamine and Single-Photon Emission Computed Tomography', *J.Nucl.Med.* 33:1741-1749, 1992.

[91] Lassen NA and Blasberg RG, 'Technetium-99m-d,l-HM-PAO, The Development of a New Class of ^{99m}Tc-Labeled Tracers: An Overview', *Journal of Cerebral Blood Flow and Metabolism* 8(S):S1-S3, 1988.

[92] Nishizawa S, Tanada S, Yonekura Y, Fujita T, Senda M, *et al.*, 'Clinical Value of Regional Cerebral Perfusion Scan with I-123 Labeled Amphetamine in Brain Tumors', *Journal of Cerebral Blood Flow and Metabolism* 7(S 1):S555, 1987.

[93] Tanada S, Yonekura Y, Senda M, *et al.*, 'Regional Distribution of N-Isopropyl-p-(I-123)Iodo-Amphetamine in Cerebrovascular Disease Compared wtih Regional Cerebral Blood Flow and Oxygen Metabolism', *Journal of Cerebral Blood Flow and Metabolism* 5(S 1):S563-S564.

[94] Murase K, Tanada S, Mogami H, *et al.*, 'Validity of Microsphere Model in Cerebral Blood Flow Measurement Using N-isopropyl-p-(I-123) Iodoamphetamine', *Med.Phys.* 17:79-83, 1990.

[95] Yokoi T, Iida H, Itoh H, *et al.*, 'A New Graphic Plot Analysis for Cerebral Blood Flow and Partition Coefficient with Iodine-123-Iodoamphetamine and Dynamice SPECT Validation Studies Using Oxygen-15-Water and PET', *J.Nucl.Med.* 34:498-505, 1993.

[96] Odano I, Ohkubo M, Takahashi N and Higuchi T, 'A New Method of Regional Cerebral Blood Flow Measurement Using One-Point Arterial Sampling Based on the Microsphere Model with N-isopropyl-p-[123I]-Iodoamphetamine SPECT', *Nucl.Med.Commun.* 15(7):560-564, 1994.

[97] Iida H, Nakazawa M and Uemura K, 'Quantitation of Regional Cerebral Blood Flow Using ^{123}I-IMP From a Single SPECT Scan and a Single Blood Sampling--Analysis on Statistical Error Source and Optimal Scan Time', *Kaku-Igaku.* 32(3):263-270, 1995.

[98] Ohkubo M, Odano I, Takahashi-M, *et al.*, 'Validation Study in Quantitative Measurement of Regional Cerebral Blood Flow Using N-Isopropyl-p-[^{123}I]Iodoamphetamine (123I-IMP) and SPECT', *Kaku-Igaku.* 33(6):647-654, 1996.

[99] Jones SC, Greenberg JH and Reivich M, 'Error Analysis for the Determination of Cerebral Blood Flow with the Continuous Inhalation of ^{15}O-labeled Carbon Dioxide and Positron Emission Tomography', *J.Comput.Assist.Tomogr.* 6(1):116-124, 1982.

[100] Ito M, Lammertsma AA, Wise RJS, *et al.*, 'Measurement of Regional Cerebral Blood Flow and Oxgyen Utilisation in Patients with Cerebral Tumours Using ^{15}O and Positron Emission Tomography: Analytical Techniques and Preliminary Results', *Neuroradiology* 23:63-74, 1982.

[101] Nelson AD, Miraldi F, Muzic-RF Jr; Leisure-GP and Semple WE, 'Noninvasive Arterial Monitor for Quantitative Oxygen-15-Water Blood Flow Studies', *J.Nucl.Med.* 34(6):1000-1006, 1993.

[102] Kanno I, Lida H, Miura S, *et al.*, 'Optimal Scan Time of Oxygen-15-Labeled Water Injection Method for Measurement of Cerebral Blood Flow', *J.Nucl.Med.* 32(10):1931-1934, 1991.

[103] Yokoi T, Kanno I, Iida H, *et al.*, 'A new Approach of Weighted Integration Technique Based on Accumulated Images Using Dynamic PET and $H_2{}^{15}O$', *Journal of Cerebral Blood Flow and Metabolism* 11(3):492-501, 1991.

[104] Gambhir SS, Huang SC, Hawkins RA, *et al.*, 'A Study of the Single Compartment Tracer Kinetic Model for the Measurement of Local Cerebral Blood Flow using 15O-Water and Positron Emission Tomorgraphy', *Journal of Cerebral Blood Flow and Metabolism* 7:15-20, 1987.

[105] Herscovitch P, Raichle ME, Kilbourn MR and Welch MJ, 'Positron Emission Tomographic Measurement of Cerebral Blood Flow and Permeability—Surface Area Product of Water Using [^{15}O]Water and [^{11}C]Butanol', *Journal of Cerebral Blood Flow and Metabolism* 7:527-543, 1987.

[106] Jones SC, Greenberg JH, Dann R, *et al.*, 'Cerebral Blood Flow with Continuous Infusion of Oxygen-15-Labeled Water', *Journal of Cerebral Blood Flow and Metabolism* 5:566-575, 1985.

[107] Fox PT, Mintun MA, Raichle ME and Herscovitch P, 'A Noninvasive Approach to Quantitative Functional Brain Mapping with $H_2{}^{15}O$ and Positron Emission Tomography', *Journal of Cerebral Blood Flow and Metabolism* 4(3):329-333, 1984.

[108] Raichle ME, Martin WRW, Herscovitch P, *et al.*, 'Brain Blood Flow Measured with Intravenous $H_2{}^{15}O$. II. Implementation and Validation', *J.Nucl.Med.* 24:790-798, 1983.

[109] West JB and Dollery CT, 'Uptake of oxygen-15 labeled CO_2 compared with carbon-11 labeled CO_2 in the lung', *J.Appl.Physiol.* 17:9-13, 1962.

[110] Kety SS, 'Human Cerebral Blood Flow and Oxygen Consumption as Related to Aging', *Res.Publ.Assoc.Res.Nerv.Ment.Dis.* 35:31-45,1965.

[111] Lassen NA, 'Cerebral Blood Flow and Oxygen Consumption in Man', *Physiol.Rev.* 39:183-238, 1959.

[112] Lammertsma AA, Jones T, Frackowiak RSJ and Lenzi GL, 'A Theoretical Study of the Steady State Technique for Measuring Regional Cerebral Blood Flow and Oxygen Utilization Using Oxygen-15', *J.Comput.Assist.Tomogr.* 5:544-550, 1981.

[113] Rhodes CG, Lenzi GL, Frackowiak RSJ, *et al.*, 'Measurement of CBF and $CMRO_2$ Using the Continuous Inhalation of $C^{15}O_2$ and $^{15}O_2$-Experimental Validation Using CO_2 Reactivity in the Anaethetized Dog', *J.Neurol.Sci.* 50:381-389, 1981.

[114] Subramanyam R, Alpert NM, Hoop B, *et al.*, 'A Model for Regional Cerebral Oxygen Distribution During Continuous Inhalation of $^{15}O_2$, $C^{15}O$, and $C^{15}O_2$', *J.Nucl.Med.* 19:48-53.

[115] Berridge MS, Adler LP, Nelson AD, *et al.*, 'Measurement of Human Cerebral Blood Flow with [^{15}O]Butanol and Positron Emission Tomography', *Journal of Cerebral Blood Flow and Metabolism* 11:707-715, 1991.

[116] Williams DS, Detre JA, Leigh JS and Koretsky AP, 'Magnetic Resonance Imaging of Perfusion Using Spin Inversion of Arterial Water', *Proc.Nat.Acad.Sci-U.S.A.* 89(1):212-216, 1992.

[117] Walsh EG, Minematsu K, Leppo J and Moor SC: 'Radioactive Microsphere Validation of a Volume Localized Continuous Saturation Perfusion Measurement', *Magn.Reson.Med.* 31(2):147-153, 1994.

[118] Kim SG, 'Quantification of Relative Cerebral Blood Flow Change by Flow-Sensitive Alternating Inversion Recovery (FAIR) Technique: Application to Functional Mapping', *Magn.Reson.Med.* 34(3):293-301, 1995.

[119] Pekar J, Jezzard P, Roberts DA, *et al.*, 'Perfusion Imaging with Compensation for Asymmetric Magnetization Transfer Effects', *Magn.Reson.Med.* 35(1):70-79, 1996.

[120] Kwong KK, Hopkins AL, Belliveau JW *et al.*, 'Communications. Proton NMR Imaging of Cerebral Blood Flow Using $H_2{}^{17}O$', *Magn.Reson.Med.* 22:154-158, 1991.

[121] Pekar J, Ligeti L, Ruttner Z *et al.*, '*In Vivo* Measurement of Cerebral Oxygen Consumption and Blood Flow Using ^{17}O Magnetic Resonance Imaging', *Magn.Reson.Med.* 21(2):313-319, 1991.

[122] Arai T, Mori K, Nakao, *et al.*, '*In Vivo* Oxygen-17 Nuclear Magnetic Resonance for the Estimation of Cerebral Blood Flow and Oxygen Consumption', *Biochem.Biophys.Res.Commun.* 179(2):954-961, 1991.

[123] Fiat D and Kang S, 'Determination of the Rate of Cerebral Oxygen Consumption and Regional Cerebral Blood Flow by Non-Invasive ^{17}O *In Vivo* NMR Spectroscopy and Magnetic Resonance Imaging. Part 2. Determination of $CMRO_2$ for the rat by ^{17}O NMR, and $CMRO_2$, rCBF and

the Partition Coefficient for the Cat by ^{17}O MRI', *Neurol.Res.* 15(1):7-22, 1993.

[124] Ligeti L, Pekar J, Ruttner Z and McLaughlin AC, 'Determination of Cerebral Blood Oxygen Consumption and Blood Flow by Magnetic Resonance Imaging', *Acta.Biomed.Ateneo.Parmense.* 66(3-4):67-74, 1995.

[125] Pekar J, Ligeti L, Sinnwell T, *et al.*, '^{19}F Magnetic Resonance Imaging of Cerebral Blood Flow with 0.4-cc Resolution', *Journal of Cerebral Blood Flow and Metabolism* 14(4):656-663, 1994.

[126] Houkin K, Kamiyama H, Iwasaki Y, *et al.*, 'Evaluation of Cerebral Blood Circulation Using Fast Magnetic Resonance Imaging (Turbo-FLASH)', *No.Shinkei.Geka.* 20(11):1155-1160, 1992.

[127] Wittlich F, Kohno K, Mies G, *et al.*, 'Quantitative Measurement of Regional Blood Flow with Gadolinium Diethylenetriaminepentaacetate Bolus Track NMR Imaging in Cerebral Infarcts in Rats: Validation with the Iodo[14C]antipyrine Technique', *Proc.Natl.Acad.Sci-U.S.A.* 92(6):1846-1850, 1995.

[128] Fiat D and Kang S, 'Determination of the Rate of Cerebral Oxygen Consumption and Regional Cerebral Blood Flow by Non-Invasive ^{17}O In Vivo NMR Spectroscopy and Magnetic Resonance Imaging: Part 1. Theory and Data Analysis Methods', *Neurol.Res.* 14(4):303-311,1992.

[129] Rempp KA, Brix G, Wenz F, *et al.*, 'Quantification of Regional Cerebral Blood Flow and Volume with Dynamic Susceptibility Contrast-Enhanced MR Imaging', *Radiology* 193(3):637-641, 1994.

[130] Perman WH, Gado MH, Larson KB and PerlmutterJS, 'Simultaneous MR Acquisition of Arterial and Brain Signal-time Curves', *Magn.Reson.Med.* 28(1):74-83, 1992.

[131] Larson KB, Perman WH, Perlmutter JS, *et al.*, 'Tracer-Kinetic Analysis for Measuring Regional Cerebral Blood Flow by Dynamic Nuclear Magnetic Resonance Imaging', *J.Theor.Biol.* 170(1):1-14, 1994.

[132] Detre JA, Leigh JS, Williams DS *et al.*, 'Perfusion Imaging', *Magn.Reson.Med.* 23(1):37-45, 1992.

[133] Jones JP, Partain CL, Mitchell MR, *et al.*, 'Principles of Magnetic Resonance', *Magn.Reson.Annual* 1985:71-111, 1985.

[134] Zhang W, Williams DS, Detre JA and Koretsky AP, 'Communications. Measurement of Brain Perfusion by Volume-Localized NMR Spectroscopy Using Inversion of Arterial Water Spins: Accounting for Transit Time and Cross-Relaxation', *Magn.Reson.Med.* 25:362-371, 1992.

[135] Zhang W, Silva AC, Williams DS and Koretsky AP, 'NMR Measurement of Perfusion Using Arterial Spin Labeling Without Saturation of Macromolecular Spins', *Magn.Reson.Med.* 33:370-376, 1995.

[136] Silva AC, Zhang W, Williams DS and Koretsky AP, 'Multi-Slice MRI of Rat Brain Perfusion During Amphetamine Stimulation Using Arterial Spin Labeling', *Magn.Reson.Med.* 33:209-214, 1995.

[137] Corbett RJT, Laptook AR and Olivares E, 'Simultaneous Measurement of Cerebral Blood Flow and Energy Metabolites in Piglets Using Deuterium and Phosphorus Nuclear Magnetic Resonance', *Journal of Cerebral Blood Flow and Metabolism* 11(1):55-65, 1991.

[138] Ewing JR, Branch CA, Helpern, JA *et al.*, 'Cerebral Blood Flow Measured by NMR Indicator Dilution in Cats', *Stroke* 20(2):259-267, 1989.

[139] Branch CA, Helpern JA, Ewing JR and Welch KM, '^{19}F NMR Imaging of Cerebral Blood Flow', *Magn.Reson.Med.* 20:151-157, 1991.

[140] Van Zijl PCM, Ligeti L, Sinnwell T, *et al.*, 'Measurement of Cerebral Blood Flow by Volume-Selective ^{19}F NMR Spectroscopy', *Magn.Reson.Med.* 16:489-495, 1990.

[141] Edelman RR, Buxton RB and Brady TJ, 'Rapid MR Imaging', *Magnetic Resonance Annual* 1988:189-216, 1988.

[142] Gore JC and Majumdar S, 'Measurement of Tissue Blood Flow Using Intravascular Relaxation Agents and Magnetic Resonance Imaging', *Magn.Reson.Med.* 14:242-248, 1990.

[143] Rosen BR, Belliveau JW, Buchbinder BR, *et al.*, 'Contrast Agent and Cerebral Hemodynamics', *Magn.Reson.Med.* 19:285-292, 1991.

[144] Dixon WT, Du LN, Faul DD, Gado M and Rossnik S, 'Projection Angiograms of Blood Labeled by Adiabatic Fast Passage', *Magn.Reson.Med.* 3:454-462, 1986.

[145] Schwarzbauer C, Morrisse SP and Haase A, 'Quantitative Magnetic Resonance Imaging of Perfusion Using Magnetic Labeling of Water Proton Spins with the Detection Slice', *Proceeding of Point Meeting* (1995), pp 130, Soc. Magn. Res. and European Soc. Magn. Res. Med. Bio.

[146] Silva AC, Zhang W, Williams DS and Koretsky AP, 'Non-invasive Measurement of the Integrity of the Blood-Brain Barrier Using Magnetic Resonance Imaging of Perfusion with Arterial Spin Labeling', *Proceeding of Point Meeting* (1995), pp 129, Soc. Magn. Res. and European Soc. Magn. Res. Med. Bio.

[147] Morris HD, Khuntia and Lauterbur PC, 'A Multislice Arterial Spin Labeling Sequence with a Single Volumetric RF Coil', *ibid.*, pp. 872, 1995.

[148] Reith W, Heiland S, Forsting M, Benner T, *et al.*, 'Perfusion Imaging in Patients with Cerebrovascular Disease', *Proceeding of Point Meeting* (1995), pp 83, Soc. Magn. Res. and European Soc. Magn. Res. Med. Bio.

[149] Levin JM, Kaufman MJ, Ross MH, *et al.*, 'Sequential Dynamic Susceptibility Contrast MR Experiments in Human Brain: Residual Contrast Agent Effect, Steady State, and Hemodynamic Perturbation', *ibid.*, pp 127, 1995.

[150] Duyn JH, van Gelderen P, Moonen CTW, *et al.*, '3D Bolus-Tracking with Frequency-Shifted BURST MRI', *ibid.*, pp 128, 1995.

[151] Strohschein R, Immler B. Maier J., *et al.*, 'Perfusion Imaging of Rat Brain Using Quantitative T_2^* Measurements During First Pass of Susceptibility Agents', *ibid.*, pp 873, 1995.

[152] Bulte JWM, De Jonge MWA, Kamman RL, Go KG, *et al.*, 'Dextran-Magnetite Particles: Contrast-Enhanced MRI of Blood-Brain Brarrier Disruption in a Rat Model', *Magn.Reson.Med*, 23:215-223, 1992.

[153] Longmaid III HE, Adams DF, Neirinckx RD, Harrison CG, *et al.*, 'In Vivo ^{19}F NMR Imaging of Liver, Tumor, and Abscess in Rats', *Investigative Radiology* 20:141-145, 1985.

[154] Mantsch HH, Saito H and Smith ICP, 'Deuterium Magnetic Resonance, Applications in Chemistry, Physics and Biology', *Progress in NMR Spectroscopy* 11(Part 4):211-272, 1977.

[155] Kim SG and Ackerman JJH, 'Quantitative Determination of Tumor Blood Flow and Perfusion *via* Deuterium Nuclear Magnetic Resonance Spectroscopy in Mice', *Cancer Research* 48:3449-3453, 1988.

[156] Pardridge WM and Fierer G, 'Blood-Brain Barrier Transport of Butanol and Water Relative to N-Isopropyl-p-iodoamphetamine as the Internal Reference', *Journal of Cerebral Blood Flow and Metabolism* 5:275-281, 1985.

[157] Neil JJ, Song SK, Ackerman JJH, 'Concurrent Quantification of Tissue Metabolism and Blood Flow *via* $^{2}H/^{31}P$ NMR in Vivo. II. Validation of the Deuterium NMR Washout Method for Measuring Organ Perfusion', *Magn.Reson.Med.* 25:56-66, 1992.

[158] Naritomi H, Kanashiro M, Sasaki M and Sawada T, '5th *Ann. Meeting Soc.Magn.Reson.Med.*, Montreal, Canada. August. 1986. Book of Abstracts,' 1:4, 1986.

Chapter 3: The Theory of Indicator Based Flow Measurement

A. Introduction

The theory of indicator based flow measurement has as its foundation four major principles and a stimulus—response theorem. The principles have been attributed to: 1. Stewart,[1] 2. Fick,[2] 3. Bergner[3] and 4. Henriques-Hamilton.[4,5] The theorem was developed by Perl (see section C for details). The Stewart and Fick principles apply to a system that has a single input and a single output. The Bergner principle applies to a system that has one input but multiple outputs. The Henriques-Hamilton principle assumes a system that has multiple inputs and a single output. The stimulus—response theorem utilizes bolus injection and residue detection.[6] All of these principles/theorem are well understood and have been reviewed by Lassen and Perl.[6] An *in vivo* flow system usually consists of multiple inputs and multiple outputs. In flow measurements, such a system is generally treated as two sub-systems connected together–a multiple input, single output system in tandem with a single input, multiple output system.

B. The Flow Principles

1. The Stewart Principle

Figure 3.1 shows a single input-single output system where both the Stewart and the Fick principles can be used. In using the Stewart principle[1] to measure the flow F of the system one injects in a continuous fashion an indicator

with concentration c_{in} [g/mL] at a flow rate of F_{in} [mL/s] at the input. In this situation the influx of indicator j_{in} into the system is

$$j_{in} = F_{in} \times c_{in} \qquad [\ g/s] \qquad \text{Eq. (3.1)}$$

Figure 3.1: A Simple Input and Output System

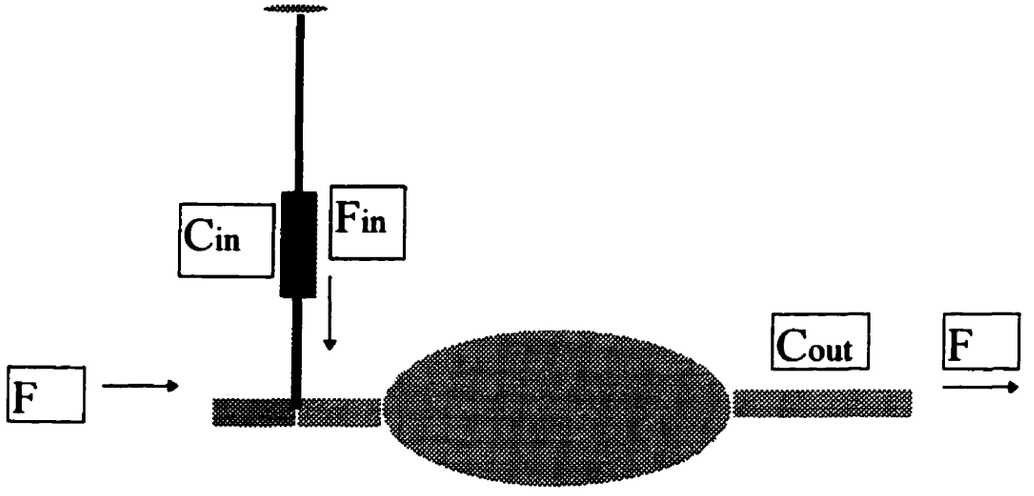

The concentration of indicator in the system increases during the injection until it eventually reaches an asymptote, or constant level c_{out}. Given c_{out}, the outflux of indicator j_{out} from the system is

$$j_{out} = (F + F_{in}) \times c_{out} \qquad [\ g\ /\ s]\ . \qquad \text{Eq. (3.2)}$$

If the inflow of indicator satisfies the condition $F_{in} << F$, then

$$j_{out} \cong F \times c_{out} \qquad [\ g\ /\ s] \qquad \text{Eq. (3.3)}$$

j_{out} is equal to j_{in} when the systemic steady state is reached. Combining Eqs. (3.1) and (3.3) we have

$$F \times c_{out} = F_{in} \times c_{in}$$

or

$$F = F_{in} \times \frac{c_{in}}{c_{out}} \qquad \text{Eq. (3.4)}$$

In other words, if: 1. disturbance of the system is small (e.g., $F_{in} << F$) and 2. the system returns to a steady state, the flow F of the system is equal to F_{in} times the indicator concentration dilution factor, c_{in}/c_{out}.

Figure 3.2: Application of Fick Principle to a Simple Input and Output System

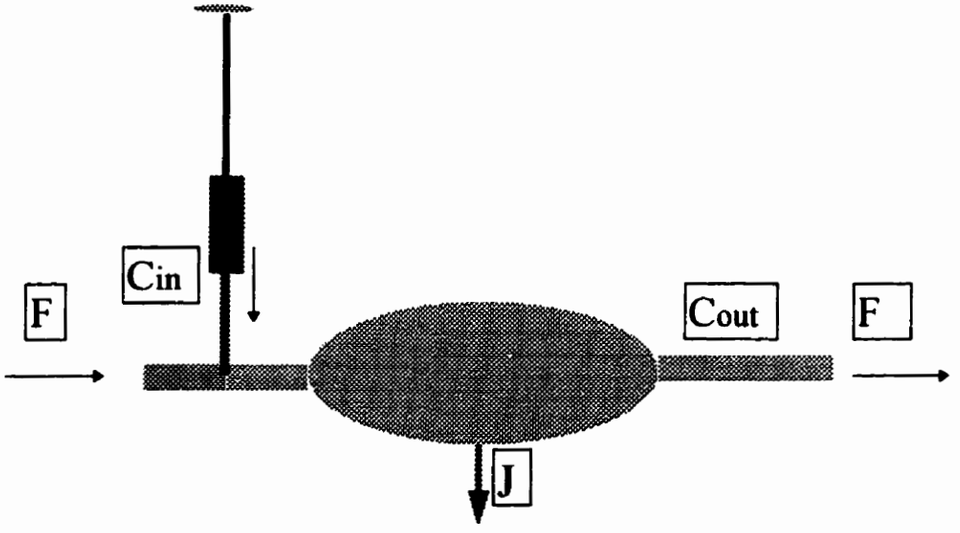

2. The Fick Principle

The Stewart principle can be utilized to determine tissue/organ flow only when two requirements are satisfied: the first is an absence of indicator recirculation and second is that indicator dissipation is due to flow alone. If the former is not satisfied, indicator recirculation needs to be accounted for; if the latter is not satisfied (due to up-take or metabolism), the Fick principle is used. Utilization of the Fick principle[2] is more or less the same as that of Stewart principle. The main difference between these two principles is in the behavior of the indicator employed. For example, if oxygen gas is used as indicator, then the amount of oxygen introduced will be reduced by tissue/organ metabolism. Assuming the indicator is disappearing at a flux rate of J, then under the systemic steady state, the flux of indicator into the system is

$$FC_{in} = J + FC_{out} \qquad \text{Eq. (3.5)}$$

where F is the system flow, C_{in} the inflowing indicator (or systematic substance, hence uppercase C is used) concentration and C_{out} the outflowing indicator (or systematic substance) concentration. Rearranging Eq. (3.5) we have

$$F = \frac{J}{C_{in} - C_{out}} \qquad \text{Eq. (3.6)}$$

Eq. (3.6) was used by Fick to determine cardiac output.[2]

3. The Henriques-Hamilton (H-H) Principle

The Henriques-Hamilton (H-H) principle[4,5] is used to calculate the flow of a system having more than one input but a single output. Figure 3.3 displays the basic configuration of the system and the technique for flow measurements using the H-H principle. In Figure 3.3 a bolus of indicator m_0 is introduced into the system at time $t = 0$. At time $t \geq 0$ the injected indicator washes out of the system. The amount of indicator leaving the system in a time interval dt about the time t is

$$dm_{out} = c_{out}(t)dV, \qquad \text{Eq. (3.8)}$$

Figure 3.3: A System with Multiple Input and Single Output

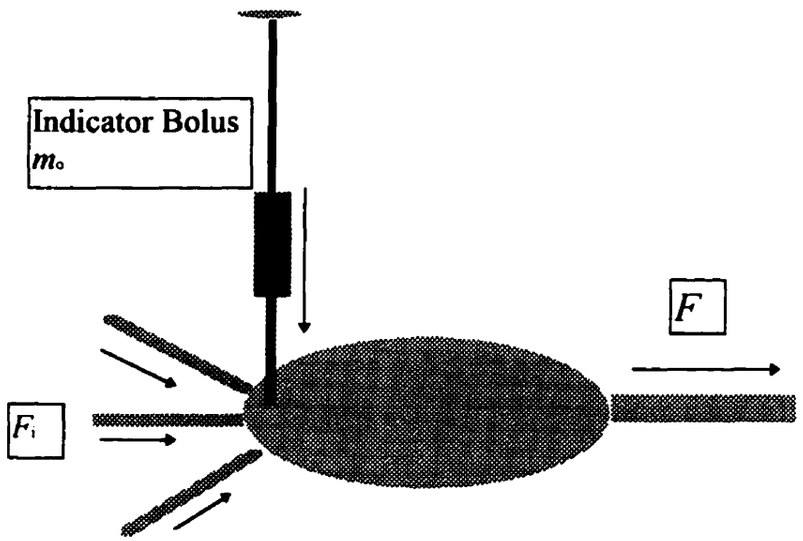

where $c_{out}(t)$ is the indicator concentration at time t and dV the volume of indicator carrier fluid that flows out of the system in time interval dt. Because dV is also the product of the system flow F and the time interval dt, Eq. (3.8) can be written as

$$dm_{out} = F \times c_{out}(t)dt \qquad \text{Eq. (3.9)}$$

or

$$m_o = \int_{\text{all t}} dm_{out} = F \times \int_{t=0}^{\infty} c_{out}(t)dt \qquad \text{Eq. (3.10)}$$

Therefore by rearranging Eq. (3.10) we have

$$F = \frac{m_o}{\int_{t=0}^{\infty} c_{out}(t)dt} \qquad \text{Eq. (3.11)}$$

That is, by using the H-H principle, the flow F through the system is equal to this amount of indicator m_o injected into the system divided by the area under the indicator concentration curve at the output.

Figure 3.4: A System with Single Input and Multiple Output

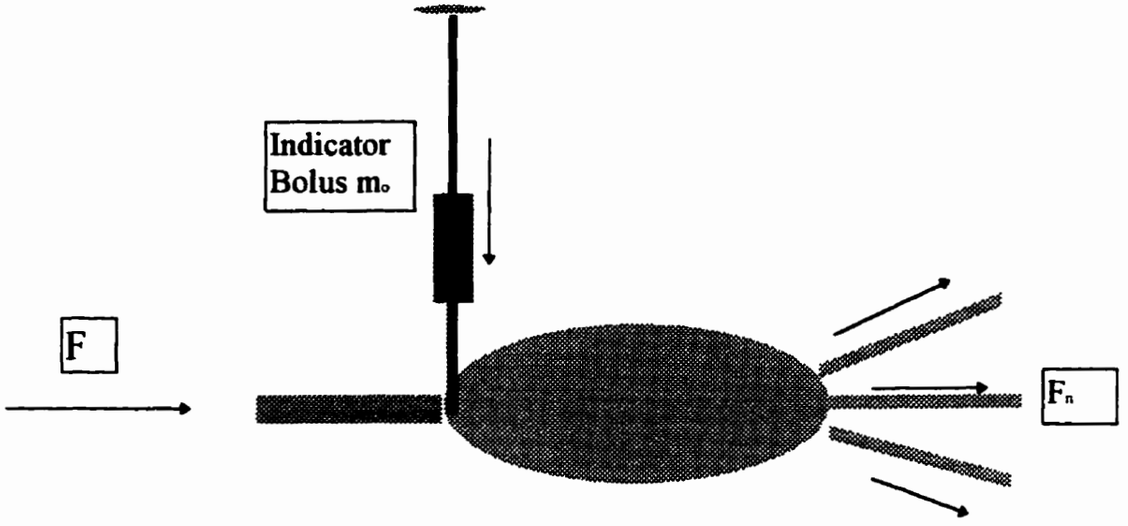

4. The Bergner Principle

The Bergner Principle[3] is applicable to a system with one input and more than one output. Figure 3.4 displays the basic configuration of the system and technique for flow measurement using this principle. For flow measurement in such a system one must first define a fraction D_n as

$$D_n = \frac{F_n}{F}, \qquad \text{Eq. (3.12)}$$

where F_n is the rate the carrier fluid is flowing out of the system at the n^{th} outlet. An alternative interpretation of D_n is

$$D_n = \frac{m_n}{m_o}, \qquad \text{Eq. (3.13)}$$

where m_n is the amount of indicator that will flow out of the system *via* outlet n, given sufficient time. Using arguments similar to those involved in the development of Eqs. (3.9) to (3.11) one arrives at the the Bergner principle

$$dm_n = F_n \times c_n(t)dt \qquad \text{Eq. (3.14)}$$

Similar to Eq. (3.13) dm_n is the amount of indicator flowing out of the system *via* the n^{th} outlet during the time interval dt about time t. Integrating over time, the amount of indicator m_n flowing out *via* the n^{th} outlet is

$$m_n = \int_{\text{all t}} dm_n = F_n \times \int_{t=0}^{\infty} c_n(t)dt \qquad \text{Eq. (3.15)}$$

Rearranging Eq. (3.15) we have

$$F_n = \frac{m_n}{\int_{t=0}^{\infty} c_n(t)dt} \Leftrightarrow D_n F = \frac{D_n m_o}{\int_{t=0}^{\infty} c_n(t)dt} \qquad \text{Eq. (3.16a)}$$

The right hand side (r.h.s.) of Eq. (3.16a) gives

$$F = \frac{m_o}{\int_{t=0}^{\infty} c_n(t)dt} \qquad \text{Eq. (3.16b)}$$

The significance of Eq. (3.16b) is that in the system flow F can be calculated using the amount (m_o) of indicator injected divided by the area under the concentration curve of **any one** of the outlets.

C. Application of the Stimulus – Response Theorem

1. Introduction to a Closed System

Let us consider a system with neither input nor output (that is, a closed system). We define V_d to be the 'virtual' volume of distribution [in mL] for a particular indicator, with respect to (w.r.t.) the closed system that has a physical volume V. This term 'virtual' is necessary because V_d need not be equal to the physical volume. This is because within a closed system there may be locations where the indicator is present in high concentration while others where the concentration is low or even zero. We define also:

1. W, the mass of the closed system [in g], including the medium (for example the carrier fluid) which allows the distribution of indicator,
2. m_o, the amount of indicator introduced into the system [in either mL or g],
3. c_l, the concentration of indicator in the carrier fluid [in amount/mL],
4. c_t, the concentration of indicator in the tissue [in amount/g], and
5. λ, (partition coefficient) $\equiv c_t/c_l$, the ratio of indicator concentration in tissue to that in carrier fluid [in mL/g] at equilibrium.

According to 5, λ can also be written as

$$\lambda = \frac{c_t}{c_i} \equiv \frac{(m_o / W)}{(m_o / V_d)} = \frac{V_d}{W} \text{ [ml / mg]} \qquad \text{Eq. (3.17)}$$

The parameters V_d, W and m_o defined above apply equally to a multiple input and multiple output system. (A multiple input and multiple output system can be visualized as connecting the closed system to multiple inputs and multiple outputs.) In the closed system, if given long enough, indicator distribution will achieve an equilibrium state; as such c_i and c_t, as well as λ will be defined by Eq. (3.17). If the indicator equilibrium can be established instantly, the c_i, c_t and λ can also be defined for the multiple input and multiple output system. In practice, indicator equilibrium in the multiple input and multiple output system need only be 'instantaneous' with respect to flow.

2. CBF Measurement Using Residue Detection and Instantaneous Bolus Injection

Consider a continuous, constant infusion of an indicator into a system that has one inlet and multiple outlets (for example, Figure 3.4). After a sufficiently long time the concentration of indicator in the system (such as the brain) reaches a steady state concentration c(∞), the indicator concentration at the inlet. Under this condition

$$V_d = \frac{m(\infty)}{c(\infty)} = \frac{\text{Residue}}{\text{Inlet concentration}}. \qquad \text{Eq. (3.18)}$$

Where $m(\infty)$ is the residue indicator in V_d after sufficient time of constant indicator infusion. Let $j(\infty)$ = F x $c(\infty)$ be indicator flux at the inlet under steady state concentration, then

$$\frac{V_d}{F} = \frac{m(\infty)}{F \times c(\infty)} = \frac{m(\infty)}{j(\infty)} = \frac{\text{Residue}}{\text{Flux}}. \qquad \text{Eq. (3.19)}$$

For such a system, the Stimulus – Response theorem[7] states that *the ratio of two parameters x and y in a continuous infusion experiment at full saturation equals the ratio of the complete time integrals of the same parameters in a bolus injection experiment.* Mathematically the theorem can be expressed as

Constant infusion Bolus Injection

$$\frac{m(\infty)}{j(\infty)} = \frac{\int_{t=0}^{\infty} m(t)dt}{\int_{t=0}^{\infty} j(t)dt} = \frac{\int_{t=0}^{\infty} m(t)dt}{m_o}. \qquad \text{Eq. (3.20)}$$

Where m_0 is the total amount of indicator injected. If m_0 can be injected so that the trailing indicator arrived at the system before the washout of the leading indicator, then the Zierler's Area – Over–Height[8] equation for the instantaneous bolus injection experiment can be used.

$$\frac{\int m(t)dt}{m_o} = \frac{\int m(t)dt}{m_{\max}}$$

where $m_{\max}$ is the maximum amount of indicator ever detected in the system. Thus

$$\frac{V_d}{F} = \frac{m(\infty)}{j(\infty)} = \frac{\int m(t)dt}{m_o} = \frac{\int m(t)dt}{m_{\max}} \qquad \text{Eq. (3.21)}$$

using Eqs. (3.19) and (3.20). In other words the Zierler's equation requires that the entire amount of indicator introduced be in the system during the determination of $m_{\max}$. In addition, if the indictor can be measured with the same efficiency at all time (such as would be the case with a stationary MR surface coil), then the residue detection with instantaneous bolus injection can be expressed as

$$\frac{Vd}{F} = \frac{\int S(t)dt}{S_{\max}}. \qquad \text{Eq. (3.22)}$$

where $S(t)$ is the MR signal recorded at a time t.

That is

$$F = \frac{Vd \times S_{\max}}{\int S(t)dt}.$$

Using the expression of Eq. (3.17) for V_d

$$F = \frac{\lambda \times W \times S_{max}}{\int S(t)dt}. \qquad \text{Eq. (3.23)}$$

The unit of tissue perfusion (f) is given in [mL/min] per unit mass [g] of tissue. As such

$$f = \frac{F}{W} = \frac{\lambda \times S_{max}}{\int S(t)dt}. \qquad \text{Eq. (3.24)}$$

By convention CBF is usually stated as 100 times f

$$CBF = 100 \times f = 100 \times \lambda \times \frac{S_{max}}{\int S(t)dt}. \qquad \text{Eq. (3.25)}$$

The above bolus injection and residue detection model, although derived for a single inlet and multiple outlet system, can be applied to a system with multiple inlets and multiple outlets[6] (Lassen and Perl, page 84). For example, in the case of MRI, the detected MR signal in an image represents signal averaged over the corresponding region of the brain imaged. In the case of MRS using a surface coil, as is the case in this study, the MRS signal intensity represents weighted signal averaged over the whole brain, (with heavier weighting given to region closer to the surface coil), turning the multiple outlets into a single one. The multiple inlets, according to fractionation principle (Lassen and Perl, page 38-39), can be taken

care of if an amount of indicator proportional to flow be injected to each of the inlets. In the case that only one inlet is injected, for example the right internal carotid artery, the CBF measured represents the weighted flow of the brain regions serves by the right internal carotid artery.

To conclude, CBF, as determined using MR in association with bolus injection and residue detection, is equal to 100 times the partition coefficient λ multiplied by the MR signal at its maximum and divided by the area under the MR signal curve. Eq. (3.25) will be used in the chapters that follow, to calculate average CBF.

3. An Approximation: Single Compartmental Analysis

If one makes the assumption that the brain can be represented by a single compartment model, then by definition the MR signal from the brain as a function of time is a mono-exponential decay curve.

$$S(t) = S_{\max} \times \exp(-kt), \quad t \geq 0, \qquad \text{Eq. (3.26)}$$

where k is the exponential rate constant. Substituting this equation into Eq. (3.25)

$$\begin{aligned} CBF &= 100 \times \frac{\lambda \times S_{\max}}{\int_{t=0}^{\infty} S_{\max} \exp(-kt)dt} \\ &= 100 \times \frac{\lambda}{\int_{t=0}^{\infty} \exp(-kt)dt} \end{aligned} \qquad \text{Eq. (3.27)}$$

Integrating

$$\int_{t=0}^{\infty} \exp(-kt)dt = \frac{1}{k}$$

yields

$$CBF = 100 \times \lambda \times k \qquad \text{Eq. (3.28)}$$

In approximating the brain as a single compartment, CBF is equal to 100 times the partition coefficient (λ), multiplied by the exponential decay constant k. If one takes the natural log of the single compartment signal function (Eq. (3.26))

$$\ln[S(t)] = -kt + \ln[S_{\max}] \qquad \text{Eq. (3.29)}$$

Eq. (3.29) is a linear function

$$y = mx + b$$

where

$$y = \ln[S(t)]$$
$$m = -k$$

and

$$b = \ln[S_{\max}]$$

Therefore another way of expressing Eq. (3.28) is

$$CBF = -100 \times \lambda \times m \qquad \text{Eq. (3.30)}$$

Where m in this case is the slope of the semi-log plot of the MR signal as a function of time. Eq. (3.30) will also be used in the Chapters that follow to calculate fast or gray matter CBF. Also, in Chapter 5 the results obtained using Eq. (3.25) will be compared with those using Eq. (3.30).

References

[1] Stewart GN, *J.Physiol.* 22:159, 1897.

[2] Fick A, Sitzungsb. *der Phys.Med.Ges. zu Würzburg*, 1870.

[3] Bergner PEE, *J.Theor.Biol.* 6:137, 1964.

[4] Henriques V, *Biochem. Zeitschr.* 56:230, 1913.

[5] Hamilton WF., *et al.*, *Am.J.Physiol.* 84:338, 1928.

[6] Lassen NA and Perl W, *Tracer Kinetic Methods in Medical Physiology*, Raven Press, NY, 1979.

[7] Perl W, Bull. Math. *Biophys.* 33:225, 1971.

[8] Zierler, K. L., *Circulat. Res.* 16:309, 1965.

Chapter 4: Experiments

This chapter has been divided into two parts. Part One provides an overview of the many experiments performed in developing the final CBF measurement protocol; Part Two is a recipe for the final protocol developed.

A. Part One: Development of the CBF Experimental Protocol

1. Introduction

Recall from Chapter 2 that flow measurement is a 'three step' process:

1. Inject an indicator into the system in which flow is to be measured.
2. Sample the system to assess the accumulation and/or dissipation of this indicator.
3. Fit mathematical models to the sampled results to predict flow.

As justified in Chapter 2 we have decided to use the following approach:

1. ^2H_2O was used as an indicator.
2. MRS was chosen to monitor the washin and washout of indicator in the brain.
3. The modeling methods were chosen to be consistent with step one and two. See Chapter 3 for details.

The following sections describe the experiments and tasks which were performed in developing the final CBF measurement protocol.

2. Developing the Final Protocol

About 40 Sprague-Dawley rats were used in developing the final CBF measurement protocol. This section justifies and details the use of the animals.

a) Gaining the Technical Expertise for CBF Measurement

In the beginning, about 10 rats were used for training. The objective of the training was to acquire expertise in the following areas:

1. microsurgery
2. anaesthesia
3. trachea intubation
4. vein and artery catheterization
5. physiological control and monitoring:
    i. temperature and blood pressure
    ii. blood gases, (especially $PaCO_2$)
    iii. pH level
    iv. level of animal sedation, etc.

The training had provided the much needed skill for the more complicated CBF experiments and an opportunity to assess how precise blood gases can be monitored. Table 4.1 demonstrates the kind of precision achievable. (See part II of this chapter for how the blood gas was measured.)

Table 4.1: Repetitive Blood Gas Measurements at Three Different Settings of Mechanical Ventilation in One Rat.

Sample No.	Trial One			Trial Two			Trial Three		
	PaCO2 (mmHg)	PaO2 (mmHg)	pH	PaCO2 (mmHg)	PaO2 (mmHg)	pH	PaCO2 (mmHg)	PaO2 (mmHg)	pH
1	40.7	460.3	7.389	56.5	124.1	7.201	44.4	288.8	7.34
2	36.1	383.6	7.377	60.7	125	7.206	35.8	241.1	7.34
3	39	366.4	7.383	58.9	121	7.202	43.9	240.6	7.328
4	38.8	347.1	7.383	59.7	126.3	7.198	45.8	234.4	7.322
5				54.6	118.9	7.193	43.2	227.5	7.316
average	**39**	**389**	**7.383**	**58**	**123**	**7.200**	**43**	**246**	**7.329**
st. dev.	**2**	**50**	**.005**	**2**	**2**	**0.005**	**4**	**24**	**0.011**

In addition to animal experiments, a number of MR studies using a flow phantom assembly were also performed. The goals of the phantom studies were: To assess in detail the capabilities, strengths and limitations of the Bruker Biospec 7T/21cm scanner, including its computer systems and software. And, to test the dynamic sampling procedures developed. A sketch of the flow phantom assembly is shown in Figure 2.2. The assembly consisted of:

1. a syringe pump connected to an upstream injection site
2. a water filled vial, representing the rat's brain, positioned at the magnetic center of the scanner, and
3. a bucket for collecting the flow exiting the phantom

The flow of fluid (water) through the phantom was initially calibrated for various syringe pump settings. Besides experiments investigating static MRI and MRS using both proton and ^2H, studies were performed to investigate:

1. dynamic proton imaging using the SNAPSHOT-FLASH sequence
2. dynamic proton imaging using the GEFI sequence (a FLASH derivative)
3. dynamic ^2H spectroscopy

With respect to the goal of this study it was concluded that dynamic ^2H spectroscopy provided both adequate temporal resolution and sufficient MR signal to noise ratio (SNR). However, for the blood flow measurement protocol to be clinically useful, it will have to be modified to yield regional information. This, in turn, will require that indicator washin/washout be measured using MRI. These phantom studies represent the initial move in this direction.

Other phantoms were developed and utilized in the course of the CBF measurements. One worth mentioning was a rigid rubber bottle of the approximate size of a rat's brain. This phantom was filled with a mixture of ~ 1.5 mL ^1H_2O and 0.2 mL ^2H_2O, the latter being typical of the amount used in an animal experiment. The phantom was used in the quality assurance (QA) of the scanner's operation. The object of the QA was to determine whether or not the scanner was performing at a level suitable for use. The QA procedure required that the phantom be set up in the same configuration as a rat in a typical animal experiment. For instance, all

the devices used to control rat physiology (such as temperature, pressure, heart beat, respiration, etc.) were activated. Similarly the same animal holder and match box for the MR surface coil were utilized. All rat experiments and QA measurements were conducted at that location inside the scanner bore possessing the most homogeneous magnetic field (very likely the magnetic center). The optimal position for the phantom (and hence the rats) was obtained as follow:

1. The manufacturer's stated magnetic center along the z-direction was read directly off the side of the scanner.
2. A plastic positioning rod was used to position the center of the surface coil at the position identified in 1.
3. A head coil was centered along the magnetic x and y directions by carrying out the following steps:
    i. Fix the surface coil at the approximate physical center of the magnetic bore along the x and y axes
    ii. Tune and shim
    iii. Perform a quality assurance (QA) measurement using MR SNR. (See below for a description)
    iv. Change the x and the y positions of the phantom and recalculate the SNR
    v. Repeat from ii. until the phantom location yielding the highest SNR is identified

The QA check consisted of the following:

1. The phantom was set-up and positioned following the procedures described above.
2. This was followed by routine tuning of the ^{2}H coil and shimming of the magnetic field; shimming was done using ^{2}H.
3. An ^{2}H FID was acquired using 2 scans in 2 seconds (time of repetition, TR = 1 second, number of scan, NS = 2, number of average, NA = 1, number of repetition, NR = 1, and the same pulse, etc., used in animal experiments).
4. The FID was processed to yield an ^{2}H spectrum by applying a base line correction and an exponential filter (line broadening = 50 Hz), Fourier Transforming and phasing. See Figure 4.5.
5. SNR was calculated and compared to the SNR threshold value (700). If the SNR was greater than the threshold value the scanner was considered acceptable for use in animal experiments.

SNR was calculated as follows:

1. The $^{2}H_{2}O$ peak height was considered to be the signal (S).
2. The maximum fluctuation in the base line of the spectrum was considered to be the noise (N).
3. SNR was calculated by dividing the signal by the noise.

Table 4.2 gives an example of the QA results obtained between Nov. 21, 94 to Dec. 20, 1994. According to the table, the SNR obtained had improved with time. This was due to better placement of the surface coil on the phantom, a skill that had increased with experience. The most frequently occurring problems that led to an unacceptable SNR included:

1. incorrect parameter settings (offset, receiver gain, pulse length, wrong nucleus, etc.)
2. improper ohmic contact between the 'match box' (the capacitor and the inductor section) and the surface coil (the resistor section) of the RLC circuit (a circuit with resistor-inductor-capacitor in a series) of the signal probe

All these problems were readily identified and easily overcome as a result of instituting the QA procedure. For example the inferior ohmic contact was due largely to the fact that the same match box was used for all other surface coils available for the scanner. The problem was two male connectors on ^{2}H surface coil were thinner than on the others. As such the use of other surface coils resulted in widening the two female connections on the match box to the extent that less than ideal ohmic contact resulted when the ^{2}H coil was configured. This problem was easily solved by adjusting the size of the two female connections before the QA procedure. In addition, grease at the two contacts could also increase impedance

(decreased quality factor (Q) of the RLC circuit—MR probe assembly). Cleaning the contacts with ethanol remedied this problem.

Table 4.2: Example of QA Results

Date	SNR
Nov. 21, 94	700
Nov. 30, 94	920
Dec. 01, 94	950
Dec. 02, 94	833
Dec. 08, 94	933
Dec. 09, 94	1057
Dec. 13, 94	1166
Dec. 20, 94	1160

b) Development of a Technique for Arterial Indicator Injection

(1) Fabrication of Injection Catheters

The catheter used for indicator injection evolved through three stages. The earliest type of catheter assembly consisted of a G24 catheter connected to a plastic tube; the other end of the plastic tube was connected to a two-way stopcock and then a 1 mL syringe. The second generation of indicator assembly consisted of a capillary tube 75 cm in length to replace the plastic tube; one end of the capillary was joined to a Teflon tip cut from a G24 catheter (for catheterizing) and the other end to a two-way stopcock and a 1 mL syringe. The much narrower diameter of

the capillary tube prevented blood from diffusing back into the indicator assembly. The dead volume associated with the catheter was 0.33 mL (with about 0.2 mL for the capillary tube itself). Finally, a special kind of catheter assembly was also fabricated to inject two different drugs alternately (e.g., Heparin and indicator). This catheter assembly used two capillary tubes of 75 cm length each. The tube with the smaller diameter was inserted into the one with the larger diameter, forming a single coaxial capillary tube. One end of this coaxial tube was connected to the Teflon tip cut from G24 catheter. The other end was separately connected to two individual two-way-stopcocks and 1mL syringes, one for the inner tube and the other for the outer tube. The two different drugs were infused into the inner and outer tubes *via* their respective syringes. The dead volume of both tubes was less than 0.1 mL, (0.23 mL if the two-way stopcock is included). A shortcoming of all the injection assemblies was the dead volume. Since this resulted in a waste of indicator. To solve this problem an indicator filling technique was employed in the deuterated alcohol studies. See the next section for details.

(2) Filling Methods of the Improved Injection Assembly (Second Generation)

In the CBF measurements, clotting of blood in and around the tip of the catheter constituted a major problem. A Teflon catheter was found to reduce clotting compared to a plastic one. However, the greatest improvement in

minimizing the problem of clotting was adding 3% (v/v) of heparin into the ^2H_2O saline that filled the catheterizing assembly. Each injection, in essence, served to flush the catheter tip and its vicinity (injections were made every 30 minutes). However, the time between the placement of the injection catheter and the first injection was typically 90 minutes (due to the time required for the placement of the surface coil and positioning the animal in the magnet as well as the setting-up of the instrumentation for the physiological controls and monitoring). In order to prevent clotting during this period, the tip of the catheter (approx. 0.005 mL) was filled with Heparin. Before this technique was adopted, the first experiment performed on a rat would usually exhibit a depressed CBF. Subsequent measurements would yield normal values for CBF and it is speculated that the first injection served to dissolve blood clots which developed during setup. The problem associated with the first injection disappeared with the introduction of 0.005 mL heparin at the catheter tip.

In the CBF measurements using dual ^2H_2O and ^2H[alcohol] indicators (heparinized, see Chapter 8 for details) the clotting prevention method used was as stated above. As mention earlier, the 0.33 mL dead volume of the catheter assembly represents a problem related to cost. In order to avoid wasting the 0.33 mL alcohol indicator in the dead volume of the catheter assembly, a different indicator filling approach was taken for bolus injections less than 0.1 mL. This approach involved:

1. initially filling the entire catheter assembly with heparin
2. drawing in an air bubble of less than 0.002 mL in size.
3. adding alcohol indicator for one injection, usually 0.05 to 0.1 mL, after the air bubble; the air bubble served to separate the heparin from this indicator
4. repeating steps 2. to 3. as many as 5 times to load the catheter for repeated injections.
5. drawing an air bubble after the last indicator bolus and filling the tip of the catheter with Heparin.

The small air bubbles not only isolate indicator boluses but most more importantly serve to separate blood from the indicator between injections. The catheter assembly was filled with heparin initially (step 1. listed above) in hope of preventing clotting between indicator injections (again every 30 minute).

(3) Injection Sites Investigated

Initially, the femoral vein was investigated as a suitable indicator injection site. For Sprague Dawley rats the catheterization of this vein is relatively easy. However, it was found that this injection site has two disadvantages:

1. On average only 15 to 25% of the indicator first passage through the heart enters the brain (See Chapter 7). As such the MR signal at the brain resulting from a femoral injection is considerably smaller than if the entire indicator is injected into the brain directly.

2. A femoral injection would also require a more complex model to describe its movement through the body and into the brain. In order to calculate CBF a knowledge of the indicator input function (see Chapter 7) is required. The input function can be obtained from continuous monitoring of artery indicator concentration by arterial blood sampling. The input function is needed in employing either the Kety or the Kety and Schmit CBF equation (see Chapter 2).

An injection site was sought to allow indicator injection as close to the brain as possible so as to simplify the CBF measurement model. There were a number of potential arteries that could satisfy this condition. These arteries included:

1. the right subclavian artery (fed retrograde from subclavian artery)
2. the common carotid arteries
3. the external carotid arteries (fed retrograde from external carotid arteries)

Catheterizing these arteries was by no means an easy operation. The higher blood pressure of the arteries was an added difficulty.

Surgically, the right subclavian was the easiest of the three and logically, was the first injection site tried. The left subclavian was not an appropriate site as it branches out downstream of the left common carotid artery. The branching of the right subclavian, however, was upstream of the right common carotid artery

and therefore, potentially appropriate. Experimentally, indicator bolus injections of up to 1 mL were performed at this site in three rats. Of the many injections only one indicator washin and washout of the brain was observed. Dissecting the animal after the experiments showed that positioning of the catheter was problematic. Ideally the tip of the catheter should have been at the junction of the right subclavian and the right common carotid. Unfortunately however, this was very difficult to achieve because it was not practical to cut through the arm and shoulder joint, to visually position the tip of the catheter at the junction. It was speculated that if the tip of the catheter was not right at the junction, the very high blood pressure of the aorta would push back the indicator injected into the many branches along the subclavian. The portion of indicator bolus that did not go into the right common carotid artery could distort the washin and washout curve, as it must circulate through part of the body (the right arm) before entering the brain. If not corrected, the late washin could cause underestimation of CBF.

The next artery investigated for catheterization was the right common carotid (CCA). Catheterizing at this site proceeded as far as inserting a catheter into the artery. Fastening the catheter with surgical thread was not allowed, as that would have stopped CCA blood flow and so super glue was employed to hold the catheter in position. Unfortunately, the attempt was not totally satisfactory, because the catheter was susceptible to slipping out of position. It was then realized that in order to catheterize the CCA, the catheter would have to be fed

retrograde from the right external carotid (ECA) where the catheter can be tied, at the expense of blood flow to the ECA.

Surgically, the right ECA catheterization was the most difficult procedure of the three. (See subsequent sections of this chapter for details.) Initially a set of 10 rats was alloted to develop this technique. MR results on the first few rats indicated that only about half the experiments showed washin and washout of indicator in the brain. In an attempt to improve the success rate, various injection rates and bolus sizes were investigated. The success rate, however, did not improve. At that point the focus of the investigation shifted to placement of the tip of the catheter in the right common carotid artery (CCA). Initial testing indicated that when a small portion of the catheter tip was in the CCA, the resistance of the catheter prevented some of the blood from moving into the right internal carotid artery (ICA) and traveling to the brain. In other words, intrusion of the catheter into the CCA compromised blood flow. It was decided therefore to position the tip of the catheter as close to the carotid bifurcation as surgically possible but still remaining completely within the ECA. Such a placement was possible due to surgical skills acquired from extensive practice. One difficulty in catheterizing at the carotid bifurcation was the fact that the usable section of the ECA was less than 5 mm in length and when the incision on the artery was made, there was only about 3 mm between the point of incision and the bifurcation, (as the ECA was imbedded deep into the neck and needed to be pulled upward before

catheterizing). In addition to the improvements in surgical technique, the use of ACCU-FLO™ (LEPAGE) super glue to hold the catheter in position was very helpful, especially during the handling of the animal after catheterizing. Consequently the catheterization site chosen was at the right ECA, with the tip of the catheter positioned at the carotid bifurcation but completely within the ECA. Results indicated a success rate of 100% when the previously mentioned technique for indicator injection was utilized to solve the blood clotting problem.

(4) Bolus Size Determination

The size of the indicator injection bolus has an effect on the following parameters:

1. SNR
2. temporal MR signal resolution
3. injection time
4. and for alcohol indicators, toxicity.

All four of these factors were investigated when selecting the optimum bolus size for CBF measurements.

(a) SNR of the MR Spectrum

The SNR of MR spectra is the ratio of the resonance peak height (S) to the baseline fluctuations (N). Given an FID, the optimal SNR for the corresponding spectrum can be obtained using a line broadening (lb) that is approximately the

same as the natural line width. Since the commissioning results indicated that the most homogenous region of the magnet (a spherical volume with 4 cm diameter) is homogeneous to 1 ppm the natural FWHM for deuterium is about 50 Hz. Thus, an exponential multiplicative filter with a lb of 50 Hz was utilized. The suitability of 50 Hz lb was experimentally confirmed to provide the best SNR under CBF measurement conditions among 4 line broadenings tested (0.3, 3, 20 and 50 Hz).

Clearly, an increased bolus size will lead to an increased SNR. However, it is desirable to keep the bolus size as small as possible in order to minimize perturbations in the system as a result of the injection. Experiments were conducted with bolus sizes ranging from 0.05 mL to 1 mL. A bolus size of 0.2 mL was found to provide an acceptable SNR.

(b) Temporal Resolution

The maximum FID sampling frequency achievable was one every 0.5 to 0.7 seconds using 1 acquisition per FID. This restriction was due to the fact that the saturated ^{2}H nuclei need time to relax their magnetization to an equilibrium level before the next pulse. However, this would require 2 times the amount of indicator (0.4 mL) to achieve a resonable SNR. This was considered to be too large and as such, it was decided to acquire an FID consisting of 2 acquisitions every two seconds.

(c) Indicator Injection Time

Various injection times were investigated *in vivo* in an attempt to ensure an instantaneous bolus. For the mathematical models utilized to be valid (see Chapter 3), the trailing edge of the bolus must enter the brain before the leading edge leaves. Only then will the maximum MRS signal recorded be proportional to amount of tracer injected — a fundamental assumption of the model employed. However, there are physical limitations on the rate at which a bolus can be injected; too high an injection rate can rupture the injection site. Bolus sizes ranging from 0.05 mL to as much as 1 mL and injection times from less than one second to 20 seconds or more were investigated. Results indicated that injecting as much as 1 mL in 5 second apparently did not alter the blood gases, pressure, pH, bases, etc., of the animal. Injecting 0.2 mL in less than or equal to one second produced a washin and washout pattern that resembled an ideal instantaneous bolus injection. In other words, the washin of indicator into the brain was almost instantaneous, rising to a very sharp peak, and the initial washout resembled a mono-exponential decay curve. (A bolus not injected instantaneously would exhibit a washout curve with a rounded peak.) The washin of the entire 0.2 mL into the brain was independently assessed by visual inspection. This was accomplished by exposing the full length of the right CCA at the end of the CBF measurements and performing the 0.2 mL bolus injection. Visually, part of the injected indicator went into the ICA and the rest overcame the blood pressure and

entered into the CCA. Nevertheless the portions that went into the CCA came right back into the internal carotid in less than 1 second. On the other hand, if the bolus was more than 0.2 mL, and the indicator injection time was equal to 1 second, a number of outcomes were observed (in addition to the outcome just mentioned):

1. It was possible for portions of the indicator to be pushed into the common carotid and only recirculate back into the brain at a later time, thereby causing errors in the CBF measurement.
2. More seriously, the catheter would often push out of position.

In the end, an injection time of less than or equal to one second and a bolus size of 0.2 mL was chosen. The choice represents a bolus possessing instantaneous indicator injection characteristics.

c) Development of a Technique for Monitoring Indicator in the Brain

(1) Fixing of the ^{2}H MR Surface Coil

Initially, it was decided to remove the skin of the animal over the frontal cortex of the brain so that the surface coil could be placed directly on the rat skull. This not only allowed one to fix the surface coil closer to the brain, but also to eliminate signal contribution from the skin. In addition, muscles around the surface coil were also removed for the same reasons. Figure 4.PA1 shows a transverse proton image of the rat brain with the surface coil in position. Note in the image the regions around the surface coil where skin and muscle were removed.

Figure 4.PA1: Proton Image of Rat Brain Using MSME, (TR=1500ms, TE=20ms, Slice Thickness = 1mm)

(2) MR Signal Acquisition

The steps taken before MR signal acquisition included tuning the ^{2}H surface coil and shimming. Tuning was necessary in order to match the LRC resonance circuit of the receiver (the surface coil plus the match box) to that of the scanner. Shimming was necessary in order to make the magnetic field as homogeneous as possible for the volume that was sensitive to the surface coil.

Tuning the ^{2}H for the surface coil was not a problem. Shimming was problematic in that it could not be performed using ^{2}H. Shimming consisted of

acquiring FIDs dynamically as the fields generated by the shim coils were adjusted, the size and shape of the FIDs providing information on the magnetic field homogeneity of the sensitive volume. Because the natural abundance of ^{2}H is so low, shimming was performed using ^{1}H instead. Unfortunately this led to its own problems. Effectively all tissues (skin, muscles) that contain water contribute MR signal to the shimming FIDs; as a result, shimming for the brain tissue alone was not possible. This was one of the reasons why the skin of the animal was removed before an experiment. If not removed, shimming using ^{1}H would have been heavily weighted for the skin and muscles. This is especially true for the skin, as the skin is closer to the surface coil than the brain, and the MR signal acquired decreases with distance cubed ($S=1/d^{3}$) from the surface coil.

It was observed in some experiments that shimming using higher order harmonics (such as using the x^{2}-y^{2} gradient coil) was not possible. The cause was attributed to the secretion of a small amount of fluid (water) on the exposed skull, immediately underneath the MR surface coil. When the secreted fluid was mopped up, shimming was successful and an acceptable SNR was obtained in the experiments that followed. This phenomenon was also verified in a phantom. It was shown that when 4 layers of single ply kimwipe were saturated with water and placed between the QA phantom and the surface coil, shimming with higher harmonics was not possible. A logical question to ask was, would the SNR change as fluid began to build-up during experiments? The answer to this question was

yes. To solve the problem, it was decided to tune the coil before each indicator injection. The initial shimming on a dry skull resulted in a magnetic field that was homogeneous in brain tissues that were near the surface coil and the presence of fluid would not have altered the homogeneity in the brain. In addition, there could not have been signal contribution from the fluid itself. It was therefore concluded that once initial shimming had been performed, it would not have to be repeated unless the rat was moved.

d) Development of a Mathematical Model to Predict Flow

The mathematical estimation of CBF required a knowledge of the indicator partition coefficient λ. (See Chapter 3 for details). The concept of partition coefficient as used in flow measurement was first defined by Kety[1] as the ratio between the tissue and blood indicator concentrations under indicator equilibrium. The H_2O partition coefficient was measured directly in four rats and the results are presented in Table 4.3. In this experimental determination, the rats were sacrificed with an injection of KCl solution at a concentration greater than 10% (w/v) *via* the femoral vein. Within 3 seconds of the KCl injection, the heads were submerged in liquid nitrogen for a sufficiently long time (long enough for the heads to freeze). Next the rats were put into a freezer at a temperature lower than -10 $^{\circ}$C, for 24 hours. Then the brains were removed, weighed and put into an oven at 90 $^{\circ}$C for 3

days. With all water evaporated from the brains they were weighed a second time and λ was calculated using

λ=(wet brain weight - dry brain weight)/wet brain weight

Table 4.3: Experimental Evaluation of Partition Coefficient (λ) for Water.

Rat No.	Wet Weight (gm)	Dry Weight (gm)	λ in (mL/gm)
rt93018	1.9150	0.4146	0.7835
rt93019	1.9629	0.4113	0.7905
rt93021	1.8797	0.3905	0.7923
rt93022	1.8309	0.3900	0.7870
		average ± s.d.	0.788 ± 0.004

The result obtained was different from the well documented[2] 0.9 mL/g by about 12%. The large 12% discrepancy could have been due to higher measured dry weights as the brains were not crushed during drying. The literature value of 0.9 mL/g was therefore used in the CBF models.

References:

[1] Kety S.S, 'The theory and applications of the exchange of inert gas at the lungs and tissues', *Pharmacol.Rev.* 3:1-141, 1951.

[2] Herscovitch P and Raichle ME, 'What is the Correct Value for the Brain-Blood Partition Coefficient for Water?', *Journal of Cerebral Blood Flow and Metabolims* 5:65-69, 1985.

Part Two: The CBF Protocol

1. Introduction

Part Two describes the final protocol utilized in CBF experiments at two levels. Section 2 is a summary and Section 3 is a detailed explanation of the protocol. Typical experimental results are presented at the end of this chapter.

2. The Final Protocol

Experiments were conducted on male Sprague-Dawley rats weighing between 300-350 grams. The animal was pre-treated with Atropine™ and anaesthetized with Na-Pentobarbital. Following anaesthetization the trachea of the animal was intubated, and the animal mechanically ventilated. The animal temperature was controlled at 38 °C and the blood pressure maintained between 90 to 110 mmHg. Animal arterial blood was sampled at an interval of 30 minutes for blood gas measurements. The partial tension of carbon dioxide ($PaCO_2$) was maintained between 35 to 45 mmHg by adjusting the rate of the mechanical ventilation.

The first surgery after initial preparation was on the tail. The tail artery was catheterized for arterial blood pressure monitoring and blood sampling. The second surgery was the placement of an indicator injection catheter which was fed retrograde from the distal side of the right external carotid artery (ECA) to the bifurcation of the common carotid artery (CCA), while making sure that the tip of

the catheter resided entirely within the external carotid artery. The third surgery was the fixing of a deuterium sensitive MR surface coil onto the skull of the rat.

The animal, after surgical preparation, was transferred to an animal holder where the required connections (such as surface coil to the transmitter/receiver etc.) were made. Then the animal holder was inserted into a Biospec 7/21 MR Scanner. After tuning and shimming, a series of 360 consecutive free induction decays (FIDs) were taken at a scan rate of 0.5 Hz (2 scans per FID). The ^{2}H labeled indicator, usually 0.2 mL, was injected as an instantaneous bolus at the beginning of the 15^{th} FID acquisition. The data acquisition procedure was repeated five times to yield 5 sets of washin/washout data per animal.

The individual FIDs in the series of 360 were base line corrected (BC). This was followed by exponential multiplication (EM), Fourier transformation (FT) and phasing to generate 360 ^{2}H spectra. The peak height of the individual spectra represented a relative measure of indicator concentration as a function of time. After picking the peak heights for the entire series the resultant data were transferred to a PC for further processing and later blood flow modeling. This additional data processing was carried out using Excel™.

The next chapter describes CBF modeling details, presents CBF results obtained and observations made.

3. Methodology and Details

This section provides a detailed step by step description of the procedures summarized above.

a) Anaesthetization and Initial Rat Preparation

The animal used in experiments was the male Sprague-Dawley rat (Figure 4.2); the male sex was chosen for its hormonal consistence. This species was ideally suited to this study because it was readily available, inexpensive, easy to care for and handle, and well investigated. The weight range of the animal chosen was between 300 to 350 grams (gm); this weight range is considered adult for the rat. Older rats were not used due to their lack of hormonal consistence.

Figure 4.2: S.D. Rat Showing i.p. Injection

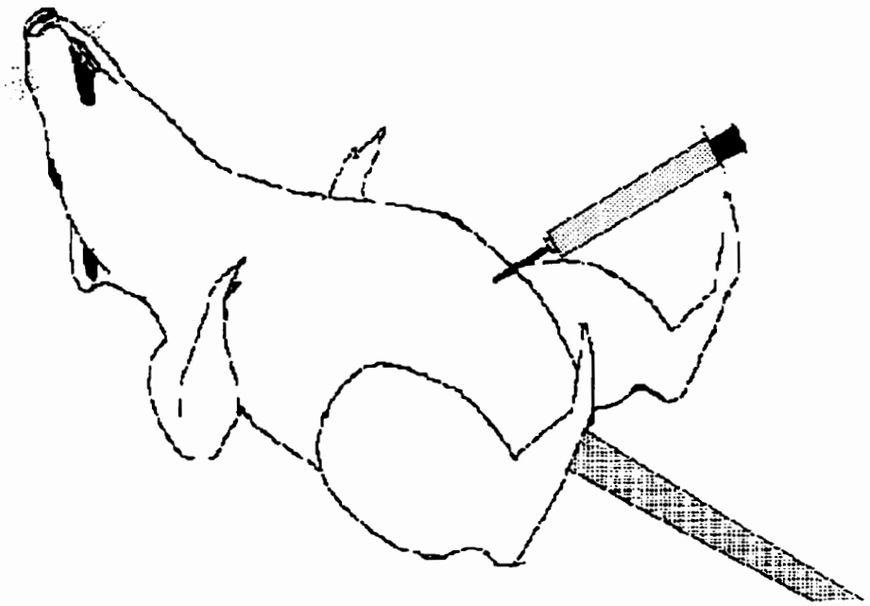

Each animal used in an experiment was pre-treated with Atropine™ (0.4 mL/kg rat, i.p.,) and anaesthetized with 50 mg/kg-rat (i.p.) Somnotol™ (Na Pentobarbital) initially and additional 15 mg/kg-rat Somnotol™ whenever needed. The additional Na Pentobarbital was introduced using a plastic capillary tube inserted into the abdomen. The additional aneasthesia injections depend on a number of factors, to be discussed later. Additional atropine after the initial injection is not necessary but if the pretreatment dose was not given the animal can choke on its own saliva.

Having achieved suitable sedation (in about 10 to 20 minutes after the Na Pentobarbital injection) the trachea of the animal is intubated using a 18G (gray) catheter for the bigger rats and a 20G (green) catheter for the smaller ones. The intubated catheter is connected to a rodent ventilator and the animal is artificially respired with a mixture of N_2O and O_2 gases. The percentage mixture of the two gases is chosen to maintain the partial tension of oxygen (PaO_2) at normal levels (110 to 130 mmHg). The respiration rate and volume are adjusted so that $PaCO_2$ remains at the desired level.

The temperature of the animal is maintained at 38 ± 0.1 °C using a water pad connected to a temperature control unit. When the animal is in the MR scanner a pair of air tubes are added for accelerated cooling when necessary.

Blood pressure is monitored continuously using a tail artery catheter. The tail artery catheterization is described fully in the section on surgical procedures. The blood pressure is monitored and maintained between 90 to 120 mmHg by injecting 5 mg/kg-rat of Na Pentobarbital whenever the blood pressure reaches 120 mmHg. The elevated blood pressure therefore functions as a crude indication for the need of additional sedation. Another crude indicator comes from heart beat regularity, which is monitored using the same blood pressure monitoring unit. For example if the heart beat is irregular, it can be due to overdosing.

Blood from the animal is sampled at a regular interval of 30 minutes. The amount of blood sampled each time is insignificant as only < 0.1mL is withdrawn.

Details of the blood sampling procedure are described later when tail artery catheterization is discussed. It is worthwhile mentioning here, for completeness, that blood gases and other physiological parameters are obtained from the sampled blood using a Radiometer ABL 330™.

b) Animal Surgery

Animal surgery was performed when a surgical plane of sedation was achieved. The surgery involved:

1. tail artery catheterization
2. MR surface coil placement, on the rat skull
3. indicator injection catheter placement at the ECA, and optionally
4. the placement of an additional indicator injection catheter at the right femoral vein (RFV)

(1) Tail Artery Catheterization

The tail artery catheter assembly consists of: (a). a 5 mL syringe, (b). a 3-way stopcock connected to the syringe, (c). a short connecting tube with a site for repetitive needle insertion, linked to the 3-way stopcock and (d). another longer connector joined to the short one, with one end attached to a 24G (yellow) Teflon catheter. The 5 mL syringe is half filled and the connections filled, with heparinized saline (1/100 Heparine Leo® by volume). Tail (caudal) artery catheterization can be achieved by first cutting open a 1 cm line along the centre of the rat tail, 2 cm from the start of the tail, while the animal lays on its back (see

Figure 4.3). Note that it is critical to have the incision at the centre, otherwise isolation of the tail artery can be difficult. An indication of a good position is that the cut is between two large tendons. Having cut open the tail, the next step is to isolate the tail artery underneath the tendons. If successful, a thread is tied at the distal end of the exposed tail artery while another thread is half tied (loosely tied) at the centre, to pull up the tail artery for temporary stoppage of blood flow. At this point a small amount of local anesthesia is applied onto the exposed artery. A small cut is then made at the artery (1/3 the artery cross section, use a surgical microscope if available[1]) and the 24G (yellow) Teflon catheter of the assembly is inserted retrograde into the hole. Finally, the catheter inside the tail artery is secured by tightening the loosely tied thread.

[1]Before a hole is cut, make sure that the artery is free of lining tissues. To check for the linings, position a pair of fine forceps underneath the artery and by partially blocking the blood flow, the uneven thickness of an artery wall indicates the presence of lining tissues. The lining tissues can be separated using two pairs of forceps.

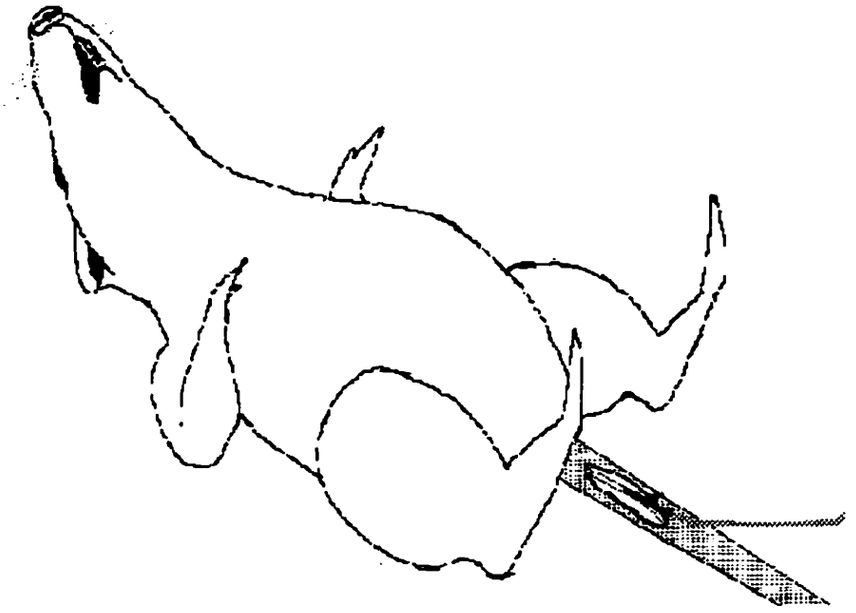

Figure 4.3: Caudal Arterial Cathetering

(2) MR Surface Coil Placement

The procedure for the placement of a ^{2}H sensitive surface coil on the skull of the rat includes:

1. Removing an oval piece of skin from the skull, starting the incision between the eyes and ending at the neck. (This step exposes the skull and tissues adjacent to the skull. Also, this step removes MR signal contributions from the skin.)
2. Removing or retracting muscles attached to skull, at the location of the surface coil (including parts of the temporalis and clavotrapezius muscles).

3. Removing a thin layer of tissue on the frontal and parietal bones, leaving only the bare skull intact at these locations. Intra-skull artery hemostasis can be achieved with bone wax.

4. Fixing the surface coil tightly onto the skull to maximize MR signal. To fix the surface coil:

   i. use a 0-silk, black braided cutting thread and tie its end at one side of the zygoma, as close to the gregma end as possible,

   ii. tie the thread to the surface coil (in a way that the position of the coil on the thread can be adjusted when needed),[2]

   iii. tie the thread to the other side of the zygoma, as symmetrically as possible.

[2]Let the thread run throught the two holes on the coil, if the same coil for this study is used.

(3) Injection Catheter Placement

The injection assembly is as follows: (a). a 1 mL syringe, connected to a stopcock; (b). a 24G catheter that has been forced into a plastic capillary tube about 0.5 meters long; the other end of the capillary tube makes use of the tip of another 24G Teflon catheter. The location for the indicator injection catheter is the ECA. (It is fed retrograde.) This location is chosen so that on the one hand it is as close to the brain as possible, while on the other hand so that the indicator bolus injection location will cause minimum perturbation of the system flow. Provided that care is taken to position the catheter within the ECA, the above mentioned objectives can be attained. It is important to be as close to the brain as possible so that an instantaneous bolus injection can be achieved. This means that although the catheter has to be within the ECA, its tip must be as close to the common carotid bifurcation as possible (Figure 4.4). Placement of this injection catheter can be accomplished by:

1. Making a right lateral incision in the neck.
2. Coagulating and cutting small exposed veins.
3. Dissecting the sternomastoid, omohyoid and the disgatric muscles.
4. Using threads to pull away the muscles dissected for a clear field of view.
5. Isolating, coagulating and cutting the occipital, ascending pharyngeal and superior thyroid branches of the ECA.

6. Isolating the ECA and fastening it at the most distal end.

7. Exposing and isolating the ICA.

8. Half tightening a thread at the centre of the ECA and pulling with enough tension to overcome blood pressure (in order to prevent bleeding when catheterizing).

9. Applying a small amount of local anesthesia to the ECA.

10. Cutting a small hole as close to the tied end as possible.

11. Inserting a 24G (yellow) Teflon injection catheter (fed retrograde) into the hole and tightening the half tied thread on the catheter; a Teflon catheter is preferred over a plastic one because of better anticoagulation; in any case a sufficient amount of anticoagulent (such as Heparin Leo®) must be used.

12. Making sure that the tip of the catheter is within the ECA; if not, hold on to the stub of the tightening thread and adjust the catheter position accordingly. The final step is critically important. When the tip crosses the carotid bifurcation, blood flow to the brain is disrupted.

Figure 4.4: Location of the Carotid Bifurcation and Position of the ECA (External Carotid Artery) Injection Catheter.

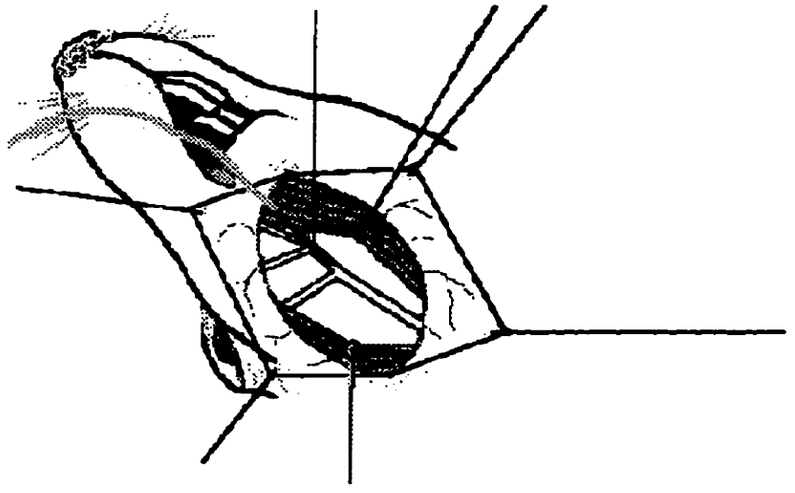

(4) Additional Injection Catheter Catheterization at the Femoral Vein

The assembly for indicator administration at the femoral vein is identical to the one used at the ECA. The right femoral vein (RFV) was catheterized for the CBF underestimation assessments described in Chapter 7. For RFV catheterization:

1. the skin is cut open 2.5 ± 0.5 cm long between the right thigh and the groin (Figure 4.5)
2. the superficial epigastric vein is coagulated and cut

3. the proximal section of the RFV (darker and bigger), which runs along side the RFA (lighter, smaller, but highly elastic) and neural fibers (white) are isolated
4. a thread is tied at the distal end of the isolated RFV and the middle is loosely tied
5. a plastic capillary indicator injection tube is inserted and the loosely tied thread is tightened
6. the catheter is positioned 0.5 cm before the point at which a slight resistance is encountered (by retreating 0.5 cm from where the resistance was felt, while holding onto the thread stub)

Figure 4.5: Location of the Right Femoral Vein Catheter.

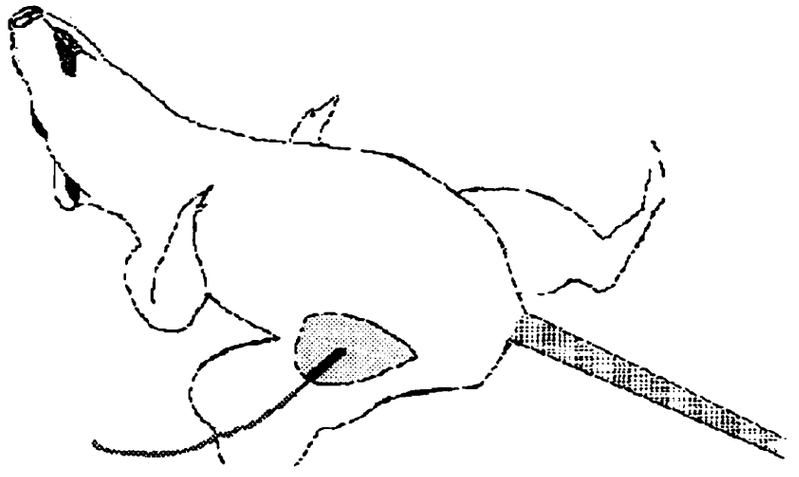

(5) Blood Sampling for Blood Gas etc. Measurements

The physiological parameters are measured at the beginning of the rat tail artery through blood sampling. The steps involved in blood sampling are:

1. withdrawal of 1.5 ± 0.1 mL of blood from the animal into the tail artery catheter assembly using the 5 mL syringe
2. filling a capillary tube with blood at the point for needle insertion on the short connector
3. pushing back the 1.5 ± 0.1 mL blood into the animal
4. measuring blood gases and other physiological parameters using the ABL 330™

c) Data Acquisition

Once the rat has been prepared according to the precedures outlined above, it is transferred into an animal holder. The position of the surface coil is such that, when the animal holder is inserted into the scanner, it coincides with the origin of the x and y gradients. All necessary connections are made before putting the animal holder into the magnet.

The MR scanner used in this study was the Bruker BIOSPEC 7/21 (7 Tesla magnetic field strength, 21 centimeter bore diameter) imager in the NMR Laboratory of the Manitoba Health Sciences Centre. The scanner computer was a Unix based X32. The operating software for imaging (as well as spectroscopy)

was UXNMR 940501. After tuning the surface coil to the ^2H resonance frequency, shimming is done using the proton signal. This is because shimming at the ^2H signal using the naturally occuring ^2H in rat brain is not possible, due to its low natural abundance. The rat at this point is ready for data acquisition. A total of 360 FIDs are acquired (NR = 360) at a rate of 1 scan per second, 2 scans per FID, using a 90° hard pulse (approximately). The indicator is injected into the ECA at the beginning of the 15th FID. The rate of indicator injection is as fast as possible, which is usually less than or equal to 1 second, for a bolus size of 0.2 mL or smaller.

At this point a right femoral vein (RFV) indicator injection experiment can be carried out alternately with the ECA experiments and used to correct for indicator recirculation. (See Chapter 7 for details.) The indicator injection procedure is identical to that for injecting at the ECA. Figure 4.8 shows a typical experimental data set.

The type of indicator used for CBF measurement was [^2H]Water (Heparinized [^2H]Saline). The size of the bolus was either 0.1 or 0.2 mL (usually 0.2 mL unless the MR signal was too strong) at the ECA and 0.2 at the RFV.

d) Data Processing

In order to pick out spectral peak heights from experimental data sets, the acquired 360 FIDs need to be processed into spectra. Figure 4.6 shows a typical

spectrum with a single peak from deuterium resonance of [^{2}H]water. Data processing includes the following:

1. arranging the data set into a 2-dimensional representation, one for the FID and the other for FID number
2. performing the following 1-dimensional operation along the FID direction:
    i. base line correction (BC)
    ii. LB = 50, line broadening
    iii. EM, exponential multiplication
    iv. FT, Fourier transformation
    v. phasing, which is normally at the [^{2}H]water signal but when an indicator mixture is used (see Chapter 8), phasing is performed at all chemical shifts
    vi. picking peak heights, an automated process performed by a subroutine built into the UXNMR software. A shortcoming of this subroutine is that it cannot find peaks when the signal is small. A merit of this subroutine is that it uses an extrapolation algorithm for picking peak heights, resulting in the selection of the highest peak value in the vicinity of the peak's CS.
3. transforming peak height values from binary to ascii

4. performing ftp to get the ascii data from the X32 MR scanner computer to a personal computer *via* the internet

5. using Excel® software for data presentation and futher processing

Figure 4.6: A $^{2}H_{2}O$ Spectrum

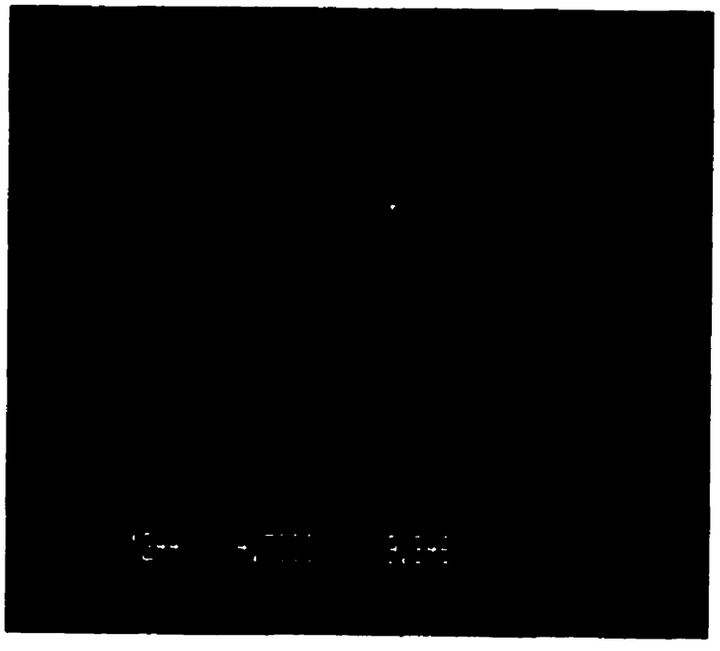

Figure 4.7a: Typical Indicator Washin and Washout Curve

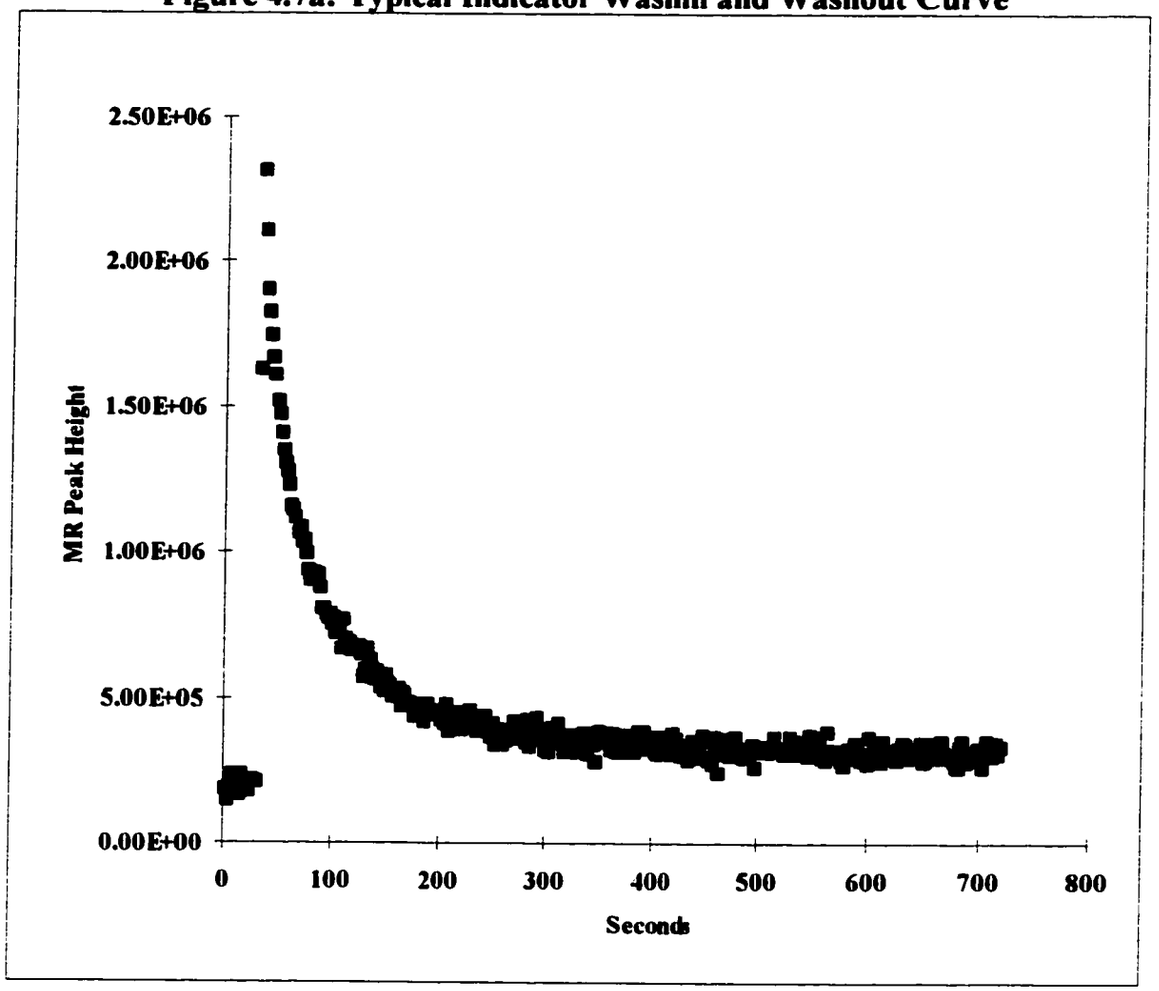

4. Observation and Discussion

Figure 4.7a shows a typical result from the CBF experiment described previously; each point in the figure represents the peak height of one acquired spectrum and is a relative measure of indicator concentration at a particular time. Figure 4.7b shows the first 120 FIDs from a typical experiment for comparison. An important feature of this result is that the data set resembles an 'ideally' instantaneous bolus injection experiment (IBID). Figure 4.8 is a conceptual IBID

sketch taken from Lassen and Perl[1]. Notice that an IBID has the following characteristics:

1. very fast indicator washin into the brain
2. fast indicator washout initially, followed by some kind of geometrical or exponential decay, and
3. asymptotic approach to a constant or base line level, depending on whether or not the indicator recirculates

In contrast to the IBID is the right femoral vein (RFV) bolus injection experiment given in Figure 4.9. In this case, indicator washin to the brain is not instantaneous and washout from the brain slower. Since the CBF modeling algorithms developed in Chapter 3 are for IBID cases, the closer an experiment resembles the IBID one the better.

Figure 4.7b: FIDs (1-120) for Typical Indicator Washin and Washout Experiment

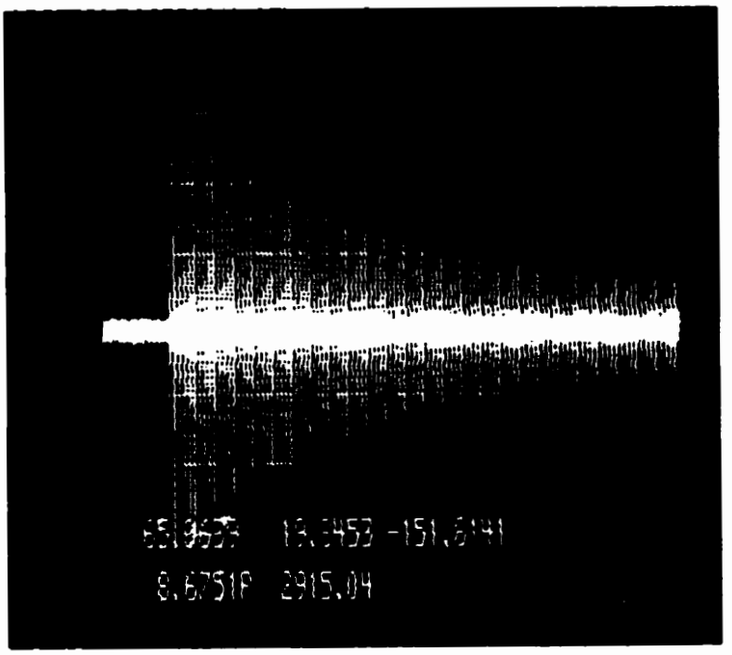

Figure 4.8: Instantaneous vs. Non-Instantaneous Injection

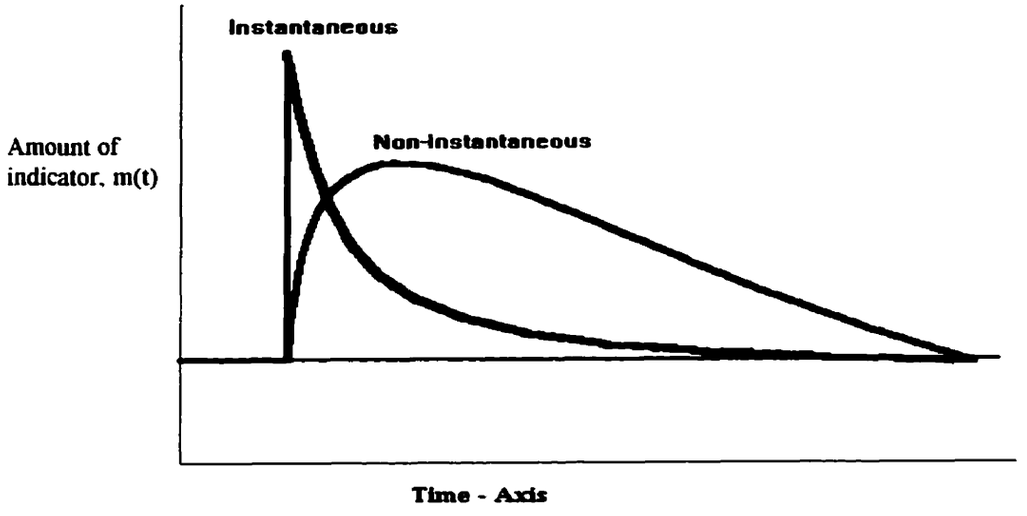

The temporal resolution of the experiment is 0.5 Hz. It was found that this resolution is sufficient, for it can resolve the direct transit of indicator *via* the intra-vascular bed. The signal from the intra-vascular indicator transit (ie. indicator which travels directly from artery to vein without being taken-up by tissue and hence moves through the brain very quickly) is essentially a spike in the semi-log plot of a typical data set (Figure 4.10). Lassen and Perl[1] suggest the spike exists in theory only and cannot be resolved by radiological methods. A sampling frequency of one datum per every 2 seconds (0.5 Hz) is fast enough for us to capture the initial spike phenomenon. Also, signal strength (and signal to noise) is high, as shown in Figure 4.10. The high signal strength can be sacrificed somewhat for even higher temporal resolution (for example with 2 Hz sampling frequency). Potentially high temporal resolution could be employed to study the kinetics of intra-vascular indicator transit.

Figure 4.9 Typical Femoral Experiment (a Non-Instantaneous Case)

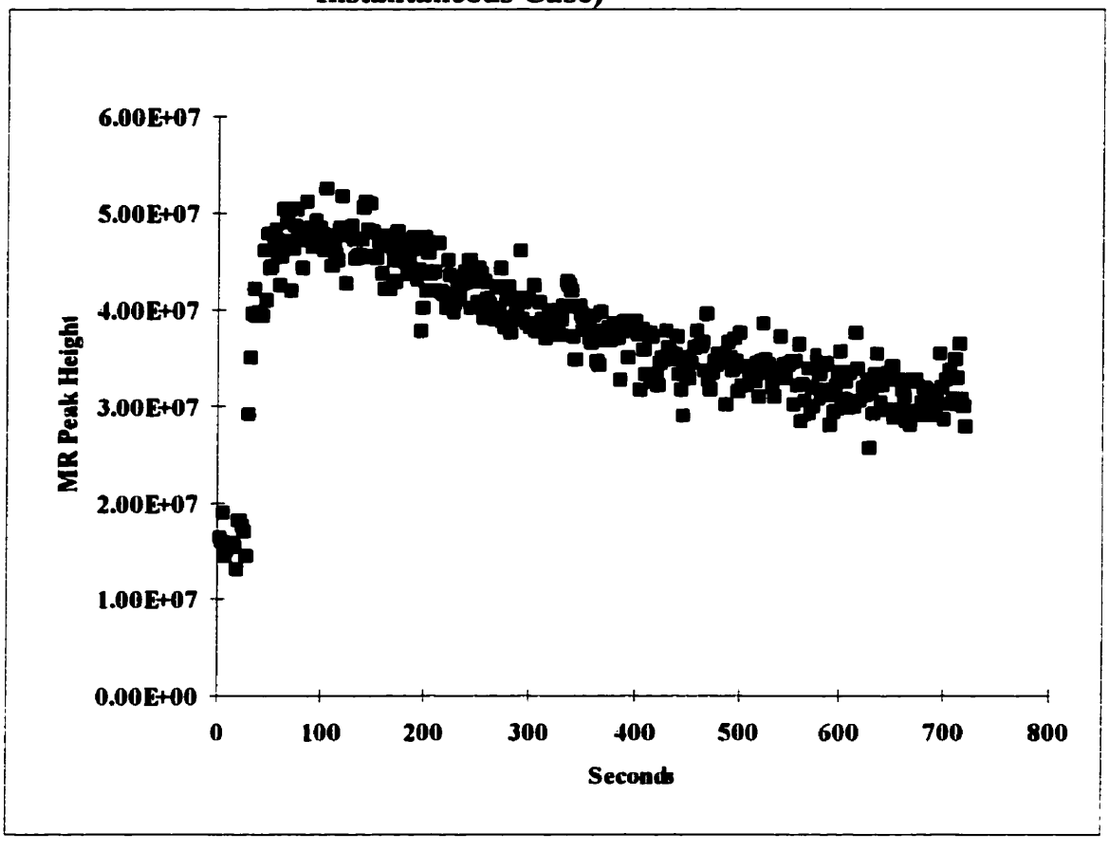

Figure 4.10: Semi-Log Plot of Typical MR Data (expt. 29c)

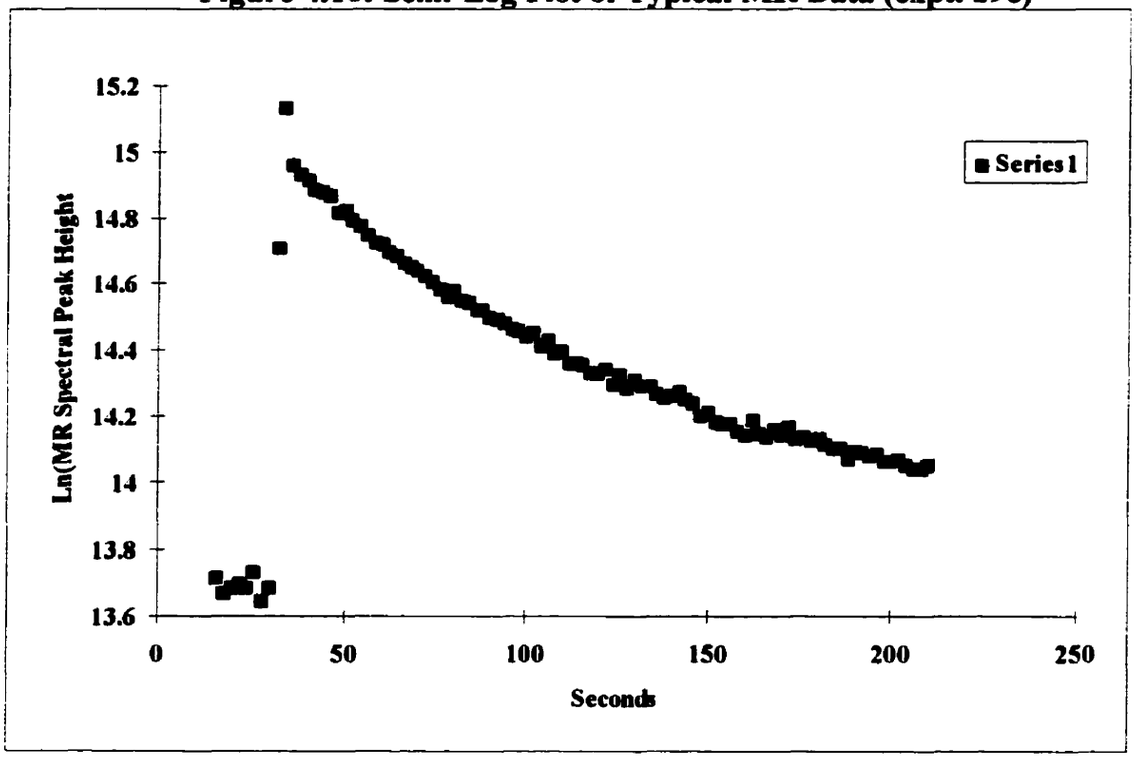

Figures 4.11(a) to 4.11(c) show CBF versus indicator injection time for three rats using the experimental techniques developed and described in this chapter. In obtaining the results of Figure 4.11, the $PaCO_2$ of the rats was maintained at normal levels (35 mmHg < $PaCO_2$ < 45 mmHg). The only parameter that was allowed to vary was the indicator injection time. The CBF values were obtained using the CBF modeling procedures outlined in Chapter 5. (See sections on fCBF(n-23) modeling). These figures show that as the indicator injection time increases, the measured CBF value decreases. The negative correlation is due to increasing spread in the bolus as injection time increases. For long injection times, part of the bolus at the leading end of the spread will have left the brain before the

trailing end arrives at the brain. A consequence is that the initial spike is less sharp, resulting in a reduction of the numerator of Eq. (3.25) (S_{max}), and ultimately an underestimation of CBF. (See Figure 4.9). This was one reason why in the final CBF protocol the indicator injection time was chosen to be less than or equal to 1 second.

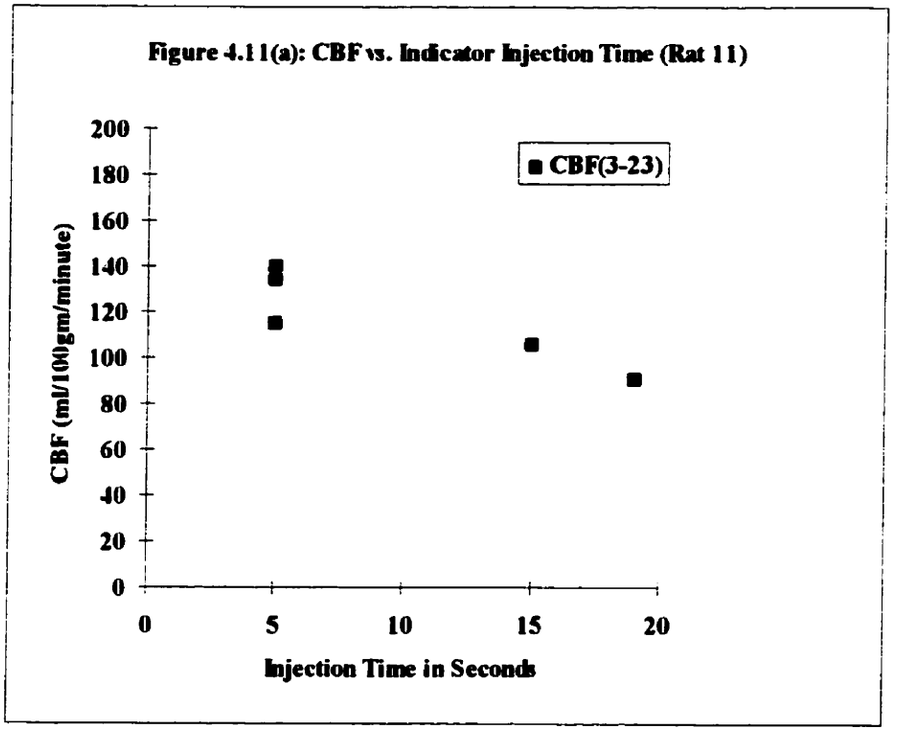

Figure 4.11(b): CBF vs. Indicator Injection Time (Rat 13)

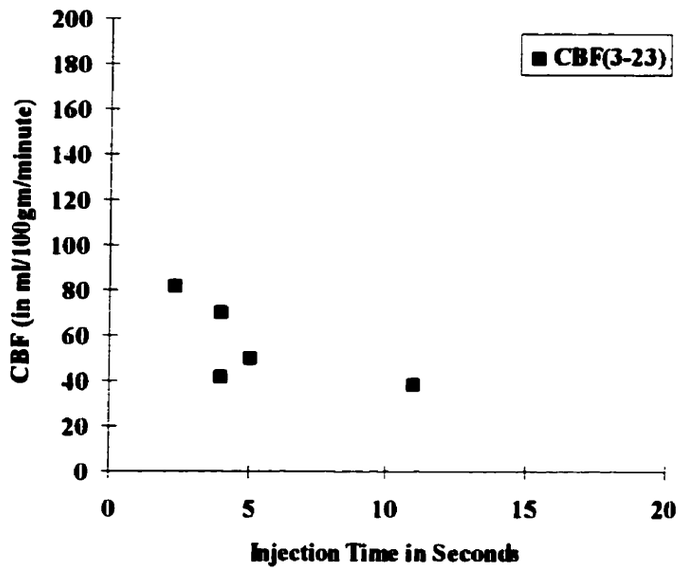

Figure 4.11(c): CBF vs. Indicator Injection Time (Rat 15)

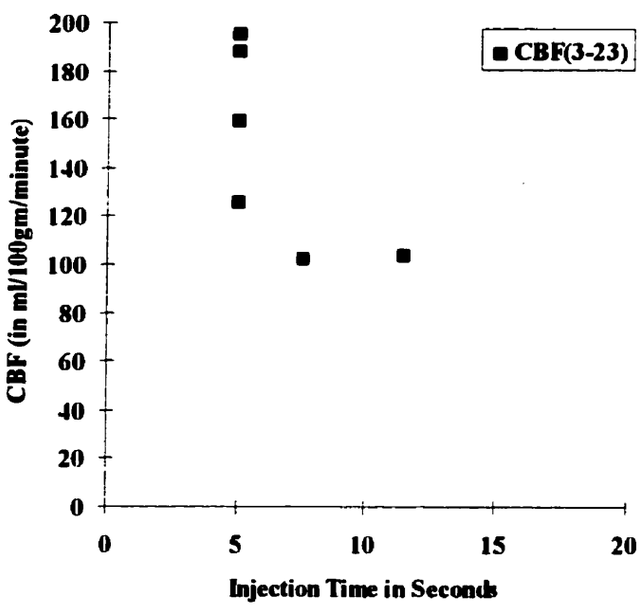

Before the ECA was chosen as the indicator injection site for the final CBF protocol, a number of the other sites were considered, for example the RFV and the right subclavian artery (RSA). Unfortunately, as mentioned before, the RFV injection experiment does not represent an IBID (Figure 4.9). On the other hand the problem with the RSA was experimental consistency. The injection site is distal from the brain (compared to the ECA), so the portion of indicator going to the brain is reduced and SNR compromised. More complicated phenomena occur in the RSA investigation, but an understanding of the phenomena was not pursued. Figures 4.12 show how results can vary between rats when using the right subclavian as the indicator injection site. Interestingly the washin and washout curve shown in Figure 4.12(b) resembles that of Figure 4.9 – a typical result for RFV injection.

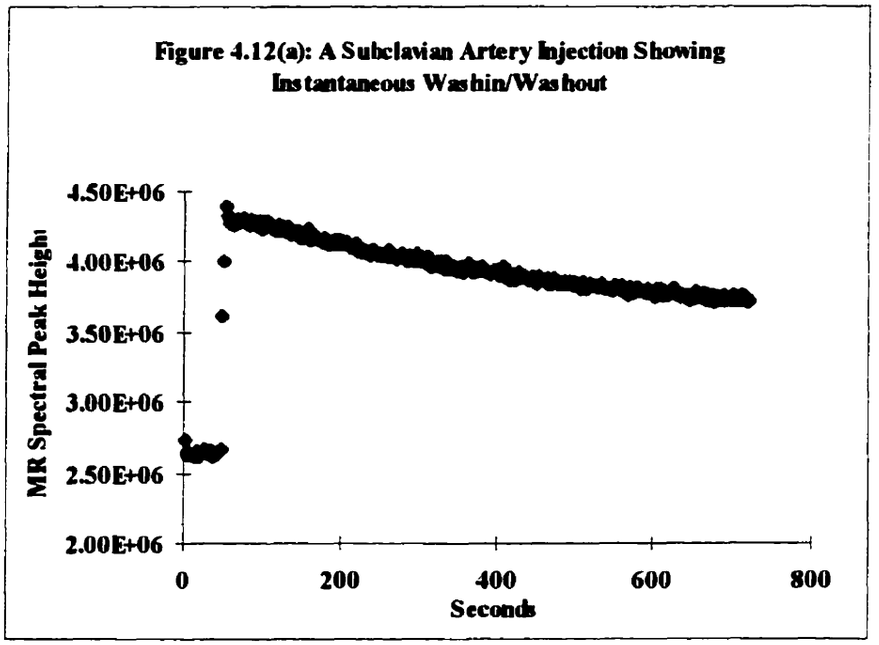

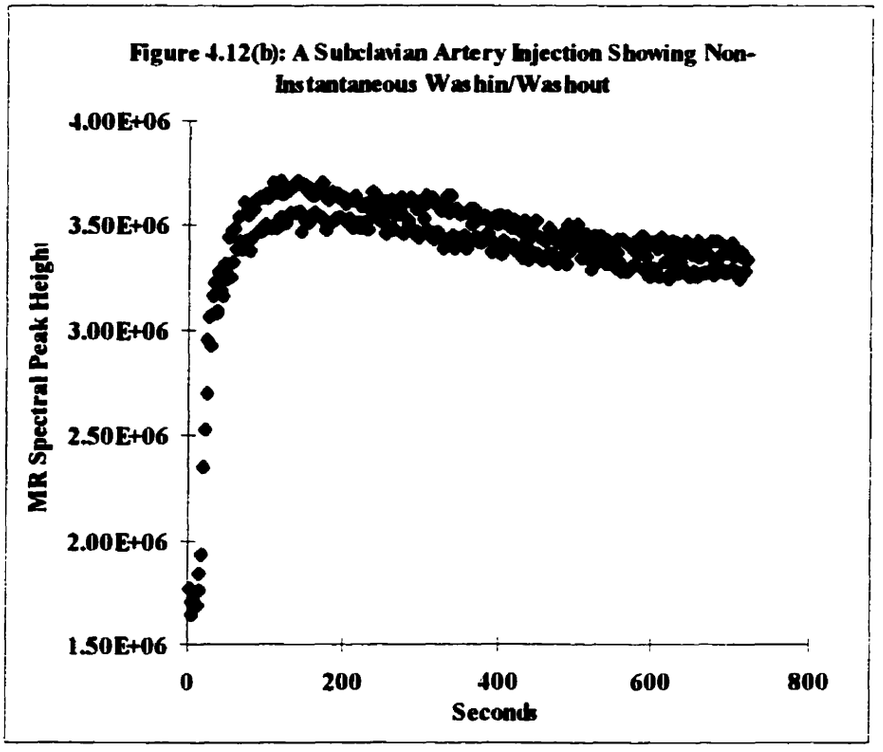

Choice of bolus size was also an important consideration in forming the final protocol. It was found that too large a bolus necessitated a longer injection time and violated the instantaneous injection requirement. At an injection rate of 0.2 mL/second (the rate used in an IBID experiment) a bolus of 1 mL will require 5 seconds to complete. On the other hand, too small a bolus means smaller SNR and uncertainty in the CBF measurement. Various bolus sizes ranging from 0.05 mL to 1 mL were tried. A 0.2 mL bolus size was chosen as a compromise.

It is well known that CBF increases as the $PaCO_2$ of blood increases. On the other hand the regulatory ability for PaO_2 is not clear. Shown in Figures 4.13 are measured CBF versus $PaCO_2$ for 5 rats performed at hyper PaO_2 levels (200

mmHg < PaO_2 < 300 mmHg). It was found that in 2 out of 5 rats (Figures 4.13(a) and 4.12(e)) hyper-oxygen tension destroyed the positive correlation of CBF and $PaCO_2$; and that in 3 out of 5 rats (Figures 4.13(b) - 4.13(d)) the measured CBF values are considerably lower than expected (see Chapter 5). Therefore, regardless of how small an effect abnormal PaO_2 can have, PaO_2 in the final CBF protocol was maintained at normal levels (110 mmHg < PaO_2 < 130 mmHg).

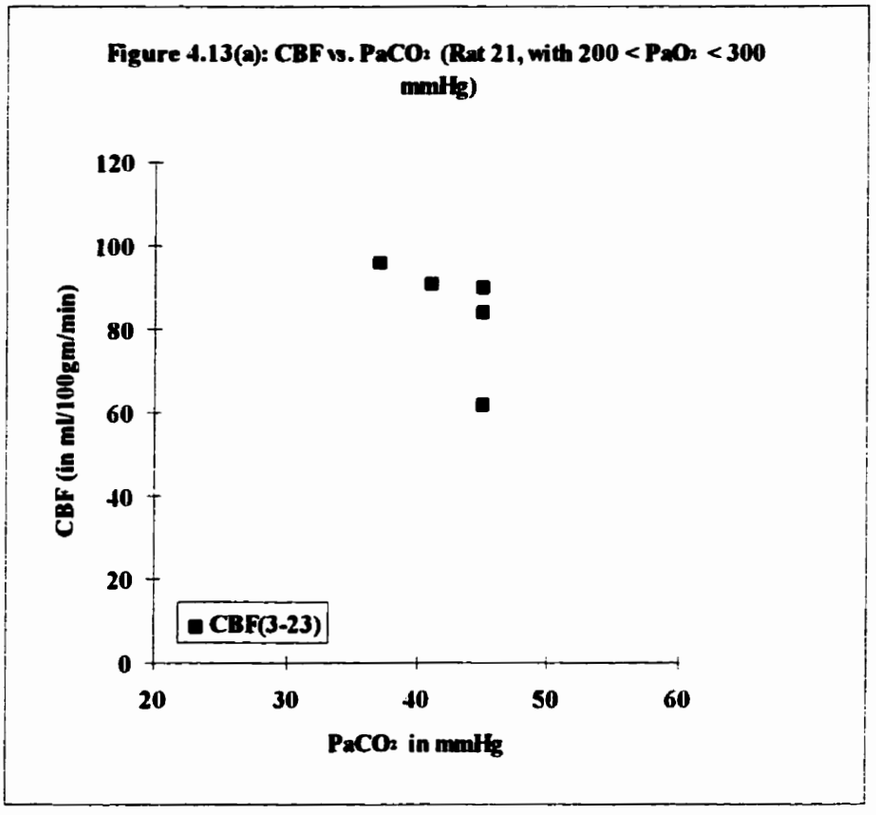

Figure 4.13(b): CBF vs. $PaCO_2$ (Rat 22, with $200 < PaO_2 < 300$ mmHg)

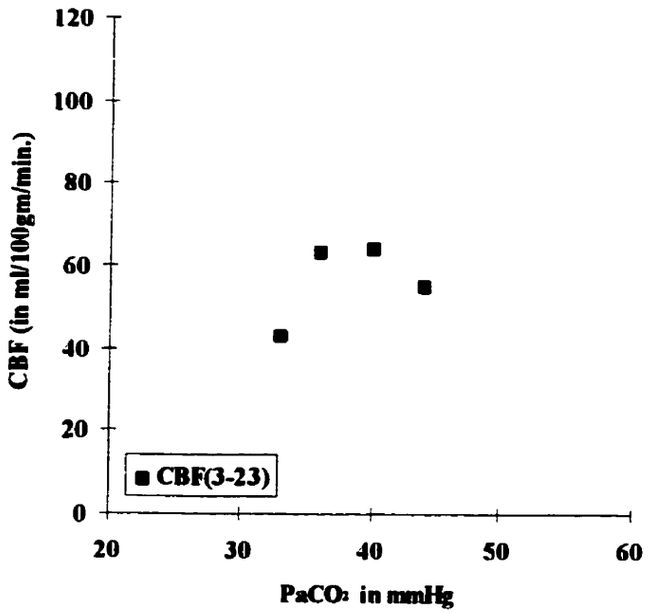

Figure 4.13(c): CBF vs. $PaCO_2$ (Rat 48, with $200 < PaO_2 < 300$ mmHg)

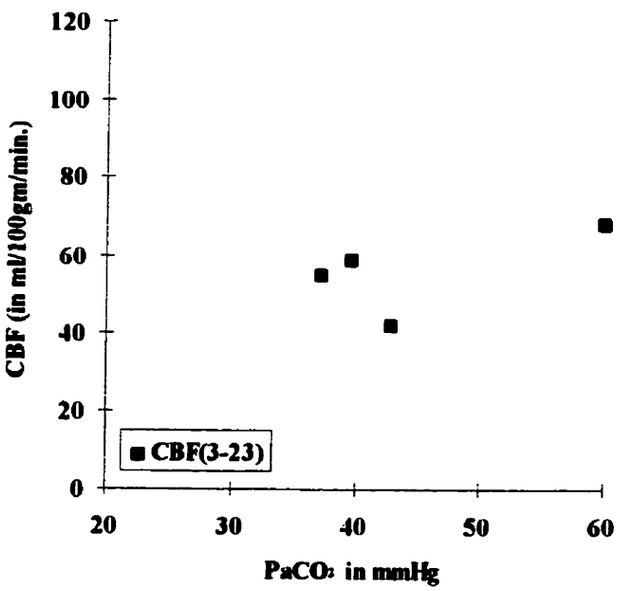

Figure 4.13(d): CBF vs. $PaCO_2$ (Rat 50, with 200 < PaO_2 < 300 mmHg)

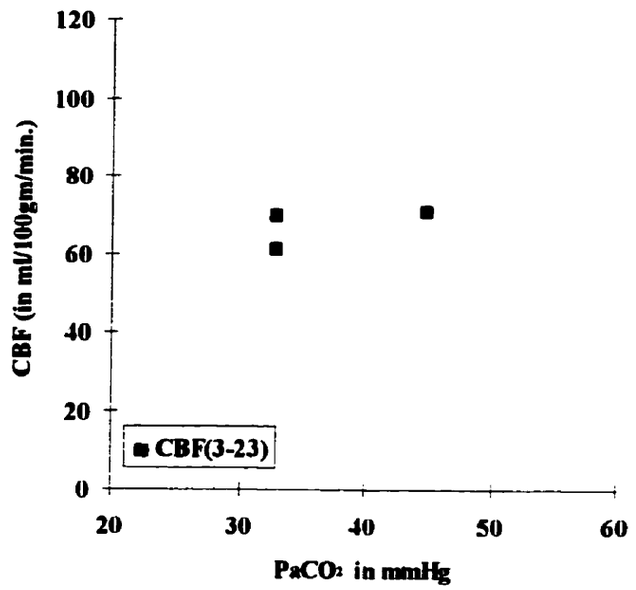

Figure 4.13(e): CBF vs. $PaCO_2$ (Rat 53, with 200 < PaO_2 < 300 mmHg)

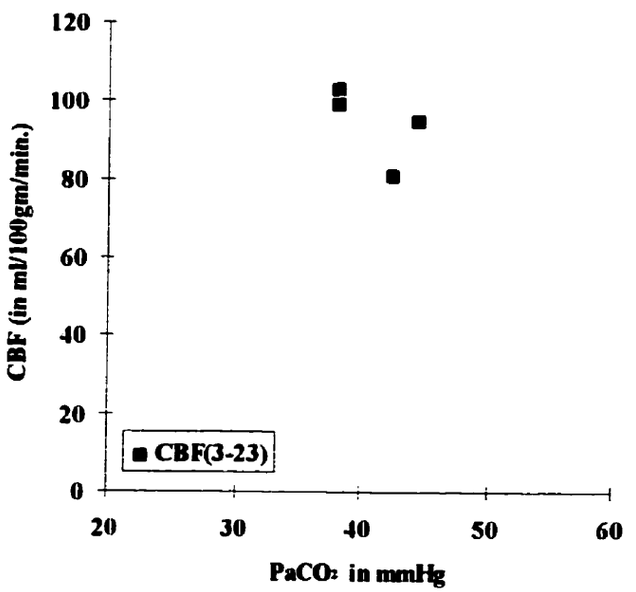

Bibliography[1]

1. Kawamura S, Yasui N, Fukasawa H, 'Rat Middle Cerebral Artery Occlusion Using an Intraluminal Thread Technique', *Acta Neurochir (Wien)* 109:126-132, 1991.

2. Longa EZ, Weinstein PR, Carlson S and Cummins R, 'Reversible Middle Cerebral Artery Occlusion Without Craniectomy in Rats', *Stroke* 20:84-91, 1989.

3. Kim SG and Ackerman JJH, 'Muticompartment Analysis of Blood Flow and Tissue Perfusion Employing D^2O as a Freely Duffusible Tracer, A Novel Deuterium NMR Technique Demonstrated *via* Application with Murine RIF-1 Tumors', *Magn.Reson.Med.* 8:410-426, 1988.

4. Kogure K Busto R, Scheinberg P, Reinmuth OM, 'Energy Metabolites and Water Content in Rat Brain During the Early Stage of Development', *Brain* 97:103-114, 1974.

References

1. Lassen NA and Perl W, *Tracer Kinetic Methods in Medical Physiology*, Raven Press, NY, 1979.

2. Kim SG and Ackerman JJH, 'Quantitative Determination of Tumor Blood Flow and Perfusion *via* Deuterium Nuclear Magnetic Resonance Spectroscopy in Mice', *Cancer Research* 48:3449-3453, 1988.

[1]These papers are not directly quoted but are of help in understanding the concepts presented.

Chapter 5: Blood Flow Analysis

A. Introduction

The goal of this chapter is to generate CBF values from the MR data obtained using the previously discussed CBF measurement protocol (See Chapter 4). The first task is to set up data discrimination criteria, so as to discern between valid and invalid experiments. The second is to analyse and interpret the valid data and to divide these data into suitable regions for CBF modeling. The third is to apply the fast (single compartment) CBF (fCBF) and the average CBF (aCBF) mathematical algorithms to calculate CBF (See Chapter 3).

B. Setting-Up Data Selection Criteria

1. The Need for a Data Discriminator

It is to be expected that mistakes will occur during an experiment, either due to human errors or faulty apparatus. This is the main reason for developing a systematic way of assessing the validity of experimental data. The many potential human experimental errors are:

1. overdosing the animal with drugs, especially with anesthetic
2. over-stressing the animal during experiment, especially towards the end of an 8 hour long experiment
3. surgical mistakes, such as incorrectly positioning a catheter or employing a poor surgical technique causing excessive bleeding, etc., (see chapter 4 for details)

4. errors during monitoring and measurement of physiological parameters, especially blood gases and
5. clogging of catheters during an experiment

Equipment malfunction can also cause errors. For example the break down of MR scanner components, the blood gas apparatus, etc., can invalidate experimental results.

In some situations the data can be rejected using common sense. For example, data sets have been collected where the washin and washout of indicator in the rat brain are not observed, (sometimes this phenomenon can be explained while at other times it cannot). Also, physiological parameters (other than $PaCO_2$) outside the normal range can be considered reason for throwing out data. Under these obvious circumstances discarding the data cannot be considered as biased. The exclusion of $PaCO_2$ as a means of invalidating will become obvious towards the end of this chapter. Briefly, the levels of $PaCO_2$ were intentionally varied, from lower than normal (hypocarbia) to normal (normocarbia) and from normal to higher than normal (hypercarbia) during the CBF measurements. Measurements made at different $PaCO_2$ levels was used to validate the CBF measurement technique.

In some other situations whether to include or exclude data was not as straightforward and an objective way of substantiating or invalidating the data was

required. For example a set of data may exhibit no obvious problems other than a low SNR. Inferior SNR can occur when:

1. animal position in the magnet is less than optimal
2. the animal moves during data acquisition
3. MR coil tuning and/or shimming are/is less than ideal
4. too small an indicator bolus enters the brain (MR SNR is directly proportional to the number of deuterated water molecules residing in the brain)

To objectively discriminate and subsequently throw out results under these circumstances, a $SNR_{threshold}$ was established. Only data that possess SNR > $SNR_{threshold}$ were included in the study.

2. Using $SNR_{threshold}$ as Data Discriminator

In a CBF experiment, indicator injection was started at the 15th datum point (See Chapter 4). Noise ($N_{s.d.}$) was defined as the standard deviation of the first 10 datum points (1st to 10th points); signal (S_{max}) was defined as the maximum MR signal (corrected for background) in the data set. From these two definitions a corresponding signal-to-noise ratio (SNR) can be derived as

$$SNR = \frac{S_{max}}{N_{s.d}}. \qquad (5.1)$$

In this study a $SNR_{threshold}$ was set arbitrarily at 50. Only washin and washout curves that satisfied the condition SNRs > 50 were accepted for CBF analysis.

C. CBF Modeling

Given the final CBF protocol (see Chapter 4), it was observed that all data sets satisfying SNRs > $SNR_{threshold}$ also satisfied the condition SNRs >> $SNR_{threshold}$. Similarly, all typical rejected data sets (such as the one given in Figure 5.2, SNR = 20 ± 1) will have SNR << $SNR_{threshold}$. This lends credibility to the discrimination criteria in that the accepted and rejected data sets are so drastically different that the latter must be associated with problematic experiments. Notice in Figure 5.2 the exceedingly high value of the background MR signal associated with the baseline in front of the peak. This is due to the fact that a number of injections (≤ 4) were performed (without succeeding in obtaining indicator washin and washout) before the result of Figure 5.2 was obtained.

Figure 5.1: A Typical Accepted Data Set

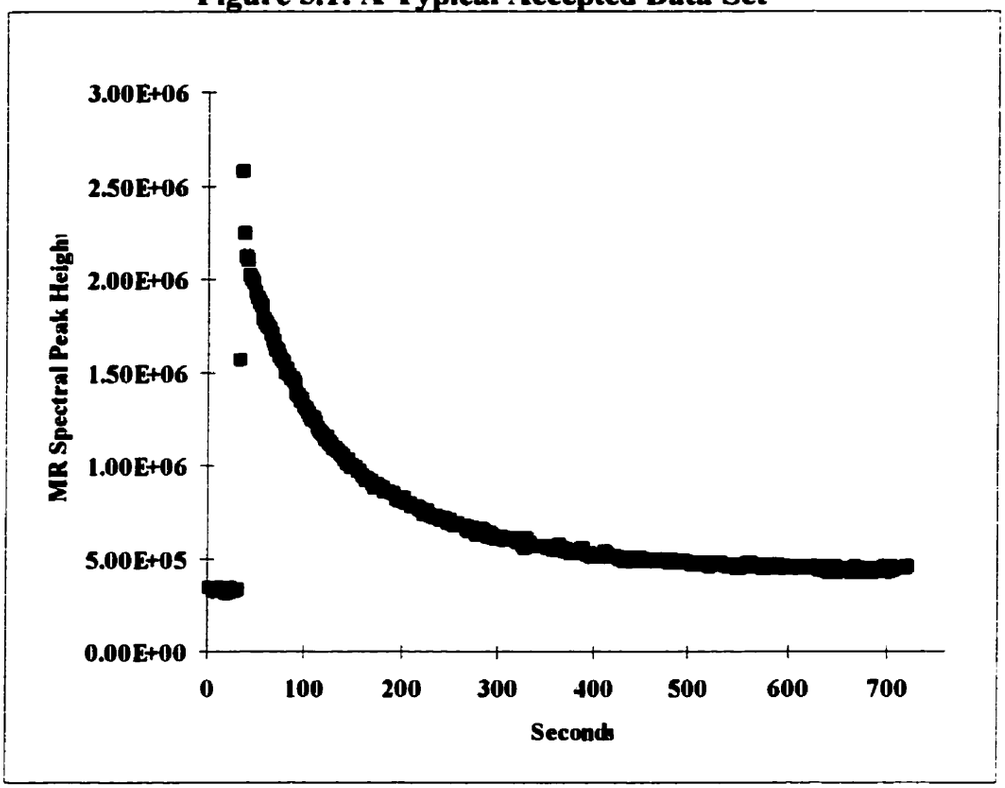

A semi-log plot of a typical accepted data set (as shown in Figure 5.1) is given in Figure 5.3. It is interesting to note that a substantial amount of information about the brain can be derived by looking at Figure 5.3 alone. To this end, it is useful to divide Figure 5.3 into three regions. The first region begins at the 15th datum (the time of injection) and ends at the 2nd point after the signal maximum. The second region begins at the 3rd point and ends at the 23rd (36 to 76 seconds after the injection) after the signal maximum. The third region encompasses all data points beyond the 2nd region. The delineation of these three regions applies equally well to all the accepted washin and washout curves used

for analysis. As will become clear in chapter 7, the end of the 2nd region conincides roughly to when indicator recirculation reaches one quarter of its maximum effect.

Figure 5.2: A Typical Rejected Data Set

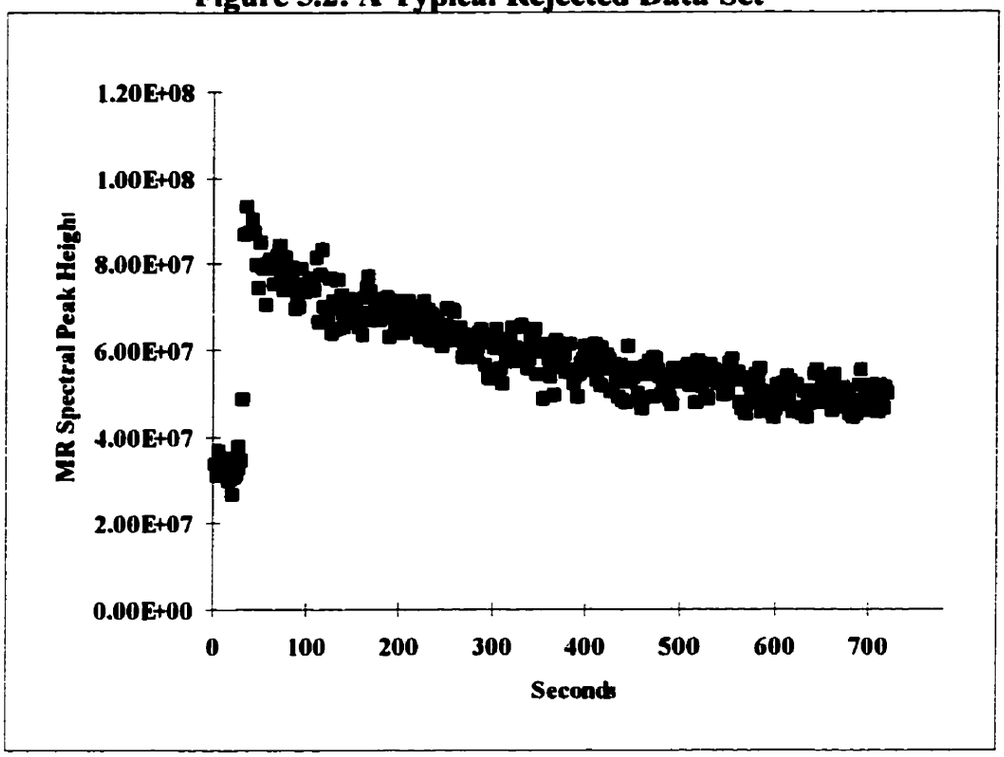

The first and the second regions combined have been referred to as the gray matter compartment[1], the fast compartment or the mono-exponential compartment[1-4] of the brain. It is called the mono-exponential compartment because this region can often be fitted with a single exponential decay curve, or with a straight line on a semi-log plot. From a conceptual point of view, this fast gray matter compartment should also contain of an ultra-fast vascular component as is predicted by Lassen and Perl.[5] Because the ultra fast indicator transit *via* the

vascular bed happens very fast, Lassen and Perl predicted that it would appear as an initial spike on a semi-log plot (that is, region I. See Figure 5.4). Briefly, when a bolus is injected into the brain, some of the indicator is extracted from the arterial bed and enters the constituent tissue. The degree of extraction depends on the type of indicator injected. For [^{2}H]water, the extraction was found to be approximately 85% for the brain tissue (or E=0.85, see Chapter 6). The remaining indicator not extracted will pass directly from the arterial supply to venous supply *via* the capillaries. In other words this component moves through the brain much more quickly than that extracted by the tissue and leads to the appearance of the initial spike. Chapter 6 gives details for calculating the extraction coefficient (E), and discusses how E is related to the initial spike. Lassen and Perl also commented that the spike could not be detected by radiographic means because it happens too fast. (The comment was made before the advent of MR scanning). Figure 5.3 shows that in a typical experiment (using the technique developed) the initial spike for the brain indeed exists. This is the reason for dividing the fast gray matter compartment into the first and second regions; the first region characterizes the intra-vascular indicator transit, and the second region represents the conventional fast gray matter compartment, that component taken up by and eventually washed out of cerebral grey matter. We attributed the detection of the initial spike to the use of:

1. a fast MR technique

2. a bolus injection, and

3. an injection site that is close to the brain (ECA, at the entrance of the brain)

In Figure 5.3 notice that the duration of the spike phenomenon is around five seconds. In order not to smear out the spike phenomenon the MR signal sampling frequency needs to be higher that 0.2 Hz. Our sampling frequency of 0.5 Hz satisfied this criterion.

If the injection is not instantaneous, indicator will enter the brain over a greater period of time. Now, the leading edge of the bolus will begin to move out of the brain before the trailing edge enters. The loss in signal due to intra-vascular transit will in part be compensated by the increased signal associated with the trailing edge of the bolus entering the brain. As such, the spike is not observed and in fact the entire peak region of the washin/washout curve takes on a more rounded appearance.

Figure 5.3: Semi-Log Plot of a Typical Accepted Data Set

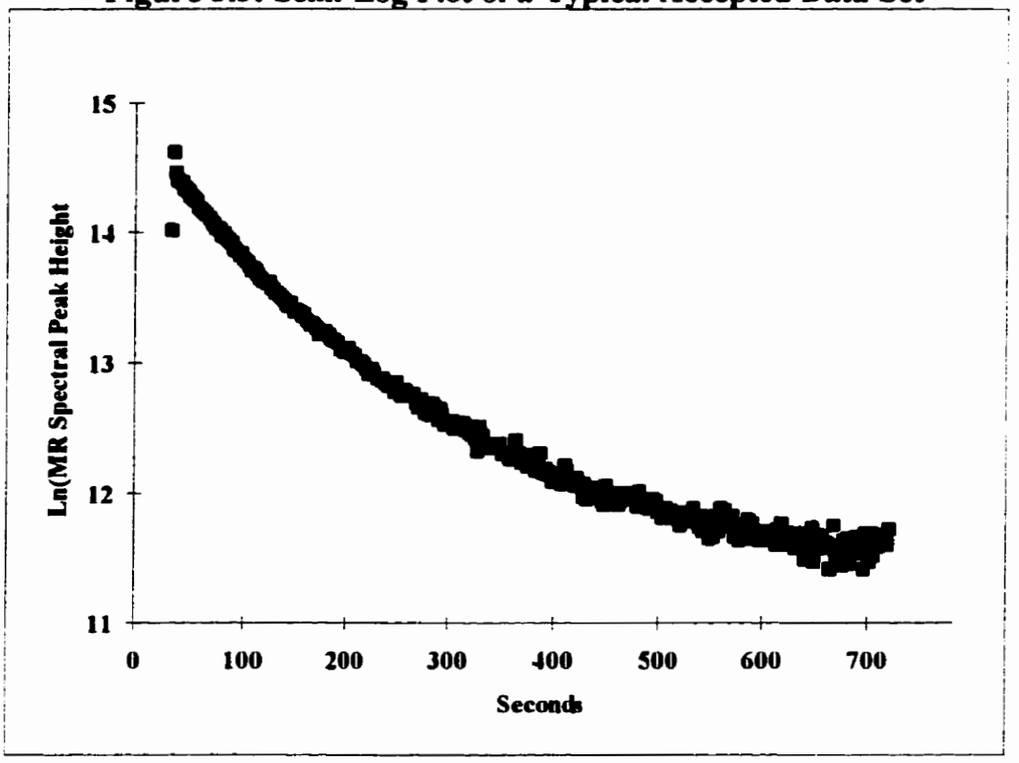

Figure 5.4: Conceptual Semi-Log Plot Showing Initial Spike, Reproduced from Lassen and Perl[5]

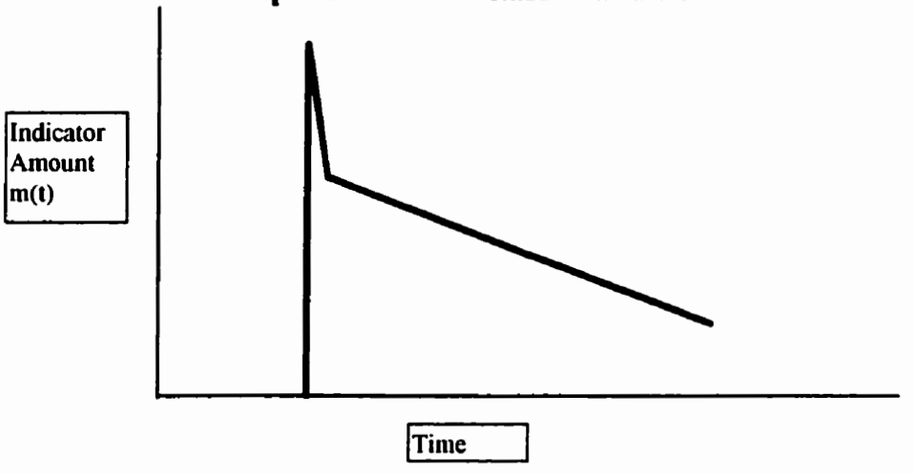

The third region represents a slow white matter compartment. In this region indicator taken up by cerebral white matter will be retained for a longer time. As a result the indicator will washout at a much slower rate than that in grey matter.[1]

This region also embodies an indicator recirculation component (see Chapter 7). The recirculation component becomes more important at larger times. It dominates when the MR signal asymptotically approaches a constant value. At the end of the experiment, indicating uniform distribution of the indicator throughout the animal.

The first and second regions defined above are used for the measurement of the fast gray matter CBF (fCBF for short). The beginning of the data range selected is at the MR signal maximum (see Figure 5.1 or 5.3) and the end at the 23^{rd} point after the maximum. The decision to end at the 23^{rd} point after the maximum (about 50 seconds after indicator injection) was somewhat arbitrary. However, a number of factors were considered before reaching this decision. The first observation is that there is no region on the semi log plot of indicator washout that is truly linear. The further into the experiment (larger time) the more pronounced this curvature becomes. The sources of this curvature are the fact that the indicator is not 100% freely diffusible, indicator recirculation and the influence of white matter flow. As such, choosing a region to analyse gray matter flow is in fact a trade-off between a more accurate and a more precise fCBF modeling method. For example, ending the 2^{nd} region at a point to the left of the 23^{rd} will give a more accurate fCBF value, due to the reduced influence of the slow white matter compartment and recirculation. However, this is at the expense of a more precise value (fewer data points and increased statistical fluctuation). The converse is also true, in that ending at a point to the right of the 23^{rd} will provide a more

precise fCBF value, but at the expense of accuracy (the fCBF will in fact be underestimated, as the region is expanded to the right due to the influence of white matter flow). Practically, ending the fCBF datum range at the 23rd point serves as a first order approximation for the CBF modeling. It also enables one to standardize the CBF technique of the study. The remaining chapters explore the strengths and weaknesses and assess the precision and accuracy of this standardized CBF technique.

The fCBF values were derived as follow:

1. Calculate the MR background signal as the average of the first 10 points of an accepted data set (such as the one given in Figure 5.1)
2. Subtract the MR background signal from each datum point
3. Take the natural logarithm of the MR background subtracted data
4. Fit a straight line to the fast data range using least squares regression, to obtain a slope m, and
5. Use Eq. (5.2) (reproduced from Chapter 3, Eq. (3.30)) to obtain the fCBF value for the experiment

$$fCBF = -100 \times \lambda \times m \qquad \text{Eq. (5.2)}$$

Figure 5.5: A Typical Processed Data Set for Fast CBF Modeling

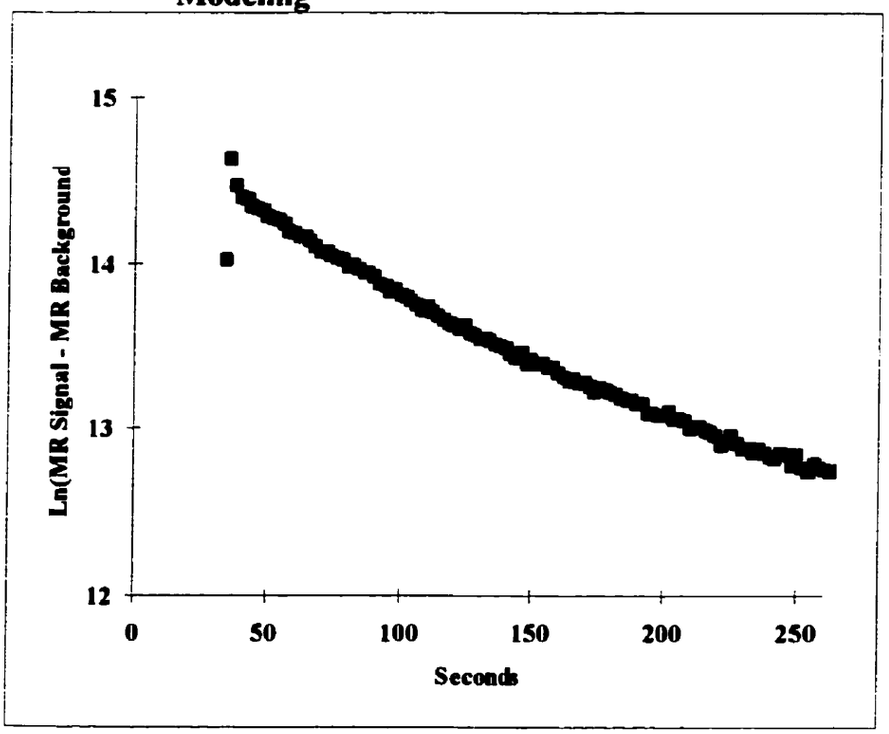

In an effort to investigate the effect of the region of analysis on fCBF, assume that fCBF(0-23) is the fCBF value obtained using the entire 'fast' CBF datum range (a combination of the first and the second regions). Similarly, fCBF(n-23) is the fCBF value obtained using the n^{th} to 23^{rd} data points. fCBF(0-23) corresponds to the fast gray matter CBF that is usually reported in the literature, while fCBF(3-23), calculated using the second region only, is in a sense the pure fast gray matter CBF value, a fCBF value that excludes the intra-vascular component.

The entire washin-washout curve (that is, the whole data set) is used for the average CBF (aCBF for short) calculation. The first step in modeling aCBF is to remove base line values from the data set. This step is accomplished by taking the average of the first 10 points as a base line value and subtracting it from all points, as discussed previously in fCBF modeling. The second step is to remove indicator recirculation. (Figure 5.1 shows that the wash-out of indicator does not return to the base-line, suggesting the presence of indicator recirculation and in particular the eventual uniform distribution of indicator throughout the rat.) In Chapter 7, a technique is described and used for the removal of indicator recirculation from the data. Here, a 'crude' method is used as a starting point for aCBF analysis. This 'crude' method takes the average (aENDs) of the last 30 points (from point 331 to 360), as in Figure 5.1, and subtracts a value of

$$(n-15)\times\frac{aENDs}{360-15} \qquad \text{Eq. (5.2)}$$

from the n^{th} datum point, for n = 15 to 360. It can be seen from the equation that the aENDs is in effect the maximum value to be subtracted and that this value is in fact subtracted from the last point in the washout (for example, n=360). For n=15 (the time injection started), the value subtracted is 0. The equation results in the subtraction of a triangular area from the washin and washout curve. The aCBF is

then obtained using the processed data set and the aCBF equation given in Chapter 3 (Eq. (3.25)) .

$$aCBF = 100 \times \lambda \times \frac{S_{max}}{\int_{t=30}^{t=720} S(t)dt} \qquad \text{[ml/100g/min.]} \qquad \text{Eq. (5.3)}$$

Note that signal integration in Eq. (5.3) is finite (from t=30 to t=720 seconds), in contrast to a 'true' aCBF that is semi-finite (from t=30 to ∞). According to Eq. (5.3) a finite integration will overestimate aCBF. Since acquiring signal from t = 30 seconds to ∞ is impossible, the t = 30 to 720 seconds (11.5 minutes) interval is used here. aCBF represents some sort of weighted average of white matter and grey matter flow, contaminated ever so slightly by a very small intra-vascular component and an inaccurate removal of indicator recirculation.

D. Results and Observations

In the process of finalizing the CBF protocol the relationship between the CBF results obtained and many experimental parameters have been investigated. Some of the results from the investigation, such as injection site, injection time, etc., are presented in the discussion section of Chapter 4. Others are presented in Chapter 6. The following presents only results obtained using the finalized CBF protocol, as described in Chapter 4.

Before presenting the results a few terms regarding the partial tension of carbon dioxide ($PaCO_2$) and oxygen (PaO_2) need to be defined. These definitions are given collectively in Table 5.1.

Table 5.1: Blood Gas Definitions

Low $PaCO_2$	20 mmHg < $PaCO_2$ ≤ 35 mmHg
Normal $PaCO_2$	35 mmHg < $PaCO_2$ ≤ 45 mmHg
High $PaCO_2$	45 mmHg < $PaCO_2$ ≤ 62 mmHg
Low PaO_2	60 mmHg < PaO_2 ≤ 100 mmHg
Normal PaO_2	100 mmHg < PaO_2 ≤ 140 mmHg
Near Normal PaO_2	140 mmHg < PaO_2 ≤ 180 mmHg
Medium High PaO_2	180 mmHg < PaO_2 ≤ 200 mmHg
High PaO_2	200 mmHg < PaO_2 ≤ 300 mmHg

1. fCBF Results and Discussion

Figures 5.6 to 5.10 show fCBF(3-23) versus $PaCO_2$ for individual animals at normal PaO_2 (see Table 5.1). Four out of the five rats have a positive correlation between fCBF and $PaCO_2$, as expected (Figure 5.6, r = 0.97; Figure 5.7, r = 0.50; Figure 5.8, r = 0.98; Figure 5.9, r = 0.96). The reason why a positive correlation between CBF and $PaCO_2$ does not exist for Figure 5.10 (r = -0.91) is not known. Figures 5.11 combines all the rat data, including the problematic data of Figure 5.10. Figures 5.12 is the same as Figures 5.11 except that rat #5 (data of Figure 5.10) is not included. It is evident, from Figures 5.11 and 5.12, that not only does the measured CBF increase with increasing $PaCO_2$ within a single animal

experiment but also for inter-animal experiments (Figure 5.11(a), r = 0.58; Figure 5.12(a), r = 0.86). This observed correlation establishes the validity of the CBF technique developed. Note that Figures 5.6 and 5.9 exhibit overlapping fCBF(3-23) values at $PaCO_2$ ~ 35 mmHg, suggesting that reproducibility may be quite good. (See also Figures 5.15 at $PaCO_2$ ~ 38 mmHg, 5.17 at $PaCO_2$ ~ 40 mmHg, 5.18 at $PaCO_2$ ~ 32 mmHg.)

Figure 5.6: fCBF vs. $PaCO_2$ (at $100 \leq PaO_2 < 180$ mmHg), Rat 93042, (n = 3, r = 0.97)

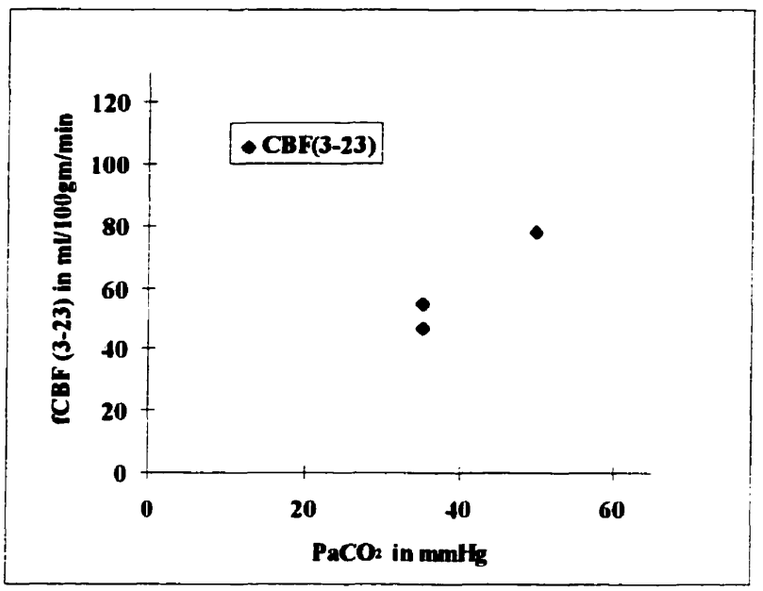

Figure 5.7: fCBF vs. $PaCO_2$ (at $100 \leq PaO_2 < 180$ mmHg), Rat 93053, (n = 3, r = 0.5)

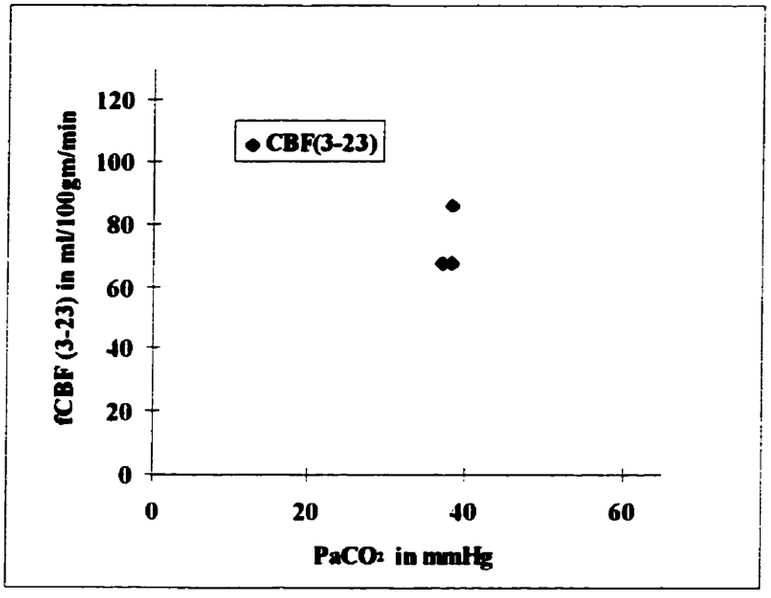

Figure 5.8: fCBF vs. $PaCO_2$ (at $100 \leq PaO_2 < 180$ mmHg), Rat 95021, (n = 3, r = 0.98)

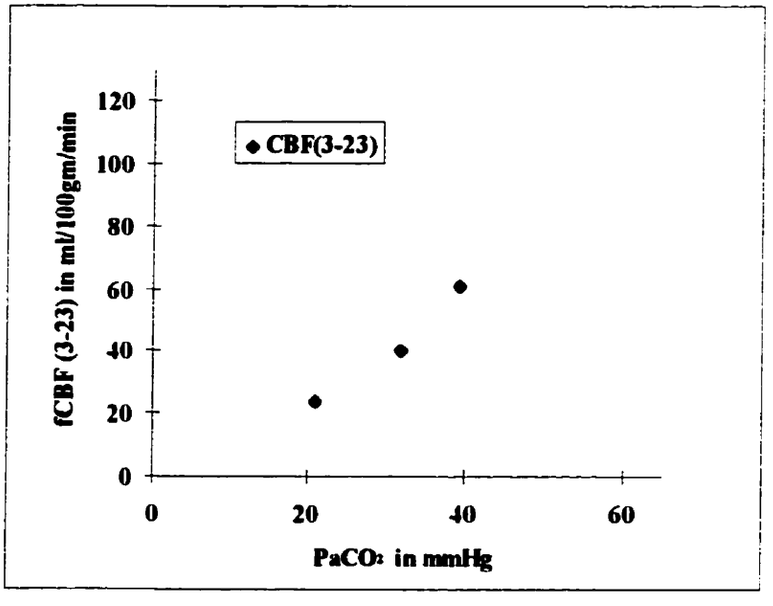

Figure 5.9: fCBF vs. $PaCO_2$ (at $100 \leq PaO_2 < 180$ mmHg), Rat 95022, (n = 3, r = 0.96)

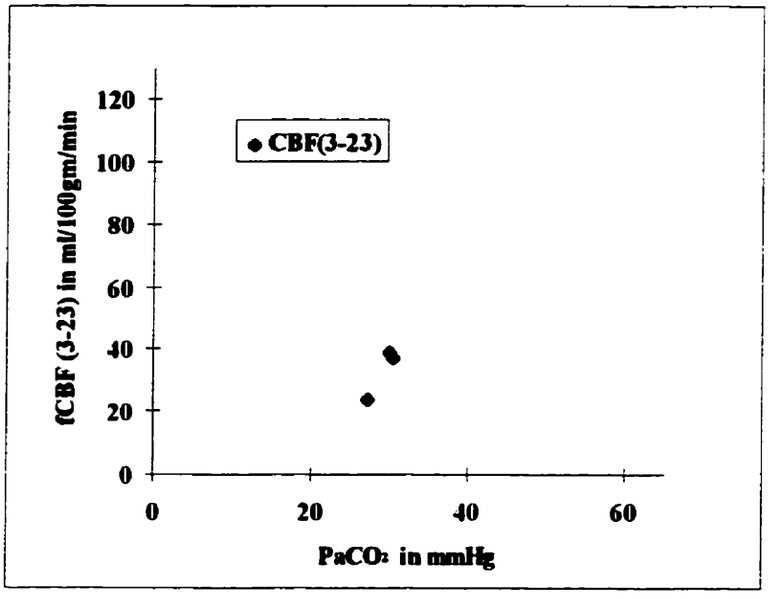

Figure 5.10: fCBF vs. $PaCO_2$ (at $100 \leq PaO_2 < 180$ mmHg), Rat 95020, (n = 5, r = -0.91)

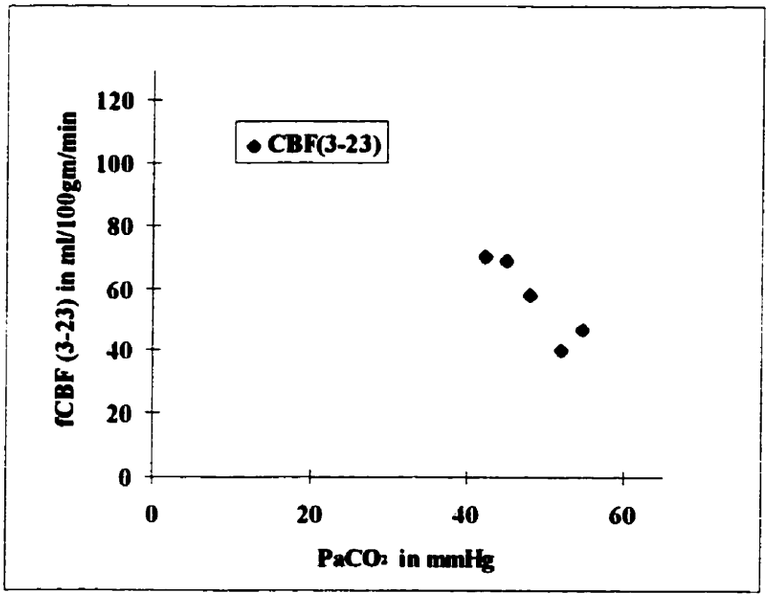

Figure 5.11(a): fCBF(3-23) vs. $PaCO_2$ (at $100 \leq PaO_2 \leq 180$ mmHg), with rat 95020, (r = 0.58)

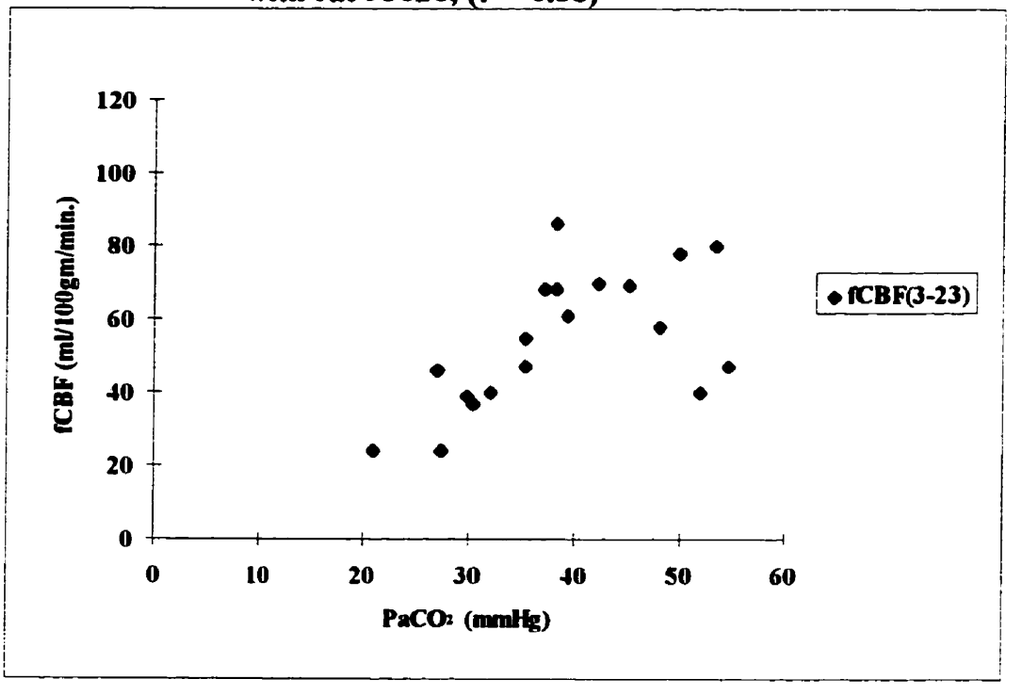

Figure 5.11(b): fCBF(n-23) vs. $PaCO_2$ (at 100 mmHg < PaO_2 < 180 mmHg), with rat 95020, for n=1, 2, 3, ..., 9.

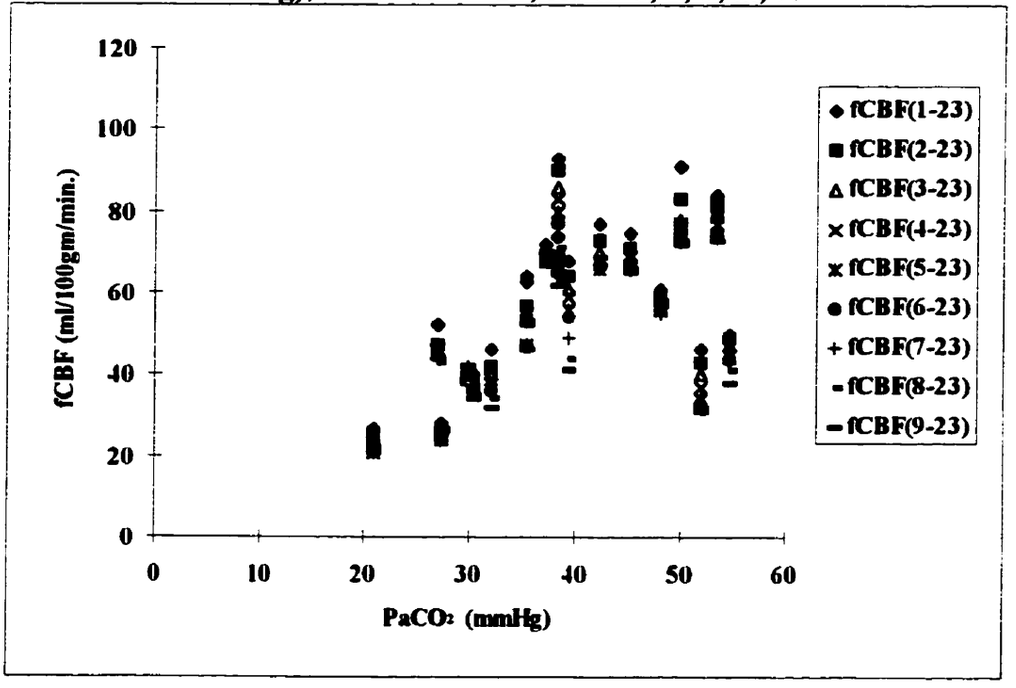

Figure 5.12(a): fCBF(3-23) vs. $PaCO_2$ (at $100 \leq PaO_2 \leq 180$ mmHg), without rat 95020, (r = 0.86)

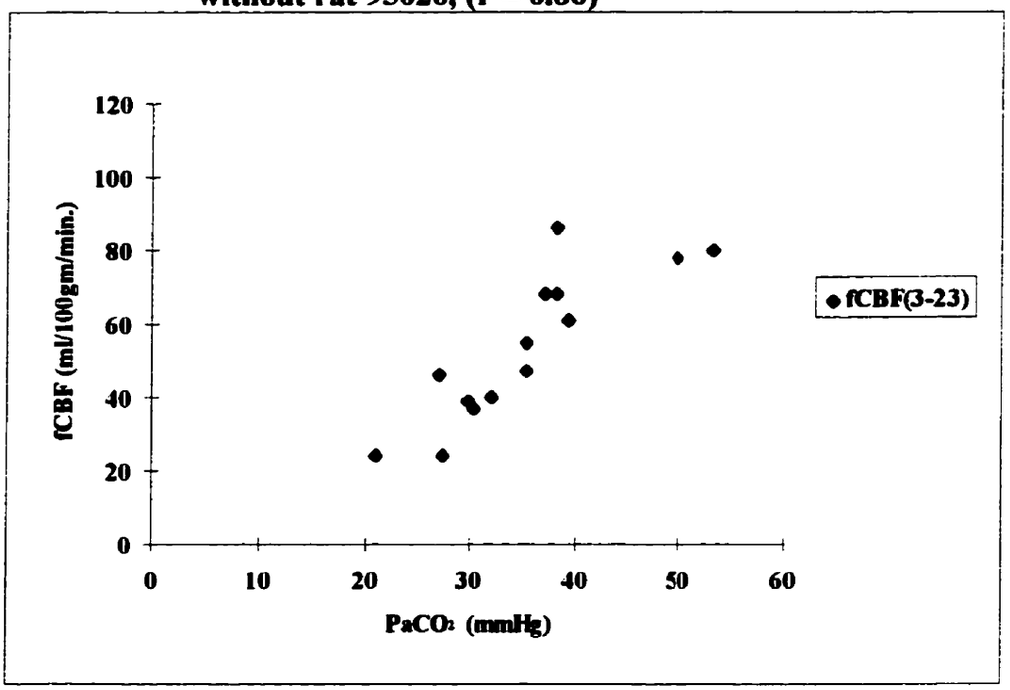

Figure 5.12(b): fCBF(n-23) vs. $PaCO_2$ (at 100 mmHg < PaO_2 < 180 mmHg), without rat 95020, for n=1, 2, 3, ..., 9.

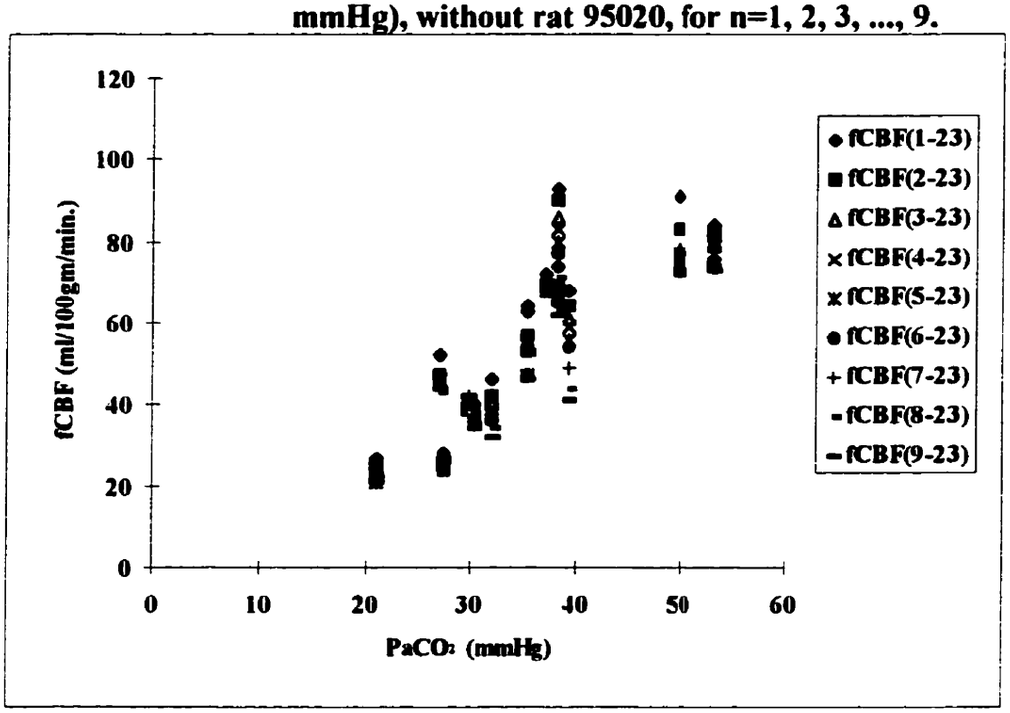

Figures 5.11(b) and 5.12(b) show fCBF(n-23) for n = 1 to 9. In these two figures observe that:

1. fCBF values depend on the choice of n, and decrease as n increases, due to indicator recirculation (see Chapter 7) and due to a more significant influence of the slower white matter flow
2. The magnitude of change in fCBF as a function of n varies, from less than 5 ml/100gm/min to more than 30 ml/100gm/min
3. The average least squares fitting errors from the first 45 experiments of 1993 that passed the data screening criteria mentioned previously are as follows:

st. dev. of	fCBF(1-23)	fCBF(2-23)	fCBF(3-23)	fCBF(4-23)	fCBF(5-23)	fCBF(6-23)	fCBF(7-23)	fCBF(8-23)	fCBF(9-23)
(n=45)	3.31	2.33	2.18	2.25	2.32	2.29	2.48	2.57	2.72

fCBF(3-23) was chosen to represent the fast CBF because the fitting error associated with it was the least. Figure 5.13 shows fCBF(n-23) versus $PaCO_2$ for two rats at low PaO_2 (see Table 5.1). In this figure the linear correlation between CBF and $PaCO_2$ is not very good. But with only three experiments one can not say for sure if this is indeed the case; more experiments will be needed before making a final conclusion. Figures 5.14 and 5.15 show two rats at medium high PaO_2 while Figure 5.16 combines the data contained in these two figures with that of a third rat.

Figure 5.13: fCBF vs. $PaCO_2$ (at $60 \leq PaO_2 < 100$ mmHg), rats 93034 & 93035, (n = 3, r = 0.68)

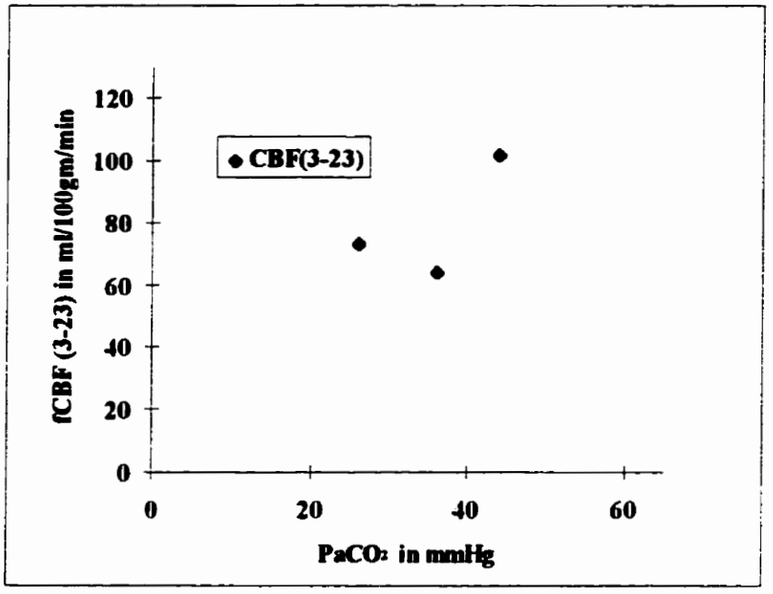

These three figures reveal the same CBF, $PaCO_2$ linear correlation as the data at normal PaO_2. In Figure 5.15, note that at $PaCO_2$ = 38 mmHg, fCBF(3-23) measured for two separate experiments have almost the identical value, indicating once again that the CBF technique developed is quite precise.

Figure 5.14: fCBF vs. $PaCO_2$ (at $180 \leq PaO_2 < 200$ mmHg), Rat 93029, n = 2

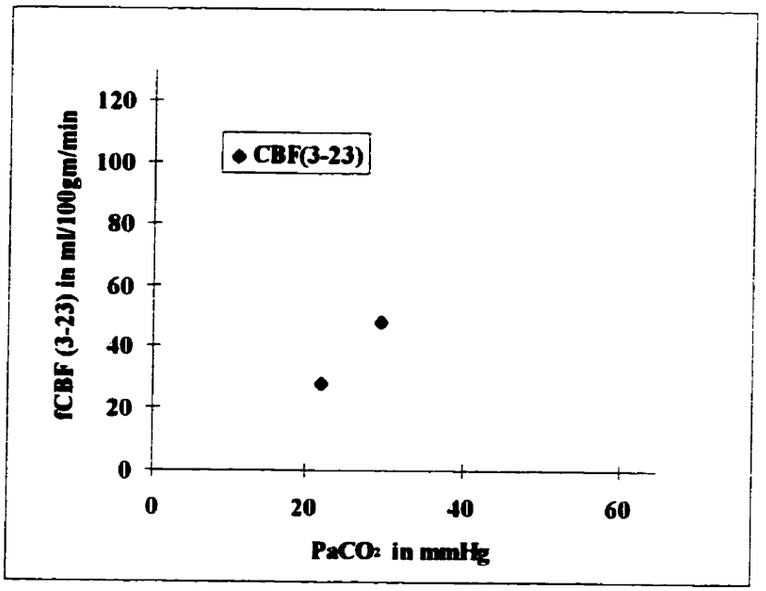

Figure 5.15: fCBF vs. $PaCO_2$ (at $180 \leq PaO_2 < 200$ mmHg), Rat 93048, (n = 3, r = 0.98)

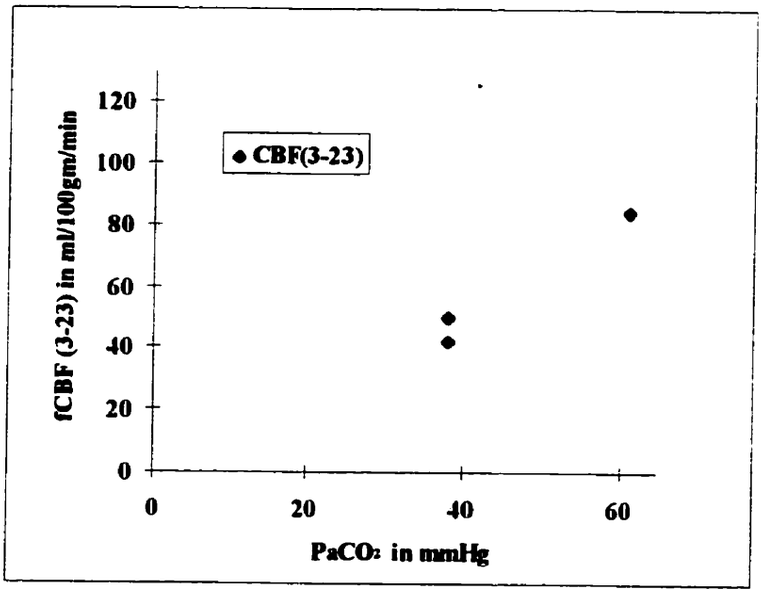

Figure 5.16: fCBF vs. $PaCO_2$ (at $180 \leq PaO_2 < 200$ mmHg), Rat 93029, 93048, 93051, (n = 6, r = 0.96)

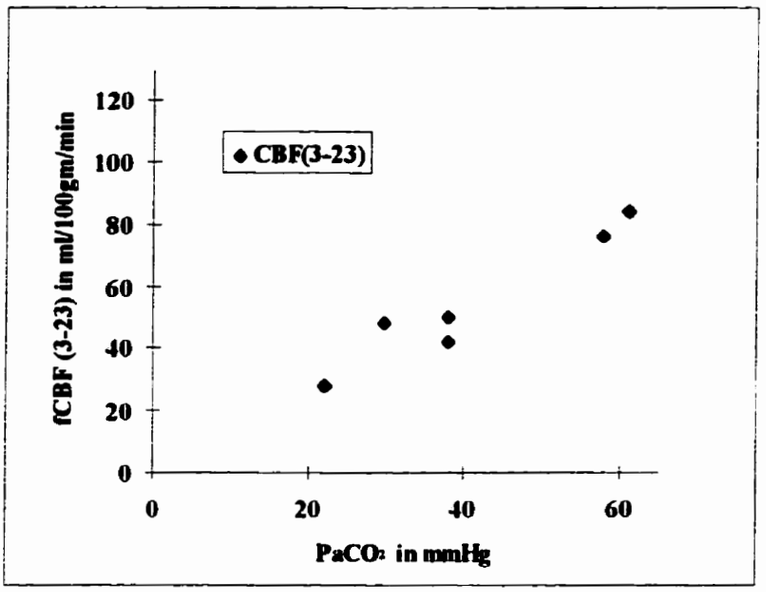

Figures 5.17 to 5.19 show fCBF(3-23) versus $PaCO_2$ for 3 rats at high PaO_2 (see Table 5.1). For an individual rat a linear correlation of CBF and $PaCO_2$ exists. The degree of this correlation (or correlation coefficient) however, is less than that of either the normal or medium high PaO_2 cases. When all the high PaO_2 results are combined (see Figure 5.20) the degree of correlation worsens. A possible explanation for the observed result could be as follows. Although it is true that under general circumstances the level of PaO_2 will not affect (or regulate) CBF, when PaO_2 is above a certain threshold (i.e. extremely high), CBF starts to drop at all levels of $PaCO_2$. If it so happens that the threshold varies from animal to

animal, the inter-animal correlation for CBF and $PaCO_2$ is destroyed, but the intra-animal correlation is maintained.

Figure 5.17: fCBF vs. $PaCO_2$ (at $200 \leq PaO_2 < 300$ mmHg), Rat 93048, (n = 4, r = 0.60)

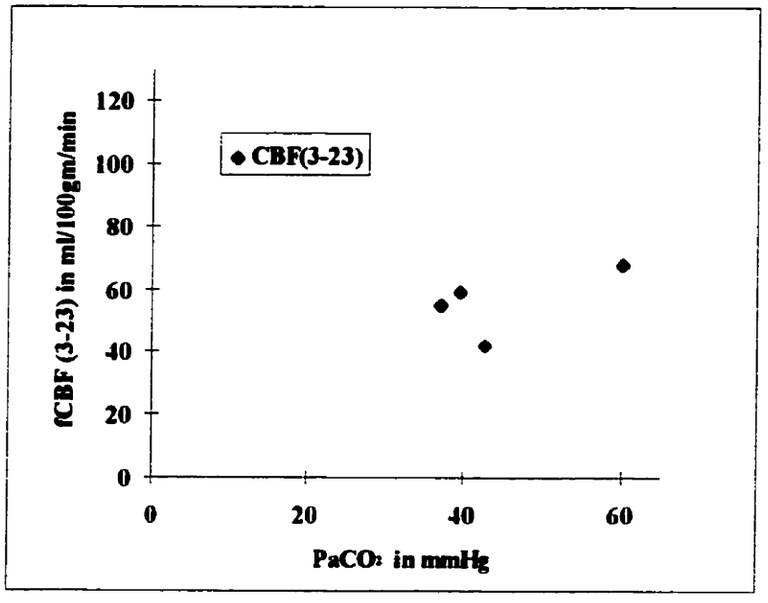

Figure 5.18: fCBF vs. $PaCO_2$ (at $200 \leq PaO_2 < 300$ mmHg), Rat 93050, (n = 3, r = 0.58)

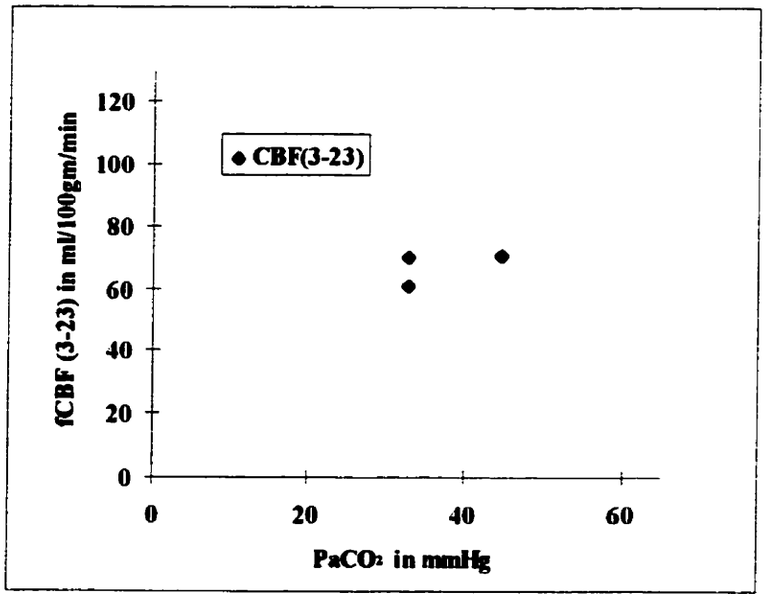

Figure 5.19: fCBF vs. $PaCO_2$ (at $200 \leq PaO_2 < 300$ mmHg), Rat 93051, n = 2

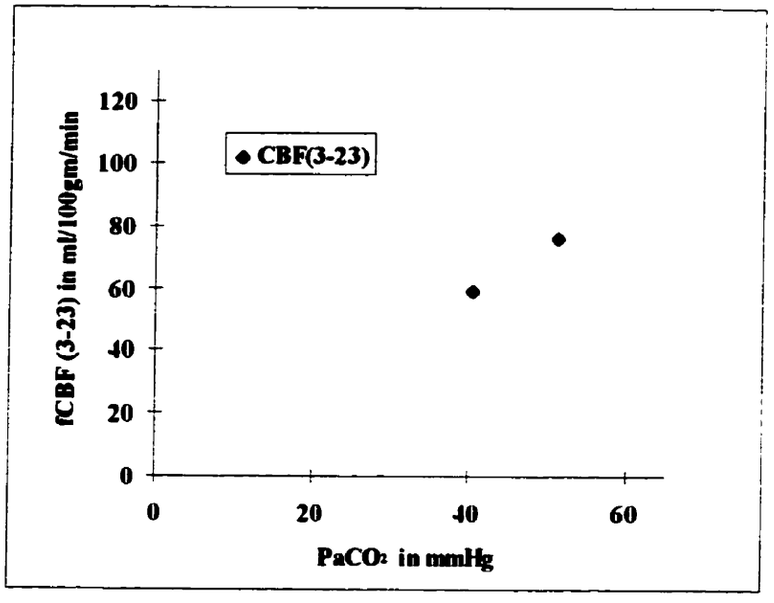

Figure 5.20: fCBF vs. $PaCO_2$ (at $200 \leq PaO_2 < 300$ mmHg), Rat 93029, 48, 50, 51, (n = 10, r = -0.02)

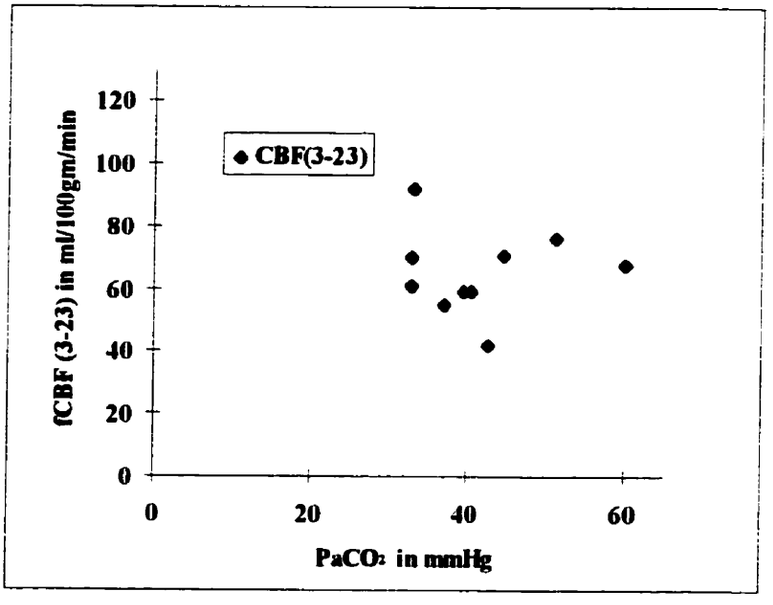

2. aCBF Results and Discussion

Figure 5.21 shows aCBF versus $PaCO_2$ results at normal and medium high PaO_2 for 8 rats. Figure 5.22 shows the same at high PaO_2 for 3 rats. The results of aCBF mirror that of fCBF. For example good correlation between aCBF and $PaCO_2$ exists for normal and medium high PaO_2 levels but inferior correlation for high PaO_2. The aCBF results for normal and medium high PaO_2 levels are put together because as in the fCBF study, results indicate that there is no difference between the two.

Figure 5.21: aCBF vs. $PaCO_2$ (at $60 \leq PaO_2 \leq 200$ mmHg, without Rat 95020), no. Rats = 8, (n = 15, r = 0.77)

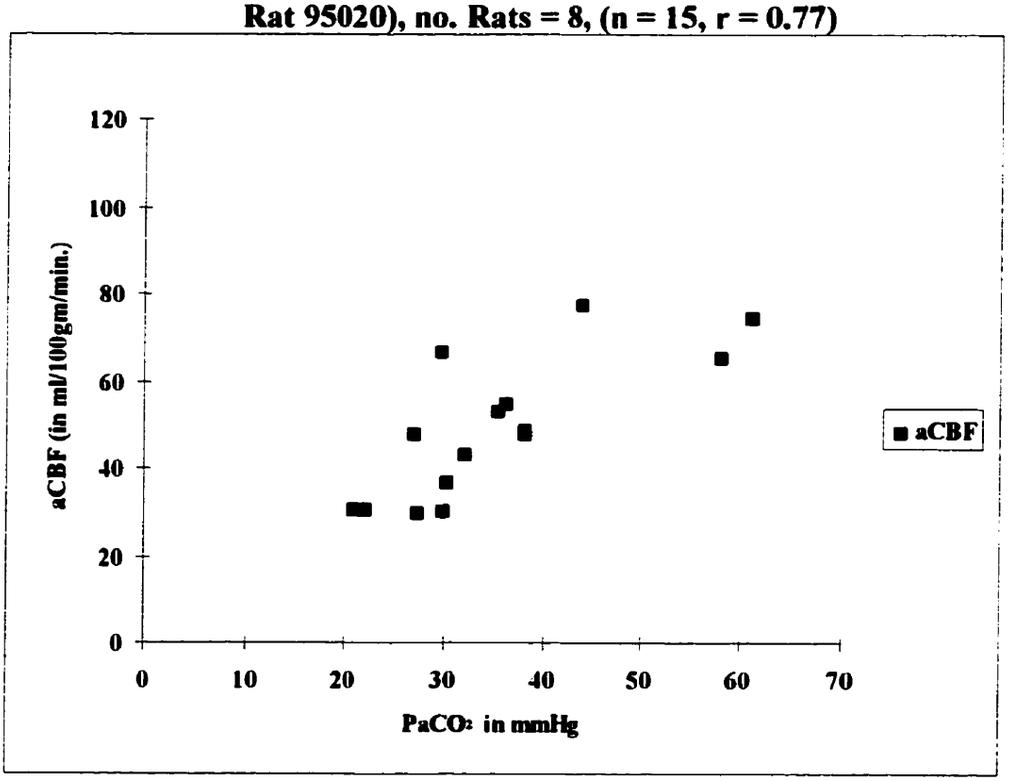

Figure 5.22: aCBF vs. $PaCO_2$ (at $200 \leq PaO_2 \leq 300$ mmHg), no. Rats = 3, (n = 8, r = 0.42)

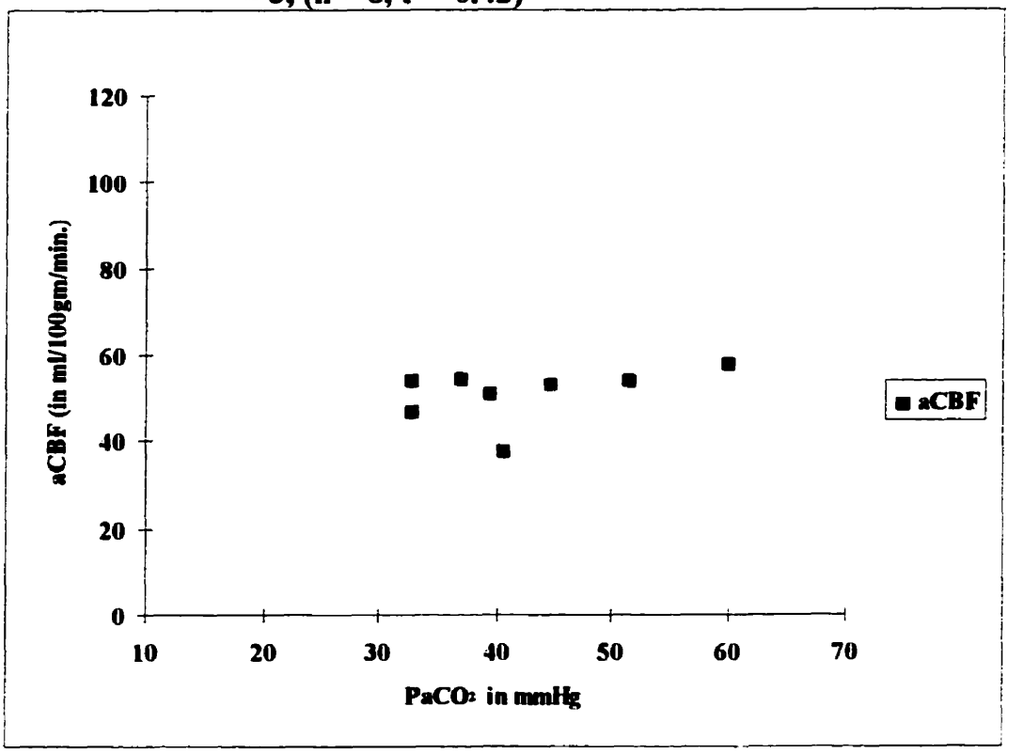

3. Observations and Comparisons

Figure 5.23 illustrates fCBF(3-23) versus $PaCO_2$ values for low, normal, medium high and high PaO_2 levels. The corresponding aCBF are given in Figure 5.24. Comparing both figures, the aCBF values are generally smaller than values for fCBF(3-23). From a theoretical point of view the aCBF values represent weighted averages of the fast gray matter and slow white matter and therefore should be lower than the fast gray matter alone. The aCBF values are smaller than fCBF(0-23) by about 25% (see Table 5.3). Clearly this is a rough comparison only

as the process utilized to correct for indicator recirculation in the former data is crude at best.

Figure 5.23: fCBF vs. $PaCO_2$ (at $60 \leq PaO_2 < 300$ mmHg), n=49

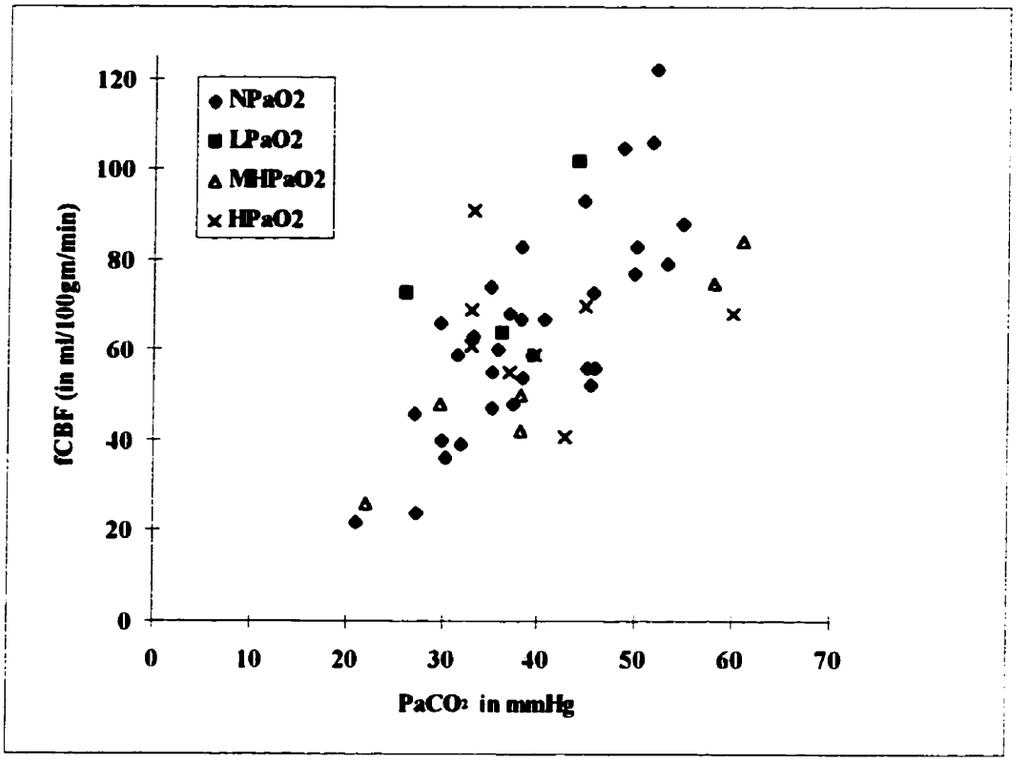

	Correlation coefficients R ($PaCO_2$, fCBF)
$NPaO_2$	0.78
LPa O_2	0.68
MHPa O_2	0.96
HPa O_2	-0.14
Average R	0.63
Average R (without HPa O_2)	0.72

Figure 5.24: aCBF vs. $PaCO_2$ for $NPaO_2$ (at $100 \leq PaO_2 < 200$ mmHg) and $HPaO_2$ (at $200 \leq PaO_2 < 300$ mmHg), [n = 39, $r(NPaO_2) = 0.77$, $r(HPaO_2) = 0.42$]

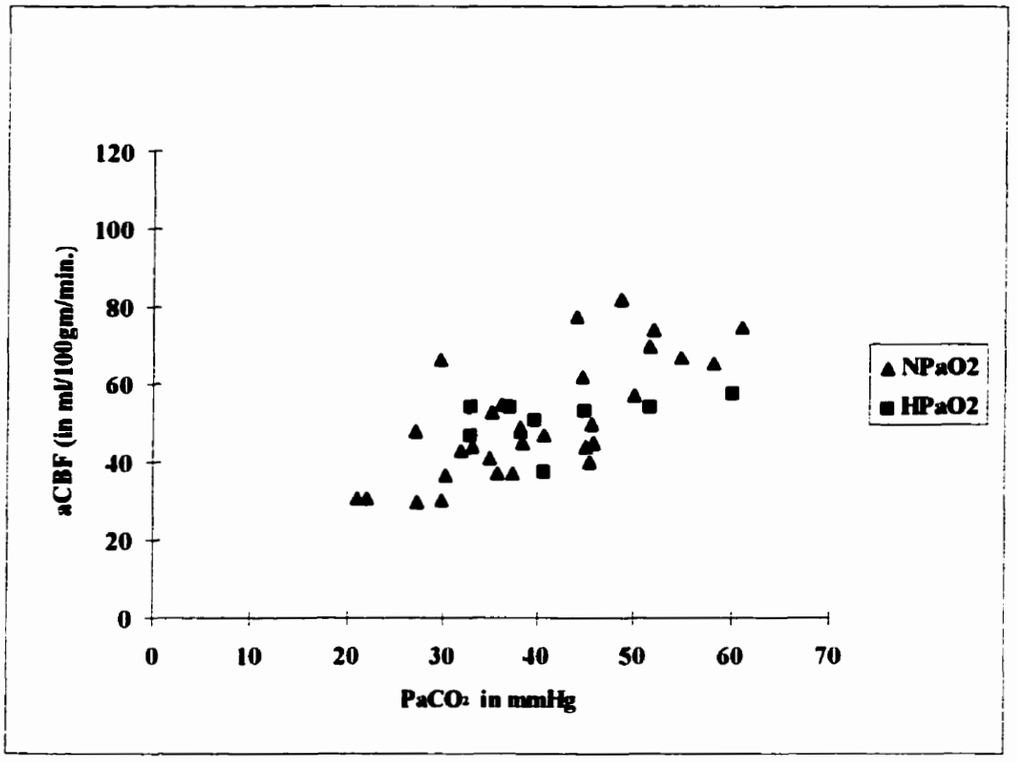

Listed in Table 5.2 are average CBF values for rats taken from the literature. Among the many values, quantitative autoradiography is usually considered as the gold standard. Table 5.3 lists the various averages CBF values obtained in this study, for comparison. The average of 115 mL/min/100g from the literature is higher that the 88 mL/min/100g obtained in this study for normal $PaCO_2$ levels (35 mmHg < $PaCO_2$ < 45 mmHg). If one compares the 88 ml/min/100g of this study to that of 97 ml/min/100g for the quantitative autoradiography the difference is smaller. In any case the reason is likely due to the less than 100% extraction of the indicator as well as the fact that results are

slightly contaminated by white matter flow due to the definition of region 2 used for the analysis is too late so that contamination from white matter flow is more significant.

Table 5.2: CBF Values from the Literature

	CBF (ml/100g/min)	s.d. CBF	Technique
	122	17	dual-autoradiographic [6]
	97	7	quantitative autoradiography [7]
	150	60	hydrogen clearance [8]
	99	19	intra-art. 133 Xe [9]
	130*		19F MR Spect. [10]
	97.1	10.6	14C butanol [11]
	83.3	7.4	hydrogen clearance [12]
	159	12	hydrogen clearance [13]
AVERAGE	**115**	**± 29**	

*This a value assumed by the authors of the paper

Table 5.3: CBF Values Using the CBF Measurement Method Developed for This Study

	CBF (ml/100g/min.)	sdCBF (ml/100g/min.)
fCBF(0-23)		
1. Normal PaCO2, Normal PaO2		
(8 rats, partition coefficient=1)	81	11
(8 rats, partition coefficient=0.9)	73	10
2. Normal PaCO2, Low PaO2		
(2 rats, partition coefficient=1)	98	30
(2 rats, partition coefficient=0.9)	88	27
3. Normal PaCO2, High PaO2		
(7 rats, partition coefficient=1)	66	22
(7 rats, partition coefficient=0.9)	59	20
aCBF		
1. Normal PaCO2, Normal PaO2		
(5 rats, partition coefficient=1)	57	17
(5 rats, partition coefficient=0.9)	51	15
2. Normal PaCO2, High PaO2		
(4 rats, partition coefficient=1)	55	9
(4 rats, partition coefficient=0.9)	49	8

Figure 5.25: fCBF(3-23) vs. aCBF [r(fCBF) = 0.74, r(aCBF) = 0.77)

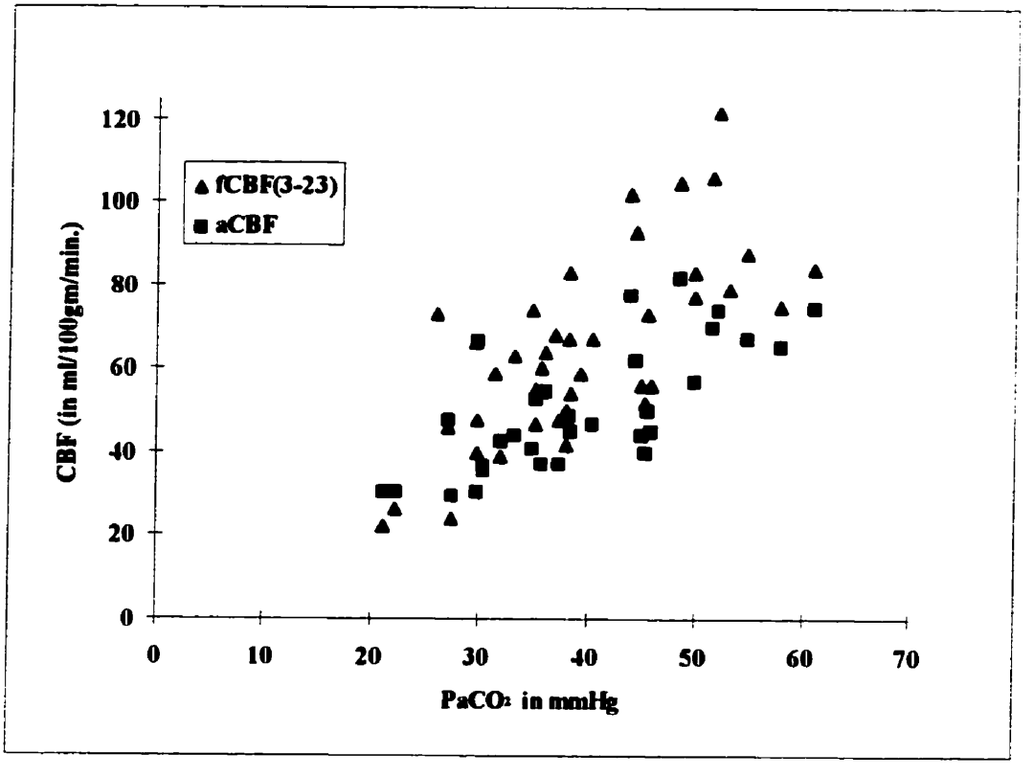

References

1. Ewing JR, Branch CA, Fagan SC, *et al.*, 'Fluorocarbon-23 Measure of Cat Cerebral Blood Flow by Nuclear Magnetic Resonance', *Stroke* 21:(1):100-106, 1990.

2. Barranco D, Sutton LN, Florin S, *et al.*, 'Use of ^{19}F NMR Spectroscopy for Measurement of Cerebral Blood Flow: A Comparative Study Using Microspheres', *Journal of Cerebral Blood Flow and Metabolism* 9:886-981, 1989.

3. Detre JA, Subramanian VH, Mitchell MD, *et al.*, 'Measurement of Regional Cerebral Blood Flow in Cat Brain Using Intracarotid $^{2}H_2O$ and ^{2}H NMR Imaging', *Magn.Reson.Med.* 14:389-395, 1990.

4. Kim SG and Ackerman JH, 'Quantification of Regional Blood Flow by Monitoring of Exogenous Tracer *via* Nuclear Magnetic Resonance Spectroscopy', *Magn.Reson.Med.* 14:266-282, 1990.

5. Lassen NA and Perl W, *Tracer Kinetic Methods in Medical Physiology*, Raven Press, New York, 1979.

6. Takizawa S, Hogan M, Hakim AM, 'The effects of a competitive NMDA receptor antagonist (CGS-19755) on cerebral blood flow and pH in focal ischemia', *Journal of Cerebral Blood Flow Metabolism* 11(5):786-93, 1991.

7. Williams JL, Shea M, Furlan AJ, Little JR, Jones-SC, 'Importance of freezing time when iodoantipyrine is used for measurement of cerebral blood flow', *Am.J.Physiol.* 261(1 Pt 2):H252-H256, 1991.

8. Metzger HP, Pante H, Heuber-Metzger S, 'Cerebrocortical oxygen supply of sclerotic rats and acute diltiazem therapy', *Adv.Exp.Med.Biol.* 277:353-361, 1990.

9. Waldemar G, 'Acute sympathetic denervation does not eliminate the effect of angiotensin converting enzyme inhibition on CBF autoregulation in spontaneously hypertensive rats', *Journal of Cerebral Blood Flow and Metabolism* 10(1): 43-7, 1990.

10. Rudin M, Sauter A, 'Non-invasive determination of cerebral blood flow changes by ^{19}F NMR spectroscopy', *NMR-Biomed.* 2(3):98-103, 1989.

11. Onesti ST, Strauss RC, Mayol B, Solomon RA, 'The effects of norepinephrine depletion on cerebral blood flow in the rat', *Brain Res.* 477(1-2):378-381, 1989.

12. Skarphedinsson JO, Harding H, Thoren P, 'Repeated measurements of cerebral blood flow in rats. Comparisons between the hydrogen clearance method and laser Doppler flowmetry', *Acta.Physiol.Scand.* 134(1):133-142, 1988.

13. Kochanek PM, Nemoto EM, Melick JA, Evans RW, Burke DF, 'cerebrovascular and cerebrometabolic effects of intracarotid infused platelet-activating factor in rats', *Journal of Cerebral Blood Flow Metabolism* 8(4):546-51,1988.

Chapter 6: Underestimation of Cerebral Blood Flow: Quantification Using Surface Permeability

A. Introduction

Chapter 5 assumes that during a CBF experiment, instantaneous indicator equilibrium exists between the blood and the tissue (brain). Unfortunately, this is not the case. If equilibrium indeed were established instantaneously, the spike, observed in a washin and washout curve would not have been observed. Its presence is due to the fact that [^{2}H]water (water for short), as an indicator, is diffusion limited. In other words, equilibrium is not established instantly. As a result, when the indicator is first introduced into the brain, its concentration in blood relative to that in tissue is higher.

At equilibrium,

$$\lambda = \frac{c_{tissue}}{c_{blood}}; \qquad \text{Eq. (6.1)}$$

where λ is the partition coefficient for the indicator used and c_{tissue} and c_{blood} represent the indicator concentration in the brain (including blood) and blood, respectively. Immediately after injection, due to indicator diffusion limitations we have

$$c_{tissue} < \lambda \times c_{blood}. \qquad \text{Eq. (6.2)}$$

The same diffusion limiting mechanism works the opposite way as blood flow continues and washout of indicator from tissue begins (average time to start of washout, t = Volume(brain)/CBF(average) ~ 2 to 3 seconds after indicator injection), this time with the tissue concentration being higher than at equilibrium. In other words,

$$c_{tissue} > \lambda \times c_{blood}. \qquad \text{Eq. (6.3)}$$

A consequence of the indicator diffusion limitation is that the rate of indicator washout from the brain is slower than predicted by our model; hence CBF is underestimated. There are two causes for the diffusion limitation of water in the brain: One is due to the fact that the water indicator is not 100% freely diffusible. For example, at equilibration, water does not diffuse through a cell membrane but rather transverses it *via* pores. As a result, diffusion is restricted at the cell membrane. The second reason is related to the fact that the diffusion processes take time to reach equilibrium, whereas the CBF model requires an unlimited rate of indicator diffusion (that is, requires an instantaneous mixing of indicator in the brain).

The goal of this chapter is to quantify the degree our model underestimates CBF. The method used to reach the goal is to employ the concepts of indicator

permeable surface (PS), diffusibility factor (M) and indicator extraction coefficient (E).

B. Surface Permeable (PS) Correction

1. The Diffusibility Factor (M)

In Chapter 3, Eq. (3.25) provides an average CBF (the aCBF used in Chapter 5) modeling method, reproduced here as Eq. (6.4):

$$aCBF \equiv 100 \times f = 100 \times \lambda \times S_{max} / \int S(t)dt \ . \qquad \text{Eq.(6.4)}$$

With fCBF modeling (See Chapters 3 and 5), it is assumed that the brain is a single compartment. For a single compartment, the washout of indicator from the brain is described by a mono-exponential curve. Using the single compartmental model, Eq. (3.25) can be replaced by the simpler Eq. (3.28) , reproduced here as Eq. (6.5)

$$fCBF = 100 \times \lambda \times k. \qquad \text{Eq.(6.5)}$$

Eq. (6.5) represents the fast compartment or the fast gray matter flow. Once again, the λ in the equation is the indicator PC and k is the time constant of the mono-exponential curve. A single compartmental washout curve is by definition a mono-exponential decay function[1], because it assumes that when the indicator is injected into the brain, instantaneous mixing of the indicator in the compartment occurs; in

other words, the indicator diffuses freely within the compartment, and the rate of diffusion is unlimited. In other words, this ideal process assumes that instantaneous indicator equilibrium between the tissues and the carrier fluid exists, for all flow rates and at all times. Given instantaneous indicator equilibrium, the rate of indicator washout from the brain is proportional to the amount of indicator in the brain, or

$$dN / dt = -kN \quad \text{or} \quad \frac{dN}{N} = -kdt$$

Upon integration,

$$\ln(\frac{N}{N_o}) = -kt \quad \text{or} \quad N(t) = N_o \exp(-kt)$$

Although in the model utilized in this study the brain is treated as a single compartment, water can not achieve instantaneous mixing in the brain due to the fact that its movement is, to some degree, restricted and it can not establish equilibrium instantaneously. The use of water, as a CBF measurement indicator, therefore does not fully satisfy the requirement of the model. A consequence of the diffusion limitation of water is an apparent slower indicator clearance. This slower washout gives rise to a slower mono-exponential decay curve and hence a smaller time constant k than one would predict to be associated with a particular value of flow. That is to say, if $k_{experiment}$ is the time constant measured using water as an indicator, then k for Eq. (6.5) can be related to $k_{experiment}$ as follows

$$k_{experiment} = Mk, \qquad 0 \le M \le 1 \qquad \text{Eq. (6.6)}$$

In Eq. (6.6), the diffusion factor M denotes the degree of equilibrium achieved by the water indicator during the clearance of indicator from the brain.[2,3,4] By substituting Eq. (6.6) into Eq. (6.5), a new fCBF, corrected for water diffusion limitation, is obtained.

$$newfCBF = 100 \times \lambda \times \frac{k_{experiment}}{M} \qquad \text{Eq. (6.7)}$$

2. The Expression of (M)

The water diffusion limitation correction factor (M) has been formulated by Kety[2,3], using a model suggested by Krogh[5] and a derivation by Bohr.[3] Kety's diffusion correction factor (M) is applied generally to all indicators that are diffusion limited. The derived formulation of this correction factor is simply stated here

$$M = 1 - \exp(-PS/F), \qquad \text{Eq. (6.8)}$$

where the multiplication of P and S is the "Permeability (P) – Surface (S) product"[6,7] and F is flow. PS, also called surface area product, was first developed by Renkin.[7] According to Renkin, it is '*a theoretical relation between blood flow*

and blood tissue clearance,' assuming uniform circulation characterised by a permeability constant P.

Herscovitch *et al.*[4] pointed out that this expression for M is equivalent to the indicator extraction coefficient (E, to be discussed later). Crone[6] derived an expression for permeability (P) as follows:

$$P = \frac{F}{S}\ln(\frac{1}{1-E}). \qquad \text{Eq. (6.9)}$$

Upon rearranging, Eq. (6.9) yields

$$E = 1 - \exp(-PS/F), \qquad \text{Eq. (6.10)}$$

supporting Herscovitch and co-workers' claim that M is equivalent to E. Another derivation by Renkin[7] shows the same expression for E as Eq. (6.10), further strengthening the argument that M is equivalent to E.

Substituting E = M into Eq. (6.8) one has

$$newfCBF = 100 \times \lambda \times \frac{k_{experiment}}{E} = \frac{fCBF_{experiment}}{E}. \qquad \text{Eq. (6.11)}$$

A parallel expression for the aCBF diffusion limitation correction, using [^{15}O]water, was derived by Herscovitch *et al.*,[4]

$$newaCBF = \frac{aCBF_{experiment}}{E}. \qquad \text{Eq. (6.12)}$$

In this chapter, both Eqs. (6.11) and (6.12) will be used to quantify the underestimation of CBF due to indicator diffusion limitations.

3. The Concept of Extraction Coefficient (E)

The definition of indicator extraction coefficient (E) is given as the ratio of indicator extracted by the brain to the amount of indicator injected, during the first pass of the indicator through the brain. In equation form, this is

$$E = \frac{m_{\text{extracted}}}{m_0}. \qquad \text{Eq. (6.13)}$$

In Eq. (6.13), m_o is the amount of indicator injected into the brain and $m_{extracted}$ is the amount extracted by the brain during indicator's first passage through the brain.

A characteristic of the final CBF protocol, as is discussed in Chapter 4, is that it allows a simultaneous measurement of the extraction coefficient (E), fCBF and aCBF. For example, Figure 6.1 is a base line corrected, indicator washin and washout curve. The initial spike superimposed on the initial straight line is a result of direct indicator transit through the brain *via* the vascular bed (i.e. that portion of the injected indicator that does not enter the tissue space). As such, the presence of this spike provides information for the estimation of E.

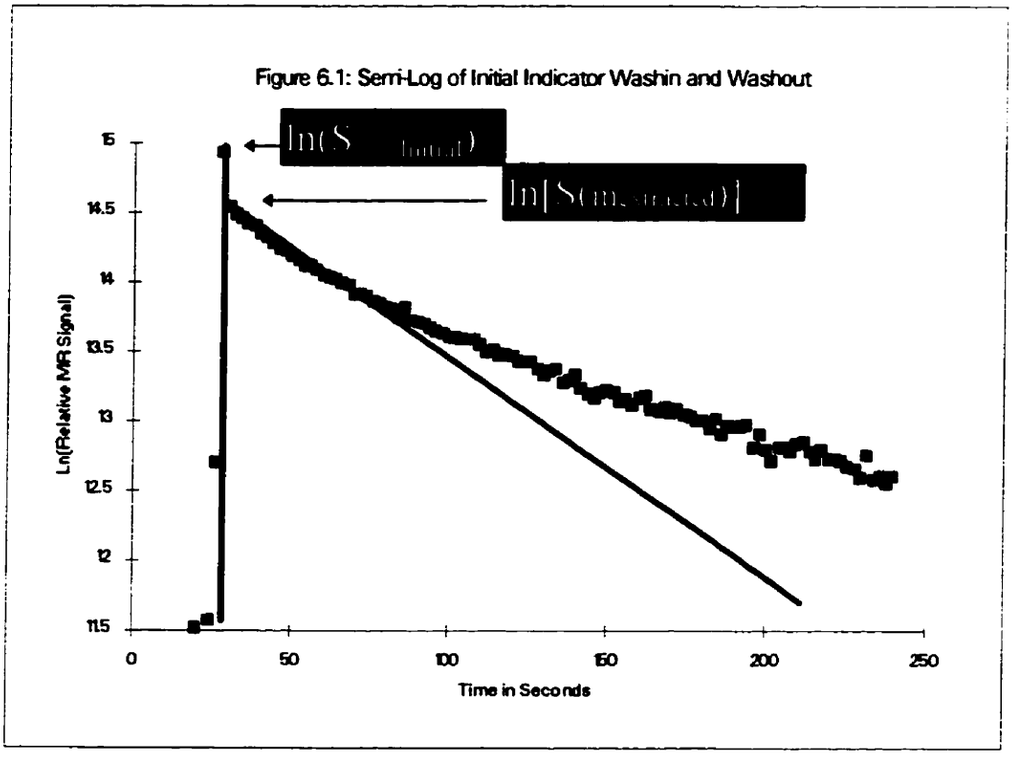

To calculate E, one can utilize the fact that the amount of indicator in the brain is proportional to the MR signal received; then Eq. (6.13) can be rewritten as

$$E = \frac{S(m_{\text{extracted}})}{S(m_0)} = \frac{S(m_{\text{extracted}})}{S_{\max}}. \qquad \text{Eq. (6.14)}$$

In Eq. (6.14), S_{max} is the MR signal, at the maximum, during indicator washin and washout. $S(m_{extracted})$ is the corresponding MR signal due to the portion of indicator extracted by the brain. $S(m_{extracted})$ can be obtained from Figure 6.1 as follows:

1. In Figure 6.1, the initial straight line is projected back to the time of S_{max}, using least square linear regression.

2. The magnitudes of S_{max} and $S(m_{extracted})$ on the semi-log plot are measured.

3. The extraction coefficient (E) is calculated using Eq. (6.15).[3]

Therefore, when CBF washin and washout is plotted in the form of Figure 6.1, the extraction coefficient (E) is calculated as

$$E = \frac{S(m_{extracted})}{S_{max}} = \frac{\exp(I_{max})}{\exp[I(m_{extracted})]}. \qquad \text{Eq. (6.15)}$$

I_{max} is the value measured at the spike and $I(m_{extracted})$ is the value measured at the intercept of the spike with the initial straight line of Figure 6.1.

Using the final CBF protocol the Full-Width-Half-Maximum (FWHM) for the intra-vascular indicator transit spike was 3 ± 2 seconds. The FWHM was derived as follow:

1. Treat the initial spike of the indicator washout as a distribution with base at $m_{extracted}$.

2. Calculate

$$H_{half} = \frac{m_{max} - m_{extracted}}{2} + m_{extracted}.$$

3. Measure the width of the initial spike at the height of H_{half}.

In essence, the FWHM of the spike is the mean of the intra-vascular transit time for the brain. The uncertainty of 2 seconds in the intra-vascular transit can be

reduced to 1 second by using a higher MR spectrum sampling frequency (for example one spectrum per second).

C. Discussion

The results of experiments described in this chapter are summarized in Figures 6.2 and 6.3. Figure 6.2(a) presents E, as a function of fCBF(3-23), for 60 mmHg < PaO_2 < 200mmHg. According to Eq. (6.10), when fCBF(3-23) increases, E decreases. This decrease can be seen in both Figures 6.2(a) and 6.2(b). Figures 6.2(a) and 6.2(b) can be used to correct for the underestimation of measured fCBF and aCBF as a result of the limitations of tracer diffusion. For example if one obtains an aCBF value of 55 ml/100g/min, then E from the figure is approximately 0.85; as such, substituting 0.85 for E into Eq. (6.12), the diffusion limitation corrected aCBF is 65 ml/100g/min.

Figure 6.2(a): Extraction Coefficient (E) versus fCBF(3-23) for 60 mmHg < PaO_2 < 200 mmHg, r = -0.30

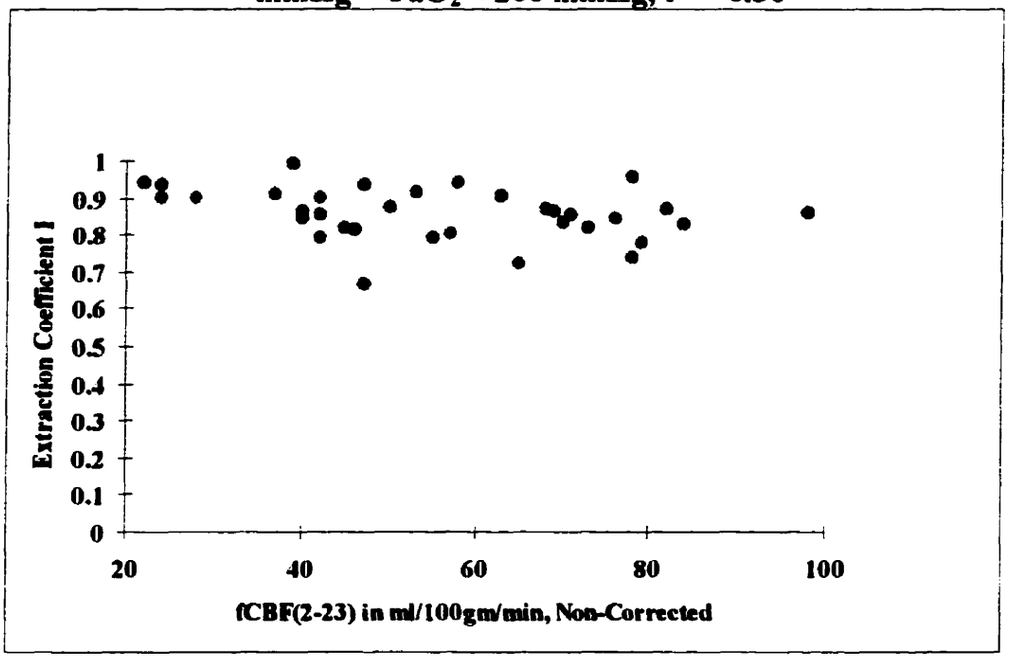

Figure 6.2(b): Extraction Coefficient (E) versus aCBF for 60 mmHg < PaO_2 < 200 mmHg, r = -0.62

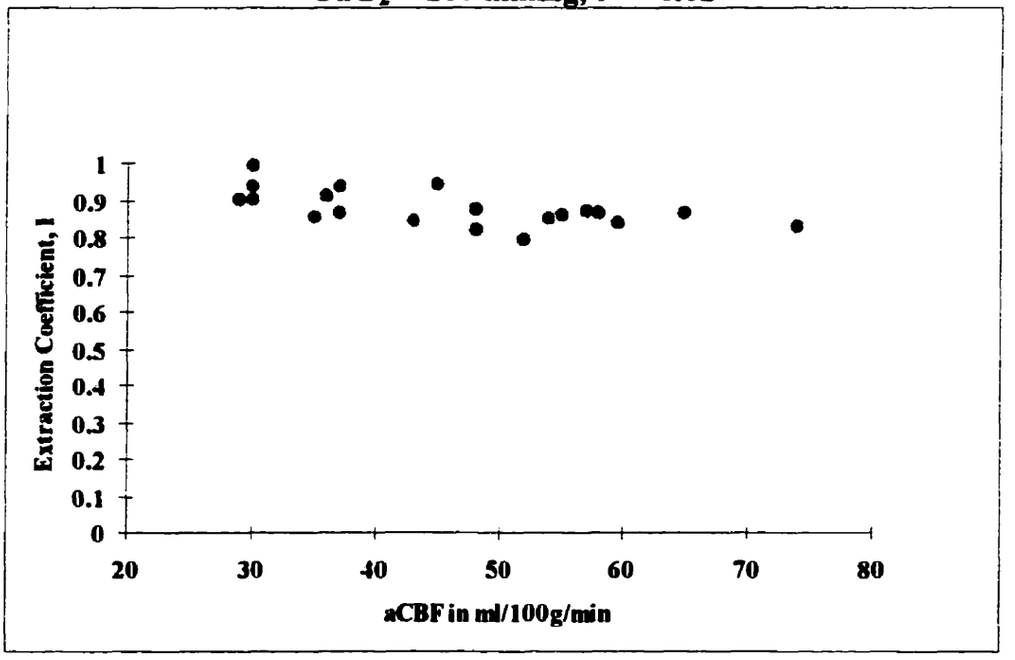

Figure 6.3(a) shows fCBF(3-23) versus $PaCO_2$, corrected for diffusion limitations. For comparison, Figure 6.3(b) shows both the corrected and the non-corrected fCBF(3-23) versus $PaCO_2$. The average percent difference between the corrected and the non-corrcted fCBF(3-23), using Eq. (6.16), was approximately 20%.

$$P.D.=\frac{(fCBF_{corrected}-fCBF_{non-corrected})}{fCBF_{non-corrected}}\times 100\% \qquad \text{Eq. (6.16)}$$

The average extraction coefficient obtained using the final CBF protocol decribed in Chapter 4, is 0.85.

Figure 6.3(a): Diffusion Limitation Corrected fCBF(3-23) versus $PaCO_2$ for 60 mmHg < PaO_2 < 200 mmHg

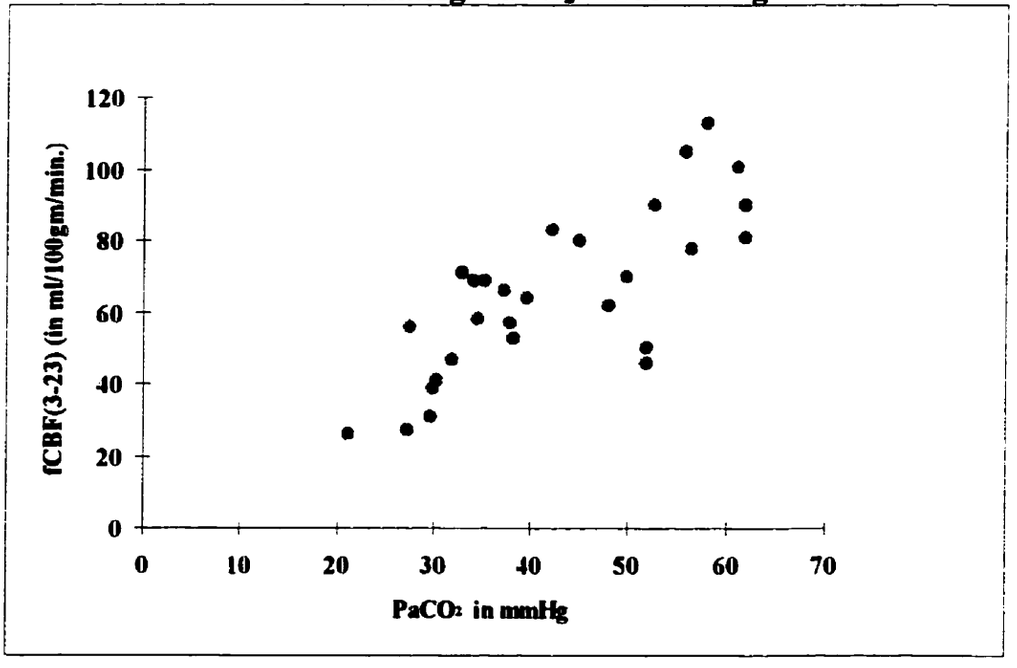

Figure 6.3(b): Diffusion Corrected and Non-Corrected fCBF(3-23) versus $PaCO_2$ for 60 mmHg < PaO_2 < 200 mmHg. Note that the diffusion corrected fCBF(3-23) (circles) is approximately 20% higher than the non-corrected (triangles).

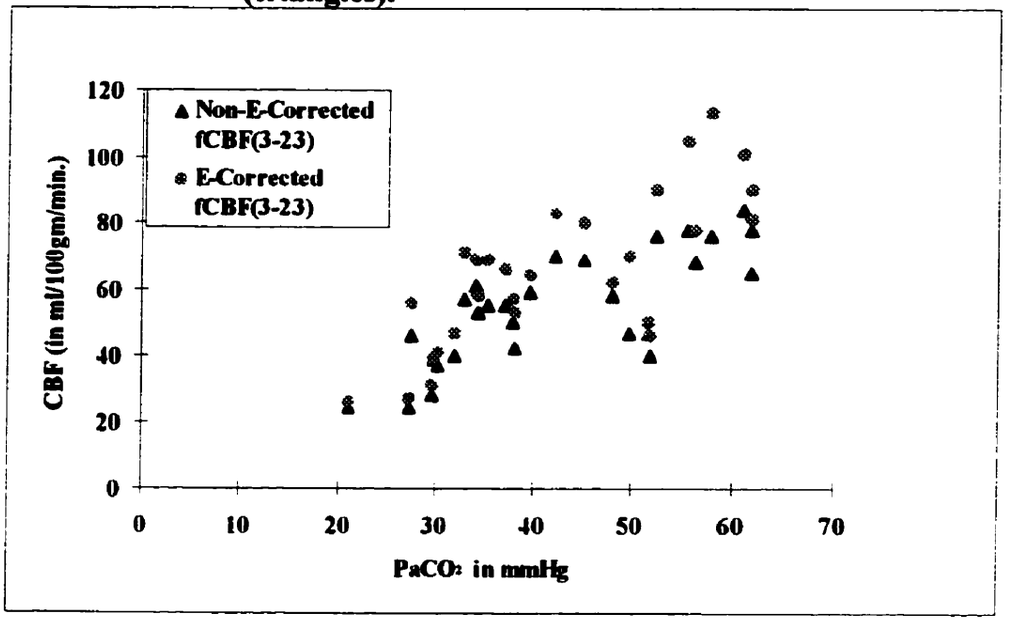

References:

[1] Lassen NA and Perl W, *Trancer Kinetic Methods in Medical Physiology*, Raven Press, NY, 1979.

[2] Kety SS, 'The Theory and Application of The Exchange of Inert Gas at The Lungs and Tissues', *Pharm.Rev.* 3:1-41, 1951.

[3] Kety SS, 'Regional Cerebral Blood Flow: Estimation by Means of Nonmetabolized Diffusible Tracers-An Overview', *Sem.Nucl.Med.* XV(4): 324-328, 1985.

[4] Herscovitch P, Raichle ME, Kilbourn MR and Welch MJ, 'Positron Emission Tomographic Measurement of Cerebral Blood Flow and Permeability-Surface Area Product of Water Using [^{15}O]Water and [^{11}C]Butanol', *Journal of Cerebral Blood Flow and Metabolism* 7: 527-542, 1987.

[5] Krogh A, 'The Number and Distribution of Capillaries in Muscles with Calculation of the Oxygen Pressure Head Necessary for Supplying the Tissue', *J.Physiol.* 52:391-408, 1919.

[6] Crone C, 'The Permeability of Capillaries in Various Organs as Determined by Use of the 'Indicator Diffusion' Method', *Acta.Physiol.Scand.* 58:292-305, 1963.

[7] Renkin EM, 'Transport of Potassium-42 from Blood to Tissue in Isolated Mammalian Skeletal Muscles', *Am.J.Physiol.* 197:1205-1210, 1959.

Chapter 7: Indicator Recirculation Correction: Impulse Response Function (IRF) and Convolution Analysis

A. Introduction

Indicator recirculation is a problem in the final CBF protocol described in Chapter 4. In CBF measurements, one way of classifying the various types of indicators is on the basis of indicator recirculation. An indicator is called a non-recirculating indicator if it is removed from the blood flow circulation, one way or another, after washout from the brain. On the other hand, a recirculating indicator remains in the system longer than the time required for the blood to go from the brain to the heart and then back to the brain, either directly or indirectly. The most serious aspect of indicator recirculation is that it introduces a distortion into the washout curve and hence an error in the CBF estimates. The error is due to the fact that indicator recirculation makes the washout appear slower. (Tracer is continually entering the brain and compensating for, in part, that which is being washed out.) In the case of fCBF modeling (see Chapter 5), indicator recirculation contributes to flow underestimation. This underestimation is mostly from shifting the semi-log plot of a washout curve to the right and up. In fCBF calculations, this problem is partially circumvented by using only a small number of points at the beginning of washout. The initial data are expected to be less distorted by recirculation, due to the fact that there is a time delay associated with the on-set of recirculation. Flow is also underestimated in the case of aCBF (Chapter 5). This is

because as the washout curve drifts to the right the area under the curve increases. According to Equation (5.3) an increase in area under the signal curve results in flow underestimation. This is more serious than with fCBF since recirculation eventually leads to a uniform distribution of indicator throughout the rat and a constant concentration over time in the brain. In Chapter 5, a crude method was employed to partially eliminate the aCBF recirculation distortion by subtracting the term

$$(n-15)\times\frac{aENDs}{360}$$

from the n^{th} datum point, for n = 15 to 360.

In this chapter, the concept of convolution integration is incorporated into the existing CBF technique in an attempt to remove the effects of indicator recirculation from the experiment. The concept of convolution integration involves obtaining a impulse response function (IRF) and an input function (INF) describing indicator recirculation. The IRF and INF are used in the convolution integral to generate the (theoretical) recirculation curve. Knowing the indicator recirculation function, its removal from the CBF experiment is only a matter of direct subtraction.

The concept of convolution integration was initially applied and evaluated in phantoms. Unlike animal experiments, phantom experiments can be performed under precisely controlled conditions. This allows simulation of various kinds of

flow in a single system (for example, flow with and without indicator recirculation using the same phantom assembly). In addition, flow parameters can be controlled at a desired level of accuracy and precision. Using a phantom, the applicability of convolution analysis for generating a recirculation curve was tested.

The phantom testing of the convolution concept consisted of five steps. The first step was to simulate washout with indicator recirculation. The second was to simulate washout without indicator recirculation. The third was to generate a recirculation curve using convolution analysis. The fourth was to add the recirculation curve to the curve acquired without indicator recirculation to predict theoretically washout with indicator recirculation. The final step was to compare the theoretical and measured washout with recirculation curves. The phantom technique developed and assessed was incorporated into the CBF animal studies, in order to eliminate indicator recirculation. In parallel to the phantom studies, the animal studies involved the following steps: (a) Performing a CBF experiment using the protocol given in Chapter 4. (b) Obtaining an IRF and an input function for this CBF experiment. (c) Using the convolution integration to generate a recirculation curve for this experiment. (d) Subtracting the recirculation curve generated from the experimental washout curve. (e) Calculating the fCBF(3-23) and aCBF using the corrected curve (see Chapter 5).

At the end of this chapter the percentage underestimation of CBF measurement due to indicator recirculation is assessed. This is accomplished by

measuring fCBF(3-23) and aCBF before and after subtraction of the recirculation curve.

B. Theory

1. The Impulse Response Function (IRF) of Indicator Recirculation

The IRF is a term borrowed from radiographic imaging. In radiographic imaging, IRF is the image generated by a radiographic technique (i.e. SPECT, PET, CT, etc.) of a point source. In a more general sense the IRF is the output (or response) of a system for a delta function input. If one treats the vascular bed of the rat as a system and the MR signal from the brain as the response, the IRF is the measured signal associated with a unit volume bolus injection of indicator. In the particular case of recirculation, the IRF of indicator recirculation is the signal response (as a function of time) from the brain, due to a unit volume bolus injection of indicator introduced at the exit of the brain, (i.e., at the jugular veins). In essence, the IRF describes the signal (as a function of time) arising at the brain as a result of an instantaneous unit volume bolus of indicator leaving the brain at a particular time.

2. The Input Function (INF) of Indicator Recirculation

The INF is the instantaneous rate of indicator leaving the brain as a function of time. Therefore it is the derivative of the indicator washout curve in the absence of indicator recirculation. In this *in-vitro* study the INF was taken from the

derivative of the washout in a CBF experiment. The INF obtained in this manner was therefore only an approximation of the actual one. In theory, using iterations, an arbitrarily precise INF can conceptually be obtained. For example, consider the following process:

1. Consider the derivative of the washout curve from a CBF experiment to be the 1st order approximation of INF.
2. Generate the 1st order approximation recirculation curve using this INF.
3. Subtract the 1st order approximation curve recirculation from the washout curve and consider the result to be a 2nd order approximation (more precise) INF.
4. Generate a 2nd order (approximation) recirculation curve using this input function.
5. Repeat steps 3 to 5 using the new recirculation curve, until a recirculation curve or input function is achieved with the desired degree of accuracy.

In practice only the 1st order INF is required, as the difference between it and the 'true' input function is normally small. The derivative of the washout represents the rate at which the amount of tracer in the brain is dropping. Because of the simple nature of the rat experiments, any tracer disappearing from the brain must be appearing at the internal jugular veins.

3. Convolution Integration

Knowing the IRF and the INF of an CBF experiment, one can calculate indicator recirculation (MR signal from brain due to tracer re-entering this organ) for that experiment using convolution integration. The IRF describes how a unit volume bolus of indicator will behave as a function of time, following its appearance at the exit of the brain. The INF can be interpreted as a function describing the size of the instantaneous bolus appearing at the exit of the brain as a function of time. Essentially convolution integration equation (Eq. (7.1)) is the sum of the time shifted IRFs, modulated by the magnitude of INF at the shifted time, t.

$$Output(t) = \int_0^t IRF(t-u)INF(u)du \qquad \text{Eq. (7.1)}$$

In Eq. (7.1) the indicator recirculation, as a function of time, is given by the left hand side.

In practice, it is not necessary to measure the IRF with a unit volume bolus of indicator. Provided the same bolus size is used for both the determinations of IRF and INF, consistency will be maintained by normalizing the IRF curve to the signal maximum of the INF curve.

C. Experimental

1. Phantom Model

A phantom based experiment was designed to assess the capability of this theory to predict recirculation. Figure 7.1 shows the set-up. The assembly consisted of a water filled chamber representing the brain of the animal. The volume of the phantom was 1.5 mL (the measured size of the rat brain is 1.2 to 1.5 mL). The detecting apparatus is a sodium iodide crystal and this simulates the MR scanner in the animal experiments. A high performance liquid chromatographic (labeled peristaltic) pump, with variable flow settings, represented the heart and served to pump water through the brain at a constant rate. The reservoir, when used in recirculation experiments, contained 20 mL of water, mimicking the vascular 'volume' of the rat. A stirring bar was also included in the reservoir. The total length of the connecting tubing was chosen so that at a flow rate of 2 ml/minute (or 2 mL/1.5g/min. = 133 mL/100g/min.) the entire length could be filled in 20 seconds. The injection devices, etc., simulated, as closely as possible, the animal situation. The indicator used in the phantom study was ^{99m}Tc pertechnetate. The injection loop shown in the figure could be arranged to inject an indicator bolus either up-stream or down-stream of the phantom chamber. Although the detector and indicator used in these experiments differ from those employed in the animal studies, the underlying principles of flow are exactly the

same, implying that any findings are directly applicable to an MR based experiment.

Figure 7.1 The Phantom Assembly

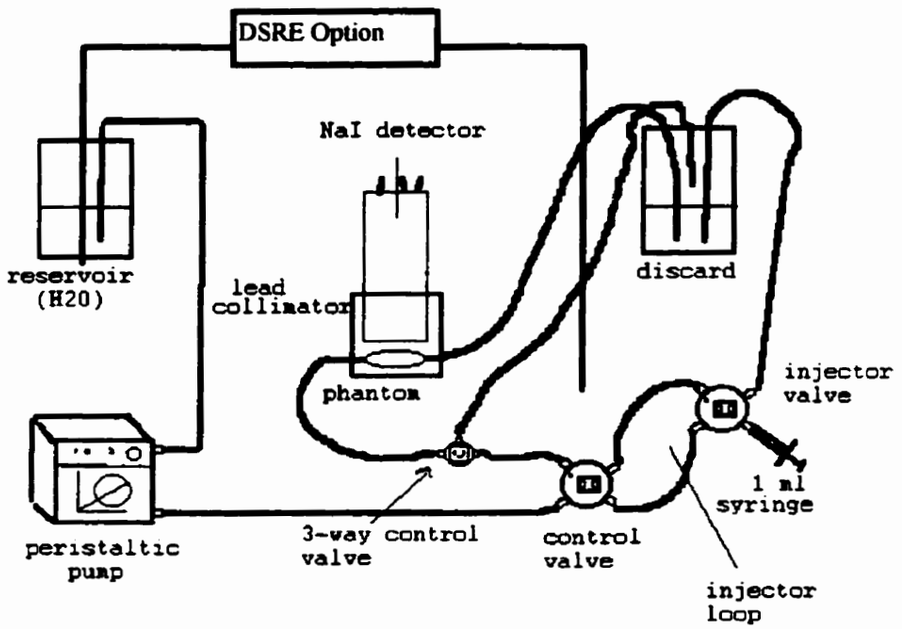

For convenience define the following terms:

1. DSRE ≡ down-stream injection with recirculation
2. USRE ≡ up-stream injection with recirculation
3. USNRE ≡ up-dtream injection without recirculation

The set-up shown in Figure 7.1 was used to perform the DSRE phantom experiment which yielded the IRF for this arrangement. It is called DSRE because

the indicator bolus was injected down-stream of the phantom chamber. From the figure it can be seen that injecting a bolus at this location simulates a bolus at the exit of the chamber or the rat brain. Monitoring the ^{99m}Tc activity at the chamber is a measure of the effect of a bolus appearing at the exit of the brain on activity recorded from the brain (ie. IRF). Flow rates of the DSRE experiments were set at: i. 2 ml/min. or 133 ml/100g/min., ii. 3 ml/min. or 200 ml/100g/min., iii. 4 ml/min. or 267 ml/100g/min. and iv. 5 ml/min. or 333 ml/100g/min. Figure 7.2 shows the DSRE data (IRF curves), for the flow setting of 3 ml/min. Note in Figure 7.2 that two experiments were performed using different amounts of activity. USRE experiments were then carried out using the same experimental set-up but with an injection site at the input to the brain.

The set-up shown in Figure 7.1 was modified in order to perform the USNRE phantom experiments. The modifications included moving the indicator injection site up-stream of the phantom chamber and collecting the outflow down stream of the phantom before it reached the resevoir so as to prevent the tracer from recirculating. To compute the input function the flow rate was set equal to that of its corresponding DSRE experiment. The same size bolus as in the DSRE experiment was also used. The negative of the derivative of the activity (count rate) versus time curve obtained in the USNRE experiment was taken to be proportional to the input function. The USNRE experiments were performed alternately with the DSREs. Figure 7.3a shows a USNRE curve for the same

experimental setup used for Figure 7.2 and Figure 7.3b shows USNRE experiments at various flow settings. The washin of USNRE was very fast compared to that of DSRE, as indicated by the sudden increase of activity in Figure 7.3a. The absence of washin in Figure 7.3b was due to the fact that injections were performed prior to the initiation of flow.

Figure 7.2: DSRE (IRF) at 3 ml/min Using Different Amounts of Activity. Data Was Normalized to Bolus Size

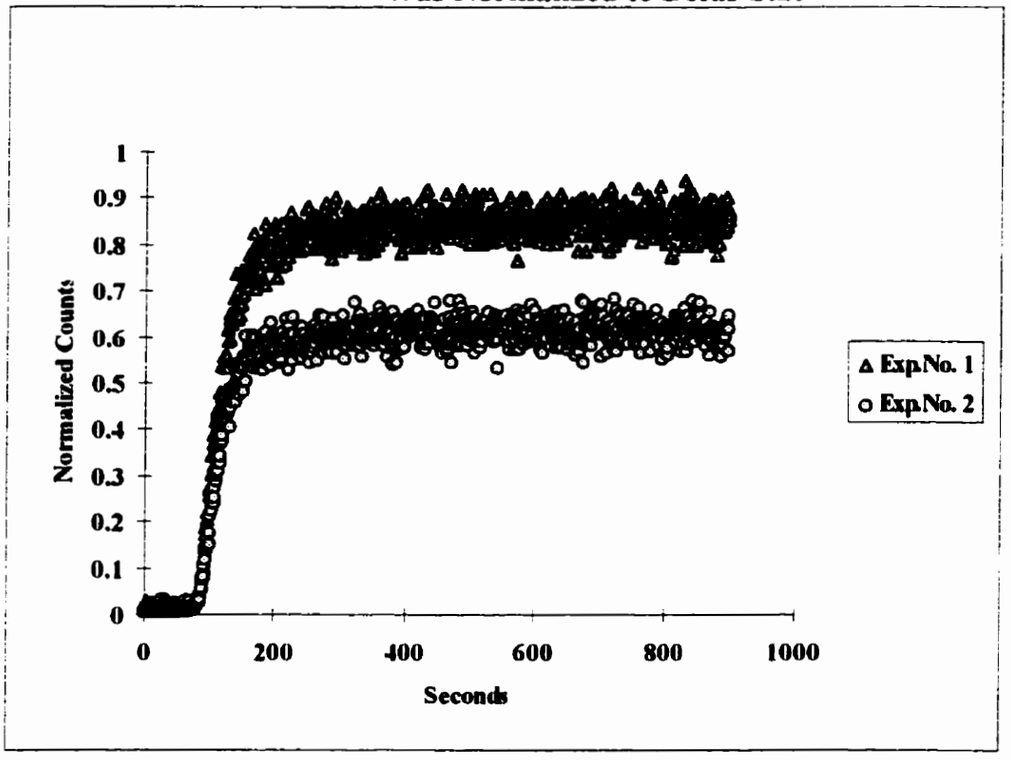

Figure 7.3(a): USNRE at 3 ml/min Using Different Amounts of Activity.

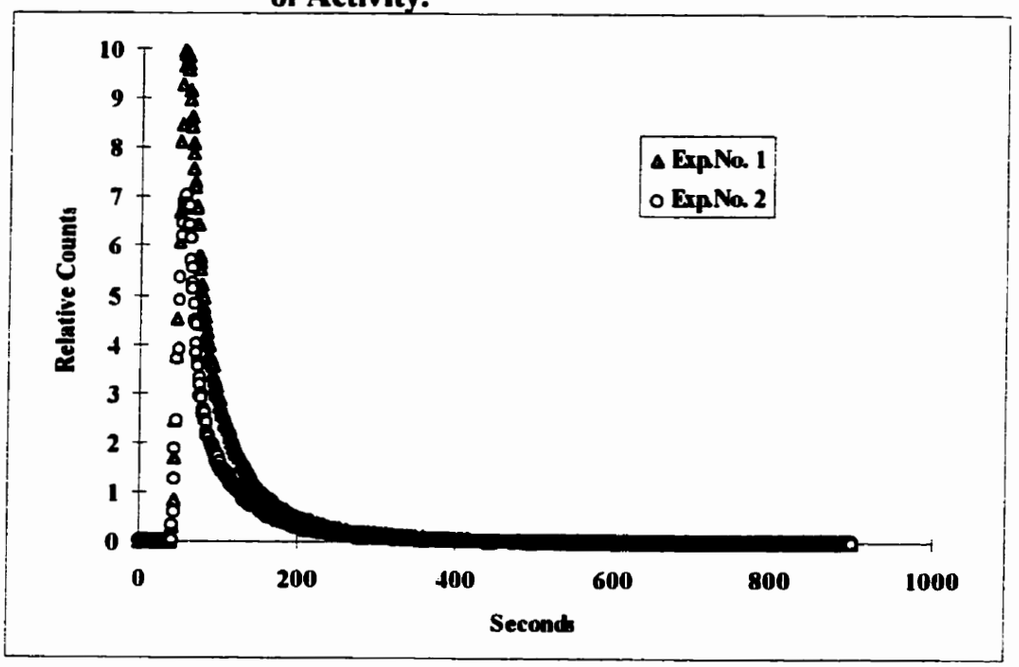

Figure 7.3b: USNRE at Various Flow Rates (with Diminishing Amounts of Activity)

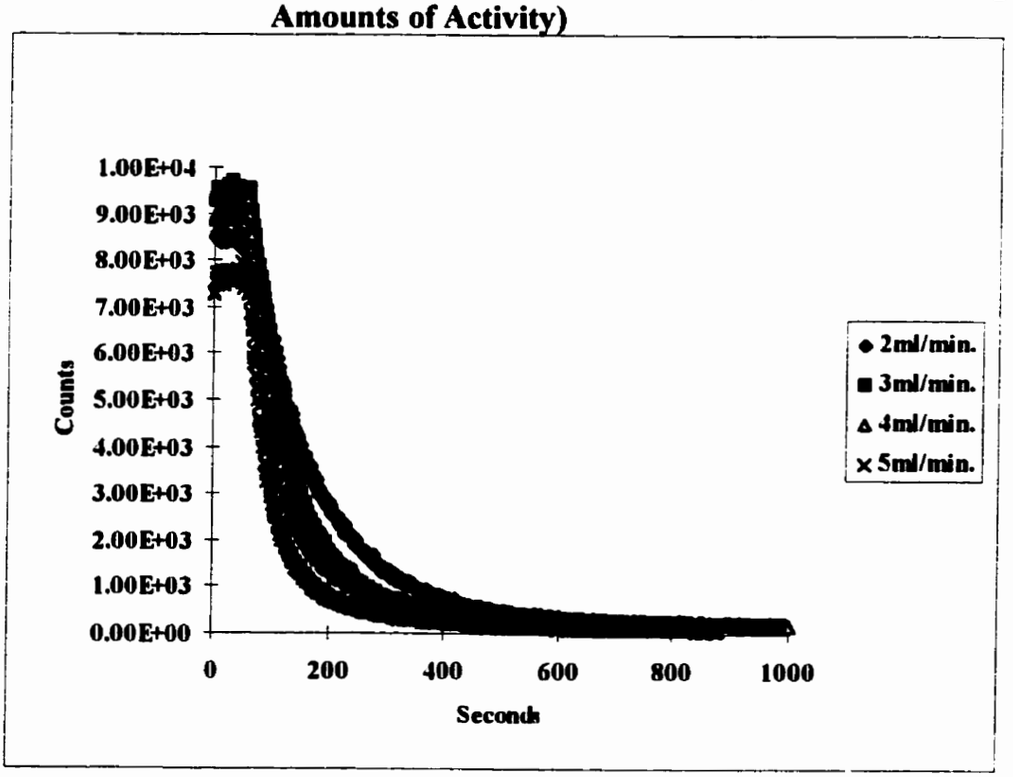

Figure 7.3(c): Input Function for Experiment No. 2 of Figure 7.3(a)

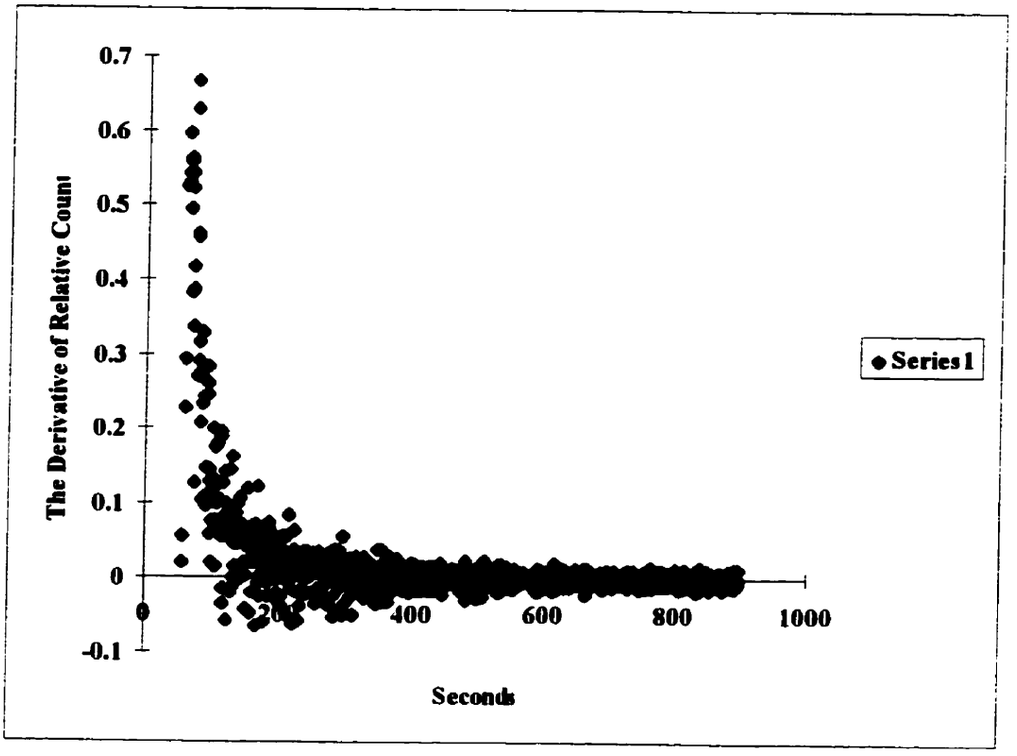

The DSRE and the USNRE experiments can be used to generate a theoretical USRE. The ability to calculate the USRE provides a method for assessing the ability of Equation (7.1) to correct for indicator recirculation (i.e. the theoretical USRE can be compared with the experimental results). However, before Equation (7.1) can be employed, the DSRE needs to be scaled to reflect the response per unit volume bolus of tracer injected. In the phantom experiments, the measured signal was related to the amount of indicator present within the brain (radiation decay was ignored as only about ten minutes of time lapsed between each injection). At each flow setting equal volumes of indicator bolus were used for both the DSRE and the USNRE experiments. Also, due to the design of the USNRE experiments, the maximum signal recorded is directly related to the amount of indicator injected. Therefore, the DSRE can be scaled by dividing by the signal maximum of the USNRE washout curve.

The Input Function, as mentioned in the theoretical section of this chapter, is the derivative of the USNRE. In taking the derivative, a number of numerical differentiation algorithms were evaluated. The algorithms included: (a) two, three-point formula[1], (b) a five-point formula[1] and (c) the negative difference. The method selected was the negative difference technique since it worked better over a larger time region. It consisted of taking the negative difference of the $(i+1)^{th}$ and the i^{th} point on the washout curve to represent the i^{th} input function value.

Figure 7.4 compare a theoretical and experiment USRE. It is evident that the convolution technique successfully predicts the USRE as the two curves are similar in shape and the area under the curves approximately the same. Although one may question the ability of the phantom experiment to simulate the CBF experiments carried out on rats, the underlying concepts of flow, impulse response function and input function are the same. As a result, the success observed in the phantom study provides the confidence needed to transfer the technique to animals.

Figure 7.4: Theoretical versus Experimental USRE Results

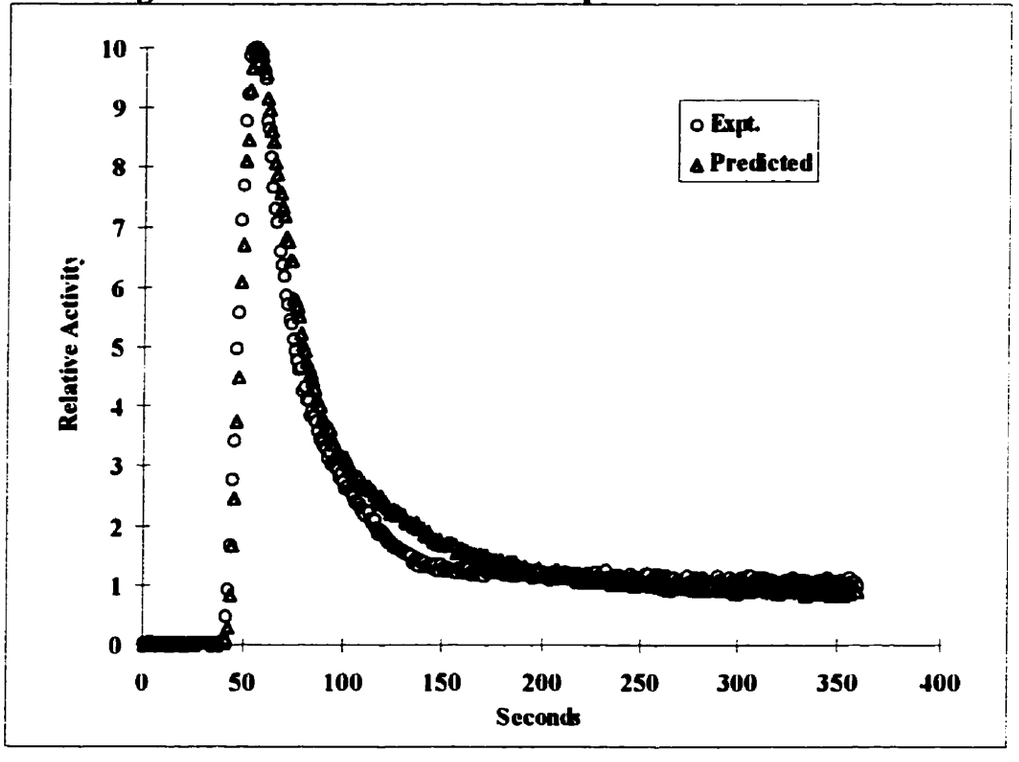

2. Animal Model

The recirculation experiments on animals differed from those on the phantom. The final CBF technique described in Chapter 4 corresponds to the USRE experiment. The goal of the recirculation experiments on animals was the reverse of the phantom study. In particular, convolution analysis in the animal experiment was employed in order to remove indicator recirculation from the USRE experiment. Having removed indicator recirculation from the USRE experiment, the derived USNRE result can be used for CBF calculation. Unfortunately, in animal experiments, a theoretical USNRE can not be compared with an experimentally obtained function (the latter is impossible to measure) – hence the need for validation of the technique through phantom studies.

In the animal study, a down-stream injection site must be selected. Initially, the left external jugular vein was chosen because it is at the exit of the brain. Unfortunately it requires an additional catheterization to be performed near the ECA (external carotid artery) catheter. This procedure is quite complicated and the additional neck incision further stresses the animal. A more practical downstream injection site and the one finally employed, was the right femoral vein (RFV). Compared to the external jugular site, the femoral is more distal to the brain. However, relative to the exit of the brain (the ideal injection site for obtaining the impulse response function of indicator recirculation), its distance from the heart is about the same; thus, the recirculation associated with a femoral injection should

be very similar to that associated with the exit of the brain. The primary advantage of the femoral site is its surgical simplicity.

A set of animal experiments for the indicator recirculation study included measuring two impulse response functions (IRFs), using the RFV indicator injection site and 0.2 ml bolus, as well as the original CBF experiment described in Chapter 4. The IRFs were scaled by the signal maximum of the washout curve obtained in the original CBF measurement in order to remain consistent with its definition. The first relative IRF (or IRF1) experiment began 30 minutes prior to the CBF experiment, and the second relative IRF (or IRF2) began 30 minutes after the start of the CBF experiment. Animal surgery and experimental parameters such as the size and injection time of the indicator bolus, etc., for the RFV experiments are described in Chapter 4. The two RFV experiments served to indicate the stability of the IRF during the 90 minutes of experimentation. Although the physiological parameters of the animal were kept as constant as possible during the experiment, the IRF could still change. It is speculated that a major reason for the change was the variation in the level of anaesthesia over the 90 minutes of measurement, an effect which could not be eliminated. Figure 7.5a shows a pair of relative IRF1 and IRF2 that are nearly equal to each other. In comparison, Figure 7.5b shows a pair of relative IRF1 and IRF2 that are dissimilar due to an increase in $PaCO_2$ level from normocarbia during IRF1 to hypercarbia during IRF2. If PSF1 is similar to IRF2, then the relative IRF at the time of the CBF experiment is taken

to be the average of the two. Such averaging, in some cases, can approximate the relative IRF even when IRF1 is not similar to IRF2; provided that during the 90 minutes of experimentation the change in animal physiological parameters are small or unidirectional (for example, with $PaCO_2$ either increasing or decreasing monotonically). In any case, the convergence of the predicted recirculation free washout curve to zero baseline can always be used to check the validity of the IRF used.

Figure 7.5a: IRF1 and IRF2 with Unchanging Animal Physiology

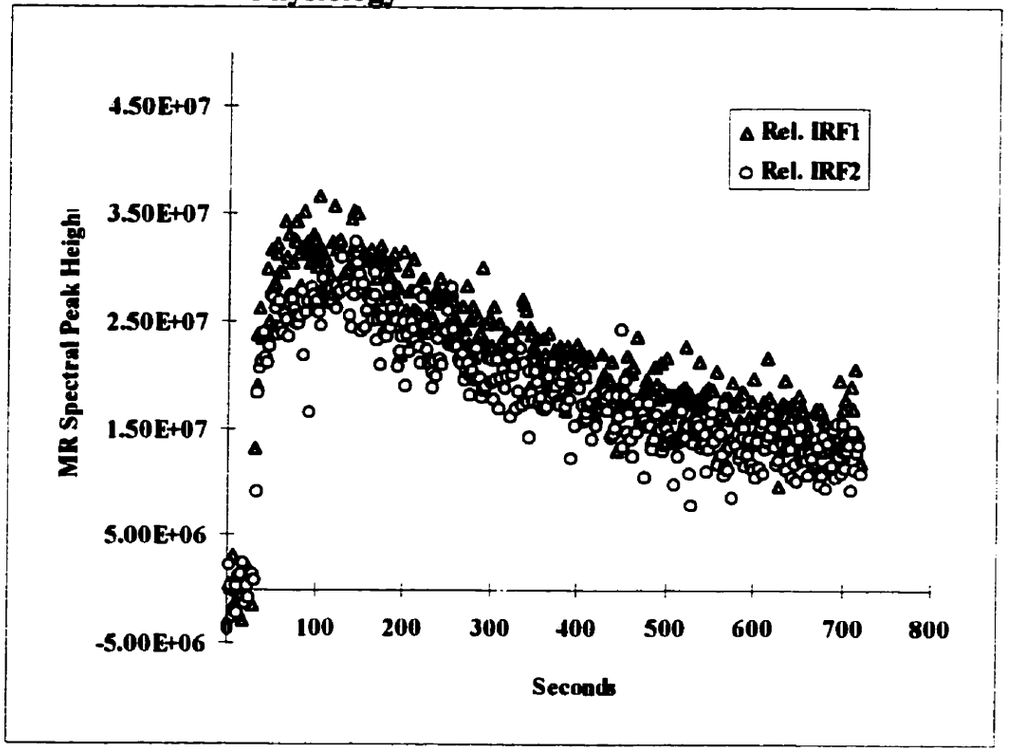

Figure 7.5b: IRF1 and IRF2 with Changing Animal Physiology

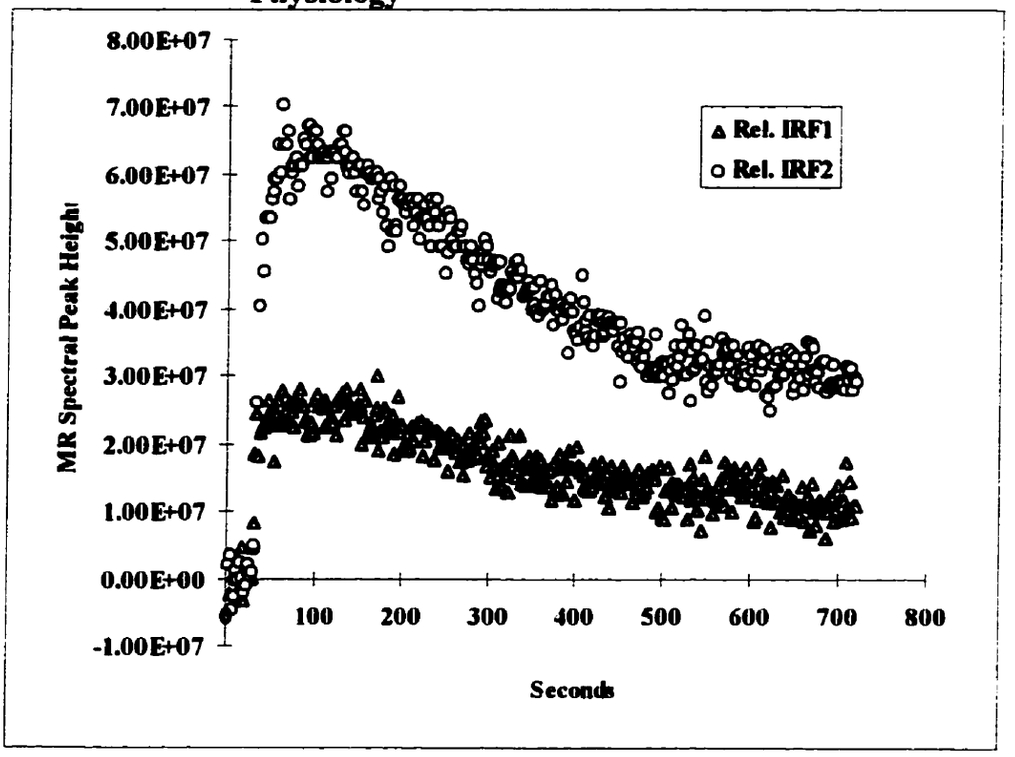

The procedure for calculating the indicator recirculation curve in the rat experiment paralleled that utilized in the phantom study. The impulse response function for the CBF experiment was scaled using the signal maximum associated with the washin/washout curve of the CBF experiment as discussed previously. The input function for the CBF experiment was taken as the derivative of the washout curve. The numerical differentiation method utilized was the same negative difference signal technique described in the phantom experiment section. Finally, Equation (7.1) was used to generate the indicator recirculation curve for the CBF experiment. Figure 7.6 shows an indicator recirculation curve, along with

its corresponding CBF washout curve. Note in this figure the convergence of the washout and recirculation curves. The convergence is a good indication of the validity of the impulse response function utilized. Note also that the gradual and smooth build-up of the recirculation is similar to that observed in the phantom experiments. At 48 seconds into the experiment (the time of the last datum point used in fCBF calculations, see Chapter 5) indicator recirculation reaches 25% of its maximum. The implication of this is that although only the initial few points are used in a fCBF calculation, the results obtained are still influenced by indicator recirculation.

Figure 7.6: Recirculation and Corresponding Washin/Washout Curves

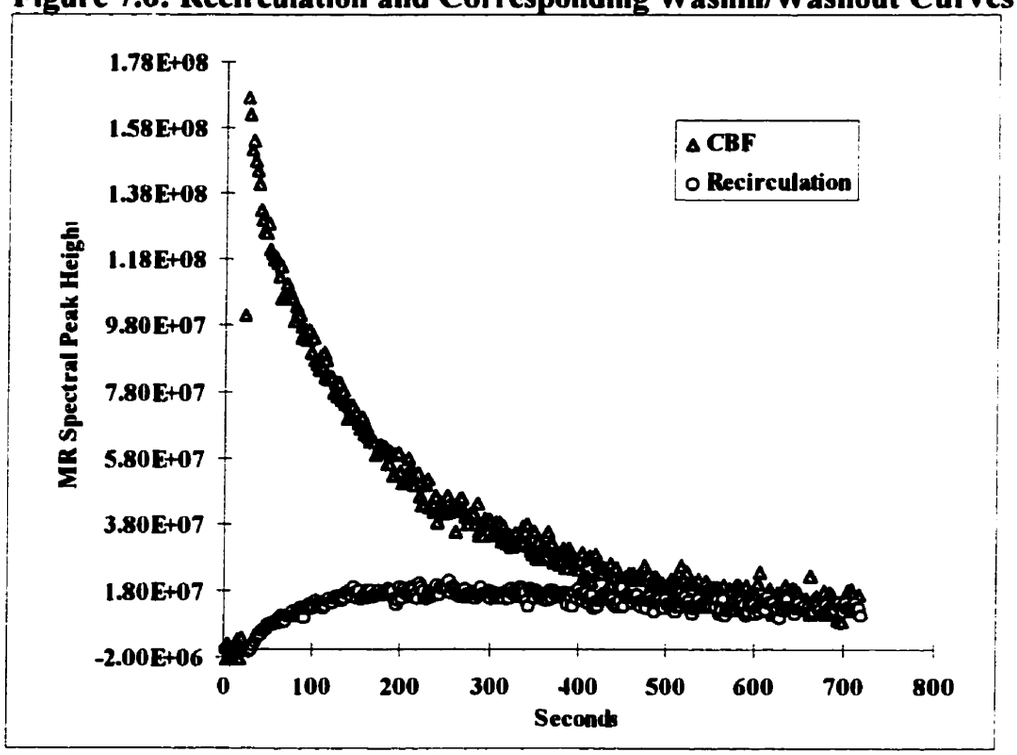

Figure 7.7 illustrates recirculation, impulse response function and CBF curves. Note the convergence of the three curves shown. Also, the maximum of the impulse response function is about 20 % that of CBF, indicating that 20% of the cardiac output went to the brain in this experiment. The average cardiac output to the brain for normal $PaCO_2$ (35 mmHg < $PaCO_2$ < 45 mmHg), as determined from 12 impulse response functions (in 6 recirculation experiments), was (18 ± 8) %. The cardiac output to the brain was also observed to increase with increasing $PaCO_2$ level as expected. The highest observed cardiac output to the brain (for $PaCO_2$ = 65 mmHg) was 45 ± 5 %.

Figure 7.7: Recirculation and Corresponding IRF and Washin/Washout (CBF) Curves

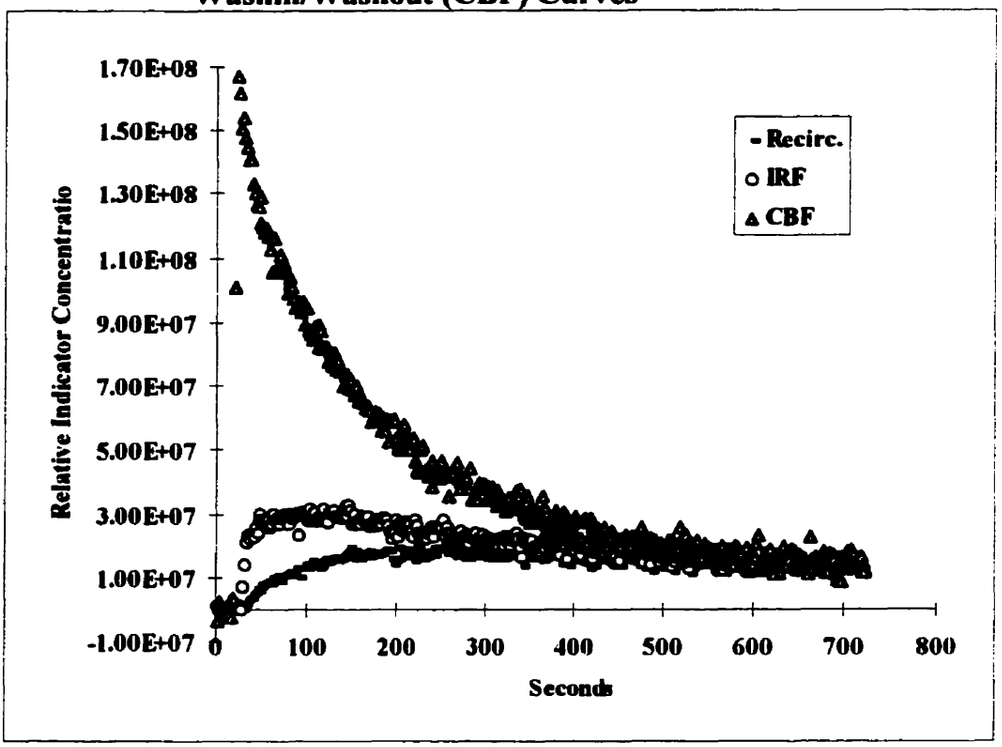

Figure 7.8 presents typical washout curves with and without correction for indicator recirculation. The recirculation corrected curve in Figure 7.8 was obtained by subtracting the recirculation curve (generated using convolution analysis) from the CBF curve. In Figure 7.8 the curve corrected for indicator recirculation converges to a base line of zero. In contrast, the curve not corrected for indicator recirculation converges to a non-zero constant base line, reflecting uniform distribution of indicator throughout the rat.

Figure 7.8: Washin and Washout Curves for CBF Experiment (With and Without Recirculation Correction).

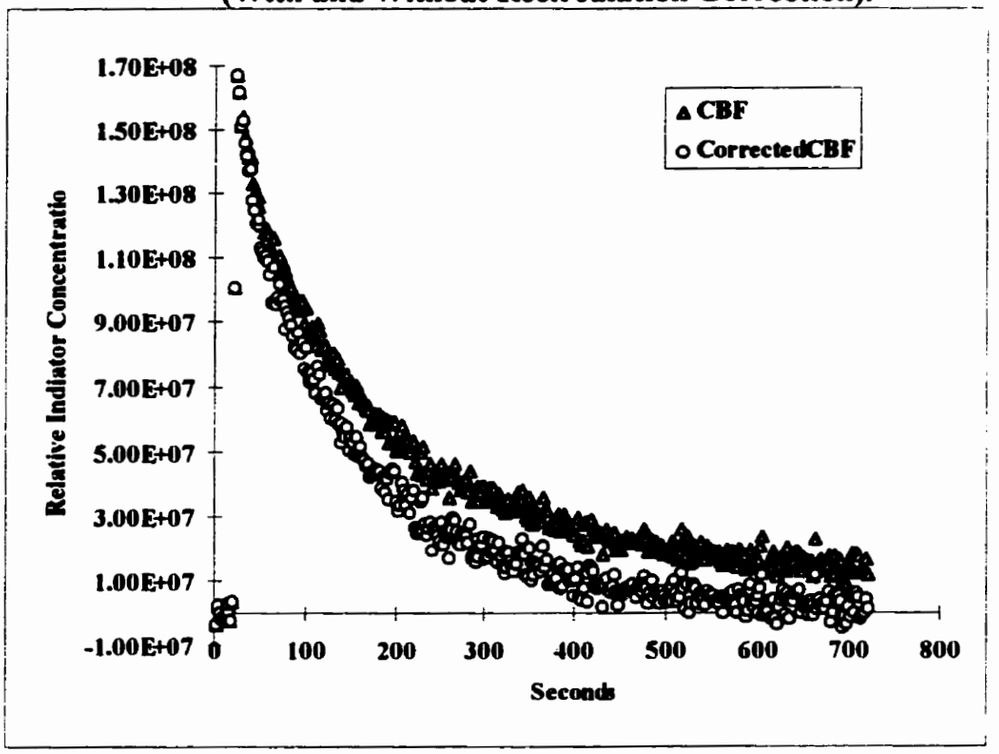

Figure 7.9 is a semi-log plot of the data presented in Figure 7.8. In this figure the recirculation corrected curve is straighter than the non-corrected one and would appear to consist of two linear segments of different slope. This shape supports the three component brain model consisting of an intra-vascular spike, a fast grey matter compartment (1st linear segment) and a slower white matter compartment (2nd linear segment). Note that in the case of the uncorrected curve, the initial section gradually shifts to the right, at no time demonstrating a linear region. This result suggests the possibility of simultaneous fCBF and sCBF calculation (with their respective recirculation corrected flows as refCBF and

resCBF), where fCBF, as before, stands for fast gray matter flow and sCBF for slow white matter flow. The procedure for this task was to use a least square linear regression to fit to each straight line portion independently and then use the slopes in conjunction with Eq. (5.1) to predict the recirculation corrected flows. (See Chapter 5). For the particular experiment shown in Figure 7.9 refCBF(3-23) was 68 and resCBF(50-100) 48 ml/100g/min; or resCBF(50-100) was 71% of refCBF(3-23) for this experiment.

Figure 7.9: Semi-Log. of Washin and Washout Curves (With and Without Recirculation Correction

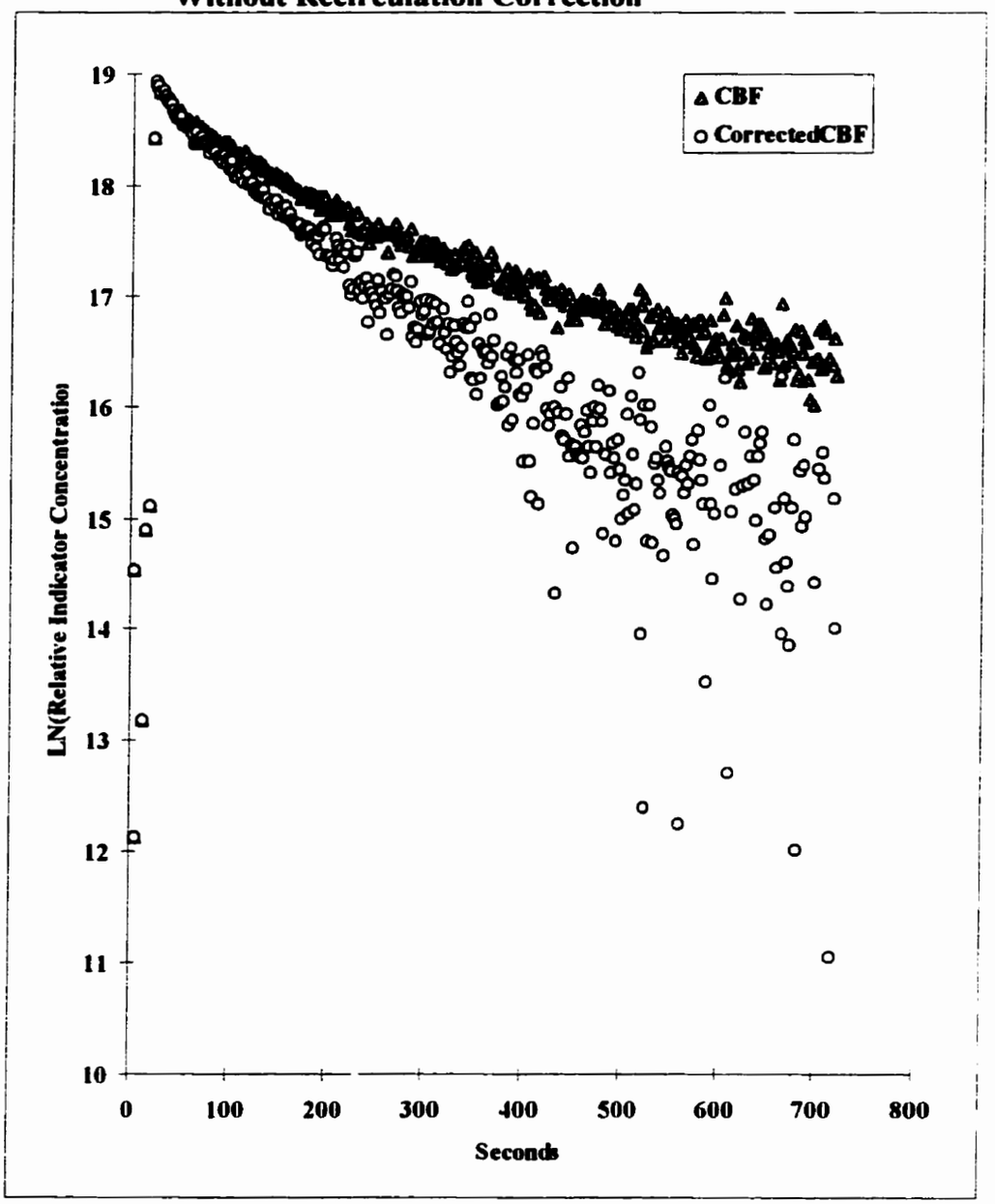

D. Non-Corrected Versus Corrected CBF Results

Figure 7.10 shows recirculation corrected (refCBF(3-23)) and non corrected fCBF(3-23) values. Figure 7.11 compares refCBF(3-23) with resCBF(50-100). The aCBF and the recirculation corrected rcaCBF values are shown in Figure 7.12, for comparison. The average percentage difference (P.D.) between corrected and non-corrected flow values of individual experiments was calculated to be 33% for aCBF and 31% for fCBF(3-23), using

$$P.D. = \frac{refCBF - fCBF}{refCBF} \times 100\%$$

If indicator recirculation were not partially corrected for using the crude aCBF technique described in Chapter 5, the percentage difference between recirculation corrected and uncorrected aCBF would have been higher.

Figure 7.10: Recirculation Corrected and Non-Corrected fCBF(3-23) versus $PaCO_2$. P.D. (ave.) = 31 ± 11

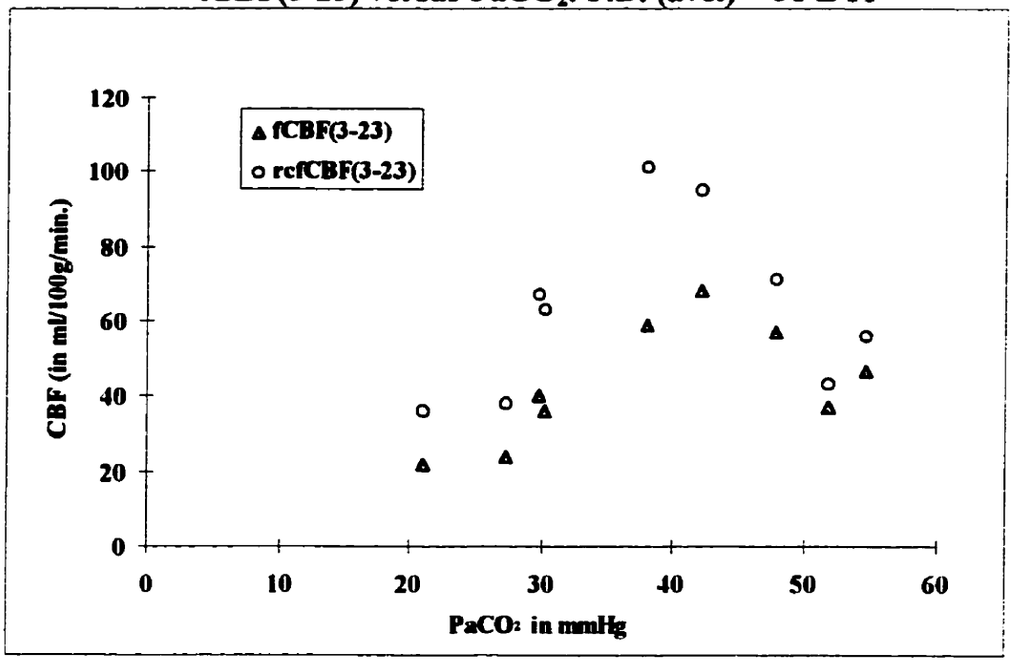

Figure 7.11: refCBF(3-23) and resCBF(50-100) versus $PaCO_2$

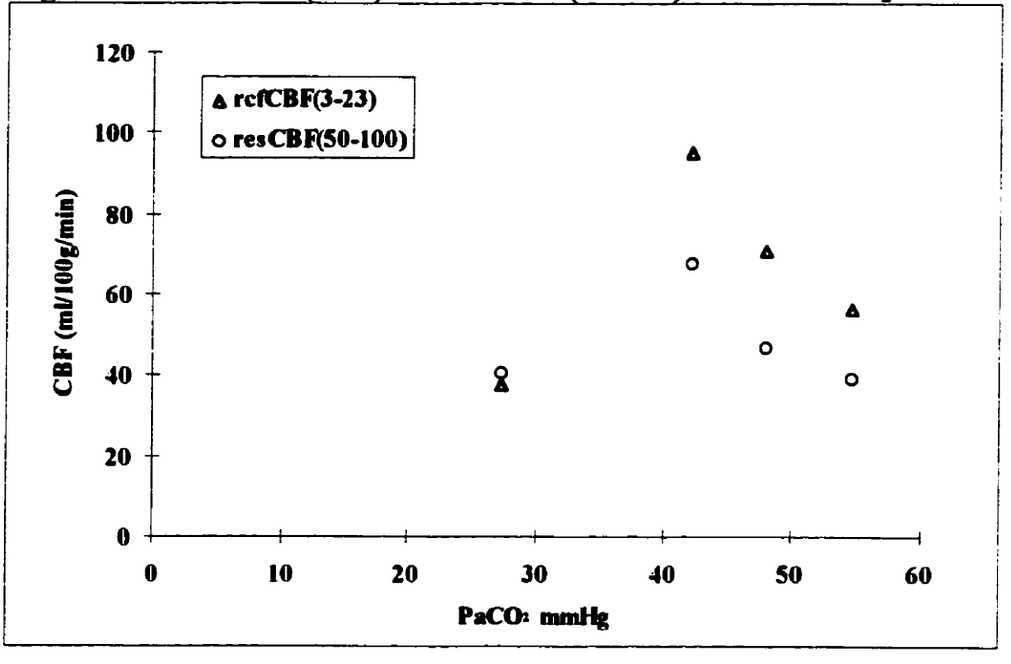

Figure 7.12: aCBF and rcaCBF versus $PaCO_2$. P.D. (ave.) = 33 ± 11.

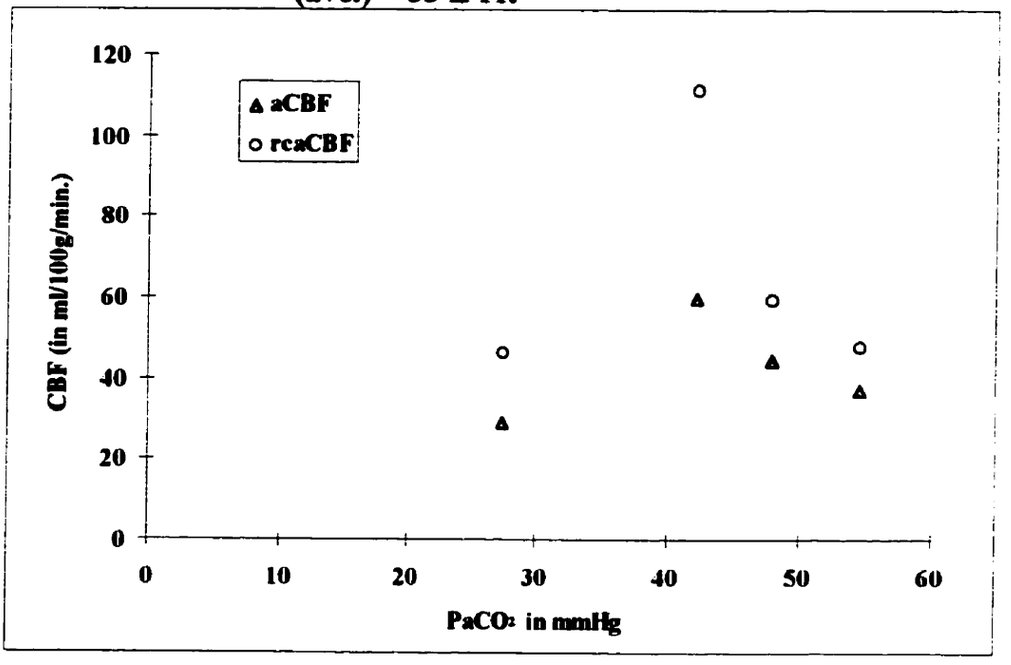

References:

1. Burden RL, Faires JD and Reynoids AC, *Numerical Analysis*, 2nd Edition, PWS Publishers, Boston, 1981.

Chapter 8: A Dual Indicator Technique for Measuring CBF: A Comparison of ^{2}H-Labeled Water and Alcohols

A. Introduction

It was pointed out in Chapter 6 that deuterated water is diffusion limited and therefore does not fully satisfy the requirements of the mathematical models used to predict CBF. This results in CBF underestimation. Also in Chapter 6, the deuterated water extraction coefficient (E) was measured in order to quantify the CBF underestimation. E is equivalent to the permeable surface (PS) area and is the reciprocal of the CBF underestimation correction factor. This chapter attempts to evaluate the CBF underestimation using a dual indicator technique. Briefly, the technique utilizes simultaneous injection of two kinds of indicator. The two kinds of indicator selected were deuterated water and deuterated alcohol. Because alcohols better satisfy the 'ideal' freely diffusible condition required by the mathematical models used for CBF calculations,[1,2,3,4,5] they can serve as a yard stick for assessing the degree of CBF underestimation associated with deuterated water. Using the deuterated water and deuterated alcohol CBF values from a dual experiment, the underestimation with respect to alcohol is given by

$$PD = 2 \times \frac{CBF(\text{alcohol}) - CBF(\text{water})}{CBF(\text{alcohol}) + CBF(\text{water})} \times 100\%, \qquad \text{Eq. (8.1)}$$

where *PD* is the percentage difference between the CBF determined using an [^{2}H]alcohol (alcohol for short) based indicator and that using [^{2}H]water (water for short).

In the dual indicator protocol developed, water and alcohol are injected simultaneously. Because of the nature of pulse MR signal acquisition (i.e. both alcohol and water signals are acquired together in a FID after an rf pulse), the washin/washout of the two indicators can be monitored simultaneously (because the FID can be Fourier transformed into a spectrum to yield both the alcohol and water lines) and as a result, CBF can be calculated for each of the two indicators under identical conditions. Hence, differences in the two values reflect only diffusion limitations of water, assuming that no individual indicator is under preferential flow regulation due to metabolism or other differential flow factors.

In this chapter, substantial efforts were given to the development of the dual indicator technique, especially in understanding acute alcohol reactions (so as to determine the most appropriate bolus size and concentration of alcohol for each injection) and determining which alcohol is most suitable for the dual indicator study. In addition, the dual indicator experiment necessitated the development of appropriate data processing procedures prior to CBF modeling. One should keep in mind while reading this chapter that the results are preliminary and qualitative only. This is due to the fact that only a small number of experiments were

performed for each of the three dual indicator techniques. More experiments are needed before statistically significant conclusions can be formulated.

B. Dual-Indicator Experiments

The dual indicator experiments were designed to measure water CBF and alcohol CBF under virtually identical conditions. To achieve this, the CBF technique presented in Chapter 4 required modification. One modification which has already been mentioned was to replace the original water indicator with a mixture of alcohol and water. Another modification was in the technique used to introduce the indicator into the system. The injection catheter of the injection assembly (See Chapter 4 on catheter fabrication) was filled with Heparin Leo® (0.33 mL). This step attempted to prevent blood from clotting during the experiment. At 5 to 10 minutes before injection, the Heparin Leo® filled injection assembly was withdrawn so that the catheter assembly was filled with blood from the animal. Then a very small air bubble ($\leq$ 0.002 mL) was introduced, and 0.32 mL of dual indicator mixture was loaded behind the air bubble. This air bubble served to isolate the indicator mixture from the blood. During indicator injection, the small air bubble was pushed into the ECA, along with the desired indicator injection bolus.

Three different indicator mixtures were used in the dual study:

1. a mixture of [^{2}H]water and [^{2}H]ethanol (dual ethanol for short)
2. a mixture of [^{2}H]water and [^{2}H]isopropanol (dual isopropanol)

3. a mixture of [^{2}H]water and [^{2}H]t-butanol (dual t-butanol)

The fact that alcohol could affect the animal physiology was assumed inconsequential, as the respective CBF values of water and alcohol were measured under the same physiologic conditions.

The ^2H_2O spectrum was simple, as it contained only the O^2H line (see Figure 4.5). The dual ethanol spectrum, besides the O^2H line of ^2H_2O, also contained the C^2H_3 line (1.3 ppm), the C^2H_2 (3 ppm) line, and the O^2H associated with deuterated ethanol ($C^2H_3C^2H_2O^2H$). These three lines are resolvable *in vitro* using large number of averages (n.a. = large number) per FID, (and hence per spectrum). Figure 8.a1 shows a dual ethanol spectrum obtained *in vitro* using n.a. = 200 per FID and line broadening (lb) = 0.3 Hz. For comparison another *in vitro* spectrum with n.a. = 3 and lb = 50 Hz is given in Figure 8.a2. Note in Figure 8.a2 that the three lines are barely resolved. The lb = 50 Hz was the line broadening used in all the animal experiments so as to achieve superior SNR at the expense of resolution (see later sections for more detail). The corresponding dual isopropanol spectra are given in Figure 8.a3 and 8.a4. Note in Figure 8.a4 that the small C^2H (3.2 ppm) line of the deuterated isopropanol is not resolved. A spectrum for dual t-butanol, with n.a. = 3 and lb = 50Hz, is given in Figure 8.a6. Note the single C^2H_3 line from deuterated t-butanol [$(C^2H_3)_3C$-O^2H].

Figure 8.a1: Deuterium Spectrum for dual Ethanol Indicator (n.a. = 200, lb = 0.3 Hz)

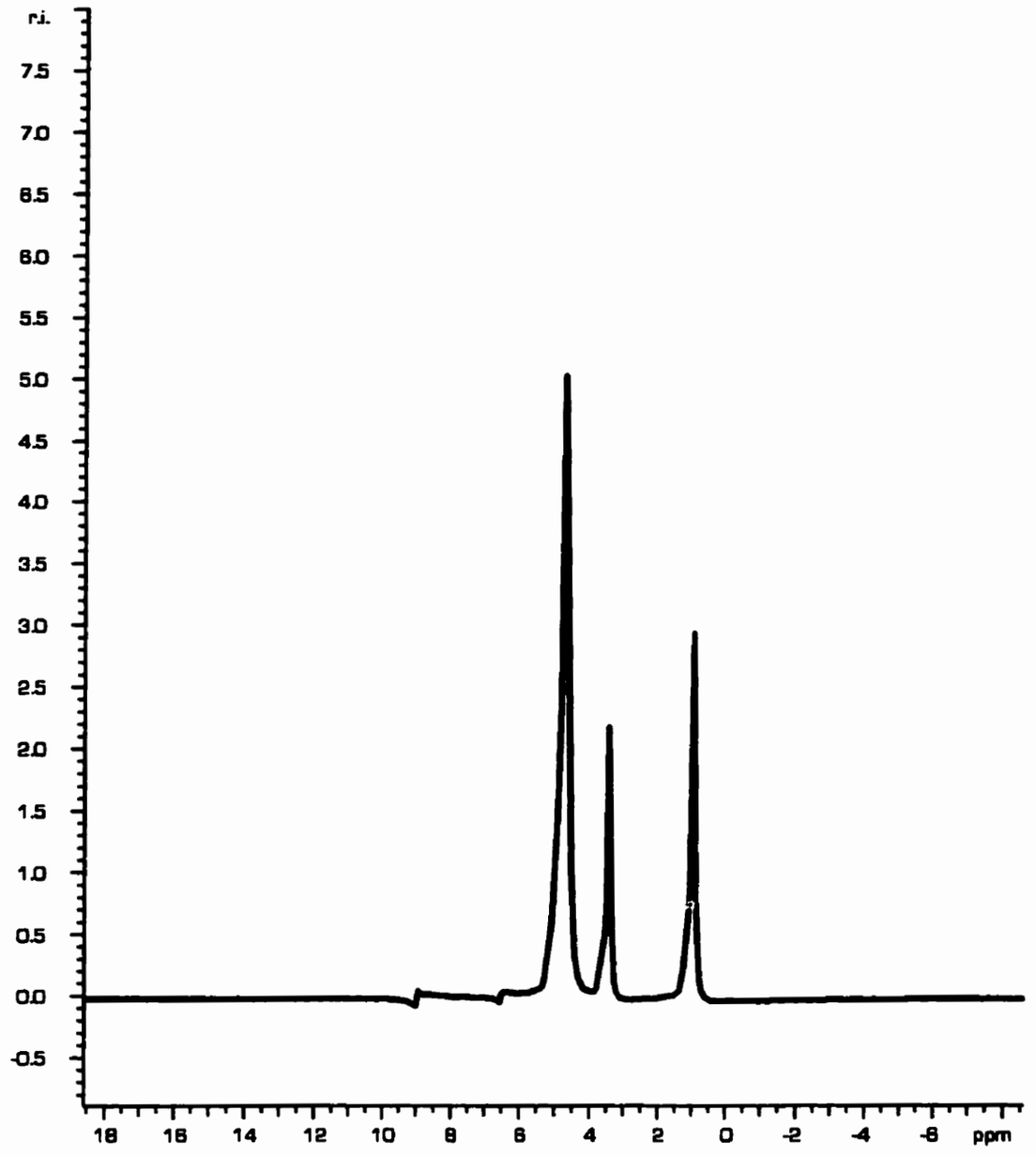

Figure 8.a2: Deuterium Spectrum for dual Ethanol Indicator (n.a. = 3, lb = 50 Hz)

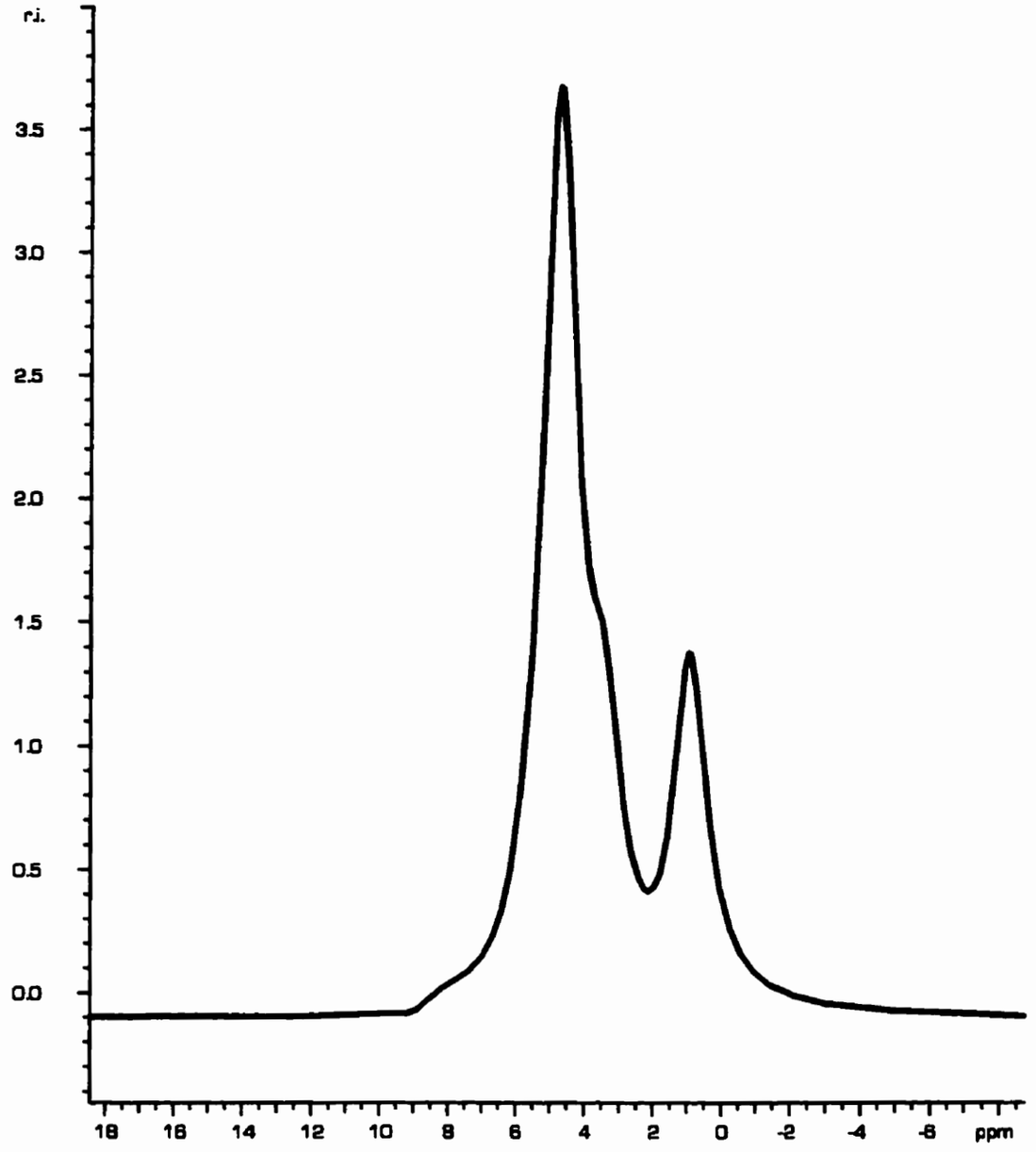

Figure 8.a3: Deuterium Spectrum for dual Isopropanol Indicator (n.a. = 100, lb = 0.3 Hz)

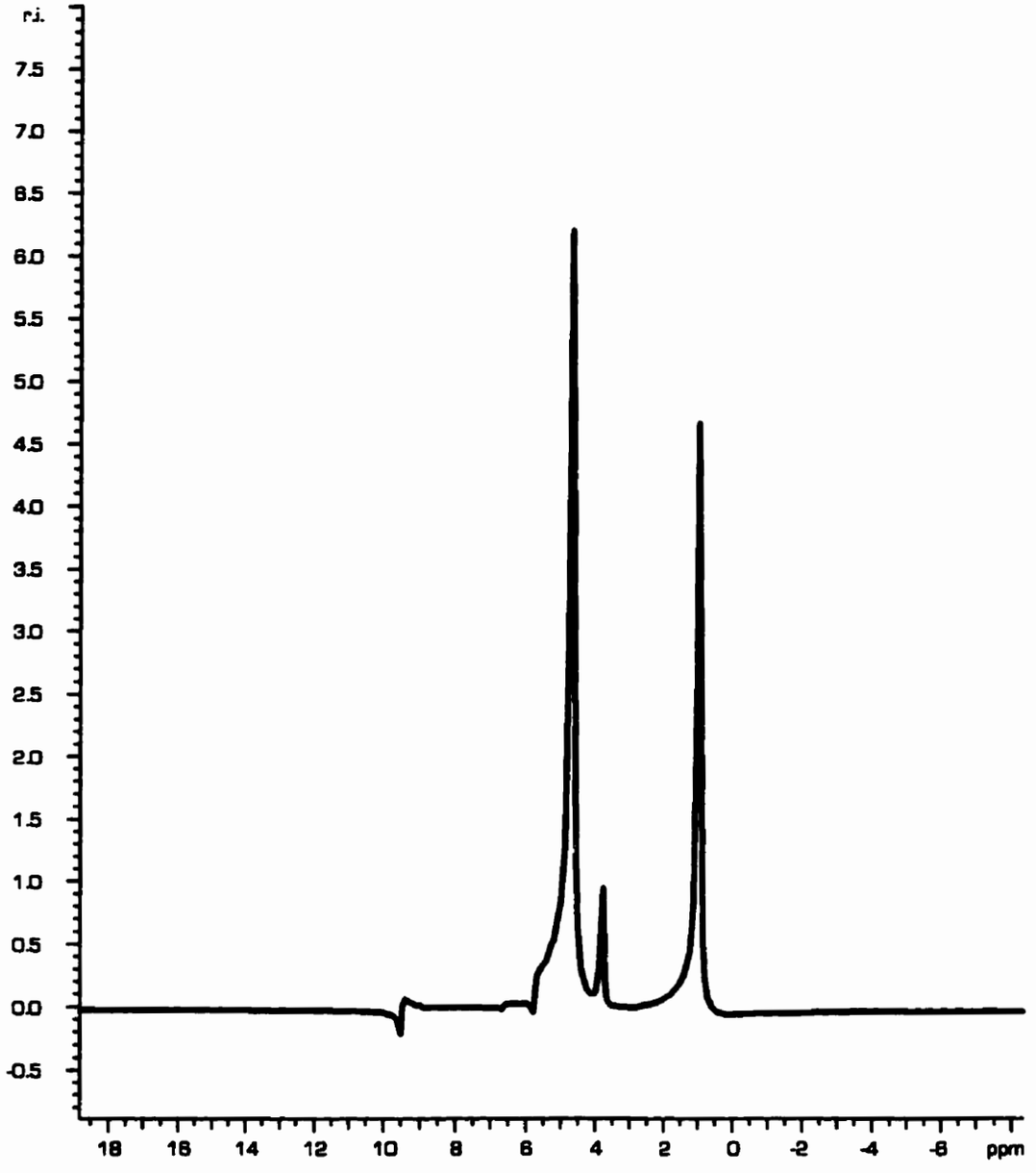

Figure 8.a4: Deuterium Spectrum for dual Isopropanol Indicator (n.a. = 3, lb = 50 Hz)

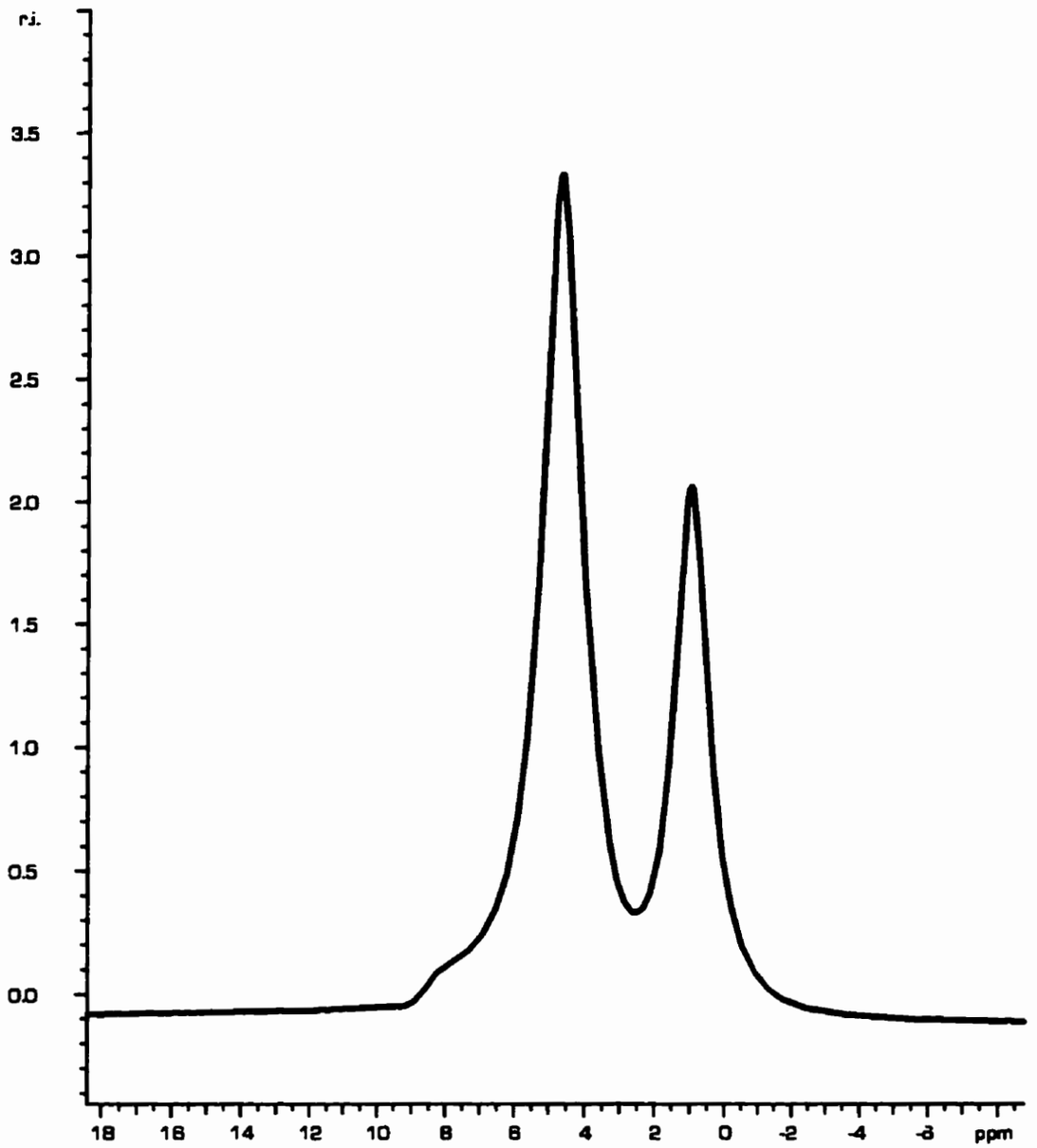

Figure 8.a5: Deuterium Spectrum for dual t-Butanol Indicator (n.a. = 100, lb = 0.3 Hz)

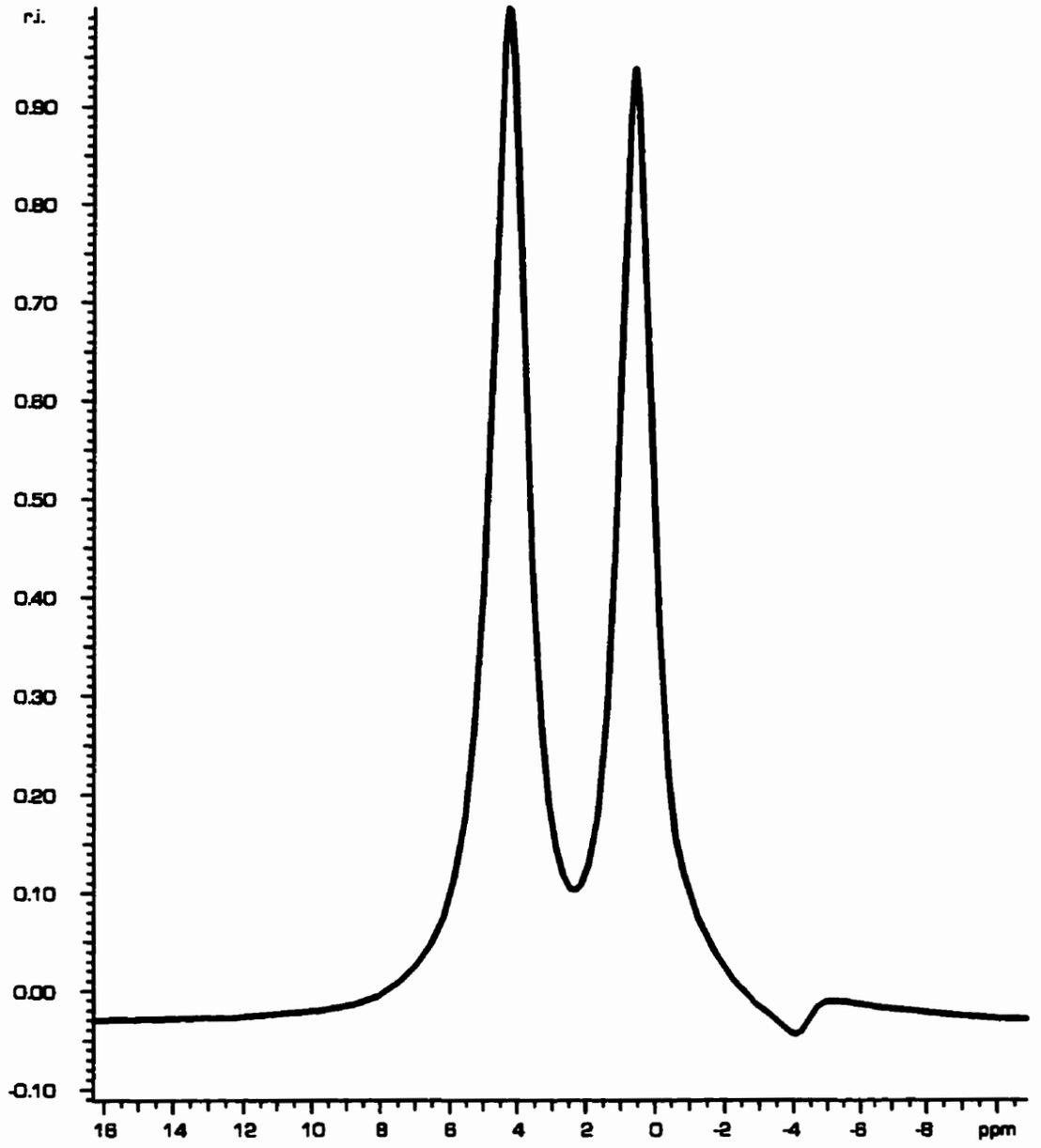

Figure 8.a6: Deuterium Spectrum for dual t-Butanol Indicator (n.a. = 3, lb = 50 Hz)

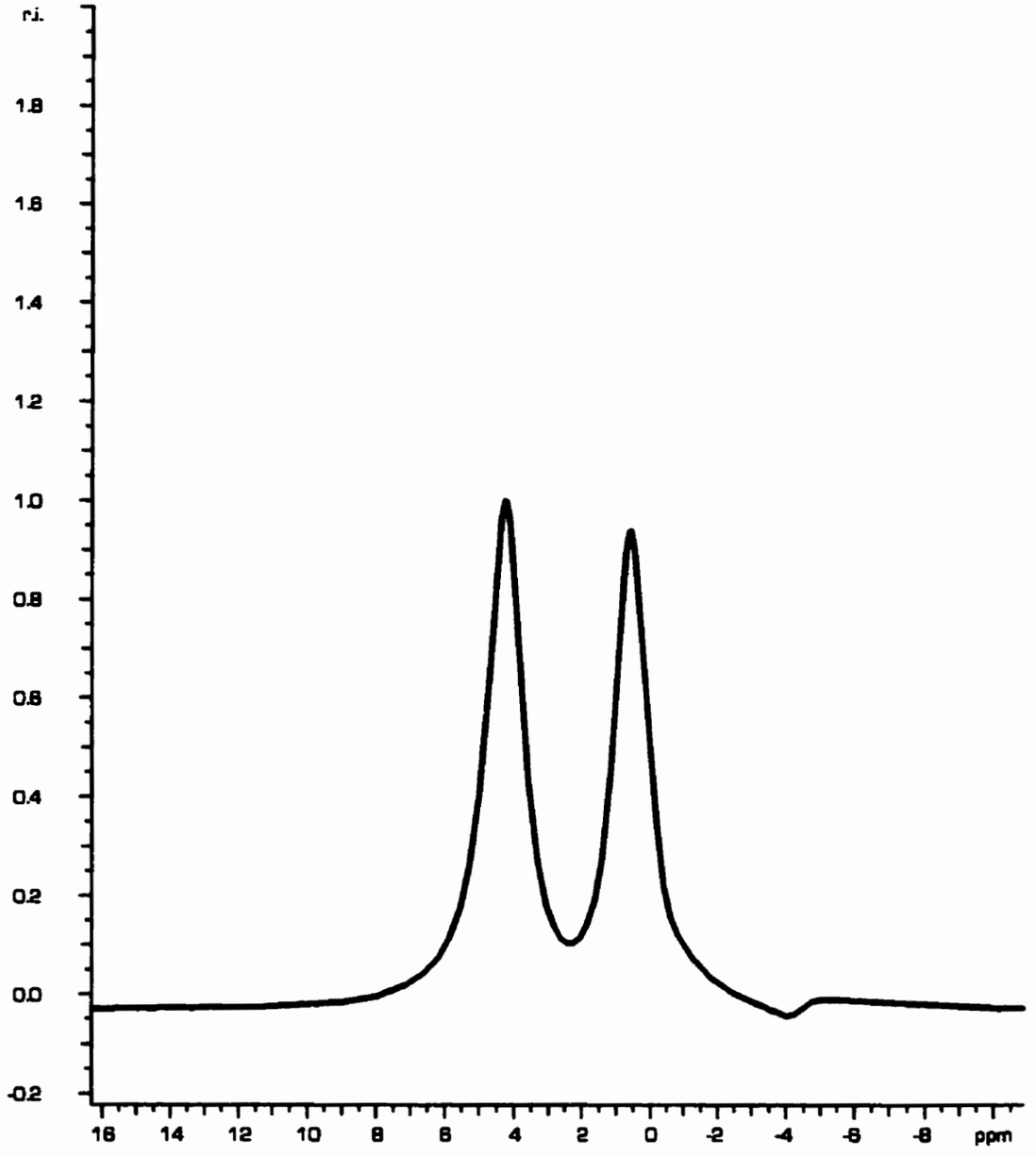

1. The Dual Ethanol Protocol

In the dual ethanol experiments, the size of the indicator bolus used was 0.2 ± 0.01 mL. (See Table 8.1). Composition of this bolus was:

1. [^{2}H]ethanol ($C^2H_3C^2H_2O^2H$, ethanol for short) 60% v/v
2. [^{2}H]water 38% v/v
3. 1% Heparin Leo® v/v
4. 0.9 mg NaCl /100mL

The time and frequency of experiments were the same as those described in the final CBF protocol of Chapter 4. With this Ethanol concentration, an animal could typically tolerate 2 to 3 injections at 30 minute intervals, after which the physiology and the CBF of the animal were affected. Figure 8.1(a) shows a typical washin and washout curve for a dual ethanol experiment. It can be seen that, although the amount of ethanol injected was quite large (0.12 mL), the SNR of the ethanol experiment was small. A more serious problem with the dual Ethanol experiments in particular, and all alcohol experiments in general, was the observation that blood pressure and presumably the CBF fluctuated drastically during the initial washout, affecting fCBF determination. The claim that CBF fluctuated during a dual alcohol experiment was supported by a number of observations. Indirect evidence was the significant change in blood pressure during the washin and washout of the indicator mixture. When the ethanol was introduced, blood pressure increased rapidly from normobaric (90 to 110 mmHg)

to hyperbaric (≥ 180 mmHg), usually in about 5 minutes. After the initial increase, blood pressure dropped continuously, at a slower pace, to hypobaric (50 to 70 mmHg), in about 15 minutes. This was followed by the blood pressure recovering to normobaric, usually in time for the next experiment (≈ 30 min) if the animal was still alive. Figure 8.1(a) served as additional evidence of CBF fluctuation during indicator washin and washout. In this figure, the characteristic exponential indicator washout shown in Figure 8.1(b) (a washout curve obtained from a deuterated water only injection) was not observed. The deviation of the washout curve from that expected suggested that the CBF might have fluctuated during the initial washout, with each change represented by a fluctuation in the linear portion of the initial washout in a semilog plot. When the fCBF values (see Chapter 5) were calculated using non-characteristic washout curves similar to that of Figure 8.1(a), the values obtained ranged from approximately 0 mL/100g/min to 30 mL/100g/min. In addition, the values were associated with large uncertainties. The large range and large uncertainties of CBF measured from the dual experiments made meaningful statistical analysis impossible. The reduction in CBF was dependent on the amount of ethanol injected per study and on the total amount accumulated in the animal. Figure 8.1(e) shows a dual ethanol experiment with less deviation due to less alcohol accumulated in the animal. CBF fluctuations during indicator washin and washout also occurred in the dual alcohol experiments using [^{2}H]t-butanol and [^{2}H]isopropanol, although the magnitude of fluctuation

was less. The CBF fluctuation indicated in Figure 8.1(a) was severe. Further alcohol injections either killed the animal, or disrupted the CBF entirely, as shown in Figure 8.1(c). This state of total absence of washout was observed in all rats after a sufficient amount of alcohol was introduced.

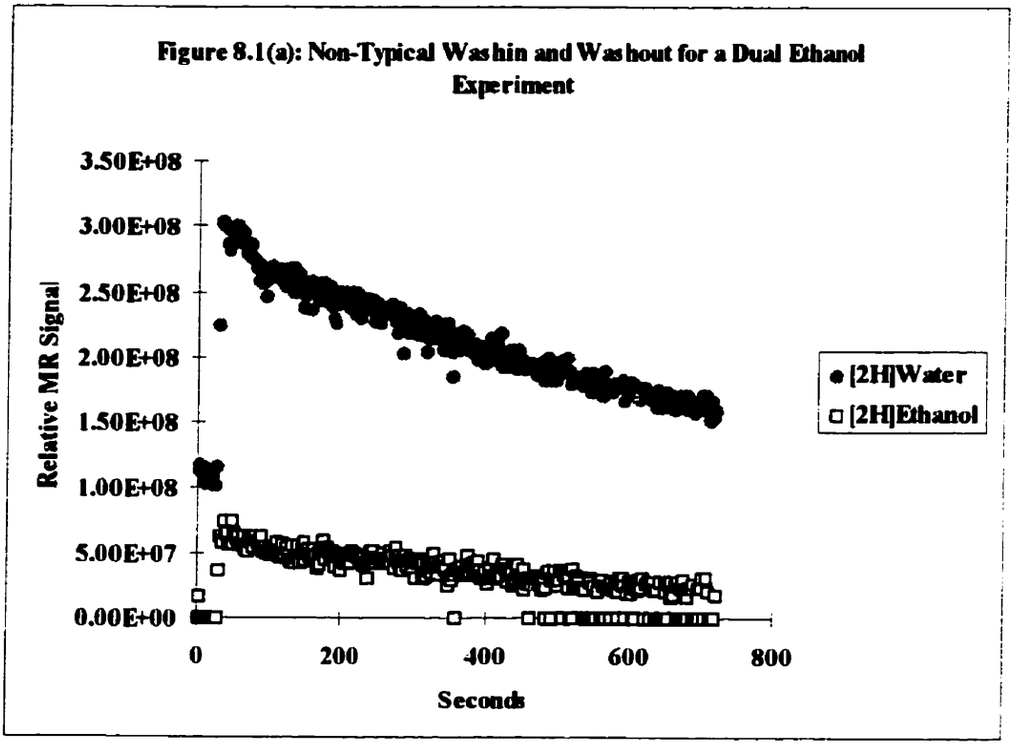

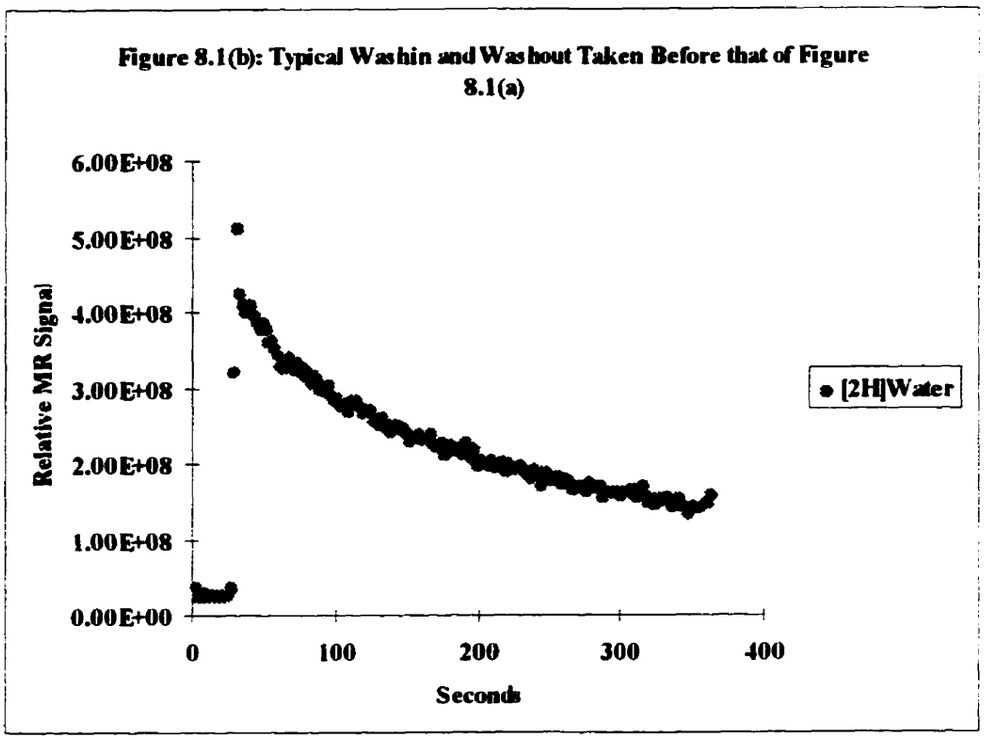

It was realized that the dual ethanol study was of limited usefulness. In order to obtain an adequate SNR, a relatively large amount of ethanol had to be injected, in turn producing a significant drop in CBF from the 'normal' value (as evident from the washin/washout curves similar to that of Figure 8.1(a)). When the CBF was disrupted, as the case in Figure 8.1(c), the flow could sometimes be restored by injecting additional [^{2}H]water (heparinized saline). The washin and washout of Figure 8.1(d) was taken after an injection of [^{2}H]water into a rat exhibiting the disrupted CBF shown in Figure 8.1(c).

Figure 8.1(c): CBF Disruption Due to Additional Alcohol Injection After that of Figure 8.1(a)

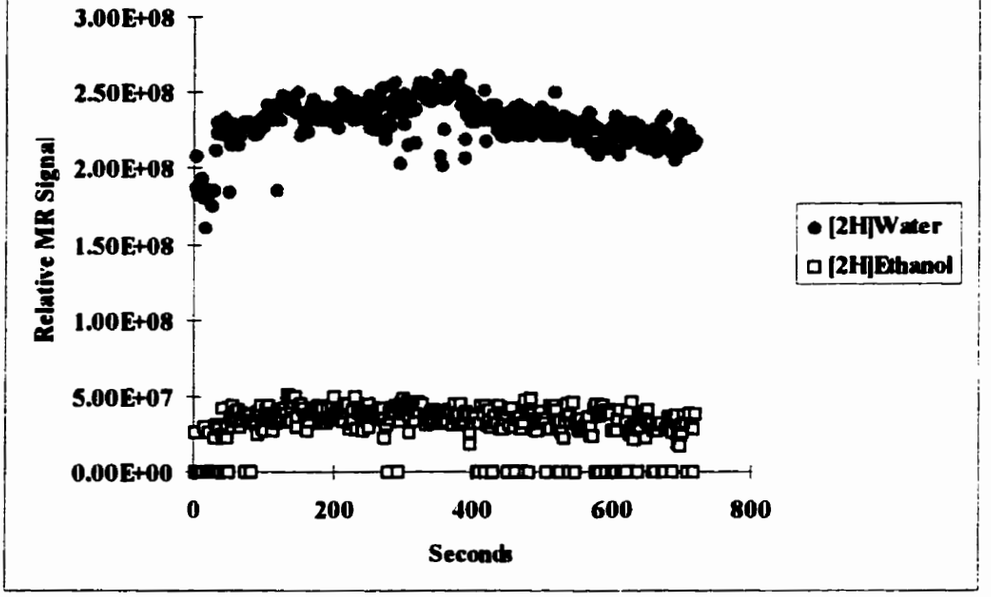

Figure 8.1(d): Restoration of Typical CBF

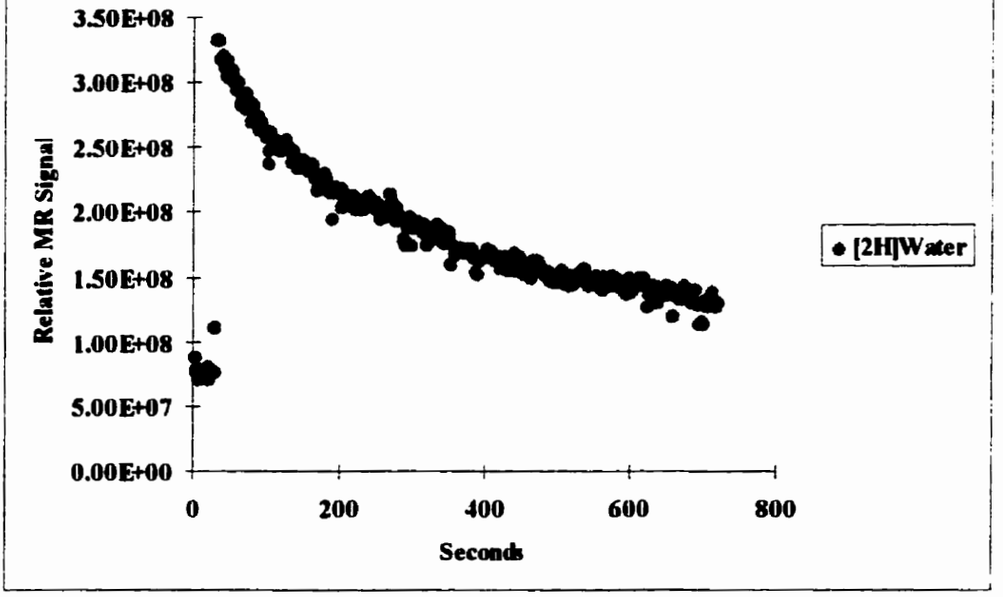

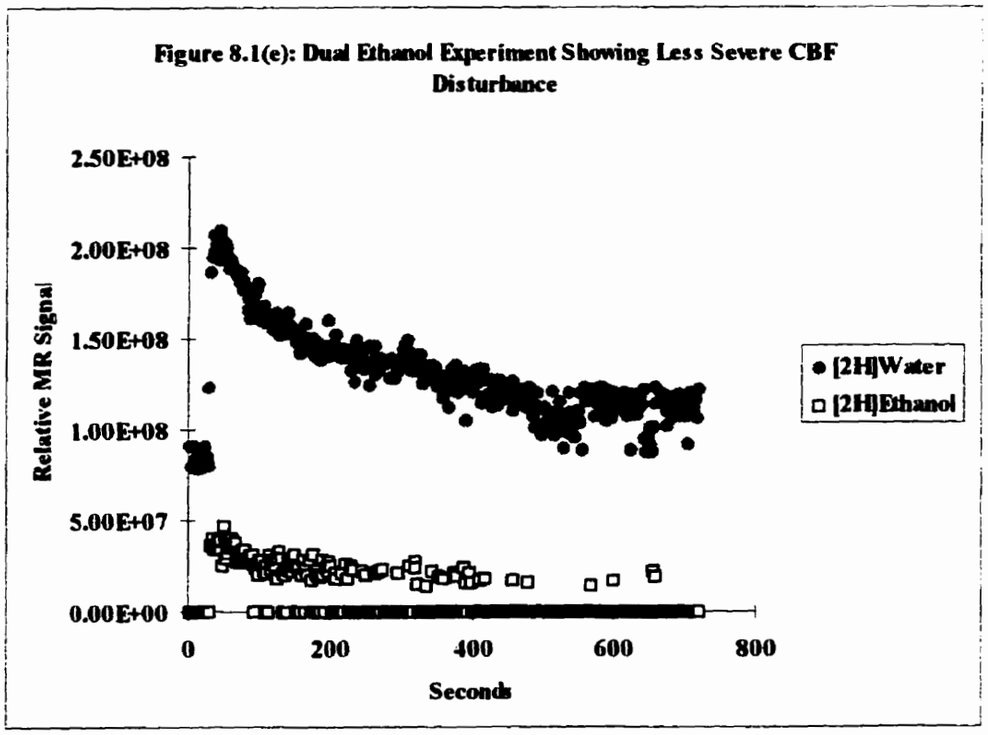

2. The Dual Isopropanol Experiment

In the dual isopropanol study, the size of the injection bolus used was 0.10 ±0.01 mL. The indicator mixture consisted of:

1. [^{2}H]isopropanol [$(C^2H_3)_2C^2HO^2H$, isopropanol for short] 30% v/v
2. [^{2}H]water 68% v/v
3. Heparin Leo® 1% v/v
4. NaCl 0.9 mg/100mL

The amount of alcohol in each experiment was therefore 30% (by volume) of that used in the dual ethanol study. The indicator injection time was less than or equal

to 1 second and an animal could tolerate typically 3 to 5 injections at 30 minute intervals before physiologic changes affecting the CBF were observed.

A typical washin and washout curve for the dual isopropanol experiments is given in Figure 8.2. Many of the observations and comments made for the dual ethanol investigation were also noted in the dual isopropanol study. These observations and comments include:

1. a reduction of CBF (see Table 8.2 (a))
2. an increase in the uncertainty of measured CBF
3. blood pressure fluctuation, which was observed to be the same as described in the previous dual ethanol experiment section
4. temporary CBF disruption and permanent CBF breakdown (similar to that given in Figure 8.1(c)), etc., when the amount of alcohol injected per study or the total amount accumulated in the animal was large

Once again, meaningful statistical analysis of CBF values was difficult. There were however important differences between the dual ethanol and the dual isopropanol experiments. First, blood pressure variation (from normobaric, at the beginning of indicator washin, to hyperbaric, followed by hypobaric and then back to normobaric) during an experiment was in general less severe for the latter. Secondly, a normal washin and washout curve (similar to that obtained using only [^{2}H]water as an indicator) was observed in some of the dual isopropanol

experiments (See Figure 5.1), usually for the first two to three dual indicator injections (within an individual animal). However, achieving the characteristic washin and washout does not imply that the CBF in the rat was not disturbed, only that the changes in physiology were less. Furthermore, the SNR for the dual isopropanol measurements was much larger than that observed in the dual ethanol experiments. Unfortunately, the prominent isopropanol line was not resolved from the shoulder of the water line in the MR spectra acquired in the dual isopropanol studies. Therefore, the isopropanol signal was severely contaminated with water, and the peak height measured at that position was not directly proportional to the alcohol concentration.

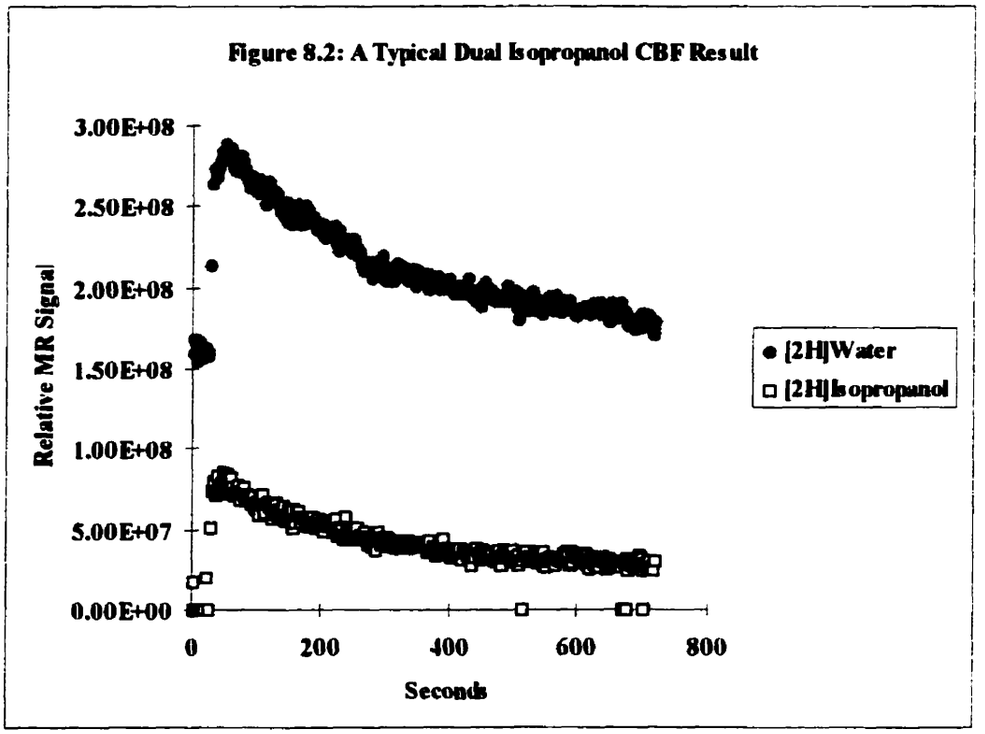

3. The Dual t-Butanol Experiment

Two types of dual t-butanol experiments were performed. Initially, the size of indicator bolus was 0.05 mL. This bolus, besides heparin and NaCl, included: [^{2}H]t-butanol [$(C^2H_3)_3C\text{-}O^2H$] (50% v/v) and [2H]water (50% v/v). Since the bolus was concentrated and small in size, special attention was given to the filling of the catheter assembly. (See Part I of Chapter 4 for details.) Briefly, in order to prevent the waste of concentrated t-butanol in the 0.33 mL dead volume of the catheter assembly, the filling of the catheter was as follows:

1. Fill the entire catheter assembly with Heparin.
2. Introduce a small air bubble into the tip of the catheter.
3. Draw in 0.05 mL of indicator, to be injected as a bolus.
4. Repeat steps 2. and 3., as much as five times, depending on number of experiments to be run.
5. Draw in the last air bubble and fill the tip of the catheter with Heparin.

The air bubbles in the filling served to separate the leading bolus from the blood of the animal after each injection.

It was believed that the t-butanol concentration in the previously discussed experiments was too great in that it significantly affected the rat physiology (similar to that of dual ethanol) and hence affected the CBF. It was decided to use approximately the same amount of alcohol (0.033 mL) but in a lower

concentration. In these later studies, the size of indicator bolus was 0.33 ± 0.05 mL. This bolus included:

1. [^{2}H]t-butanol (t-butanol for short), 10 % v/v
2. [^{2}H]water, 88% v/v
3. Heparin Leo®, 1%
4. NaCl (0.90 mg/100 mL)

Due to the larger total bolus size, the injection time was increased to less than or equal to 2 seconds. In terms of CBF modeling, a 2 second injection time was acceptable, as can be seen from Figure 8.3(a) which suggests that the washin of indicator was sufficiently fast. The frequency of experiments was every 30 minutes, as before. Usually an animal remained alive for 3 to 5 injections (an improvement from the 2 to 3 injections of the earlier t-butanol study) indicating that the attempt to reduce the effects of alcohol on the rat physiology was successful.

A typical dual t-butanol washin and washout curve obtained with the lower concentration of alcohol is given in Figure 8.3(a). The results were similar to the dual isopropanol studies and most of the observations and comments for Figure 8.3(a) were similar to that for dual isopropanol, namely:

1. a reduction of CBF
2. an increase in uncertainty associated with measured CBF
3. blood pressure fluctuation

4. temporary CBF disruption

5. permanent CBF breakdown, etc., when the amount of alcohol injected per study or the total amount of accumulated alcohol in the animal was large

The level of t-butanol water contamination was approximately 24% (derived using deconvolution method, see later) compared to 100% for isopropanol (the latter was estimated by visual inspection; for example, the peak height of the isopropanol line was smaller than the height of the shoulder of the water line it sat on). This observation might have been due to the fact that all dual isopropanol experiments were performed on rats having a large ^{2}HOH background). If t-butanol is less contaminated with water in general, then the dual t-butanol technique is the method of choice for quantifying CBF underestimation. (See later for details of how the water contamination in dual t-butanol studies was eliminated using a de-convolution method.) After 3 to 4 experiments, the washin and washout began to resemble that of a typical dual ethanol study, as is shown in Figure 8.3(b); additional alcohol injections either killed the animal, or interrupted CBF entirely. See Figure 8.3(c).

Figure 8.3(a): A Typical Washin and Washout [2H]t-Butanol Result

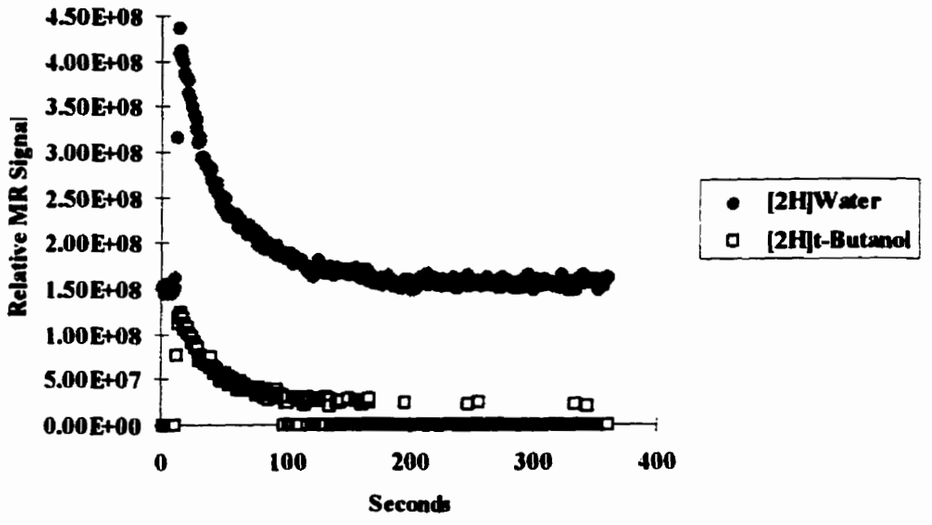

Figure 8.3(b): Typical Washin and Washout after 4 to 5 dual t-Butanol Experiments

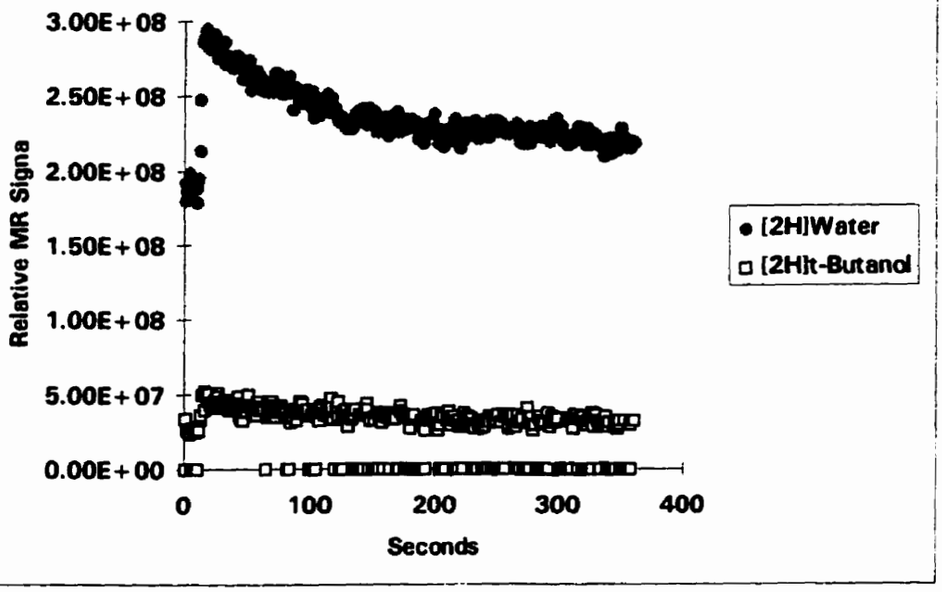

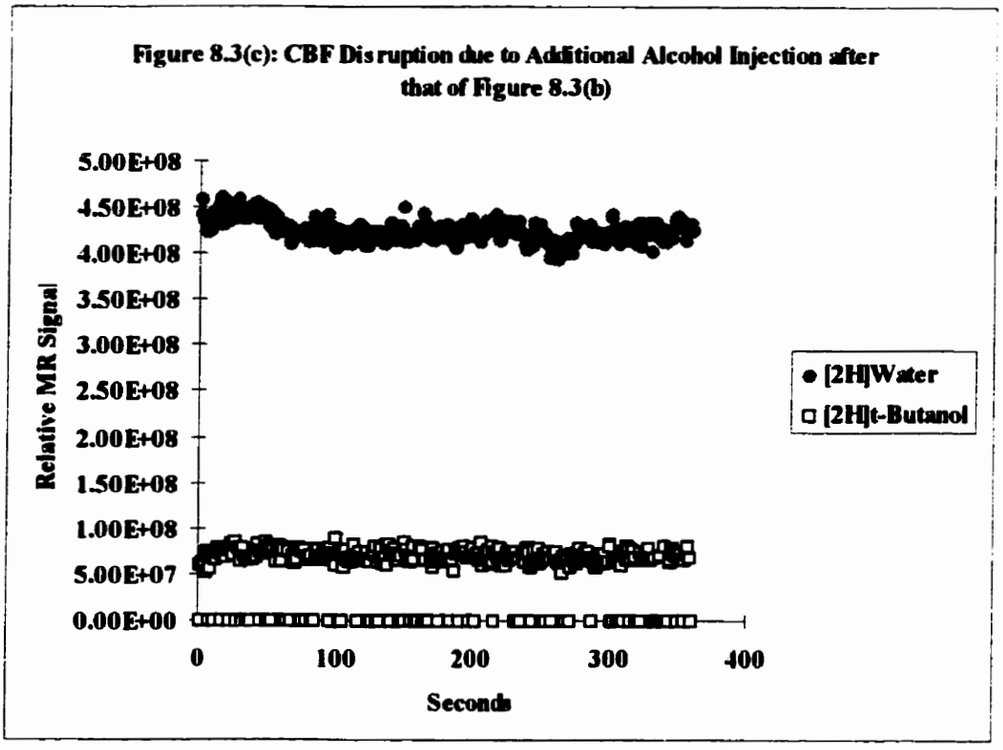

Table 8.1: Parameters for Dual Indicator Experiments

Experiment	Indicator		Bolus size (mL)	Inj. time (seconds)
	Alcohol (%v/v)	2H2O (%v/v)		
Dual Ethanol (n=3)	60%	38%	0.2	1
Dual Isopropanol (n=6)	30%	68%	0.1	1
Dual t-Butanol I (n=3)	50%	50%	0.05	1
Dual t-Butanol II (n=4)	10%	88%	0.33	2

C. CBF Comparison

1. Characteristics of the Alcohol Data

In comparing the washout curves for alcohol and water, it is evident that the former is characterized by fewer data points in the low signal regions; the only

exception is in those dual t-butanol experiments with 50/50 (v/v) concentrations of alcohol and water. This is because the software used to detect the MR spectral peak heights (See chapter 4) ignores signals less than a threshold value. This becomes an important factor in alcohol measurements where the signal is considerably smaller than that of water. It can be seen that the low signal regions include the initial pre-injection base line and the tail of the washout curve. This makes aCBF (See Chapter 5) modeling difficult, since the aCBF results depend critically on the asymptotic region, the region where missing data points frequently occur. On the other hand, fCBF modeling only requires a base line correction, which is a single averaged value and the missing data points are less of a concern (Chapter 5). It is worth pointing out that regions with too many missing data points cannot be used for CBF prediction. This was because, in low signal regions the noise that adds to the MR signal was preferentially picked up by the peak selection program while noise that reduces the MR signal was selectively ignored. This preferential selection made the washout of indicator and hence CBF appear slower (for both fCBF and aCBF).

2. Baseline Correction

As mentioned above (and in Chapter 5), in order to calculate fCBF using the alcohol washin and washout data one needs the alcohol base line. In some of the alcohol experiments the base line information was not available. This was due to the fact that the Bruker peak height picking software selectively ignores MR signals under a threshold. An attempt was made to locate the source code of the software but without success. In the absence of the alcohol baseline information, the corresponding water base line information was used to determine the alcohol base line

$$B_{\text{alcohol}} = \frac{n_{\text{alcohol}}}{n_{\text{water}}}\left[\frac{1}{10}\sum_{i=1}^{10} S_i(\text{water}) \times \frac{S_{\max}(\text{alcohol})}{S_{\max}(\text{water})}\right] \qquad \text{Eq. (8.2)}$$

where n_{alcohol} and n_{water} are the respective number of alcohol and water injections before the current experiment; $S_{\max}$(alcohol) and $S_{\max}$(water) are the respective maxima of the alcohol and water washin and washout curves; and S_i(water) is the signal for the i^{th} point of the water washin and washout curve (datum points 1 to 10, represent the baseline before washin). Eq. (8.2) was used to obtain the alcohol baselines in those experiments where baseline information was not available; that is, in those alcohol experiments characterized by a significant number (e.g, 25% or more) of missing data points (from the initial base line just before washin). Eq. (8.2) was used in all dual isopropanol experiments and three (out of six) of the dual t-butanol experiments (25en6, 25en7 and 25en8).

3. Partition Coefficients

As before, fCBF was calculated using

$$fCBF = -100 \times \lambda \times m. \qquad \text{Eq. (8.3m)}$$

where λ is the partition coefficient and m the slope of the initial washout curve on a semi-log plot. The partition coefficient (λ) for water, as before, was taken as 0.9 mL/mg. (See Chapter 5.) The λ for ethanol was taken as 1.14 mL/gm,[1] a value for cortical gray matter and hence one that is quite suitable for our present experimental technique. (See Chapter 4). At present, the λ for isopropanol has not been reported and was assumed 1.0 mL/gm. The λ for t-butanol was 0.77 mL/gm. This value, published by Gjedde *et al.*,[6,7] was measured according to the definition given by Kety[8] and therefore is appropriate for our experiments.

4. Fast CBF Component Comparisons

The CBF modeling technique used to analyse the dual indicator experiments was identical to methods discussed previously. (See Chapters 4 and 5.)

Table 8.2(a): Dual Alcohol fCBF Results

Experiment	[2H]Water (mL/100g/min)	s.dev. [2H]Water	[2H]Alcohol (mL/100g/min)	s.dev. [2H]Alcohol
Dual Ethanol n = 3	20	16	31	18
Dual Isopropanol n = 6	35	19	31	15
Dual t-Butanol n = 7	42	25	36	28

Table 8.2(a) summarizes the dual alcohol and water fCBF(3-23) results. Not included in the fCBF summary were a number of low alcohol signal experiments, (rejected using the SNR data discriminating Eq. (5.1) of Chapter 5 and the same threshold value of 50 as with water). Also not included were those experiments with too many missing t-butanol peaks in the initial washout region.

Note the large standard deviations in the CBF values obtained. This made statistical analysis impossible. The main reason, as given before, was the large range of CBF values associated with alcohol experiments. In addition, the level of $PaCO_2$ of these experiments was not controlled (in fact, attempts to control the level of $PaCO_2$ in the experiments failed; the failure was due to the influence of alcohol, for it was observed that $PaCO_2$ could change substantially in these experiments). However, the standard deviations for both water and alcohol measurements are roughly equal, suggesting the precision of the two measurements is similar and thus lending credibility to the technique. In all experiments it was observed that as the fCBF value for water increased so too did the value for alcohol and by the same proportion.

Table 8.2(b) shows the average fCBF percentage difference (PD) between the water and the alcohol values using the results of Table 8.2(a) and Eq. (8.1). The negative signs for the dual isopropanol and t-butanol indicate that the average fCBF values were less than that for water.

Table 8.2(b): Dual Alcohol fCBF Percentage Differences

Experiment	Percentage Difference fCBF(3-23)
Dual Ethanol n = 3	43
Dual Isopropanol n = 6	-12
Dual t-Butanol n = 7	-15

Table 8.2(b) shows that the fCBF measured using ethanol was greater than that for water by 43%. If this value is statistically meaningful (which is probably not due to the large standard deviation associated with the fCBF values), one can infer that water is diffusion limited and as a result will underestimate CBF. Results presented in the table for isopropanol and t-butanol are however contrary to what one would predict based on the fact that alcohol is more freely diffusible than water (alcohol should exhibit a higher CBF value). CBF values obtained for isopropanol were suspect due to the fact that λ was unknown. Because of this no further investigation was made into the isopropanol results. Keeping in mind the number of experiments is too small to yield statistical significance, the t-butanol findings are examined further in the next section.

5. An Explanation for Lower t-Butanol CBF Obtained

The dual t-butanol study was performed using the same experimental protocol as the dual ethanol study (which yielded a CBF that was greater than that measured using deuterated water), with only three exceptions (See Table 8.1): 1.

concentration, 2. bolus size and 3. duration of injection. Our previous CBF studies using water (Chapter 4) indicated that CBF measurements using bolus sizes ranging from 0.05 mL to 0.35 mL and injection times from 1 to 2 seconds did not significantly affect CBF results. In addition, the effects of bolus size and injection time on the t-butanol and water results would have been the same. Clearly, the remaining difference (alcohol concentration) is the only possible reason for the conflicting results obtained with ethanol and t-butanol.

Note in Table 8.1 that the ethanol bolus concentration was 60% (v/v) and the t-butanol concentration was 50% (v/v) for 3 experiments and 10% for 4 experiments. Table 8.3 lists the individual results of all t-butanol experiments and presents the PD (using Eq. (8.1)) for the dual t-butanol at 50% and 10% concentrations separately. When the t-butanol concentration was close to that used in the ethanol experiments (50% versus 60%) the measured fCBF was higher than for water. On the other hand, when the t-butanol concentration was 10%, the measured fCBF was lower than for water. This suggested that the fCBF values for t-butanol and water obtained in the dual alcohol experiments were dependent on the relative concentrations (v/v) of two indicators used. The chemical shift (CS) between the ^{2}H labeled water and t-butanol was approximately 3.5 ppm (Figure 8.a6, ^{2}HOH on the left and t-butanol on the right) and their FWHM was approximately 2 ppm. The large FWHM of water and t-butanol was due largely to the fact the Bruker Biospec 7T/21 cm scanner was optimized for imaging and SNR

at lb = 50 Hz (~ 1ppm). This resulted in a magnetic field that was quite homogeneous over a considerably large volume, but the homogeneity may not be as high as would be expected with a dedicated MR spectrometer at the same field strength over a smaller volume. In addition, the small bolus size (in some cases 25 μL each or 50 μL total) also played a role in the SNR obtained (for example SNR is proportional to the amount of the indicator injected). From the knowledge of the CS difference and FWHMs for water and t-butanol it was concluded that the peaks over lapped. The degree of cross contamination between t-butanol and water was determined using a deconvolution technique to fit the water and t-butanol peaks. The deconvolution

Table 8.3(a): Dual t-Butanol Results

Exp. No	t-Butanol (v/v)	i. time (s)	b. size (mL)	fCBF(3-23) ^2H_2O	st.dev. ^2H_2O	fCBF(3-23) t-Butanol	st.dev. t-Butanol
6en4	50%	1	0.05	60	5.7	75	3.5
6en6	50%	1	0.05	22	1.4	22	1.3
12en1	50%	1	0.05	24	6.3	38	7.6
			ave.	**35**		**45**	
			P.D.	**+25%**			
25en6	10%	2	0.35	40	1.5	31	6.1
25en7	10%	2	0.35	34	1.7	4	5.2
25en8	10%	2	0.35	90	2.7	72	4.5
25en9	10%	2	0.30	21	4.2	13	5.7
			ave.	**46**		**30**	
			P.D.	**-42%**			

employed two lines (one at the $^{2}HO^{1}H$ resonance and the other at the t-butanol resonance) with a Lorentz lineshape. Results show that 24% of t-butanol peak height was due to water contamination and close to 0% of water peak height was due to t-butanol contamination. Table 8.4. shows the deconvolution results. This indicates that the contribution of water signal to the t-butanol peaks is more serious as the t-butanol concentration decreases. A similar process could also have been applied to dual ethanol experiments but was not performed due to the low SNR of the data obtained. In the case of the 50/50 (v/v) dual t-butanol experiment, the height and FWHM of the water and the t-butanol lines were nearly equal and it is expected that cross contamination of water in t-butanol and vice versa would be nearly equal. A conclusion is that the effects of mutual contamination on this type of experiment was minimal (the effect of water cancels the effect of alcohol and vice versa), and that the respective fCBF values obtained for water and for t-butanol can be compared directly without deconvolution analysis. The results of Table 8.4 were obtained using data measured with 10% t-butanol (25en6). Similar results are expected from experiment 25en7 to 25en9 because they all utilized 10% alcohol concentration. There are two reasons for the higher water peak: the obvious one is it has much higher concentration in the bolus and the second is due to the fact that the dual t-butanol experiments were performed after 5 injections of deuterated water which would increase the deuterated water background. The second reason should only affect background as the time between consecutive injections was relatively long (30 minutes); hence the background effect is removed with deconvolution and background subtraction.

In order to more accurately calculate fCBF using t-butanol, the water contamination needs to be removed from the t-butanol peaks. In the case of experiment 25en6 a simple approximation would be to:

1. subtract 24% from the measured t-butanol peak heights

2. calculate a new 'water contamination removed background' for t-butanol using

$$B_{\text{alcohol}}(\text{new}) = B_{\text{alcohol}}(\text{observed}) \times 0.76$$

where $B_{alcohol}$(observed) is obtained from Eq. (8.2)

3. subtract the $B_{alcohol}$(new) from the t-butanol peaks and calculate fCBF for t-butanol as before using the new peak height and background values

Table 8.4: Dual t-Butanol Deconvolution Results for Experiment 25en6

Spec. No.	Water Peak			t-Butanol Peak		
	Before	After	P.D.	Before	After	P.D.
15	1.34E+05	1.36E+05	-0.64013	2.60E+04	2.09E+04	21.7484
16	1.37E+05	1.38E+05	-0.40095	2.39E+04	1.84E+04	26.00473
17	1.37E+05	1.39E+05	-0.68979	2.39E+04	1.90E+04	22.84382
18	1.35E+05	1.36E+05	-0.35662	2.20E+04	1.69E+04	26.22108
19	1.37E+05?	1.37E+05?		2.12E+04	1.61E+04	27.34584
20	1.31E+05	1.33E+05	-0.64647	2.38E+04	1.90E+04	22.42991
21	1.30E+05	1.31E+05	-0.44984	2.04E+04	1.54E+04	27.93296
22	1.27E+05	1.29E+05	-0.95205	2.30E+04	1.88E+04	20.09569
23	1.25E+05	1.27E+05	-0.61704	1.98E+04	1.61E+04	20.61281
24	1.23E+05	1.25E+05	-0.78834	2.03E+04	1.61E+04	23.07692
25	1.22E+05	1.24E+05	-0.92001	2.00E+04	1.56E+04	24.7191
26	1.21E+05	1.23E+05	-1.00307	1.96E+04	1.47E+04	28.57143
27	1.19E+05	1.21E+05	-0.87769	1.99E+04	1.60E+04	21.72702
28	1.15E+05	1.17E+05	-1.10953	2.08E+04	1.74E+04	17.80105
29	1.17E+05	1.19E+05	-0.85472	1.80E+04	1.43E+04	22.91022
30	1.20E+05	1.21E+05	-0.64332	1.95E+04	1.51E+04	25.43353
31	1.18E+05	1.20E+05	-0.86425	1.79E+04	1.35E+04	28.02548
32	1.14E+05	1.16E+05	-0.75676	2.23E+04	1.84E+04	19.16462
33	1.12E+05	1.14E+05	-0.50429	2.12E+04	1.69E+04	22.57218
34	1.11E+05	1.13E+05	-0.80167	2.06E+04	1.68E+04	20.32086
35	1.08E+05	1.09E+05	-0.37768	1.83E+04	1.38E+04	28.03738
36	1.10E+05	1.12E+05	-0.61406	1.87E+04	1.49E+04	22.61905
		ave.	-0.70801		ave.	23.64609
		st.dev.	0.213324		st.dev.	3.169187

Using this method the fCBF for t-butanol of 25en6 obtained is 40 ± 8 mL/100g/min. Table 8.5 are the results from experiments (25en7, 25en8, 25en9), recalculated assuming 24% water contamination of the t-butanol peak. In conclusion, the water contamination must be removed to obtain more accurate t-butanol results. When this is done, t-butanol fCBF values obtained are greater than those for water, as one would predict on the basis of diffusibility.

Table 8.5: New Dual t-Butanol Results

Exp. No	t-Butanol (v/v)	i. time (s)	b. size (mL)	fCBF(3-23) 2H2O	st.dev. 2H2O	fCBF(3-23) t-Butanol	st.dev. t-Butanol
6en4	50%	1	0.05	60	5.7	75	3.5
6en6	50%	1	0.05	22	1.4	22	1.3
12en1	50%	1	0.05	24	6.3	38	7.6
			ave.	**35**		**45**	
			P.D.	**+25%**			
25en6	10%	2	0.35	40	1.5	40	8
25en7	10%	2	0.35	34	1.7	39	19
25en8	10%	2	0.35	90	2.7	156	8
25en8	10%	2	0.30	21	4.2	24	16
			ave.	**46**		**64**	
			P.D.	**+33%**			

To summarize: 1. using the dual t-butanol experiments at 50/50 (v/v) concentrations of t-butanol and water, the measured fCBF for alcohol was higher than for water, 2. using the dual t-butanol experiments at 10% t-butanol concentration and deconvolution to account for water contamination, the measured fCBF for alcohol was also higher than for water.

D. Observations and Discussion

Unlike the water CBF experiments, the use of alcohols disturbed the CBF due to alcohol toxicity. A cumulative alcohol injection of about 0.15 ± 0.05 mL altered the CBF to a point where CBF would stop completely. This is the reason why only a limited number of injections were performed in a rat. Within the time span of an experiment (typically 30 minutes) the alcohol toxicity was similar for all three alcohols (that is, acute toxicity dominated). However, the results of the study were indifferent to the alcohol toxicity as the water and alcohol CBF values were determined under identical measurement conditions.

The SNR for t-butanol and isopropanol was at least 9 times higher than ethanol. The apparent higher SNR for isopropanol was due to excessive water contamination under the *in-vivo* experimental conditions. An attempt to eliminate water contamination in both dual t-butanol and isopropanol using a line broadening of 20 Hz (lb = 20) was not successful. It was speculated that due to the intrinsically large *in-vivo* FWHM of the water and alcohol lines, the use of lb = 20 only serves to reduce SNR in the spectra obtained. This led to the development of the deconvolution technique for the removal of water contamination in the dual t-butanol experiments with low alcohol concentration described above.

Under the given experimental conditions, the dual t-butanol approach was the preferred technique. Other findings of the study include:

1. Water, as CBF indicator, is limited by diffusion; on the other hand, alcohol is limited by toxicity.
2. Results of the study presented in Tables 8.5 are independent of alcohol toxicity.
3. t-butanol is the best of the alcohol indicators.
4. Water is preferred over alcohol indicators, if one keeps in mind that according to Chapter 6 it underestimates the CBF by an average of 25%. This 25% underestimation of CBF using the water method was qualitatively confirmed in this chapter using the dual t-butanol at 50/50 (v/v) of alcohol and water and using the dual t-butanol at 10/90 (v/v) of alcohol and water in combination with deconvolution.
5. Results obtained are preliminary and qualitative only, due to the poor statistics associated with the small number of measurements.

Reference:

1. Eklof B, Lassen NA, Nilsson L, *et al.*, 'Regional Cerebral Blood Flow in the Rat Measured by the Tissue Sampling Technique: a Critical Evaluation Using Four Indicators C14-Antipyrine, C14-Ethanol, H3-Water and Xenon-133', *Acta.Physiol.Scand.* 91:1-10, 1974.

2. Raichle ME, Eichling JO, Straatman MG, *et al.*, 'Blood-Brain Barrier Permeability of ^{11}C-Labeled Alcohols and ^{15}O-Labeled Water', *Am.J.Physiol.* 230:543-552, 1976.

3. Sage JI, Van Uitert RI, and Duffy TE, 'Simultaneous Measurement of Cerebral Blood Flow and Unidirectional Movement of Substances Across the Blood-Brain Barrier: Theory, Method, and Application to Leucine', *J.Neurolchem.* 36:1731-1738.

4. Van Uitert RL, Sage JI, Levy DE and Duffy TE, 'Comparison of Radio-Labeled Butanol and Iodoantiprine as Cerebral Blood Flow Markers', *Brain Res.* 222:365-372, 1983.

5. Herscovitch P, Raichle ME, Kilbourn R and Welch MJ, 'Positron Emission Tomographic Measurement of Cerebral Blood Flow and Permeability-Surface Area Product of Water Using [^{15}O] Water and [^{11}C] Butanol', *Journal of Cerebral Blood Flow and Metabolism* 7:527-542, 1987.

6. Gjedde A and Rasmussen M, 'Blood Brain Glucose Transport in the Conscious Rat: Comparison of the Intravenous and Intracarotid Injection Method', *J.Neurochem.* 35:1375-1381, 1980.

7. Gjedde A, Hansen AJ and Siemkowicz E, 'Rapid Simultaneous Determination of Regional Blood Flow and Blood-Brain Glucose Transfer in the Brain of Rat', *Acta.Physiol.Scand.* 108:321-330, 1980.

8. Kety SS, 'The Theory and Applications of the Exchange of Inert Gas at the Lungs and Tissues', *Pharm. Rev.* 3:1, pp1-41, 1951.

Chapter 9: Conclusion

The goal of the CBF project is to develop a method of measuring CBF in humans using MR, with eventual application of the method to brain tumor management. Three phases of research were identified as necessary in achieving this goal. They were:

1. To develop a non invasive CBF measurement method in an animal model and gain an understanding of the underlying fundamental principles on which it is based.
2. To assess in detail the accuracy and precision of the CBF method.
3. To modify the CBF method for use in humans.

The first phase was successfully completed in the present study. In the first phase the CBF measurement method was developed and investigated thoroughly to better understand all aspects of the technique (Chapters 4 and 5). For example, the effect of bolus size, injection time and injection location on results were studied. The second phase, an assessment of accuracy and precision, was also completed. The accuracy of the method was assessed using the concept of extraction coefficient (Chapter 6) to investigate the diffusion limitations of the tracer and by developing a method for recirculation correction (Chapter 7). Precision was quantified through repeated measurements on the same animal, using three rats. The third phase, to modify the CBF method for use in humans, remains to be tackled.

A. Development of the Animal Model

The goal of the study imposed a number of constraints on the CBF method developed. For example, invasive CBF (invasive with respect to indicator sampling) methods were not considered, as the method is to be applied eventually to humans. With the above conditions in mind the literature was reviewed (Chapter 2). In the end deuterated water was chosen as the indicator and MRS as the sampling method. In light of the MRS sampling method chosen, the mathematical models for the CBF measurement were formulated (Chapter 3), fCBF and aCBF. In developing the CBF method, many experiments were performed to evaluate the suitability of indicator injection sites (femoral vein, right subclavian, common carotid, external carotid and external jugular), duration of injection (from less than 1 to 25 seconds) and bolus size (from 50 μL to 1 mL), etc. Chapter 4 presented these experiments, as well as a recipe for the final protocol (which employed an instantaneous bolus injection at the right carotid bifurcation).

Using the CBF method developed it was noted that the indicator washin and washout curve suggested that the brain consists of three components:

1. the vascular bed, as was evident from the initial spike of indicator washout presented on a semi-log scale (see Figure 5.3)
2. the fast gray matter, represented by the initial linear section of the washout curve

3. the slower white matter, represented by the second linear portion of the washout curve (after removal of recirculation)

Using the three component picture of the brain it was found that the intra-vascular fluid (blood, plasma) transit time in the brain was of the order of 3 ± 2 seconds and that, the extraction coefficient of ^2H_2O indicator was 0.85 (from Figure 6.2). The transit time was obtained from measuring the FWHM of the initial spike (which in all cases was equal to 3 seconds); the ± 2 seconds was due to the limitation in sampling frequency.

1. Precision

Repeat measurements on the same rat under identical experimental conditions were extremely difficult due to fluctuations in $PaCO_2$ and animal sedation. However, in those instances where conditions remained constant (Figures 5.6, 5.7, 5.9, 5.15, 5.16, 5.18, etc.) results were found to be reproducible.

2. Validity

It is expected that a valid CBF method should be capable of tracking changes in $PaCO_2$ levels. Under normal conditions, the CBF results, as presented in Chapter 5, correlated positively to $PaCO_2$. As the $PaCO_2$ increased, the CBF increased accordingly. The increase in CBF at normocarbia was directly proportional to $PaCO_2$ levels, with a positive correlation coefficient greater than 0.78. This fact lends credibility to the CBF method developed.

To summarize: We have developed a CBF measurement method that is valid and precise. This method involved:

1. Instantaneous bolus injection of deuterated water at the right external carotid of the animal
2. Monitoring the washout of the indicator from the brain using ^{2}H MRS
3. Estimating CBF by fitting the appropriate mathematical model to the measured data.

The measured fCBF and aCBF values for:

1. hypocarbia
2. normocarbia
3. hypercarbia

were summarized in Table 5.3 (reproduced in this chapter for ease of reference). These values are at the lower end of the CBF range appearing in the literature (Table 5.2). Among the literature values it is difficult to say which is the gold standard. Results obtained in this study were lower than the median of the literature data. There are two possible reasons for this. The first is due to indicator recirculation which is not accounted for in the data presented in Table 5.3 and the second due to the indicator not being completely 'freely' diffusible.

Table 5.3: CBF Values Using the CBF Measurement Method Developed for This Study

	CBF (ml/100g/min.)	sdCBF (ml/100g/min.)
fCBF(0-23)		
1. Normal PaCO2, Normal PaO2		
(8 rats, partition coefficient=1)	81	11
(8 rats, partition coefficient=0.9)	73	10
2. Normal PaCO2, Low PaO2		
(2 rats, partition coefficient=1)	98	30
(2 rats, partition coefficient=0.9)	88	27
3. Normal PaCO2, High PaO2		
(7 rats, partition coefficient=1)	66	22
(7 rats, partition coefficient=0.9)	59	20
aCBF		
1. Normal PaCO2, Normal PaO2		
(5 rats, partition coefficient=1)	57	17
(5 rats, partition coefficient=0.9)	51	15
2. Normal PaCO2, High PaO2		
(4 rats, partition coefficient=1)	55	9
(4 rats, partition coefficient=0.9)	49	8

B. Accuracy of the CBF Method

Chapter 6 quantified the underestimation of CBF due to deuterated water not being an 'ideal' freely diffusible indicator using the extraction coefficient correction method. It was found that the underestimation of CBF was 20%.

Chapter 7 quantified the underestimation of CBF due to indicator recirculation by means of convolution analysis. It was found that the underestimation of CBF due to indicator recirculation was 30% for both fCBF and aCBF.

Chapter 8 was a preliminary investigation into using deuterated alcohol compounds as an alternative approach in assessing the diffusion limitations of water as a tracer. Although the number of rats utilized in this study was too small to draw statistically significant conclusions, the chapter does outline a very elegant protocol for simultaneous measurements using two tracers.

Table 9.1: Corrected versus Non-Corrected CBF Values

fCBF(0-23)	**CBF (uncorrected) (mL/100g/min)**	**CBF (recirculation and extraction corrections) (mL/100g/min)**
1. Normal PaCO2, Normal PaO2 (8 rats, $\lambda = 0.9$)	73	114
2. Normal PaCO2, Low PaO2 (2 rats, $\lambda = 0.9$)	88	137
3. Normal PaCO2, High PaO2 (7 rats,$\lambda = 0.9$)	59	92
aCBF		
1. Normal PaCO2, Normal PaO2 (5 rats, $\lambda = 0.9$)	51	80
2. Normal PaCO2, High PaO2 (4 rats, $\lambda = 0.9$)	49	76

C. Future Prospects

Having completed the first two phases of the CBF study, the next logical step will be to apply the CBF method to brain cancer management. To make this possible, the technique will have to be modified to make it more appropriate for use on humans (the injection site will have to be moved to a peripheral vein) and to provide spatial resolution (sampling will have to be performed using magnetic resonance imaging).